

Contents

Contents	I
List of Figures	IV
List of Tables	VI
1 Introduction	1
2 The Minimal Supersymmetric Standard Model	4
2.1 General Aspects	4
2.2 Electroweak Gauge Bosons and Higgs Bosons	5
2.3 Gauginos and Higgsinos	6
2.3.1 Charginos	6
2.3.2 Neutralinos	7
2.3.3 The Gluino	8
2.4 Leptons and Quarks	8
2.5 Sfermions	9
2.6 Experimental bounds	10
3 Decay Widths	11
3.1 General Remarks	11
3.2 The relevant parts of the Lagrangian	12
3.3 Two body decays	15
3.4 Three Body Decays of the Light Stop	16
3.4.1 The Decay of the Light Stop into a W-Boson, a Bottom Quark and the Lightest Neutralino	16
3.4.2 The Decay of the Light Stop into a charged Higgs Boson, a Bottom Quark and the Lightest Neutralino	18
3.4.3 The Decay of the Light Stop into a Bottom Quark, a Slepton and a Lepton	18
3.5 The Decay of the light Stop into a Charm-quark and a Neutralino . .	20

4	Numerical results for LEP2	22
4.1	Light Stop	22
4.2	Light Sbottom	29
4.3	Light Stau	32
4.4	Tau Sneutrino	34
5	Production of sfermions at a Linear Collider	37
6	Masses and mixing angles	43
6.1	Outlook on the following chapters	43
6.2	Masses and mixing angles of staus and sbottoms	44
6.3	Masses and mixing angles of the stops	46
6.4	Higgs masses and mixing angle	48
7	Numerical results for sleptons	50
7.1	Decays of $\tilde{\nu}_\tau$	50
7.2	Decays of $\tilde{\tau}_1$	52
7.3	Decays of $\tilde{\tau}_2$	54
8	Numerical results for $\tilde{t}_{1,2}$	59
8.1	Decays of \tilde{t}_1	59
8.2	Decays of \tilde{t}_2	63
9	Numerical results for $\tilde{b}_{1,2}$	70
9.1	Decays of \tilde{b}_1	70
9.2	Decays of \tilde{b}_2	73
10	Higher order decays of \tilde{t}_1 and \tilde{b}_1	79
10.1	Three body decays of \tilde{t}_1	79
10.2	The decay $\tilde{b}_1 \rightarrow c \tilde{\chi}_1^-$	84
11	Summary	87
A	Formulae for the three body decay widths	89
A.1	Light Stop into W, Bottom, and Neutralino	89
A.2	Light Stop into charged Higgs, Bottom, and Neutralino	99
A.3	Light Stop into Bottom, Slepton and Lepton	105
A.4	Some analytical solutions of integrals	109
A.4.1	The integrals J_i	109
A.4.2	The solution of $J_t^0(m_1)$	110
A.4.3	The solution of $J_t^1(m_1)$	110
A.4.4	The solution of $J_t^2(m_1)$	111

A.4.5	The solution of $J_{tt}^0(m_1, m_2)$	111
A.4.6	The solution of $J_{tt}^1(m_1, m_2)$	111
A.4.7	The solution of $J_{tt}^2(m_1, m_2)$	112
A.4.8	The solution of $J_{st}^0(s, m_1, m_2)$	113
A.4.9	The solution of $J_{st}^1(s, m_1, m_2)$	113
B	Calculation of sfermion parameters	114
C	Production cross sections	116
C.1	Tree Level	116
C.2	SUSY-QCD Corrections	117
C.3	Initial-State Radiation	120
	Bibliography	121
	Zusammenfassung	126
	Lebenslauf	129

List of Figures

3.1	Feynman diagrams for the decay $\tilde{t}_1 \rightarrow b W \tilde{\chi}_1^0$	17
3.2	Feynman diagrams for the decay $\tilde{t}_1 \rightarrow b H^+ \tilde{\chi}_1^0$	19
4.1	Production cross sections for a light stop at LEP2	22
4.2	Parameter domains in the (M, μ) plane for \tilde{t}_1 decays at LEP2	23
4.3	Total decay widths of a light stop at LEP2 for $\tan \beta = 1.5$	24
4.4	Total decay widths of a light stop at LEP2 for $\tan \beta = 40$	24
4.5	Branching ratios for stop decays into sleptons at LEP2	26
4.6	Total decay widths of a light stop at LEP2 (three body decays)	27
4.7	Branching ratios of the stop decay into stau at LEP2	27
4.8	Production cross sections for a light sbottom at LEP2	30
4.9	Parameter domains in the (M, μ) plane for \tilde{b}_1 decays at LEP2	30
4.10	Decay widths of a light sbottom at LEP2 for $\tan \beta = 40$	31
4.11	Branching ratios for $\tilde{b}_1 \rightarrow b \tilde{\chi}_1^0$ at LEP2 for $\tan \beta = 40$	31
4.12	Production cross sections for a light stau at LEP2	32
4.13	Parameter domains in the (M, μ) plane for $\tilde{\tau}_1$ decays at LEP2	32
4.14	Branching ratios for $\tilde{\tau}_1$ decays at LEP2 for $\tan \beta = 40$	33
4.15	Production cross sections for $\tilde{\nu}_\tau$ at LEP2	34
4.16	Parameter domains in the (M, μ) plane for $\tilde{\nu}_\tau$ decays at LEP2	34
4.17	Branching ratios for $\tilde{\nu}_\tau$ decays at LEP2 for $\tan \beta = 1.5$	35
5.1	Total cross section $\sigma(e^+e^- \rightarrow \tilde{\nu}_\tau \overline{\tilde{\nu}_\tau})$	38
5.2	Total cross section $\sigma(e^+e^- \rightarrow \tilde{\tau}_1 \overline{\tilde{\tau}_1})$	38
5.3	Total cross section $\sigma(e^+e^- \rightarrow \tilde{\tau}_2 \overline{\tilde{\tau}_2})$	39
5.4	Total cross section $\sigma(e^+e^- \rightarrow \tilde{t}_1 \overline{\tilde{t}_1})$	39
5.5	Total cross section $\sigma(e^+e^- \rightarrow \tilde{t}_1 \overline{\tilde{t}_2})$	40
5.6	Total cross section $\sigma(e^+e^- \rightarrow \tilde{t}_2 \overline{\tilde{t}_2})$	41
5.7	Total cross section $\sigma(e^+e^- \rightarrow \tilde{b}_1 \overline{\tilde{b}_1})$	42
5.8	Total cross section $\sigma(e^+e^- \rightarrow \tilde{b}_2 \overline{\tilde{b}_2})$	42
6.1	Stau masses and mixing angle as a function of μ	45
6.2	Sbottom masses and mixing angle as a function of μ	46

6.3	Stop masses and mixing angle as a function of μ for $\tan\beta = 1.5$. . .	47
6.4	Stop masses and mixing angle as a function of A_t for $\tan\beta = 1.5$. . .	47
6.5	Higgs masses and mixing angle as a function of μ	48
6.6	Higgs masses and mixing angle as a function of $A_t = A_b$	49
7.1	Branching ratios for $\tilde{\nu}_\tau$ decays as a function of μ	51
7.2	Branching ratios for $\tilde{\nu}_\tau$ decays as a function of μ	51
7.3	Branching ratios for $\tilde{\tau}_1$ decays as a function of μ	53
7.4	Branching ratios for $\tilde{\tau}_2$ decays as a function of μ	55
7.5	Branching ratios for $\tilde{\tau}_2$ decays as a function of μ for $\tan\beta = 40$. . .	55
7.6	Branching ratios for $\tilde{\tau}_2$ decays as a function of A_τ for $\tan\beta = 40$. . .	56
7.7	Branching ratios for $\tilde{\tau}_2$ decays as a function of μ for $\tan\beta = 40$. . .	57
8.1	Branching ratios for \tilde{t}_1 decays as a function of μ	60
8.2	Total decay widths of \tilde{t}_1 as a function of μ	61
8.3	Branching ratios for \tilde{t}_1 decays as a function of $A_t (= A_b)$	62
8.4	Branching ratios for \tilde{t}_2 decays as a function of μ for $\tan\beta = 1.5$. . .	64
8.5	Branching ratios for \tilde{t}_2 decays as a function of μ for $\tan\beta = 40$. . .	66
8.6	Branching ratios for \tilde{t}_2 decays as a function of A_t for $\tan\beta = 40$. . .	67
8.7	Branching ratios for \tilde{t}_2 decays as a function of $\tan\beta$ for $A_t = 500$ GeV	68
9.1	Branching ratios for \tilde{b}_1 decays as a function of μ	71
9.2	Branching ratios for \tilde{b}_1 decays as a function of $A_b (= A_t)$	72
9.3	Branching ratios for \tilde{b}_1 decays as a function of μ	72
9.4	Branching ratios for \tilde{b}_2 decays as a function of μ and A_b for $\tan\beta = 1.5$	73
9.5	Branching ratios for \tilde{b}_2 decays as a function of $\tan\beta$ for $A_b = 500$ GeV	74
9.6	Branching ratios for \tilde{b}_2 decays as a function of μ for $\tan\beta = 40$. . .	76
9.7	Branching ratios for \tilde{b}_2 decays as a function of A_b for $\tan\beta = 40$. . .	77
10.1	Branching ratios for three body decays of \tilde{t}_1 as a function of $\cos\theta_{\tilde{t}}$. .	80
10.2	Branching ratios for three body decays of \tilde{t}_1 as a function of $\tan\beta$. .	81
10.3	Branching ratios for three body decays of \tilde{t}_1 as a function of $\cos\theta_{\tilde{t}}$. .	82
10.4	Branching ratios for three body decays of \tilde{t}_1 as a function of $\tan\beta$. .	83
10.5	Branching ratios for three body decays of \tilde{t}_1 as a function of M_D . . .	84
10.6	Branching ratios for $\tilde{b}_1 \rightarrow c \tilde{\chi}_1^-$	85
C.1	Feynman diagrams for the process $e^+e^- \rightarrow \tilde{f}_i \overline{\tilde{f}_j}$ ($f \neq e, \nu_e$).	117

List of Tables

2.1	Particle content of the Minimal Supersymmetric Standard Model. . .	4
4.1	Parameters for different scenarios at LEP2	24
10.1	Parameters and physical quantities used in Fig. 10.1	80
10.2	Parameters and physical quantities used in Fig. 10.3	82

Chapter 1

Introduction

Our understanding of the fundamental forces appearing in nature rests to a large extent on our increasing understanding of the underlying symmetries. Parallel to this happened the development of quantum field theories for the electromagnetic, weak and strong interactions (see e.g. [1]). In these theories the fundamental states are described by fields whose interactions obey the underlying symmetries. The theory which explains up to now all experimental facts is the so-called Standard Model (SM) which is based on the gauge group $SU(3) \times SU(2) \times U(1)$ (see e.g. [2, 3, 4] and references therein).

Despite its enormous success the SM still leaves many questions open, e.g.: Is it possible to explain the origin of the various parameters of the model ? Can gravity be included ? What is the origin of fermion masses ? What is the origin of electroweak symmetry breaking ? A first step to answering these questions could be the embedding of the SM in a Grand Unified Theory (GUT) [3, 5]. In this case the SM appears as the low energy limit of a GUT with only one gauge coupling. However, the simplest possibility based on $SU(5)$ has been ruled out by experiment [6]. Besides this, the SM and its simple GUT extensions exhibit the so-called hierarchy problem [7]. Here the question arises how one can stabilize the masses of fundamental scalars in the range of the electroweak scale. Radiative corrections push these masses up either to the GUT- or the Planck-scale. The stabilization can be achieved through cancellation between terms, each of the order 10^{15} GeV. This seems to be rather unnatural, because these terms have to be adjusted up to 13 digits.

One possibility to solve this problem is supersymmetry (SUSY)[8]. SUSY is a symmetry, which relates bosons to fermions and vice versa [9, 10]. Due to the fact that fermionic loops enter with the opposite sign of bosonic loops, one gets an automatic cancellation between different contributions of the radiative corrections to scalar masses. Moreover, repeated applications of supersymmetric transformations are equivalent to a Poincaré transformation. Therefore, supersymmetry, if it is a local symmetry, contains the graviton among its gauge fields and includes Einstein's

theory of gravity (see e.g. [11]). For this reason local supersymmetry is called supergravity (SUGRA). Beside these more theoretical advantages it has been shown that within supersymmetric GUTs a unification of gauge couplings consistent with experiments can be achieved [6].

Some other appealing features of SUSY are:

- It can be shown that the SUSY algebra is the only nontrivial extension of the set of spacetime symmetries which forms one of the building blocks of relativistic quantum field theory [12].
- Electroweak symmetry breaking can be achieved due to radiative effects caused by the large top mass [13].
- Some models contain a stable lightest supersymmetric particle which serves as a good candidate for dark matter [14].

Therefore, it is very interesting to study the phenomenological aspects of supersymmetric theories. For technical details and how to construct a phenomenological acceptable theory we would like to refer the interested reader to the literature, e.g. [11, 15, 16, 17, 18, 19, 20].

The simplest supersymmetric extension of the SM is called Minimal Supersymmetric Standard Model (MSSM). In this model every known SM particle obtains a supersymmetric partner. One has to enlarge the Higgs sector to obtain a consistent theory by adding an extra Higgs doublet of opposite hypercharge. The second Higgs doublet is needed to give mass to both up- and down-type quarks and to cancel the triangle anomaly caused by the supersymmetric partners of the Higgs-doublets. Due to the fact that no supersymmetric partner of the SM particles has been found up to now, SUSY has to be broken. This can be achieved by adding by hand soft SUSY breaking terms. These consist of scalar and gaugino mass terms, as well as trilinear (A-terms) and bilinear (B-terms) interactions [21]. Such a model is the most conservative approach to realistic model building, but the large parameter space causes it to be rather unpredictable. However, there are many different ways to construct a more fundamental theory which reduces the number of free parameters. For example in minimal supergravity models there are only five additional parameters which remain as free parameters (see e.g. [18, 19, 20]).

In this work we will use the MSSM as framework. In this model there exists a conserved quantum number called R-parity $R = (-1)^{3B+L+2S}$, where B , L and S denote baryon number, lepton number and spin, respectively. This leads to two important phenomenological implications: Firstly, SUSY particles can only be produced in pairs. Secondly, the lightest supersymmetric particle (LSP) is stable. In recent years it has turned out that third generation sfermions (the scalar partners of the top- and bottom quark, the tau and the tau-neutrino) are of special interest. This is mainly due to two reasons: Firstly, large Yukawa couplings lead to a different

phenomenology compared to the sfermions of the first two generations. Secondly, if a SUSY GUT is realized in nature, studies of renormalization group equations (RGEs) [18, 22] indicate, that third generation sfermions are in general lighter than the sfermions of the first two generations (for the stop which is the scalar partner of the top quark this has been pointed out in [23]). For these reasons it is possible that one of them is the lightest charged SUSY particle and hence its appearance could be the first experimental evidence of SUSY. In the following we will study their phenomenology at e^+e^- colliders. However, most of our results can also be applied to hadron colliders.

This work is organized in the following manner: In Chapter 2 we present the particle content of the MSSM. The relevant interaction Lagrangian and the formulae for the various decay widths of the sfermions are given in Chapter 3. In Chapter 4 we discuss the phenomenology of sfermions at LEP2 ($\sqrt{s} = 192$ GeV). In particular the influence of the Yukawa couplings on the decay pattern will be discussed. The production of sfermions at an e^+e^- Linear Collider (LC) with an energy range between 500 GeV and 2 TeV is discussed in Chapter 5. In Chapter 6 we discuss our strategy for exploring the phenomenology of sfermions with masses of several hundred GeV which will be presented in Chapters 7, 8, and 9. Here we put special emphasis on the decays into gauge and Higgs bosons. Higher order decays of the light stop and the light sbottom are discussed in Chapter 10. In Chapter 11 we give a summary of the main topics. Appendix A gives the analytical solutions for the three body decay widths. In Appendix B we present the formulae for computation of the MSSM parameters from sfermion masses and mixing angles. Finally, the formulae for the production cross sections including ISR- and QCD-corrections are given in Appendix C .

Chapter 2

The Minimal Supersymmetric Standard Model

2.1 General Aspects

The simplest linear extension of the Standard Model (SM) is the so-called Minimal Supersymmetric Standard Model (MSSM). It has the same gauge group as the SM: $SU(3)_C \times SU(2)_L \times U(1)_Y$ which breaks spontaneously to $SU(3)_C \times U(1)_{em}$. This spontaneous symmetry breaking can be achieved through radiative corrections due to the large top mass [13]. In addition to the SM particles we have a second Higgs doublet, spin $\frac{1}{2}$ partners for the Higgs fields called higgsinos, spin $\frac{1}{2}$ partners for the gauge bosons called gauginos and two spin 0 partners for each fermion called sfermions (one for each helicity state). In Tab. 2.1 all particles of the MSSM are listed except the graviton and its partner, the gravitino.

In the following we will briefly discuss the mass eigenstates of this model.

SM particles + additional Higgs		SUSY particles	
$j = \frac{1}{2}$	$q_{L_i} = \begin{pmatrix} u_{L_i} \\ d_{L_i} \end{pmatrix}, u_{R_i}, d_{R_i}$ $l_{L_i} = \begin{pmatrix} \nu_{L_i} \\ e_{L_i} \end{pmatrix}, e_{R_i}$	$j = 0$	$\tilde{q}_{L_i} = \begin{pmatrix} \tilde{u}_{L_i} \\ \tilde{d}_{L_i} \end{pmatrix}, \tilde{u}_{R_i}, \tilde{d}_{R_i}$ $\tilde{l}_{L_i} = \begin{pmatrix} \tilde{\nu}_{L_i} \\ \tilde{e}_{L_i} \end{pmatrix}, \tilde{e}_{R_i}$
$j = 1$	g^a γ, Z, W^\pm	$j = \frac{1}{2}$	\tilde{g}^a $\tilde{\chi}_i^0 = a_i \tilde{\gamma} + b_i \tilde{Z} + c_i \tilde{H}_1^0 + d_i \tilde{H}_2^0$
$j = 0$	$H_1 = \begin{pmatrix} H_1^0 \\ H_1^- \end{pmatrix}, H_2 = \begin{pmatrix} H_2^+ \\ H_2^0 \end{pmatrix}$		$\tilde{\chi}_k^\pm = \alpha_k \tilde{W}^\pm + \beta_k \tilde{H}_{2,1}^\pm$

Table 2.1: Particle content of the Minimal Supersymmetric Standard Model.

2.2 Electroweak Gauge Bosons and Higgs Bosons

As already mentioned there are two Higgs doublets H_1 and H_2 in the MSSM. The scalar potential V_{Higgs} reads at tree-level [17]

$$V_{Higgs} = m_1^2 H_1^\dagger H_1 + m_2^2 H_2^\dagger H_2 - m_3^2 (H_{1i}^T \epsilon_{ij} H_{2j} + h.c.) + \frac{g^2}{2} \sum_{k=1}^3 \left(H_{1i}^\dagger \frac{\sigma_{ij}^k}{2} H_{1j} + H_{2i}^\dagger \frac{\sigma_{ij}^k}{2} H_{2j} \right)^2 + \frac{g'}{4} (H_1^\dagger H_1 + H_2^\dagger H_2)^2. \quad (2.1)$$

The phases of the fields can be chosen such that $m_3^2 > 0$. Note, that the quadric terms are determined through the gauge couplings in contrast to the Standard Model or a general two Higgs doublet model where these couplings are free parameters.

Due to spontaneous symmetry breaking of $SU(2)_L \times U(1)_Y$ one gets for the vacuum expectation values (vevs) of the Higgs fields:

$$\langle H_1 \rangle = \begin{pmatrix} v_1 \\ 0 \end{pmatrix} \quad \langle H_2 \rangle = \begin{pmatrix} 0 \\ v_2 \end{pmatrix}. \quad (2.2)$$

The diagonalization of the mass matrices for the charged and the neutral Higgs fields leads to five physical Higgs bosons and three Goldstone bosons. The physical Higgs bosons are two charged Higgs bosons H^\pm , two scalar Higgs bosons h^0, H^0 and a pseudoscalar Higgs boson A^0 . The three Goldstone-bosons form together with the $SU(2) \times U(1)$ gauge-bosons the photon and the Z^0 - and W^\pm -bosons. The masses of the gauge bosons

$$m_W^2 = \frac{g^2 v^2}{2}, \quad m_Z^2 = \frac{(g'^2 + g^2) v^2}{2} \quad (2.3)$$

fix the sum of the vevs $v^2 = v_1^2 + v_2^2$. The ratio $\tan \beta \equiv v_2/v_1$ remains as a free parameter of the model.

At tree-level one gets the following mass relations:

$$m_{A^0}^2 = m_1^2 + m_2^2 \quad (2.4)$$

$$m_{h^0, H^0}^2 = \frac{1}{2} \left(m_{A^0}^2 + m_Z^2 \mp \sqrt{(m_{A^0}^2 + m_Z^2)^2 - 4m_{A^0}^2 m_Z^2 \cos^2 2\beta} \right) \quad (2.5)$$

$$m_{H^\pm}^2 = m_{A^0}^2 + m_W^2 \quad (2.6)$$

and thus

$$m_{h^0} \leq \min(m_Z, m_{A^0}), \quad m_{H^0} \geq m_Z, \quad m_{H^\pm} \geq m_W. \quad (2.7)$$

It has been shown that one-loop corrections are important for the Higgs-masses. In the effective potential approach [24] the potential V_{Higgs} modifies to $V_{one-loop}$

$$V_{one-loop} = V_{Higgs} + \frac{1}{64\pi^2} \text{STr} \mathcal{M}^4 \left(\ln \frac{\mathcal{M}^2}{Q_0^2} - \frac{3}{2} \right). \quad (2.8)$$

A total one-loop computation has been given in [25, 26]. For the discussions in Chapter 6-9 the most important corrections stemming from third generation quarks and squarks [27, 28] have been included.

2.3 Gauginos and Higgsinos

2.3.1 Charginos

The mass eigenstates of the charged gauginos and higgsinos are called charginos $\tilde{\chi}_{1,2}^\pm$. In the basis

$$\tilde{\psi}_j^+ = (-i\lambda^+, \psi_{H_2}^1) \quad \tilde{\psi}_j^- = (-i\lambda^-, \psi_{H_1}^2) \quad (2.9)$$

one finds the following mass term [29, 30]

$$\mathcal{L}_{m_{\tilde{\chi}^\pm}} = -\frac{1}{2}(\tilde{\psi}_j^+, \tilde{\psi}_j^-) \begin{pmatrix} 0 & X^T \\ X & 0 \end{pmatrix} \begin{pmatrix} \tilde{\psi}_j^+ \\ \tilde{\psi}_j^- \end{pmatrix} \quad (2.10)$$

with

$$X = \begin{pmatrix} M & \sqrt{2} m_W \sin \beta \\ \sqrt{2} m_W \cos \beta & \mu \end{pmatrix}. \quad (2.11)$$

The mass matrix X can be diagonalized by two real, unitary matrices U and V

$$M_D = U^* X V^{-1}. \quad (2.12)$$

The mass eigenstates are defined through:

$$\tilde{\chi}_i^+ = V_{ij} \tilde{\psi}_j^+, \quad \tilde{\chi}_i^- = U_{ij} \tilde{\psi}_j^- \quad i, j = 1, 2. \quad (2.13)$$

For the eigenvalues $m_{\tilde{\chi}_{1,2}^\pm}$ and the matrix elements U_{ij} and V_{ij} one gets [29] for $\tan \beta > 1$:

$$m_{\tilde{\chi}_{1,2}^\pm} = \frac{1}{2} \left(\sqrt{(M - \mu)^2 + 2m_W^2(1 + \sin 2\beta)} \mp \sqrt{(M + \mu)^2 + 2m_W^2(1 - \sin 2\beta)} \right) \quad (2.14)$$

$$U_{22} = -U_{11} = \frac{\epsilon_U}{\sqrt{2}} \sqrt{1 - \frac{M^2 - \mu^2 - 2m_W^2 \cos 2\beta}{W}} \quad (2.15)$$

$$U_{12} = U_{21} = \frac{1}{\sqrt{2}} \sqrt{1 + \frac{M^2 - \mu^2 - 2m_W^2 \cos 2\beta}{W}} \quad (2.16)$$

$$V_{11} = V_{22} = \frac{1}{\sqrt{2}} \sqrt{1 - \frac{M^2 - \mu^2 + 2m_W^2 \cos 2\beta}{W}} \quad (2.17)$$

$$V_{21} = -V_{12} = \frac{\epsilon_V}{\sqrt{2}} \sqrt{1 + \frac{M^2 - \mu^2 + 2m_W^2 \cos 2\beta}{W}} \quad (2.18)$$

with

$$W = \sqrt{(M^2 + \mu^2 + 2m_W^2)^2 - 4(M\mu - m_W^2 \sin 2\beta)^2} \quad (2.19)$$

$$\epsilon_U = \text{sign}(M \cos \beta + \mu \sin \beta) \quad \text{and} \quad \epsilon_V = \text{sign}(M \sin \beta + \mu \cos \beta). \quad (2.20)$$

For $\tan \beta < 1$ one has to replace U_{ij} by $\epsilon_U U_{ij}$ and V_{ij} by $\epsilon_V V_{ij}$. In the chosen phase convention the mass eigenvalue of the heavier chargino is always positive. For $M\mu - m_W^2 \sin 2\beta < 0$ (> 0) the lighter mass eigenvalue is positive (negative). The following asymptotic behavior can be deduced from Eqs. (2.14)–(2.18): for $M \gg |\mu|$ the lighter chargino is mainly a higgsino whereas the heavier chargino is mainly gaugino-like. For $|\mu| \gg M$ the charginos interchange their nature.

2.3.2 Neutralinos

Analogous to the chargino case a mixture takes place between neutral gauginos and neutral higgsinos [30, 31]. The mass eigenstates are called neutralinos $\tilde{\chi}_j^0$ ($j = 1, \dots, 4$). In the basis

$$\psi_j^0 = (-i\lambda_\gamma, -i\lambda_Z, \psi_{H_1}^1 \cos \beta - \psi_{H_2}^2 \sin \beta, \psi_{H_1}^1 \sin \beta + \psi_{H_2}^2 \cos \beta) \quad (2.21)$$

the mass matrix has the form [31]:

$$Y = \begin{pmatrix} M' \cos^2 \theta_W + M \sin^2 \theta_W & (M - M') \sin \theta_W \cos \theta_W & 0 & 0 \\ (M - M') \sin \theta_W \cos \theta_W & M' \sin^2 \theta_W + M \cos^2 \theta_W & m_Z & 0 \\ 0 & m_Z & \mu \sin 2\beta & -\mu \cos 2\beta \\ 0 & 0 & -\mu \cos 2\beta & -\mu \sin 2\beta \end{pmatrix} \quad (2.22)$$

This matrix can be diagonalized by a 4×4 unitary matrix N . The neutralino mass eigenstates are given by:

$$\tilde{\chi}_i^0 = N_{ij} \tilde{\psi}_j^0 \quad i, j = 1, \dots, 4. \quad (2.23)$$

Here $\tilde{\psi}^0 = (\psi_j^0, \bar{\psi}_j^0)$ denotes a four component spinor whereas the ψ_j^0 are two component Weyl spinors. The ordering of the neutralino mass eigenstates is given by $|m_{\tilde{\chi}_1^0}| < |m_{\tilde{\chi}_2^0}| < |m_{\tilde{\chi}_3^0}| < |m_{\tilde{\chi}_4^0}|$. Under the assumption that the neutral gaugino–higgsino mixing contains no source of CP violation, the matrix N is real. The mass eigenvalues can be either positive or negative. This sign is related to the CP eigenvalue of the corresponding neutralino [32]. In the following, the GUT relation

$$M' = 5/3 \tan^2 \theta_W M \quad (2.24)$$

is assumed for the $U(1)$ gaugino mass M' and the $SU(2)$ gaugino mass M . For $M \gg |\mu|$ the lighter two neutralinos are mainly higgsinos and the heavier two are mainly gauginos (where the heaviest is mainly the zino and the second heaviest mainly the photino). For $|\mu| \gg M$ the lightest neutralino is mainly the photino, the second one is mainly the zino and the two heaviest states are mainly higgsinos.

2.3.3 The Gluino

For the gluino there is the following mass term

$$\mathcal{L}_{m_{\tilde{g}}} = \frac{1}{2} m_{\tilde{g}} \tilde{g} \tilde{g}. \quad (2.25)$$

In the framework of a GUT the gluino mass $m_{\tilde{g}}$ is related to the $SU(2)$ gaugino mass M through

$$M = m_{\tilde{g}} \alpha / (\alpha_s \sin^2 \theta_W). \quad (2.26)$$

where α and α_s are the electroweak and strong coupling respectively. It has been shown that QCD corrections to this relation can be important [33].

2.4 Leptons and Quarks

The leptons and quarks have similar mass terms as in the SM:

$$\mathcal{L}_f = -v_1 \bar{E}_{La} h_{ab}^e E_{Rb} - v_1 \bar{D}_{La} h_{ab}^d D_{Rb} - v_2 \bar{U}_{La} h_{ab}^d U_{Rb} - h.c.. \quad (2.27)$$

With the help of the unitary 3×3 matrices V_{jk}^l one gets the mass eigen states:

$$E_{La,Ra}^{phys} = V_{e,ab}^{L,R} E_{La,Ra}, \quad D_{La,Ra}^{phys} = V_{d,ab}^{L,R} D_{La,Ra}, \quad U_{La,Ra}^{phys} = V_{u,ab}^{L,R} U_{La,Ra} \quad (2.28)$$

with $E^{phys} = (e, \mu, \tau)$, $D^{phys} = (d, s, b)$ and $U^{phys} = (u, c, t)$. For the masses one finds

$$\begin{aligned} \text{diag}(m_e, m_\mu, m_\tau) &= v_1 V_e^L h^e V_e^{R\dagger}, & \text{diag}(m_d, m_s, m_b) &= v_1 V_d^L h^d V_d^{R\dagger}, \\ \text{diag}(m_u, m_c, m_t) &= v_2 V_u^L h^u V_u^{R\dagger}. \end{aligned} \quad (2.29)$$

Note, that there are no interactions between neutral gauge bosons and fermions of different generations (GIM-mechanism [34]). However, there are interactions between the W^\pm and quarks of different generations. The strength of these interactions is related to the so-called Cabbibo–Kobayashi–Maskawa (CKM) matrix K_{CKM} [35, 36] which is given by $K_{CKM} \equiv (V_u^L)^\dagger V_d^L$. The analogous matrix in the lepton sector does not exist because there are no right-handed neutrinos in the MSSM.

Note, that the masses of the u-quarks are proportional to v_2 whereas the masses of the d-quarks and the leptons are proportional to v_1 . Therefore, we have $h^t = h^b$ if $\tan \beta = m_t/m_b$. In such a case the τ Yukawa coupling is also of the order of the top Yukawa coupling. This has important consequences for the phenomenology of the supersymmetric partners of the τ lepton and the b quark in high $\tan \beta$ scenarios as will be shown in Chapters 4, 9 and 7.

2.5 Sfermions

As already mentioned every SM fermion has two spin 0 partners denoted by \tilde{f}_L and \tilde{f}_R , one for each helicity state. The obvious exception are the neutrinos which are only left-handed states in our model. In the following the scalar partners for the fermions (quarks, leptons) will be called sfermions (squarks, sleptons). A similar notation will be used for the scalar partners of a specific fermion, e.g. the scalar partners of the top-quarks will be called stops. For the sfermions one gets the following mass terms:

$$\mathcal{L}_{\tilde{f}} = -(\tilde{f}_L^*, \tilde{f}_R^*) \begin{pmatrix} \mathcal{M}_{\mathcal{L}\mathcal{L}}^2 & \mathcal{M}_{\mathcal{L}\mathcal{R}}^2 \\ \mathcal{M}_{\mathcal{R}\mathcal{L}}^2 & \mathcal{M}_{\mathcal{R}\mathcal{R}}^2 \end{pmatrix} \begin{pmatrix} \tilde{f}_L \\ \tilde{f}_R \end{pmatrix} \quad (2.30)$$

with

$$\begin{aligned} \mathcal{M}_{\mathcal{L}\mathcal{L}}^2 &= M_F^2 + v_i^2 (h^f)^\dagger h^f + (T_I^3 - e_f \sin^2 \theta_W) \cos 2\beta m_Z^2 \mathbf{1}_3 \\ \mathcal{M}_{\mathcal{L}\mathcal{R}}^2 &= \mathcal{M}_{\mathcal{R}\mathcal{L}}^{2\dagger} = v_i (A_f g^f - \mu h^f) \\ \mathcal{M}_{\mathcal{R}\mathcal{R}}^2 &= M_{F'}^2 + v_i^2 (h^f)^\dagger h^f + e_f \sin^2 \theta_W \cos 2\beta m_Z^2 \mathbf{1}_3. \end{aligned} \quad (2.31)$$

Here F denotes Q in case of squarks and L in case of sleptons, F' denotes E, D, U , and f denotes e, d, u . T_I^3 is the third component of the weak isospin and e_q is the electric charge of the corresponding fermion. In case of up-type squarks v_i is v_2 whereas in case of down-type squarks and charged sleptons $v_i = v_1$. A_f is a scalar quantity whereas $M_{F,F'}^2$ and g^f are 3×3 matrices. In principal the entries of these matrices are free quantities, but especially for the first two generations they are very constrained in order to avoid oversized Flavour Changing Neutral Currents (FCNCs) [37, 38]. Therefore, we will assume that M_F^2 and $M_{F'}^2$ are diagonal and that $g^f = h^f$. In this case one can perform a rotation in the sfermion sector analogous to the fermion sector to decouple the generations. The only exception will be the mixing between the stops and the scalar left charm. This will be discussed in section 3.5.

With the above assumptions the masses of the sneutrinos are given by

$$m_{\tilde{\nu}}^2 = M_L^2 + \frac{1}{2} \cos 2\beta m_Z^2. \quad (2.32)$$

For the other sfermions one gets 2×2 mass matrices of the following form [39]:

$$M_f^2 = \begin{pmatrix} M_F^2 + (T_I^3 - e_f \sin^2 \theta_W) \cos 2\beta m_Z^2 + m_f^2 & m_f (A_f - \mu \Theta(\beta)) \\ m_f (A_f - \mu \Theta(\beta)) & M_{F'}^2 + e_f \sin^2 \theta_W \cos 2\beta m_Z^2 + m_f^2 \end{pmatrix} \quad (2.33)$$

with

$$\Theta(\beta) = \begin{cases} \cot \beta & \text{for } T_I^3 = \frac{1}{2} \\ \tan \beta & \text{for } T_I^3 = -\frac{1}{2} \end{cases}$$

The mass eigenvalues are given by:

$$m_{\tilde{f}_{1,2}}^2 = \frac{1}{2}(M_{\tilde{f}_{LL}}^2 + M_{\tilde{f}_{RR}}^2) \mp \frac{1}{2}\sqrt{(M_{\tilde{f}_{LL}}^2 - M_{\tilde{f}_{RR}}^2)^2 + 4M_{\tilde{f}_{LR}}^2} \quad (2.34)$$

with the eigenstates

$$\begin{pmatrix} \tilde{f}_1 \\ \tilde{f}_2 \end{pmatrix} = \begin{pmatrix} \cos \theta_{\tilde{f}} & \sin \theta_{\tilde{f}} \\ -\sin \theta_{\tilde{f}} & \cos \theta_{\tilde{f}} \end{pmatrix} \begin{pmatrix} \tilde{f}_L \\ \tilde{f}_R \end{pmatrix} \quad (2.35)$$

$$\cos \theta_{\tilde{f}} = \frac{-m_f (A_f - \mu \Theta(\beta))}{\sqrt{(M_{\tilde{f}_{LL}}^2 - m_{\tilde{f}_1}^2)^2 + M_{\tilde{f}_{LR}}^4}} \quad (2.36)$$

$$\sin \theta_{\tilde{f}} = \frac{M_{\tilde{f}_{LL}}^2 - m_{\tilde{f}_1}^2}{\sqrt{(M_{\tilde{f}_{LL}}^2 - m_{\tilde{f}_1}^2)^2 + M_{\tilde{f}_{LR}}^4}}. \quad (2.37)$$

$\cos \theta_{\tilde{f}}$ is proportional to the fermion mass as can be read of Eq. (2.36). Therefore, one can safely neglect the mixing for the first two generations but not for the third generation. Especially for the stops one expects a strong mixing and mass splitting between the heavier and the lighter state due to the large top mass. For large $\tan \beta$ (≥ 10) the product $\mu \tan \beta$ can be large leading to a strong mixing and large mass splitting in the sbottom and in the stau sector too. Note, that in this convention $\sin \theta_{\tilde{f}}$ is always positive because

$$M_{\tilde{f}_{LL}}^2 - m_{\tilde{f}_1}^2 = \frac{1}{2}(M_{\tilde{f}_{LL}}^2 - M_{\tilde{f}_{RR}}^2) + \frac{1}{2}\sqrt{(M_{\tilde{f}_{LL}}^2 - M_{\tilde{f}_{RR}}^2)^2 + 4M_{\tilde{f}_{LR}}^2}. \quad (2.38)$$

A more detailed discussion on sfermion masses and mixing angles will be given in Chapter 6.

2.6 Experimental bounds

LEP1 has obtained a model independent experimental mass-bound on charged supersymmetric particles which is $\tilde{m} \gtrsim 45$ GeV [4, 40]. Stronger limits have been reported during the last two years from the various LEP runs at higher energy [41, 42, 43, 44, 45]. In the first half year LEP was running at $\sqrt{s} = 170 - 172$ GeV. There the following limits have been obtained [46, 47]: $m_{\tilde{t}_1} \gtrsim 73.3$ GeV, $m_{\tilde{b}_1} \gtrsim 73$ GeV, $\tilde{\mu}_R \gtrsim 59$ GeV, $\tilde{e}_R \gtrsim 58$ GeV, $\tilde{\tau}_R \gtrsim 53$ GeV, $m_{h^0} \gtrsim 69.5$ GeV, $m_{A^0} \gtrsim 62.5$ GeV, $m_{H^+} \gtrsim 51.5$ GeV, $m_{\tilde{\chi}_1^+} \gtrsim 84.5(67.6)$ GeV if $m_{\tilde{\nu}_\tau} = 1(\sim 0.1)$ TeV. Note, that these bounds depend on various assumptions. The D0 experiment at FNAL obtained additional mass limits for the stop [47, 48] excluding the mass range $40 \text{ GeV} \lesssim m_{\tilde{t}_1} \lesssim 100$ GeV if the mass difference $(m_{\tilde{t}_1} - m_{\tilde{\chi}_1^0}) \gtrsim 30$ GeV. The bound on the gluino mass is $m_{\tilde{g}} \gtrsim 175$ GeV [49].

Chapter 3

Decay Widths

3.1 General Remarks

As already mentioned, in the MSSM exists a conserved quantum number called R-parity leading to the existence of a lightest stable supersymmetric particle (LSP). We will assume that the lightest neutralino is the LSP for cosmological reasons (see e.g. [50] and references therein).

In general, sfermions decay according to $\tilde{f}_k \rightarrow \tilde{\chi}_i^0 + f$ and $\tilde{f}_k \rightarrow \tilde{\chi}_j^\pm + f'$. Normally, the flavour conserving decay into the lightest neutralino is always possible except in case of the light stop because of the large t -quark mass. Nevertheless, the decay of a light stop into the lighter chargino and a b -quark can still be accessible in this case. As we will show later there is a wide range of SUSY parameters where all two body decays of the light stop are forbidden at tree level. Therefore, the flavour changing decay into a c -quark and the LSP becomes important [51]. Moreover, three body decays of the light stop can be competitive: $\tilde{t}_1 \rightarrow b + W^+ + \tilde{\chi}_1^0$, $b + H^+ + \tilde{\chi}_1^0$, $b + \tilde{f}_{1,2} + \nu_f$, $b + f^+ + \tilde{\nu}_f$ where f denotes e, μ, τ .

In the next section we collect the relevant terms of the interaction Lagrangian which are needed for the computation of the decay widths. After this we will list the formulae for the two body decays of the sfermions. In the subsequent section we present the matrix elements, the Feynman diagrams and the formulae for the above mentioned three body decays of the light stop. For completeness we also present the formulae for the decay $\tilde{t}_1 \rightarrow c + \tilde{\chi}_1^0$ in our notation.

3.2 The relevant parts of the Lagrangian

The part of the Lagrangian, which is needed for the calculation of the subsequent decay widths, is given by:

$$\begin{aligned}
\mathcal{L}_I = & g \sum_{\substack{f=\nu_\tau, t \\ f'=\tau, b}} \left[\bar{f} \left(k_{ij}^{\tilde{f}'} P_L + l_{ij}^{\tilde{f}'} P_R \right) \tilde{\chi}_j^+ \tilde{f}' + \bar{f}' \left(k_{ij}^{\tilde{f}} P_L + l_{ij}^{\tilde{f}} P_R \right) \tilde{\chi}_j^- \tilde{f} + h.c. \right] \\
& + g \sum_{f=\tau, \nu_\tau, b, t} \left[\bar{f} \left(b_{ki}^f P_L + a_{ki}^f P_R \right) \tilde{\chi}_i^0 \tilde{f}_k + h.c. \right] \\
& - g \left[W_\mu^+ \tilde{\chi}_k^0 \left(O'_{L_{kj}} P_L + O'_{R_{ki}} P_R \right) \gamma^\mu \tilde{\chi}_j^+ + h.c. \right] \\
& - g \left[H^+ \tilde{\chi}_k^0 \left(Q'_{R_{kj}} P_L + Q'_{L_{ki}} P_R \right) \tilde{\chi}_j^+ + h.c. \right] \\
& - \frac{g}{\sqrt{2}} \left[W_\mu^+ \bar{t} \gamma^\mu P_L b + h.c. \right] \\
& - g \left[i W_\mu^+ \left(\sum_{i,j=1,2}^2 A_{\tilde{t}_i \tilde{b}_j}^W \tilde{t}_i \overset{\leftrightarrow}{\partial}_\mu \tilde{b}_j + \sum_{i=1,2}^2 A_{\tilde{\nu}_\tau \tilde{\tau}_i}^W \tilde{\nu}_\tau \overset{\leftrightarrow}{\partial}_\mu \tilde{\tau}_i \right) + h.c. \right] \\
& + \frac{g}{\sqrt{2} m_W} \left[H^+ \bar{t} (m_b \tan \beta P_R + m_t \cot \beta P_L) b + h.c. \right] \\
& - g \left[H^+ \left(\sum_{i,j=1,2}^2 C_{\tilde{t}_i \tilde{b}_j}^H \tilde{t}_i \tilde{b}_j + \sum_{i=1,2}^2 C_{\tilde{\nu}_\tau \tilde{\tau}_i}^H \tilde{\nu}_\tau \tilde{\tau}_i \right) + h.c. \right] \\
& - \frac{i g}{2 \cos \theta_W} Z_\mu \left[\cos \theta_{\tilde{t}} \sin \theta_{\tilde{t}} \left(\tilde{t}_1 \overset{\leftrightarrow}{\partial}_\mu \tilde{t}_2 - \tilde{t}_2 \overset{\leftrightarrow}{\partial}_\mu \tilde{t}_1 \right) \right. \\
& \quad \left. - \sum_{f=\tau, b} \cos \theta_{\tilde{f}} \sin \theta_{\tilde{f}} \left(\tilde{f}_1 \overset{\leftrightarrow}{\partial}_\mu \tilde{f}_2 - \tilde{f}_2 \overset{\leftrightarrow}{\partial}_\mu \tilde{f}_1 \right) \right] \\
& - g h^0 \left(\sum_{f=\tau, b, t} B_{h^0}^{\tilde{f}} \tilde{f}_1 \tilde{f}_2 + h.c. \right) - g H^0 \left(\sum_{f=\tau, b, t} B_{H^0}^{\tilde{f}} \tilde{f}_1 \tilde{f}_2 + h.c. \right) \\
& + i g A^0 \left[\sum_{f=\tau, b, t} B_{A^0}^{\tilde{f}} \left(\tilde{f}_1 \tilde{f}_2 - \tilde{f}_2 \tilde{f}_1 \right) \right] \\
& - \sqrt{2} g_s T_{jk}^a \left[\sum_{q=b, t} \left(\bar{q}_j (\cos \theta_{\tilde{q}} P_R - \sin \theta_{\tilde{q}} P_L) \tilde{g}_a \tilde{q}_1^k \right. \right. \\
& \quad \left. \left. - \bar{q}_j (\sin \theta_{\tilde{q}} P_R + \cos \theta_{\tilde{q}} P_L) \tilde{g}_a \tilde{q}_2^k \right) + h.c. \right]
\end{aligned} \tag{3.1}$$

where $P_{R,L} = (1 \pm \gamma_5)/2$. The T_{jk}^a are the generators of $SU(3)$. In the following we will use the abbreviation $\mathcal{R}^{\tilde{f}}$ for the mixing matrix (Eq. (2.35)):

$$\mathcal{R}^{\tilde{f}} = \begin{pmatrix} \cos \theta_{\tilde{f}} & \sin \theta_{\tilde{f}} \\ -\sin \theta_{\tilde{f}} & \cos \theta_{\tilde{f}} \end{pmatrix}. \tag{3.2}$$

The Yukawa couplings of the sfermions are given by:

$$Y_\tau = \frac{m_\tau}{\sqrt{2} m_W \cos \beta}, \quad Y_b = \frac{m_b}{\sqrt{2} m_W \cos \beta}, \quad Y_t = \frac{m_t}{\sqrt{2} m_W \sin \beta}. \quad (3.3)$$

The \tilde{q}_i - q' - $\tilde{\chi}_j^\pm$ couplings read

$$l_{ij}^{\tilde{q}} = \mathcal{R}_{in}^{\tilde{q}} \mathcal{O}_{jn}^q, \quad k_{ij}^{\tilde{q}} = \mathcal{R}_{i1}^{\tilde{q}} \mathcal{O}_{j2}^{q'} \quad (3.4)$$

with

$$\mathcal{O}_j^t = \begin{pmatrix} -V_{j1} \\ Y_t V_{j2} \end{pmatrix}, \quad \mathcal{O}_j^b = \begin{pmatrix} -U_{j1} \\ Y_b U_{j2} \end{pmatrix}. \quad (3.5)$$

In case of sleptons we have:

$$l_{ij}^{\tilde{\tau}} = \mathcal{R}_{in}^{\tilde{\tau}} \mathcal{O}_{jn}^\tau, \quad k_{ij}^{\tilde{\tau}} = 0, \quad l_j^{\tilde{\nu}} = -V_{j1}, \quad k_j^{\tilde{\nu}} = Y_\tau U_{j2}. \quad (3.6)$$

with

$$\mathcal{O}_j^\tau = \begin{pmatrix} -U_{j1} \\ Y_\tau U_{j2} \end{pmatrix}. \quad (3.7)$$

The \tilde{f}_i - f - $\tilde{\chi}_k^0$ couplings are given by

$$a_{ik}^{\tilde{f}} = \mathcal{R}_{in}^{\tilde{f}} \mathcal{A}_{kn}^f, \quad b_{ik}^{\tilde{f}} = \mathcal{R}_{in}^{\tilde{f}} \mathcal{B}_{kn}^f \quad (3.8)$$

with

$$\mathcal{A}_k^f = \begin{pmatrix} f_{Lk}^f \\ h_{Rk}^f \end{pmatrix}, \quad \mathcal{B}_k^f = \begin{pmatrix} h_{Lk}^f \\ f_{Rk}^f \end{pmatrix}, \quad (3.9)$$

and

$$\begin{aligned} h_{Lk}^t &= Y_t (\sin \beta N_{k3}^* - \cos \beta N_{k4}^*) \\ f_{Lk}^t &= \frac{-2\sqrt{2}}{3} \sin \theta_W N_{k1} - \sqrt{2} \left(\frac{1}{2} - \frac{2}{3} \sin^2 \theta_W \right) \frac{N_{k2}}{\cos \theta_W} \\ h_{Rk}^t &= Y_t (\sin \beta N_{k3} - \cos \beta N_{k4}) \\ f_{Rk}^t &= \frac{-2\sqrt{2}}{3} \sin \theta_W (\tan \theta_W N_{k2}^* - N_{k1}^*) \end{aligned} \quad (3.10)$$

$$\begin{aligned} h_{Lk}^b &= -Y_b (\cos \beta N_{k3}^* + \sin \beta N_{k4}^*) \\ f_{Lk}^b &= \frac{\sqrt{2}}{3} \sin \theta_W N_{k1} + \sqrt{2} \left(\frac{1}{2} - \frac{1}{3} \sin^2 \theta_W \right) \frac{N_{k2}}{\cos \theta_W} \\ h_{Rk}^b &= -Y_b (\cos \beta N_{k3} + \sin \beta N_{k4}) \\ f_{Rk}^b &= \frac{\sqrt{2}}{3} \sin \theta_W (\tan \theta_W N_{k2}^* - N_{k1}^*) \end{aligned} \quad (3.11)$$

$$\begin{aligned} h_{Lk}^\tau &= -Y_\tau (\cos \beta N_{k3}^* + \sin \beta N_{k4}^*) \\ f_{Lk}^\tau &= \sqrt{2} \sin \theta_W N_{k1} + \sqrt{2} \left(\frac{1}{2} - \sin^2 \theta_W \right) \frac{N_{k2}}{\cos \theta_W} \\ h_{Rk}^\tau &= -Y_\tau (\cos \beta N_{k3} + \sin \beta N_{k4}) \\ f_{Rk}^\tau &= \sqrt{2} \sin \theta_W (\tan \theta_W N_{k2}^* - N_{k1}^*) \end{aligned} \quad (3.12)$$

In case of $\tilde{\nu}_\tau$ we get $a_k^{\tilde{\nu}_\tau} = -\frac{N_{k2}}{\sqrt{2} \cos \theta_W}$ and $b_k^{\tilde{\nu}_\tau} = 0$. The couplings $\bar{t}_i\tilde{b}_j-W^+$ read

$$A_{\tilde{t}_i\tilde{b}_j}^W = (A_{\tilde{b}_i\tilde{t}_j}^W)^T = \frac{1}{\sqrt{2}} \begin{pmatrix} \cos \theta_{\tilde{b}} \cos \theta_{\tilde{t}} & -\sin \theta_{\tilde{b}} \cos \theta_{\tilde{t}} \\ -\cos \theta_{\tilde{b}} \sin \theta_{\tilde{t}} & \sin \theta_{\tilde{b}} \sin \theta_{\tilde{t}} \end{pmatrix} \quad (3.13)$$

The couplings $\tilde{\tau}_i\tilde{\nu}_\tau-W^+$ are given by

$$A_{\tilde{\tau}_1\tilde{\nu}_\tau}^W = \frac{\cos \theta_{\tilde{\tau}}}{\sqrt{2}}, \quad A_{\tilde{\tau}_2\tilde{\nu}_\tau}^W = -\frac{\sin \theta_{\tilde{\tau}}}{\sqrt{2}}. \quad (3.14)$$

The couplings between light sfermion, heavy sfermion and neutral Higgs read:

$$\begin{aligned} B_{h^0}^{\tilde{f}} &= -\frac{m_Z \sin 2\theta_{\tilde{f}}}{2 \cos \theta_W} \left(\frac{1}{2} + 2e_f \sin^2 \theta_W \right) \sin(\alpha + \beta) - \frac{m_f \cos 2\theta_{\tilde{f}}}{2 m_W \cos \beta} (\mu \cos \alpha + A_f \sin \alpha) \\ B_{H^0}^{\tilde{f}} &= \frac{m_Z \sin 2\theta_{\tilde{f}}}{2 \cos \theta_W} \left(\frac{1}{2} + 2e_f \sin^2 \theta_W \right) \cos(\alpha + \beta) - \frac{m_f \cos 2\theta_{\tilde{f}}}{2 m_W \cos \beta} (\mu \sin \alpha - A_f \cos \alpha) \\ B_{A^0}^{\tilde{f}} &= -\frac{m_f}{2 m_W} (A_f \tan \beta + \mu) \end{aligned} \quad (3.15)$$

if $f = b, \tau$ and in case of $f = t$ we get

$$\begin{aligned} B_{h^0}^{\tilde{t}} &= -\frac{m_Z \sin 2\theta_{\tilde{t}}}{2 \cos \theta_W} \left(\frac{4}{3} \sin^2 \theta_W - \frac{1}{2} \right) \sin(\alpha + \beta) + \frac{m_t \cos 2\theta_{\tilde{t}}}{2 m_W \sin \beta} (\mu \sin \alpha + A_t \cos \alpha) \\ B_{H^0}^{\tilde{t}} &= \frac{m_Z \sin 2\theta_{\tilde{t}}}{2 \cos \theta_W} \left(\frac{4}{3} \sin^2 \theta_W - \frac{1}{2} \right) \cos(\alpha + \beta) - \frac{m_t \cos 2\theta_{\tilde{t}}}{2 m_W \sin \beta} (\mu \cos \alpha - A_t \sin \alpha) \\ B_{A^0}^{\tilde{t}} &= -\frac{m_t}{2 m_W} (A_t \cot \beta + \mu) \end{aligned} \quad (3.16)$$

The couplings $\bar{t}_i\tilde{b}_j-H^+$ are given by

$$\begin{aligned} C_{\tilde{t}_i\tilde{b}_j}^H &= (C_{\tilde{b}_i\tilde{t}_j}^H)^T \\ &= \frac{1}{\sqrt{2} m_W} \mathcal{R}^{\tilde{t}} \begin{pmatrix} m_b^2 \tan \beta + m_t^2 \cot \beta - m_W^2 \sin 2\beta & m_b(A_b \tan \beta + \mu) \\ m_t(A_t \cot \beta + \mu) & 2m_b m_t / \sin 2\beta \end{pmatrix} (\mathcal{R}^{\tilde{b}})^\dagger \end{aligned} \quad (3.17)$$

and the couplings $\tilde{\tau}_i\tilde{\nu}_\tau-H^+$ are given by

$$C_{\tilde{\tau}_i\tilde{\nu}_\tau}^H = \frac{1}{\sqrt{2} m_W} \mathcal{R}^{\tilde{\tau}} \begin{pmatrix} m_\tau^2 \tan \beta - m_W^2 \sin 2\beta \\ m_\tau(A_\tau \tan \beta + \mu) \end{pmatrix} \quad (3.18)$$

The $W^+-\tilde{\chi}_j^--\tilde{\chi}_k^0$ couplings read:

$$O'_{L_{kj}} = \frac{V_{j2}}{\sqrt{2}} (\sin \beta N_{k3} - \cos \beta N_{k4}) + V_{j1} (\sin \theta_W N_{k1} + \cos \theta_W N_{k2}) \quad (3.19)$$

$$O'_{R_{kj}} = \frac{U_{j2}}{\sqrt{2}} (\cos \beta N_{k3} + \sin \beta N_{k4}) + U_{j1} (\sin \theta_W N_{k1} + \cos \theta_W N_{k2}) \quad (3.20)$$

The $H^+-\tilde{\chi}_j^--\tilde{\chi}_k^0$ couplings are given by:

$$Q'_{L_{kj}} = \cos \beta \left[V_{j1} (\cos \beta N_{k4} - \sin \beta N_{k3}) + \frac{V_{j2}}{\sqrt{2}} (2 \sin \theta_W N_{k1} + (\cos \theta_W - \sin \theta_W \tan \theta_W) N_{k2}) \right] \quad (3.21)$$

$$Q'_{R_{kj}} = \sin \beta \left[U_{j1} (\cos \beta N_{k3} + \sin \beta N_{k4}) - \frac{U_{j2}}{\sqrt{2}} (2 \sin \theta_W N_{k1} + (\cos \theta_W - \sin \theta_W \tan \theta_W) N_{k2}) \right] \quad (3.22)$$

3.3 Two body decays

The decay widths for the electroweak two body decays of the sfermions \tilde{f}_i are given by (\tilde{f}_i denotes $\tilde{t}_{1,2}$, $\tilde{b}_{1,2}$, $\tilde{\tau}_{1,2}$ or $\tilde{\nu}_\tau$):

$$\Gamma(\tilde{f}_i \rightarrow f + \tilde{\chi}_k^0) = \frac{g^2 \lambda^{\frac{1}{2}}(m_{\tilde{f}_i}^2, m_f^2, m_{\tilde{\chi}_k^0}^2)}{16\pi m_{\tilde{f}_i}^3} * \left[(a_{ik}^{\tilde{f}})^2 + (b_{ik}^{\tilde{f}})^2 (m_{\tilde{f}_i}^2 - m_f^2 - m_{\tilde{\chi}_k^0}^2) - 4a_{ik}^{\tilde{f}} b_{ik}^{\tilde{f}} m_f m_{\tilde{\chi}_k^0} \right] \quad (3.23)$$

$$\Gamma(\tilde{f}_i \rightarrow f' + \tilde{\chi}_k^\pm) = \frac{g^2 \lambda^{\frac{1}{2}}(m_{\tilde{f}_i}^2, m_{f'}^2, m_{\tilde{\chi}_k^\pm}^2)}{16\pi m_{\tilde{f}_i}^3} * \left[(k_{ik}^{\tilde{f}})^2 + (l_{ik}^{\tilde{f}})^2 (m_{\tilde{f}_i}^2 - m_{f'}^2 - m_{\tilde{\chi}_k^\pm}^2) - 4k_{ik}^{\tilde{f}} l_{ik}^{\tilde{f}} m_{f'} m_{\tilde{\chi}_k^\pm} \right] \quad (3.24)$$

$$\Gamma(\tilde{f}_i \rightarrow W^\pm + \tilde{f}_j) = \frac{g^2 (A_{\tilde{f}_i \tilde{f}_j}^W)^2 \lambda^{\frac{3}{2}}(m_{\tilde{f}_i}^2, m_W^2, m_{\tilde{f}_j}^2)}{16\pi m_W^2 m_{\tilde{f}_i}^3} \quad (3.25)$$

$$\Gamma(\tilde{f}_i \rightarrow H^\pm + \tilde{f}_j) = \frac{g^2 (C_{\tilde{f}_i \tilde{f}_j}^H)^2 \lambda^{\frac{1}{2}}(m_{\tilde{f}_i}^2, m_H^2, m_{\tilde{f}_j}^2)}{16\pi m_{\tilde{f}_i}^3} \quad (3.26)$$

$$\Gamma(\tilde{f}_2 \rightarrow Z + \tilde{f}_1) = \frac{g^2 \sin^2 2\theta_{\tilde{f}} \lambda^{\frac{3}{2}}(m_{\tilde{f}_2}^2, m_Z^2, m_{\tilde{f}_1}^2)}{256\pi m_W^2 m_{\tilde{f}_2}^3} \quad (3.27)$$

$$\Gamma(\tilde{f}_2 \rightarrow H + \tilde{f}_1) = \frac{g^2 (B_{\tilde{f}_i}^{\tilde{f}})^2 \lambda^{\frac{1}{2}}(m_{\tilde{f}_2}^2, m_H^2, m_{\tilde{f}_1}^2)}{16\pi m_{\tilde{f}_2}^3} \quad (3.28)$$

with $\lambda(x, y, z) = x^2 + y^2 + z^2 - 2xy - 2xz - 2yz$. In Eq. (3.28) H denotes h^0 , H^0 or A^0 . Squarks can also decay into a gluino and a quark:

$$\Gamma(\tilde{q}_1 \rightarrow \tilde{g} + q) = \frac{2\alpha_s \lambda^{\frac{1}{2}}(m_{\tilde{q}_1}^2, m_{\tilde{g}}^2, m_q^2)}{3 m_{\tilde{q}_1}^3} \left(m_{\tilde{q}_1}^2 - m_{\tilde{g}}^2 - m_q^2 + 2 \sin 2\theta_{\tilde{q}} m_{\tilde{g}} m_q \right) \quad (3.29)$$

$$\Gamma(\tilde{q}_2 \rightarrow \tilde{g} + q) = \frac{2\alpha_s \lambda^{\frac{1}{2}}(m_{\tilde{q}_2}^2, m_{\tilde{g}}^2, m_q^2)}{3 m_{\tilde{q}_2}^3} \left(m_{\tilde{q}_2}^2 - m_{\tilde{g}}^2 - m_q^2 - 2 \sin 2\theta_{\tilde{q}} m_{\tilde{g}} m_q \right) \quad (3.30)$$

3.4 Three Body Decays of the Light Stop

3.4.1 The Decay of the Light Stop into a W-Boson, a Bottom Quark and the Lightest Neutralino

In Fig. 3.1 we show the Feynman diagrams for the decay $\tilde{t}_1 \rightarrow W^+ + b + \tilde{\chi}_1^0$. The matrix element for this decay is given by:

$$\begin{aligned} T_{fi} = & -\frac{g^2}{\sqrt{2}} \sum_{i=1}^2 A_{\tilde{t}_1 \tilde{b}_i}^W \frac{(p_{\tilde{t}} + p_{\tilde{b}_i})^\mu}{p_{\tilde{b}_i}^2 - m_{\tilde{b}_i}^2 - i m_{\tilde{b}_i} \Gamma_{\tilde{b}_i}} \bar{u}(p_b) \left[b_{i1}^{\tilde{b}} P_L + a_{i1}^{\tilde{b}} P_R \right] v(p_{\tilde{\chi}_1^0}) \epsilon_\mu(p_W) \\ & + g^2 \sum_{i=1}^2 \bar{u}(p_b) \left[l_{1i}^{\tilde{t}} P_R + k_{1i}^{\tilde{t}} P_L \right] \frac{\not{p}_{\tilde{\chi}_i^\pm} - m_{\tilde{\chi}_i^\pm}}{p_{\tilde{\chi}_i^\pm}^2 - m_{\tilde{\chi}_i^\pm}^2 - i m_{\tilde{\chi}_i^\pm} \Gamma_{\tilde{\chi}_i^\pm}} \\ & \quad * \left[O'_{L1i} P_L + O'_{R1i} P_R \right] \gamma^\mu v(p_{\tilde{\chi}_1^0}) \epsilon_\mu(p_W) \\ & - \frac{g^2}{\sqrt{2}} \bar{u}(p_b) \gamma^\mu P_L \frac{\not{p}_t + m_t}{p_t^2 - m_t^2 - i m_t \Gamma_t} \left[b_{11}^{\tilde{t}} P_L + a_{11}^{\tilde{t}} P_R \right] v(p_{\tilde{\chi}_1^0}) \epsilon_\mu(p_W) \end{aligned} \quad (3.31)$$

The decay width is given by

$$\begin{aligned} \Gamma(\tilde{t}_1 \rightarrow W^+ + b + \tilde{\chi}_1^0) = & \\ = & \frac{\alpha^2}{16 \pi m_{\tilde{t}_1}^3 \sin^4 \theta_W} \int_{(m_b + m_{\tilde{\chi}_1^0})^2}^{(m_{\tilde{t}_1} - m_W)^2} ds \left(F_{\tilde{\chi}^+ \tilde{\chi}^+} + F_{\tilde{\chi}^+ t} + F_{\tilde{\chi}^+ \tilde{b}} + F_{tt} + F_{t\tilde{b}} + F_{\tilde{b}\tilde{b}} \right). \end{aligned} \quad (3.32)$$

The explicit expressions for the F_{ij} is given are Appendix A.

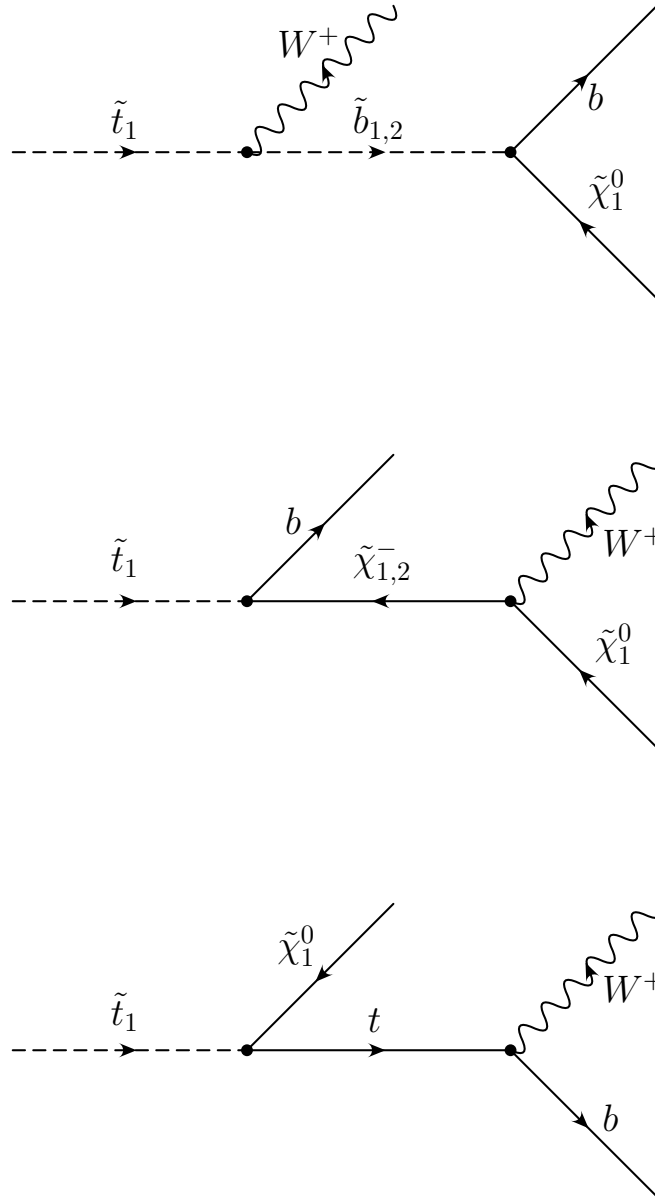


Fig. 3.1: Feynman diagrams for the decay $\tilde{t}_1 \rightarrow W^+ + b + \tilde{\chi}_1^0$. The arrow of a fermionic line defines a fermion flow and is not necessarily identical with the momentum flow used in our calculations.

3.4.2 The Decay of the Light Stop into a charged Higgs Boson, a Bottom Quark and the Lightest Neutralino

In Fig. 3.2 we show the Feynman diagrams for the decay $\tilde{t}_1 \rightarrow H^+ + b + \tilde{\chi}_1^0$. The matrix element for this decay is given by:

$$\begin{aligned}
T_{fi} = & -g^2 \sum_{i=1}^2 C_{\tilde{t}_1 \tilde{b}_i}^H \frac{\bar{u}(p_b) [b_{i1}^{\tilde{b}} P_L + a_{i1}^{\tilde{b}} P_R] v(p_{\tilde{\chi}_1^0})}{p_{\tilde{b}_i}^2 - m_{\tilde{b}_i}^2 - im_{\tilde{b}_i} \Gamma_{\tilde{b}_i}} \\
& - g^2 \sum_{i=1}^2 \frac{\bar{u}(p_b) [l_{1i}^{\tilde{t}} P_R + k_{1i}^{\tilde{t}} P_L] [\not{p}_{\tilde{\chi}_i^\pm} - m_{\tilde{\chi}_i^\pm}] [Q'_{L1i} P_L + Q'_{R1i} P_R] v(p_{\tilde{\chi}_1^0})}{p_{\tilde{\chi}_i^\pm}^2 - m_{\tilde{\chi}_i^\pm}^2 - im_{\tilde{\chi}_i^\pm} \Gamma_{\tilde{\chi}_i^\pm}} \\
& + \frac{g^2}{\sqrt{2} m_W} \frac{\bar{u}(p_b) [m_b \tan \beta P_L + m_t \cot \beta P_R] [\not{p}_t + m_t] [b_{11}^{\tilde{t}} P_L + a_{11}^{\tilde{t}} P_R] v(p_{\tilde{\chi}_1^0})}{p_t^2 - m_t^2 - im_t \Gamma_t}
\end{aligned} \tag{3.33}$$

The decay width is given by

$$\begin{aligned}
\Gamma(\tilde{t}_1 \rightarrow H^+ + b + \tilde{\chi}_1^0) &= \\
&= \frac{\alpha^2}{16 \pi m_{\tilde{t}_1}^3 \sin^4 \theta_W} \int_{(m_b + m_{\tilde{\chi}_1^0})^2}^{(m_{\tilde{t}_1} - m_{H^\pm})^2} ds \left(G_{\tilde{\chi}^+ \tilde{\chi}^+} + G_{\tilde{\chi}^+ t} + G_{\tilde{\chi}^+ \tilde{b}} + G_{tt} + G_{t\tilde{b}} + G_{\tilde{b}\tilde{b}} \right)
\end{aligned} \tag{3.34}$$

The explicit expressions for the G_{ij} are given in Appendix A.

3.4.3 The Decay of the Light Stop into a Bottom Quark, a Slepton and a Lepton

Here we have the following possibilities:

- $\tilde{t}_1 \rightarrow b + \tilde{\nu}_e + e^+, b + \tilde{\nu}_\mu + \mu^+$
- $\tilde{t}_1 \rightarrow b + \tilde{e}_L^+ + \nu_e, b + \tilde{\mu}_L^+ + \nu_\mu$
- $\tilde{t}_1 \rightarrow b + \tilde{\nu}_\tau + \tau^+$
- $\tilde{t}_1 \rightarrow b + \tilde{\tau}_{1,2}^+ + \nu_\tau$

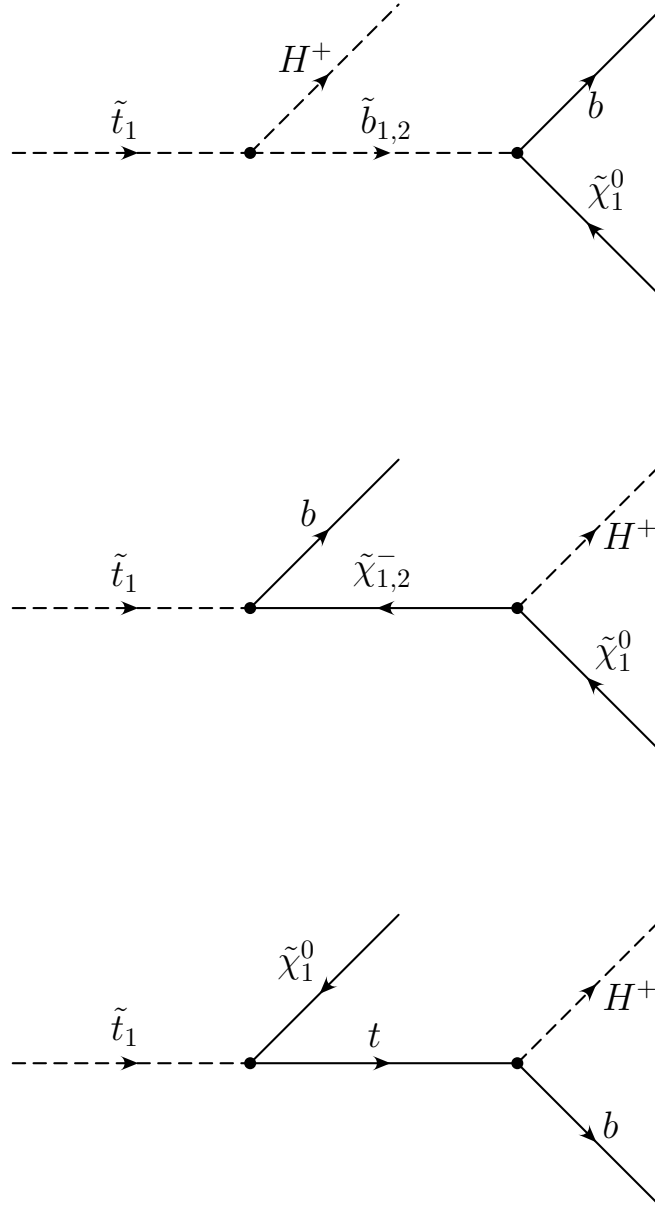


Fig. 3.2: Feynman diagrams for the decay $\tilde{t}_1 \rightarrow H^+ + b + \tilde{\chi}_1^0$. The arrow of a fermionic line defines a fermion flow and is not necessarily identical with the momentum flow used in our calculations.

Note, that the decays into \tilde{e}_R and $\tilde{\mu}_R$ are negligible because the couplings to the charginos are proportional to m_e/m_W and μ/m_W respectively. In the case of decays into sneutrinos and leptons the matrix elements have the generic form:

$$T_{fi} = g^2 \sum_{i=1}^2 \frac{\bar{u}(p_b) \left[l_{1i}^{\tilde{t}} P_R + k_{1i}^{\tilde{t}} P_L \right] \left[\not{p}_{\tilde{\chi}_i^\pm} - m_{\tilde{\chi}_i^\pm} \right] \left[l_{ki}^{\tilde{f}} P_R + k_{ki}^{\tilde{f}} P_L \right] v(p_{f'})}{p_{\tilde{\chi}_i^\pm}^2 - m_{\tilde{\chi}_i^\pm}^2 - im_{\tilde{\chi}_i^\pm} \Gamma_{\tilde{\chi}_i^\pm}}, \quad (3.35)$$

whereas for the decays into sleptons and neutrinos we get:

$$T_{fi} = g^2 \sum_{i=1}^2 \frac{\bar{u}(p_b) \left[l_{1i}^{\tilde{t}} P_R + k_{1i}^{\tilde{t}} P_L \right] \left[\not{p}_{\tilde{\chi}_i^\pm} - m_{\tilde{\chi}_i^\pm} \right] \left[l_{ki}^{\tilde{f}} P_L \right] v(p_{f'})}{p_{\tilde{\chi}_i^\pm}^2 - m_{\tilde{\chi}_i^\pm}^2 - im_{\tilde{\chi}_i^\pm} \Gamma_{\tilde{\chi}_i^\pm}}, \quad (3.36)$$

In both cases the decay width is given by

$$\begin{aligned} \Gamma(\tilde{t}_1 \rightarrow b + \tilde{l} + l') &= \\ &= \frac{\alpha^2}{16 \pi m_{\tilde{t}_1}^3 \sin^4 \theta_W} \int_{(m_{l'} + m_{\tilde{l}})^2}^{(m_{\tilde{t}_1} - m_b)^2} ds W_{l'\tilde{l}}(s) \sum_{i=1}^3 \left(\sum_{j=1}^5 c_{ij} s^{(j-4)} \right) D_i(s) \end{aligned} \quad (3.37)$$

with

$$D_{1,2}(s) = \frac{1}{(s - m_{\tilde{\chi}_{1,2}^\pm}^2)^2 + m_{\tilde{\chi}_{1,2}^\pm}^2 \Gamma_{\tilde{\chi}_{1,2}^\pm}^2} \quad (3.38)$$

$$D_3(s) = \text{Re} \left(\frac{1}{(s - m_{\tilde{\chi}_1^\pm}^2 + im_{\tilde{\chi}_1^\pm} \Gamma_{\tilde{\chi}_1^\pm})(s - m_{\tilde{\chi}_2^\pm}^2 - im_{\tilde{\chi}_2^\pm} \Gamma_{\tilde{\chi}_2^\pm})} \right). \quad (3.39)$$

The explicit expressions for the $W_{l'\tilde{l}}$ and c_{ij} are given in Appendix A.

3.5 The Decay of the light Stop into a Charm-quark and a Neutralino

For completeness we will also rewrite the results of [51] for the two body decay $\tilde{t}_1 \rightarrow c + \tilde{\chi}_1^0$. They found that the decay is dominated by top-charm squark mixing, which is induced at one loop level. In the limit $m_c \rightarrow 0$ only the left charm squark contributes to this mixing. In the basis of Eq. (2.35) the respective $\tilde{t}_1 - \tilde{t}_2 - \tilde{c}_L$

mixing matrix is given by

$$\mathcal{M}_{\tilde{t}_1 \tilde{t}_2 \tilde{c}_L}^2 = \begin{pmatrix} m_{\tilde{t}_1}^2 & 0 & \Delta_L \cos \theta_t + \Delta_R \sin \theta_t \\ 0 & m_{\tilde{t}_2}^2 & -\Delta_L \sin \theta_t + \Delta_R \cos \theta_t \\ \Delta_L^* \cos \theta_t + \Delta_R^* \sin \theta_t & -\Delta_L^* \sin \theta_t + \Delta_R^* \cos \theta_t & m_{\tilde{c}_L}^2 \end{pmatrix} \quad (3.40)$$

Δ_L (Δ_R) are $\tilde{t}_L - \tilde{c}_L$ ($\tilde{t}_R - \tilde{c}_L$) mixing terms with

$$\Delta_L = -\frac{g^2}{16\pi^2} \ln \left(\frac{M_X^2}{m_W^2} \right) \frac{K_{tb}^* K_{cb} m_b^2}{2m_W^2 \cos^2 \beta} (M_Q^2 + M_D^2 + M_{H_1}^2 + A_b^2) \quad (3.41)$$

$$\Delta_R = \frac{g^2}{16\pi^2} \ln \left(\frac{M_X^2}{m_W^2} \right) \frac{K_{tb}^* K_{cb} m_b^2}{2m_W^2 \cos^2 \beta} m_t A_b \quad (3.42)$$

where M_X is a high scale which we assume to be the Planck mass to get a maximal mixing. M_Q , M_D and M_{H_1} are soft SUSY breaking squark and Higgs mass terms and K_{tb} and K_{cb} are the respective elements of the CKM matrix.

One gets Eq. (3.41) and (3.42) as one step solutions in $\ln(M_P^2/M_W^2)$ of the renormalization group equation in the framework of supergravity theories. Note, that one should stay away from $A_b = 0$ because in this case higher order terms in $\ln(M_P^2/M_W^2)$ become important for Δ_R . Note, also that in this approximation M_D , M_Q and M_{H_1} can be evaluated at any scale because the induced error is of higher order. Therefore, the expressions should be treated as rough estimates giving the order of magnitude for the mixing. For that reason we will use the formula for the decay width in Eq. (3.43) mainly as a check if this decay clearly dominates or if it is negligible.

In the following ϵ gives the size of the charm squark component of the lighter stop, which we calculated numerically. Therefore, in this decay mode the charm-squark component of the lighter stop couples with the charm quark and the LSP $\tilde{\chi}_1^0$ and the width is given by

$$\Gamma(\tilde{t}_1 \rightarrow c \tilde{\chi}_1^0) = \frac{g^2}{16\pi} \epsilon^2 |f_{L1}^c|^2 m_{\tilde{t}_1} \left(1 - \frac{m_{\tilde{\chi}_1^0}^2}{m_{\tilde{t}_1}^2} \right)^2 \quad (3.43)$$

where $f_{L1}^c = f_{L1}^t$ as given in Eq. (3.10). Before discussing our results in detail we give the conditions leading to a large ϵ : (i) $m_{\tilde{t}_1}$ and $m_{\tilde{c}_L}$ have almost the same size, (ii) $\tan \beta$ becomes large ($\cos \beta$ small) which will enhance Δ_L and Δ_R (iii) $\tan \theta_t \sim \Delta_L/\Delta_R$ which will maximize the \mathcal{M}_{13}^2 and \mathcal{M}_{31}^2 components of the mixing matrix $\mathcal{M}_{\tilde{t}_1 \tilde{t}_2 \tilde{c}_L}^2$ (Eq. (3.40)) and (iv) the parameters M_D , M_Q , M_{H_1} and A_b entering Δ_L and Δ_R are big.

Chapter 4

Numerical results for LEP2

4.1 Light Stop

The total cross sections for the process $e^+e^- \rightarrow \tilde{t}_1\bar{\tilde{t}}_1$ at $\sqrt{s} = 200$ GeV are shown in Fig. 4.1 as a function of $|\cos\theta_{\tilde{t}}|$ for several mass values of \tilde{t}_1 . Here ISR- and SUSY-QCD-corrections are included [52, 53]. For completeness the formulae are given in Appendix C. The main corrections are due to ISR- and gluonic QCD-corrections [54]. For $m_{\tilde{t}_1} = 80$ GeV the cross section reaches 0.41 pb. Therefore, one can expect ~ 60 to 123 $\tilde{t}_1\bar{\tilde{t}}_1$ events assuming an integrated luminosity of 300 pb^{-1} . Moreover, the cross section shows a clear dependence on the mixing angle for $m_{\tilde{t}_1} \lesssim 80$ GeV and $|\cos\theta_{\tilde{t}}| \gtrsim 0.6$. In this region cross section measurements should therefore allow to determine the stop mixing angle once $m_{\tilde{t}_1}$ is known.

Assuming $m_{\tilde{t}_1} < m_{\tilde{l},\tilde{\nu}}$ the main decay modes are $\tilde{t}_1 \rightarrow c\tilde{\chi}_1^0$ and $\tilde{t}_1 \rightarrow b\tilde{\chi}_1^+$. As already mentioned in Chapter 3 the first decay is a FCNC decay occurring at one loop level whereas the second one occurs at tree level. Therefore, $\tilde{t}_1 \rightarrow b\tilde{\chi}_1^+$ dominates with practically 100 % branching ratio if it is kinematically allowed. As $\tilde{\chi}_1^+$ further decays into $\tilde{\chi}_1^0 l^+ \nu_l$ or $\tilde{\chi}_1^0 q \bar{q}'$ the signature is two acoplanar b jets accompanied

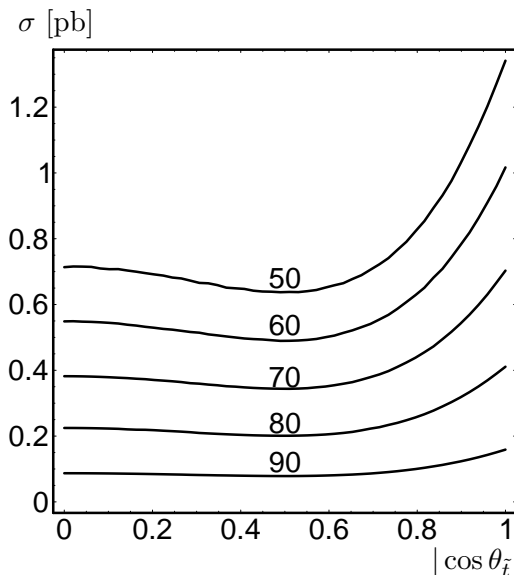


Fig. 4.1: Total cross section for $e^+e^- \rightarrow \tilde{t}_1\bar{\tilde{t}}_1$ in pb at $\sqrt{s} = 200$ GeV as a function of $|\cos\theta_{\tilde{t}}|$ for \tilde{t}_1 masses 50, 60, 70, 80 and 90 GeV. ISR- and QCD-corrections are included.

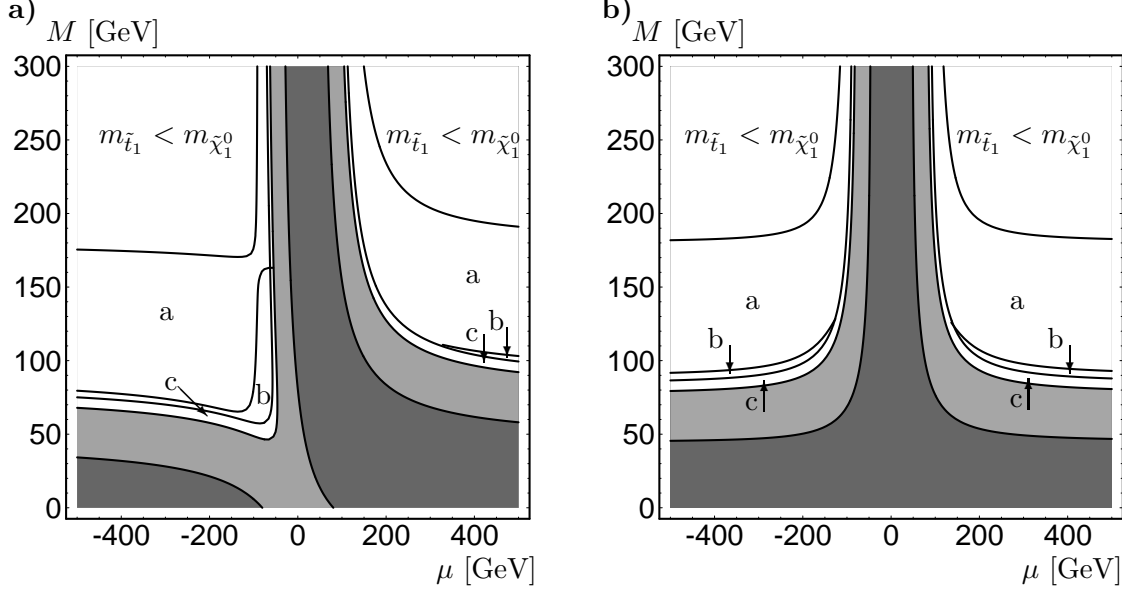


Fig. 4.2: Kinematically allowed parameter domains in the (M, μ) plane for $m_{\tilde{t}_1} = 90$ GeV, a) $\tan \beta = 1.5$ and b) $\tan \beta = 40$ for the decays: a) $\tilde{t}_1 \rightarrow c \tilde{\chi}_1^0$, b) $\tilde{t}_1 \rightarrow c \tilde{\chi}_2^0$, c) $\tilde{t}_1 \rightarrow b \tilde{\chi}_1^+$. The dark grey area is excluded by LEP1 and the bright grey area is excluded by LEP1.5 ($\sqrt{s} = 170$ GeV, $m_{\tilde{\nu}_e} = 90$ GeV).

by two charged leptons + large missing energy (\cancel{E}), or a single charged lepton + jets + \cancel{E} , or jets + \cancel{E} . Here b tagging techniques can be used to extract the signal. Moreover, in this case it is most likely that $\tilde{\chi}_1^+$ will be observed first and its decay properties can be used for identifying \tilde{t}_1 . If $m_{\tilde{t}_1} < m_b + m_{\tilde{\chi}_1^+}$ the decay $\tilde{t}_1 \rightarrow c \tilde{\chi}_1^0$ has practically 100 % branching ratio. The signature is then two acoplanar jets + \cancel{E} . Generally, in this case the invisibly energy will be larger than in the case of $\tilde{t}_1 \rightarrow b \tilde{\chi}_1^+$. In Fig. 4.2 a (b) we show the domains of the stop decay modes in the (M, μ) plane for $m_{\tilde{t}_1} = 90$ GeV and $\tan \beta = 1.5$ (40). Note, that there is a small strip where the decay $\tilde{t}_1 \rightarrow c \tilde{\chi}_2^0$ is also possible.

If the lifetime of \tilde{t}_1 is longer than the typical hadronization time of $\mathcal{O}(10^{-23}s)$, i.e. $\Gamma_{\tilde{t}_1} \lesssim 0.2$ GeV, it will first hadronize into a colourless $(\tilde{t}_1 \bar{q})$ or $(\tilde{t}_1 qq)$ bound state before decaying. The process of \tilde{t}_1 fragmentation was discussed in detail in [55]. Fast moving stops first radiate off gluons at small angles. This process can be treated perturbatively. After that the non-perturbative hadronization phase follows leading to $(\tilde{t}_1 \bar{q})$ and $(\tilde{t}_1 qq)$ hadrons. If the velocity $\beta_{\tilde{t}_1}$ is $\sim 1/2$ the energy loss of the stop due to gluon radiation and due to hadronization is of comparable size. Near the threshold, the gluon emission is suppressed by $\beta_{\tilde{t}_1}^4$.

Hadronization is generally expected in case of $\tilde{t}_1 \rightarrow c \tilde{\chi}_1^0$, $\tilde{t}_1 \rightarrow b l^+ \tilde{\nu}_l$ and $\tilde{t}_1 \rightarrow b \nu \tilde{l}^+$ since these decays involve the electroweak coupling twice (see Fig. 4.6). However, also in case of $\tilde{t}_1 \rightarrow b \tilde{\chi}_1^+$ this can happen as illustrated in Fig. 4.3 and 4.4.

Scenario	μ	M_2	$\tan \beta$	$m_{\tilde{\chi}_1^0}$	$m_{\tilde{\chi}_2^0}$	$m_{\tilde{\chi}_1^\pm}$	$m_{\tilde{\chi}_2^\pm}$
pt1	-500.0	70.0	1.5	37.3	80.7	80.0	511.2
pt2	-138.0	55.0	1.5	31.5	82.1	80.0	168.7
pt3	-64.9	300.0	1.5	63.5	88.6	80.0	317.2
pt4	230.6	120.0	1.5	43.3	89.7	80.0	272.0
pt5	-500.0	81.4	40	40.4	80.0	80.0	512.9
pt6	-138.0	110.0	40	48.4	82.4	80.0	193.8
pt7	-84.8	300.0	40	64.7	98.0	80.0	321.9
pt8	133.9	120.0	40	49.4	85.8	80.0	196.8
pt9	-250.0	75.0	1.5	41.1	93.0	91.6	269.3
pt10	-67.0	90.0	1.5	50.5	64.2	91.5	130.4

Table 4.1: Parameters used in the the different scenarios for LEP2. In addition, we give the respective values for the masses (in GeV) of the two lighter neutralinos and the charginos. The other parameters are given in the text.

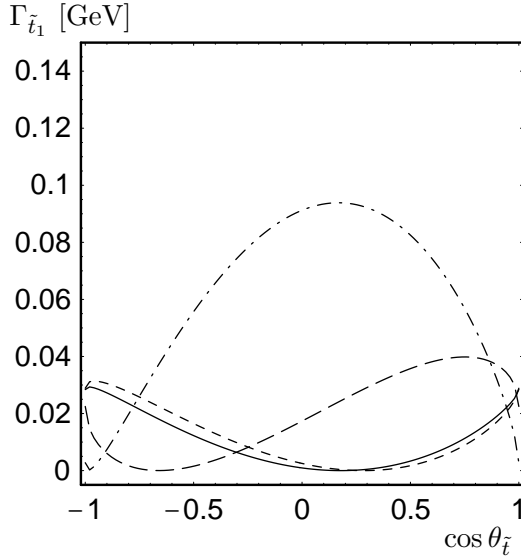


Fig. 4.3: Total decay width of the light stop as a function of $\cos \theta_{\tilde{t}}$ for the scenarios pt1 (solid line), pt2 (dashed line), pt3 (dashed dotted line) and pt4 (long dashed line) of Tab. 4.1. ($\tan \beta = 1.5$)

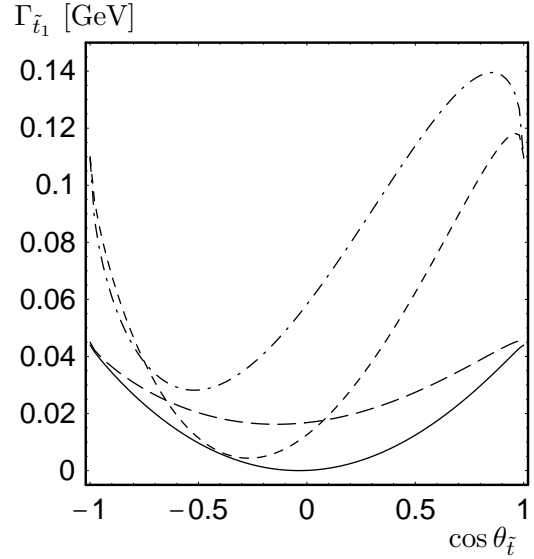


Fig. 4.4: Total decay width of the light stop as a function of $\cos \theta_{\tilde{t}}$ for the scenarios pt5 (solid line), pt6 (dashed line), pt7 (dashed dotted line) and pt8 (long dashed line) of Tab. 4.1. ($\tan \beta = 40$)

In Fig. 4.3 (4.4) we show the width of $\tilde{t}_1 \rightarrow b \tilde{\chi}_1^+$ as a function of $\cos \theta_{\tilde{t}}$ for $m_{\tilde{t}_1} = 90$ GeV, $m_{\tilde{\chi}_1^+} \simeq 80$ GeV, $\tan \beta = 1.5$ (40), and four different sets of M and μ as given in Tab. 4.1. In addition we present there the masses of the two lighter neutralinos and of both charginos. In case of pt1 (pt5) the chargino is mainly gaugino-like ($M \ll \mu$), in case of pt3 (pt7) the chargino is mainly higgsino-like ($M \gg \mu$), whereas in the other cases we have a strongly mixed chargino ($M \sim \mu$). In the last case we have taken two different points in the (M, μ) plane with a different sign for μ .

For small $\tan \beta$ and gaugino-like charginos (pt1 in Fig. 4.3) the $\tilde{t}_1 - b - \tilde{\chi}_1^+$ interaction is dominated by $V_{11} \cos \theta_{\tilde{t}}$. The deviation of the decay width from the $\cos^2 \theta_{\tilde{t}}$ shape is due to constructive and destructive interference with the term proportional to the top Yukawa coupling ($Y_t V_{12} \sin \theta_{\tilde{t}}$) which becomes especially important for $\tilde{t}_1 \sim \tilde{t}_R$ and increases with decreasing $|\mu|$. In the case of pt3 this part of the coupling leads to a $\sin^2 \theta_{\tilde{t}}$ shape. If the gaugino- and higgsino-components of the chargino are of comparable size (pt2 and pt4) a more complicated interplay of the gaugino and higgsino couplings give rise to an intricate dependence on the mixing angle and a large asymmetry in the sign of μ .

In Fig. 4.4 we show the total decay widths for the large $\tan \beta$ ($=40$) scenarios pt5, pt6, pt7 and pt8 of Tab. 4.1. Here the term $Y_b U_{12} \cos \theta_{\tilde{t}}$ becomes important if the chargino has a sizable higgsino-component. This leads to an enhancement of the decay width and to a shift of the maxima compared to the case $\tan \beta = 1.5$ (Fig. 4.3).

Let us now turn to the case that three body decays of \tilde{t}_1 into sleptons are kinematically possible and that $m_{\tilde{\chi}_1^+} > m_{\tilde{t}_1}$. In this case the decay chain will be either $\tilde{t}_1 \rightarrow b l^+ \tilde{\nu}_l \rightarrow b l^+ \nu_l \tilde{\chi}_1^0$ or $\tilde{t}_1 \rightarrow b \nu_l \tilde{l}_{1,2}^+ \rightarrow b l^+ \nu_l \tilde{\chi}_1^0$. These decays compete with the decay $\tilde{t}_1 \rightarrow c \tilde{\chi}_1^0$. The signature is 2 b jets + 2 charged leptons + \cancel{E} or 1 b jet + 1 c jet + 1 charged lepton + \cancel{E} or 2 c jets + \cancel{E} . If the three body decays dominate, one may ask if there is a chance to distinguish between the different sleptons. It should be no problem to identify the generation by identifying the nature of the charged lepton. To answer the question whether the final state occurs through sneutrinos and/or charged sleptons requires most likely the study of the angular distribution of the b -jets, the lepton and the angle between the jet and the lepton.

In the following examples we will assume that the parameters $M_{\tilde{E}}$ and $M_{\tilde{L}}$ are the same for every generation. For small $\tan \beta$ this is justified by RGE studies. The modifications for a high $\tan \beta$ scenario will be discussed later. Before going into detail we want to remark that: (i) The charged sleptons are expected to be heavier than the sneutrinos because of the D -term contributions. Therefore, the discovery of those decay modes is not only an evidence for a light stop but at the same time most likely the first evidence of light sneutrinos. The sneutrino decays invisibly into $\nu_l \tilde{\chi}_1^0$. Therefore, it is difficult to detect. (ii) Even for small $\tan \beta$ the influence of the τ Yukawa coupling and stau mixing can lead to sizable effects. (iii) In case that the

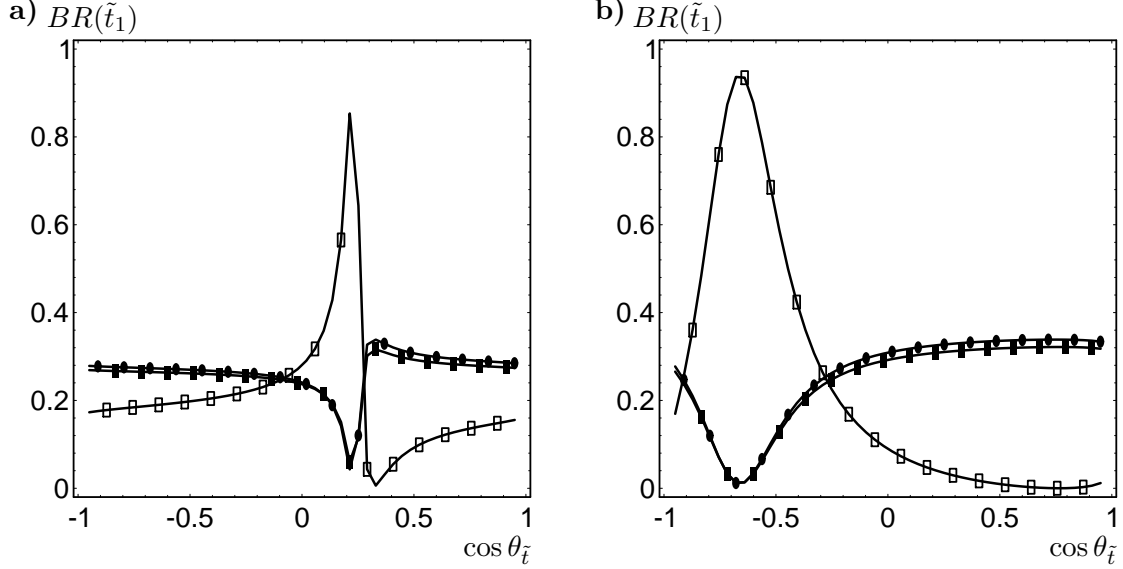


Fig. 4.5: Branching ratios for stop decays into sleptons for the scenarios pt9 (a) and pt10 (b) of Tab. 4.1. The other parameters are given in the text. The curves correspond to the following decays: \square $\tilde{t}_1 \rightarrow b \nu_\tau \tilde{\tau}_1$, \bullet $\tilde{t}_1 \rightarrow b e^+ \tilde{\nu}_e$ ($b \mu^+ \tilde{\nu}_\mu$), and \blacksquare $\tilde{t}_1 \rightarrow b \tau^+ \tilde{\nu}_\tau$.

chargino is mainly higgsino-like there is only a small mass difference between the chargino and the lightest neutralino. Therefore, the charged particles will most likely have too little energy to pass the experimental cuts [56]. We will therefore discuss examples where the lighter chargino is either mainly a gaugino (pt9 of Tab. 4.1) or where it is highly mixed (pt10 of Tab. 4.1). (iv) The existence of this decay and the fact that the stop should be heavier than the lightest neutralino implies an upper bound on the lighter chargino which is approximately given by $m_{\tilde{\chi}_1^+} \lesssim 2 m_{\tilde{t}_1}$. Here it is assumed that $\tilde{\chi}_1^0$ is the LSP and that the GUT relation 2.24 between the gaugino masses M' and M is valid.

In Fig. 4.5 we show the branching ratios for the three body decays for the scenarios pt9 and pt10 of Tab. 4.1 and for $m_{\tilde{t}_1} = 80$ GeV. Both cases are low $\tan \beta$ scenarios ($\tan \beta = 1.5$). We have used the following (flavor independent) parameters in the slepton sector: $M_{\tilde{E}} = 59.8$ GeV, $M_{\tilde{L}} = 72.1$ GeV and $A_\tau = 500$ GeV (774.5 GeV) in case of scenario pt9 (pt10). They lead to the following physical quantities: $m_{\tilde{\nu}_i} = 60$ GeV ($i = e, \mu, \tau$), $m_{\tilde{e}_L} = 77.9$ GeV, $m_{\tilde{e}_R} = 65.7$ GeV, $m_{\tilde{\tau}_1} = 58.4$, $m_{\tilde{\tau}_2} = 83.5$ and $\cos \theta_{\tilde{\tau}} = -0.5$. Therefore, the decays into all sneutrinos and the lighter stau are possible. Note, that also the decays into \tilde{e}_R and $\tilde{\mu}_R$ are kinematically allowed. However, as already mentioned in Chapter 3, these decays are negligible because the coupling of $\tilde{\chi}_i^+ - \tilde{e}_R - \nu_e$ ($\tilde{\chi}_i^+ - \tilde{\mu}_R - \nu_\mu$) is proportional m_e (m_μ). We expect that the numbers of produced electrons and muons are nearly equal and that they are smaller than the number of produced τ leptons.

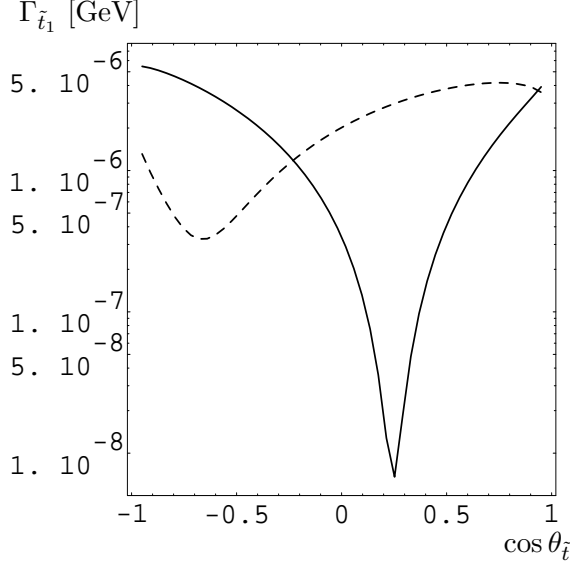


Fig. 4.6: Total decay widths of a light stop for the scenarios pt9 (full line) and pt10 (dashed line) as given in Tab. 4.1. The other parameters are given in the text.

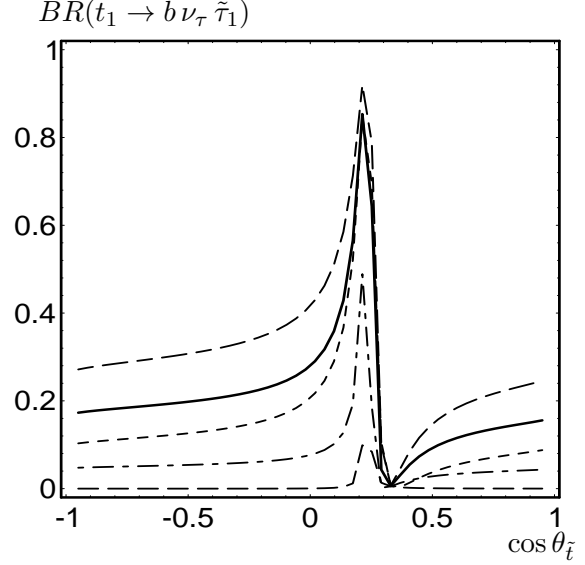


Fig. 4.7: Branching ratio for the decay $\tilde{t}_1 \rightarrow b \nu_\tau \tilde{t}_1$ as a function of $\cos \theta_{\tilde{t}}$ for $M = 75$ GeV, $\mu = -250$ GeV and $\tan \beta = 1.5$ (pt9 of Tab. 4.1). The masses of the sleptons are: $m_{\tilde{\nu}_i} = 60$ GeV ($i = e, \mu, \tau$), $m_{\tilde{\tau}_1} = 58.4$ and $\cos \theta_{\tilde{\tau}} = 0$ (long dashed line), -0.24 (short long dashed line), 0.39 (short dashed line), -0.5 (full line) and -0.68 (middle long dashed line). The other parameters are given in the text.

In Fig. 4.5a the situation for scenario pt9 is shown. The decays into sneutrinos dominate over the decays into $\tilde{\tau}_1$ except in the region $0 \lesssim \cos \theta_{\tilde{t}} \lesssim 0.25$. This behaviour can be understood by combining the following facts: i) The sleptons couple mainly to $\tilde{\chi}_1^+$ because $\tan \beta$ is small. ii) $\cos \theta_{\tilde{\tau}} = -0.5$ and therefore $\tilde{\tau}_1 \simeq \tilde{\tau}_R$. iii) The \tilde{t}_1 - $\tilde{\chi}_{1,2}^+$ - b couplings are dominated by $l_{11,12}^{\tilde{t}}$. iv) Near $\cos \theta_{\tilde{t}} = 0.25$ the coupling $l_{11}^{\tilde{t}}$ vanishes whereas $l_{12}^{\tilde{t}}$ is near its maximum. Therefore, the exchange of the heavier chargino becomes important. Note, that $\tilde{\chi}_2^+$ couples stronger to $\tilde{\tau}_1$ than to $\tilde{\nu}_\tau$ in this example. Moreover, the interference terms have opposite signs: in case of the stau (sneutrino) it is positive (negative) for $\cos \theta_{\tilde{t}} \lesssim 0.25$ and negative (positive) for $\cos \theta_{\tilde{t}} \gtrsim 0.25$.

Let us now turn to scenario pt10 where we have two main differences compared to the above example: (i) the heavier chargino has rather large gaugino components ($U_{12} = 0.997$ and $V_{12} = -0.651$). (ii) The mass difference between the charginos is much smaller compared to the previous example (see Tab. 4.1). The decay into the stau proceeds mainly through $\tilde{\chi}_2^\pm$ exchange whereas the decays into the sneutrinos

proceed mainly through $\tilde{\chi}_1^+$ exchange. Looking at the $\tilde{t}_1\text{-}\tilde{\chi}_{1,2}^+\text{-}b$ couplings one sees that $|l_{11}^{\tilde{t}}| < |l_{12}^{\tilde{t}}|$ ($|l_{11}^{\tilde{t}}| > |l_{12}^{\tilde{t}}|$) if $\cos\theta_{\tilde{t}} \lesssim 0.1$ ($\cos\theta_{\tilde{t}} \gtrsim 0.1$). $l_{11}^{\tilde{t}}$ ($l_{12}^{\tilde{t}}$) vanishes near $\cos\theta_{\tilde{t}} = -0.8$ ($\cos\theta_{\tilde{t}} = 0.8$). Moreover, the interference term is negative for all decay modes if $|\cos\theta_{\tilde{t}}| \lesssim 0.8$. The combination of all facts leads to the pronounced maximum of $BR(\tilde{t}_1 \rightarrow b\nu_{\tau}\tilde{\tau}_1)$ near $\cos\theta_{\tilde{t}} = -0.7$. Because of the large asymmetry it should be possible to determine the sign of $\cos\theta_{\tilde{t}}$ if $BR(\tilde{t}_1 \rightarrow b\nu_{\tau}\tilde{\tau}_1)$ can be measured.

In Fig. 4.6 we show the total decay width for both examples. One can easily see that the decay width has a minimum near the above mentioned $\cos\theta_{\tilde{t}}$ values where $l_{11}^{\tilde{t}}$ vanishes. In case of scenario pt9 (pt10) the decay width varies over 2 (1) orders of magnitude. This difference in the order is due to the different mass of the heavier chargino. In both cases the stop will hadronize before decaying.

The branching ratios depend not only on the kinematics but also on the stau mixing angle. To get a feeling for this dependence let us first look at the possible range for $\cos\theta_{\tilde{\tau}}$. As can be seen from the formulae given in Appendix B we can fix μ and $\tan\beta$, vary A_{τ} and calculate $\cos\theta_{\tilde{\tau}}$. Keeping $m_{\tilde{\tau}_1}$ and $m_{\tilde{\nu}_{\tau}}$ fixed one can first calculate $m_{\tilde{\tau}_2}$ (see Eq. (B.12)) and then $M_{\tilde{E}}$ (Eq. (B.10)) to get a feeling if the parameters are reasonable. One gets $0.39 > \cos\theta_{\tilde{\tau}} > -0.68$, $77.9 \text{ GeV} < m_{\tilde{\tau}_2} < 91.1 \text{ GeV}$ and $64.3 \text{ GeV} < M_{\tilde{E}} < 79.9 \text{ GeV}$ if A_{τ} is varied between -1 TeV and 1 TeV in scenario pt9. In Fig. 4.7 we show the branching ratio for the decay into a stau for the following $(A_{\tau}, M_{\tilde{E}}, \cos\theta_{\tilde{\tau}}, m_{\tilde{\tau}_2})$ sets: $(-1000, 55.97, 0.39, 80.8)$, $(-375, 51.69, 0, 77.9)$, $(0, 53.27, -0.24, 78.9)$, $(500, 59.8, -0.5, 83.5)$ and $(1000, 70.04, -0.68, 91.1)$. The masses are given in GeV. A large ratio $A_{\tau}/M_{\tilde{E}}$ implies the possible danger of a charge breaking minimum. However, to our knowledge there is no sufficient way to treat this problem. Therefore, we will leave it aside for the moment. For a discussion of this topic see e.g. [57] and references therein. One can easily see that the importance of the decay $\tilde{t}_1 \rightarrow b\nu_{\tau}\tilde{\tau}_1$ grows with $|\cos\theta_{\tilde{\tau}}|$ because this implies a stronger coupling to the lighter chargino. We have checked that the dependence on $\cos\theta_{\tilde{\tau}}$ is similar in scenario pt10. An interesting detail is that even for $\cos\theta_{\tilde{\tau}} = 0$ there is small range of $\cos\theta_{\tilde{t}}$ where $BR(\tilde{t}_1 \rightarrow b\nu_{\tau}\tilde{\tau}_1)$ is of $O(0.1)$ because of the Yukawa coupling to the heavier chargino.

In the case that a large $\tan\beta$ scenario is realized in nature, it is expected that the lighter stau is the lightest slepton. In the energy range of LEP2 the most likely scenario would be that the stau is lighter than the stop and the stop lighter than the other sleptons. This can be seen in the following way: let us first assume $M_{\tilde{E}} = M_{\tilde{L}}$ for simplicity. The mass of the lighter stau is then given by:

$$\begin{aligned} m_{\tilde{\tau}_1}^2 &= M_{\tilde{L}}^2 + m_{\tau}^2 - \frac{1}{4}m_Z^2 \cos 2\beta - \sqrt{\frac{1}{4}m_Z^4 \cos^2 2\beta (1/2 - 2\sin\theta_W)^2 + (m_{\tau}\mu \tan\beta)^2} \\ &\sim M_{\tilde{L}}^2 + m_{\tau}^2 - \frac{1}{4}m_Z^2 \cos 2\beta - m_{\tau}|\mu| \tan\beta. \end{aligned} \quad (4.1)$$

The last relation holds because $1/2 - 2\sin\theta_W \sim 0.04$. The mass of the tau sneutrino

is given by

$$m_{\tilde{\nu}_\tau}^2 = M_{\tilde{L}}^2 + \frac{1}{2}m_Z^2 \cos 2\beta. \quad (4.2)$$

Therefore, $\tilde{\tau}_1$ is lighter than $\tilde{\nu}_\tau$ if

$$-m_\tau |\mu| \tan \beta < \frac{3}{4}m_Z^2 \cos 2\beta < 0 \quad (4.3)$$

There is only a small parameter range in the large $\tan \beta$ regime where $\tilde{\chi}_1^+$ is mainly a higgsino and at the same time $m_{\tilde{\chi}_1^0} < \min(m_{\tilde{\tau}_1}, m_{\tilde{\nu}_\tau})$. Therefore, $|\mu|$ is larger than $m_{\tilde{\chi}_1^\pm}$ implying that relation 4.3 will be fulfilled in most cases. Now we should remember that RGE studies [18, 22] indicate that $M_{\tilde{E}}$ and $M_{\tilde{L}}$ are smaller for the third generation than for the other two and that $M_{\tilde{E}} < M_{\tilde{L}}$. For these reasons even the tau sneutrino is expected to be heavier than the lighter stau in such a scenario. This finishes our chain of hints for the above assumption. Therefore, the two competing modes are $\tilde{t}_1 \rightarrow c \tilde{\chi}_1^0$ and $\tilde{t}_1 \rightarrow b \nu_\tau \tilde{\tau}_1 \rightarrow b \nu_\tau \tau \tilde{\chi}_1^0$. As mentioned in Section 3.5 we use the formula for the decay-width $\Gamma(\tilde{t}_1 \rightarrow c \tilde{\chi}_1^0)$ only as indication of the order of magnitude. Therefore, we show no figures for the large $\tan \beta$ scenarios.

Let us shortly comment on the possibility of $m_{\tilde{\chi}_1^0} < \min(m_{\tilde{\tau}_1}, m_{\tilde{\nu}_\tau})$. This, for example is realized in gauge mediated SUSY models (see e.g. [58] and references therein) if $\tan \beta$ is large. In this class of models, the gravitino \tilde{G} is the LSP and the lighter stau is the next heavier SUSY particle. In such a scenario the lighter stop can decay in the following way: $\tilde{t}_1 \rightarrow b \nu_\tau \tilde{\tau}_1 \rightarrow b \nu_\tau \tau \tilde{G}$. This leads to the same signature as in the previous case.

Monte Carlo studies for \tilde{t}_1 pair production have been performed within the CERN-LEP2 Workshop 1995 [56]. They have mainly concentrated on the decay $\tilde{t}_1 \rightarrow c \tilde{\chi}_1^0$ since in this case the \tilde{t}_1 would most likely be the first SUSY particle to be discovered. For the simulation of \tilde{t}_1 hadronization different approaches have been used. The conclusions have been a 5σ discovery reach for $m_{\tilde{t}_1} \simeq 75$ to 90 GeV and a 95% confidence level exclusion of $m_{\tilde{t}_1} = 84$ to 92 GeV at $\sqrt{s} = 190$ GeV, for $\mathcal{L} = 300\text{pb}^{-1}$ depending on $\cos \theta_{\tilde{t}}$ and $m_{\tilde{\chi}_1^0}$. In case of $\tilde{t}_1 \rightarrow b \tilde{\chi}_1^+$ the experimental reach for $m_{\tilde{t}_1}$ is ~ 85 GeV. Here b -tagging is important for identifying the stop. For the case of dominance of the three body decays the limits on $m_{\tilde{t}_1}$ given in [43] are about 5 GeV lower than in the case where the main decay mode is $\tilde{t}_1 \rightarrow c \tilde{\chi}_1^0$.

4.2 Light Sbottom

A considerable \tilde{b}_L - \tilde{b}_R mixing is possible if $\tan \beta$ is large (see Eq. (2.36)). In this case \tilde{b}_1 can be rather light. Therefore, it is interesting to discuss the phenomenology of \tilde{b}_1 at LEP2.

The total cross sections of \tilde{b}_1 pair production at $\sqrt{s} = 200$ GeV are shown in Fig. 4.8 as a function of $|\cos \theta_{\tilde{b}}|$ for several mass values of \tilde{b}_1 including ISR- and

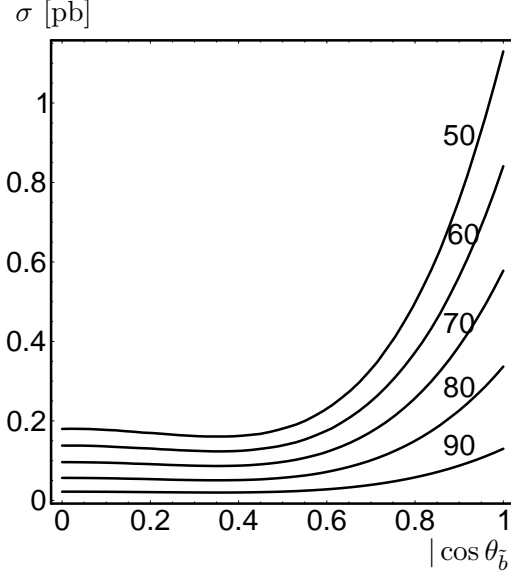


Fig. 4.8: Total cross section for $e^+e^- \rightarrow \tilde{b}_1\bar{\tilde{b}}_1$ in pb at $\sqrt{s} = 200$ GeV as a function of $|\cos \theta_{\tilde{b}}|$ for \tilde{b}_1 masses 50, 60, 70, 80 and 90 GeV. ISR- and QCD-corrections are included.

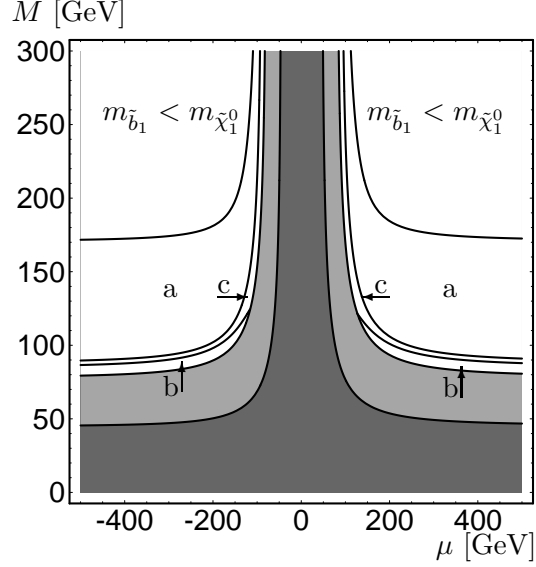


Fig. 4.9: Kinematically allowed parameter domains in the (M, μ) plane for $m_{\tilde{b}_1} = 90$ GeV and $\tan \beta = 40$ for the decays: a) $\tilde{b}_1 \rightarrow b\tilde{\chi}_1^0$, b) $\tilde{b}_1 \rightarrow b\tilde{\chi}_2^0$ and c) $\tilde{b}_1 \rightarrow c\tilde{\chi}_1^\pm$. The dark grey area is excluded by LEP1 and the bright grey area is excluded by LEP1.5 ($\sqrt{s} = 170$ GeV, $m_{\tilde{\nu}_e} = 90$ GeV).

QCD-corrections. If $|\cos \theta_{\tilde{b}}| \gtrsim 0.6$ the dependence on the mixing angle is even more pronounced than in the case of \tilde{t}_1 production. The production cross section of $e^+e^- \rightarrow \tilde{b}_1\bar{\tilde{b}}_1$ is smaller than in the case of \tilde{t}_1 production by a factor $\sim 5/4$ to 5. For a sbottom mass of 80 GeV the cross section varies between 0.05 and 0.34 pb. Therefore, 15 to 100 events per year are expected for an integrated luminosity of 300 pb^{-1} .

The main decay modes of \tilde{b}_1 are $\tilde{b}_1 \rightarrow b\tilde{\chi}_1^0$ and $\tilde{b}_1 \rightarrow b\tilde{\chi}_2^0$ if $m_{\tilde{b}_1} < m_{\tilde{g}}$. The domains of the \tilde{b}_1 decays in the (M, μ) plane are shown in Fig. 4.9 for $m_{\tilde{b}_1} = 90$ GeV and $\tan \beta = 40$. If only $\tilde{b}_1 \rightarrow b\tilde{\chi}_1^0$ is kinematically allowed, the signature is two b -jets plus \cancel{E} . In order to distinguish the sbottom from a stop b -tagging can be necessary because the decay $\tilde{t}_1 \rightarrow c\tilde{\chi}_1^0$ leads to a similar signature. If in addition, the decay into the second lightest neutralino is possible, there can be additional charged leptons and/or jets stemming from $\tilde{\chi}_2^0 \rightarrow \tilde{\chi}_1^0 q\bar{q}$ and $\tilde{\chi}_2^0 \rightarrow \tilde{\chi}_1^0 l^+l^-$. In any case b -tagging will enhance the signal. In principal the flavour changing decay $\tilde{b}_1 \rightarrow c\tilde{\chi}_1^\pm$ is also possible (region b and c in Fig. 4.9). Assuming that the mixing between different squark generations is of the same order as in the quark sector, it turns

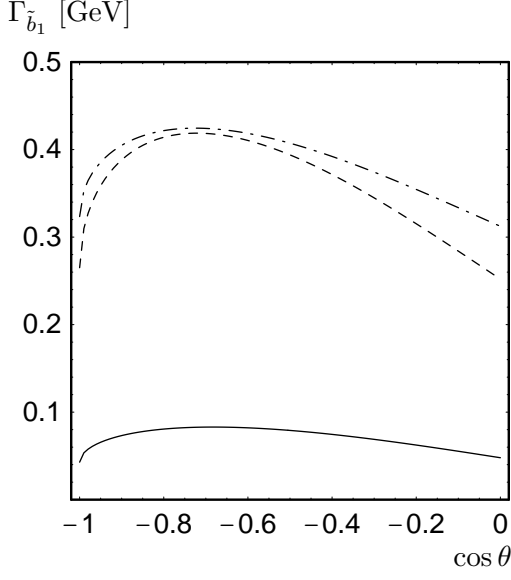


Fig. 4.10: Decay width of the light sbottom as a function of $\cos \theta_{\tilde{b}}$ for the scenarios pt5 (solid line), pt6 (dashed line), and pt7 (dashed dotted line) of Tab. 4.1.

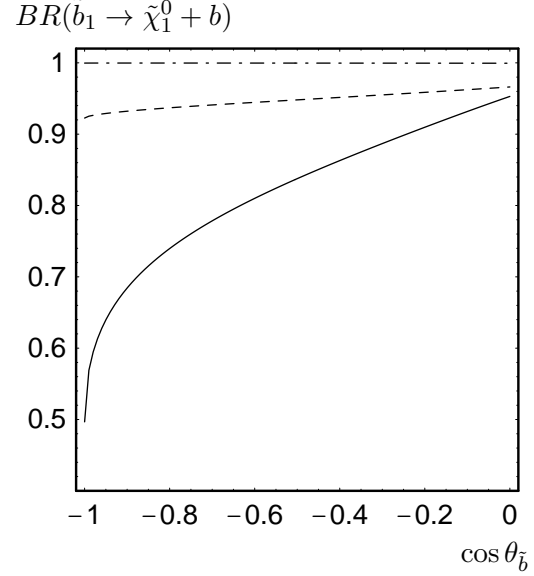


Fig. 4.11: Branching ratio for $\tilde{b}_1 \rightarrow b \tilde{\chi}_1^0$ as a function of $\cos \theta_{\tilde{b}}$ for the scenarios pt5 (solid line), pt6 (dashed line) and pt7 (dashed dotted line) of Tab. 4.1.

out that this decay mode is negligible. Nevertheless, this decay can be important if one studies the flavour structure of the squark sector. Moreover, this mode gains some importance for larger $m_{\tilde{b}_1}$ as will be shown in Section 10.2.

In Fig. 4.10 we show the total decay width of \tilde{b}_1 for the scenarios pt5, pt6 and pt7 of Tab. 4.1 and for $m_{\tilde{b}_1} = 90$ GeV. Scenario pt8 gives nearly the same result as scenario pt6 for equal $|\cos \theta_{\tilde{b}}|$. Here we show only the dependence on negative values of $\cos \theta_{\tilde{b}}$ because for large $\tan \beta$ the sign of $\cos \theta_{\tilde{b}}$ is determined by the sign of μ (Eq. (2.36)) if one wants to avoid unnaturally large A_b . As can be seen, the total decay width is smaller than 0.2 GeV if the neutralinos are mainly gaugino-like (pt5). Therefore, hadronization becomes important. Its effects are the same as in the case of \tilde{t}_1 because QCD is flavour blind. If $\tilde{\chi}_1^0$ and $\tilde{\chi}_2^0$ have a sizable higgsino-component (pt6 and pt7) the total decay widths increase because of the large bottom Yukawa coupling although the neutralino masses are larger when compared to the previous case.

The branching ratio for $\tilde{b}_1 \rightarrow b \tilde{\chi}_1^0$ is shown in Fig. 4.11 as a function of $\cos \theta_{\tilde{b}}$ for the above examples. If the neutralinos are mainly gauginos the branching ratio depends strongly on $\cos \theta_{\tilde{b}}$ (pt5). This is because \tilde{b}_L has a strong coupling to the zino components whereas \tilde{b}_R couples only to the bino components. Due to the assumption $M' = 5/3 \tan^2 \theta_W M$ the lightest neutralino is mainly a bino and the second lightest neutralino is mainly a zino for the parameter choices of pt5. Evidently,

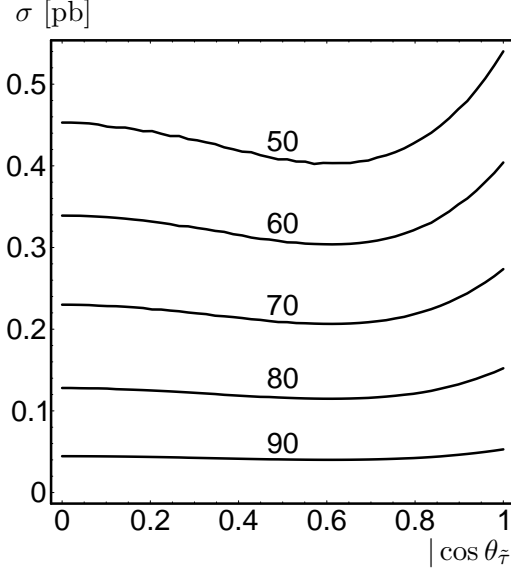


Fig. 4.12: Total cross section for $e^+e^- \rightarrow \tilde{\tau}_1 \tilde{\tau}_1^*$ in pb at $\sqrt{s} = 200$ GeV as a function of $|\cos \theta_{\tilde{\tau}}|$ for $\tilde{\tau}_1$ masses 50, 60, 70, 80 and 90 GeV. ISR-corrections are included.

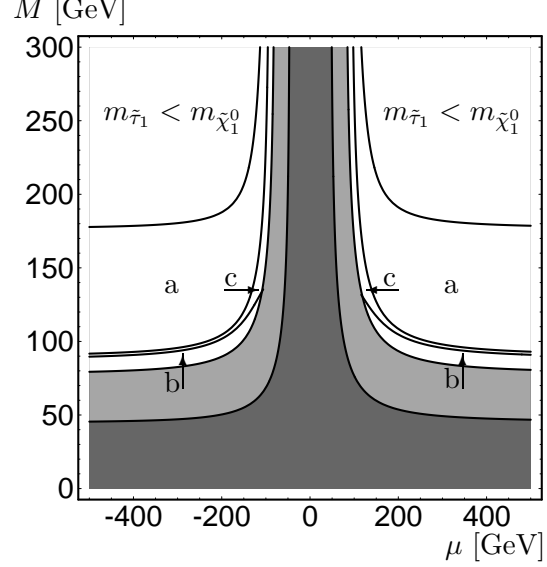


Fig. 4.13: Kinematically allowed parameter domains in the (M, μ) $m_{\tilde{\tau}_1} = 90$ GeV and $\tan \beta = 40$ for the decays: a) $\tilde{\tau}_1 \rightarrow \tau \tilde{\chi}_1^0$, b) $\tilde{\tau}_1 \rightarrow \tau \tilde{\chi}_2^0$ and c) $\tilde{\tau}_1 \rightarrow \nu_\tau \tilde{\chi}_1^-$. The dark grey area is excluded by LEP1 and the bright grey area is excluded by LEP1.5 ($\sqrt{s} = 170$ GeV, $m_{\tilde{\nu}_e} = 90$ GeV).

the dependence on the mixing angle will decrease if the mass of the second lightest neutralino increases. The increase of $BR(\tilde{b}_1 \rightarrow b \tilde{\chi}_1^0)$ in case of the mixed scenario pt6 is an effect of the larger higgsino components of $\tilde{\chi}_{1,2}^0$.

DELPHI has studied \tilde{b}_1 search for the case that only the decay $\tilde{b}_1 \rightarrow b \tilde{\chi}_1^0$ is possible [56]. Their conclusion was that the discovery potential for \tilde{b}_1 is similar to $\tilde{t}_1 \rightarrow c \tilde{\chi}_1^0$ ($m_{\tilde{b}_1} \lesssim 75$ to 90 GeV depending on $\cos \theta_{\tilde{b}}$ and $m_{\tilde{\chi}_1^0}$).

4.3 Light Stau

There are two reasons that at least one of the staus could be within the mass range which will be explored by LEP2: Firstly, the soft SUSY breaking mass terms for sleptons are expected to be smaller than the corresponding ones for squarks. Secondly, as in the sbottom sector one expects a large $\tilde{\tau}_L$ - $\tilde{\tau}_R$ mixing for large $\tan \beta$.

The cross sections for stau pair production are plotted in Fig. 4.12 as a function of $|\cos \theta_{\tilde{\tau}}|$ for $\sqrt{s} = 200$ GeV. Here we have included ISR-corrections. As can be seen, the dependence on the mixing angle is much weaker for stau production than in case of squark production. The cross section is of $\mathcal{O}(0.15)$ pb for $m_{\tilde{\tau}_1} = 80$ GeV

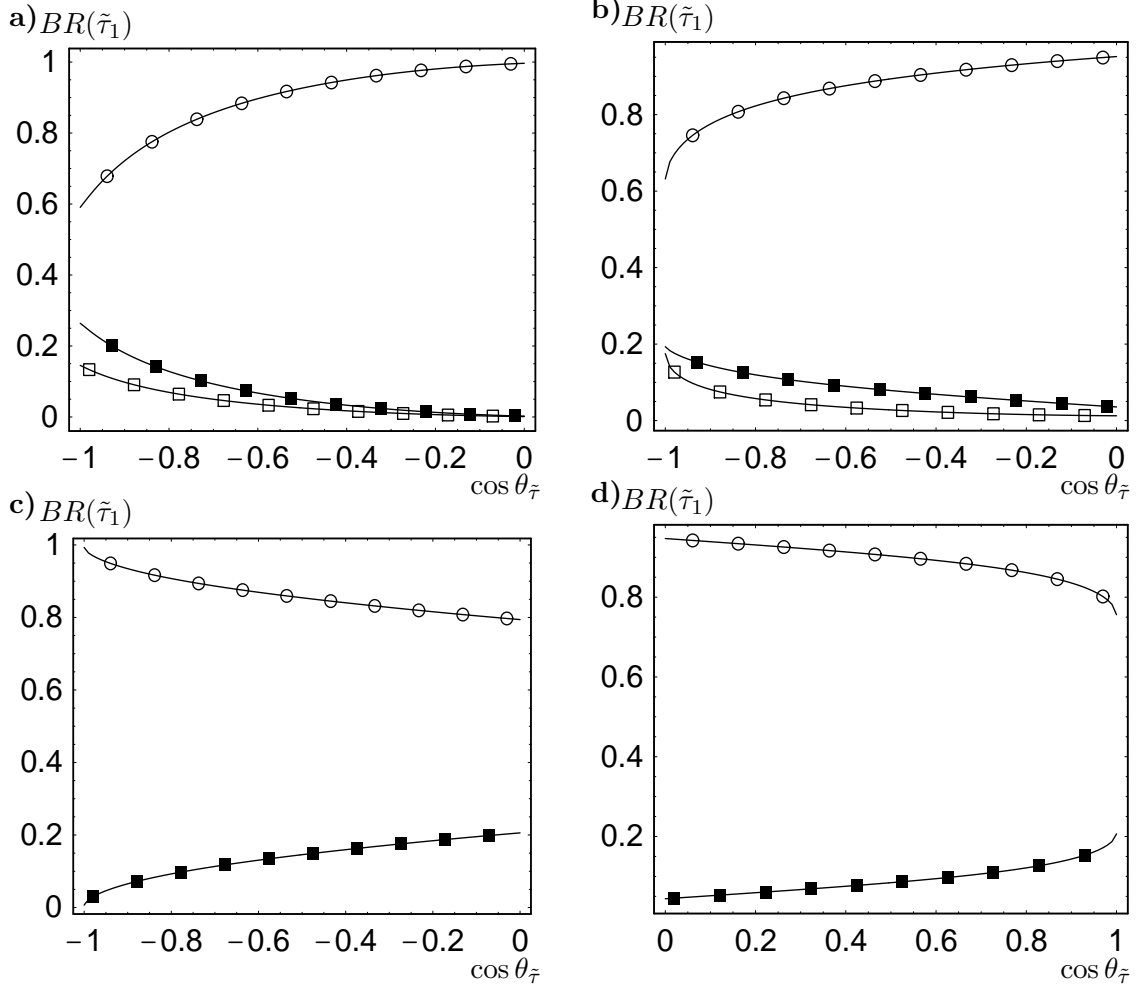


Fig. 4.14: Branching ratios for the decays of the lighter stau as a function of $\cos \theta_{\tilde{\tau}}$ for the scenarios pt5 (a), pt6 (b), pt7 (c) and pt8 (d) of Tab. 4.1, $m_{\tilde{\tau}_1} = 90$ GeV. The graphs correspond to the following decays: $\circ \tilde{\tau}_1 \rightarrow \tau \tilde{\chi}_1^0 + \tau$, $\square \tilde{\tau}_1 \rightarrow \tau \tilde{\chi}_2^0 + \tau$, and $\blacksquare \tilde{\tau}_1 \rightarrow \tau \tilde{\chi}_1^- + \nu_\tau$.

corresponding to ~ 45 events for an integrated luminosity of $\mathcal{L} = 300 \text{ pb}^{-1}$.

We get the classical SUSY signature consisting of 2 τ -leptons + \cancel{E} if only the decay $\tilde{\tau}_1 \rightarrow \tau \tilde{\chi}_1^0$ is kinematically allowed. The decays $\tilde{\tau}_1 \rightarrow \tau \tilde{\chi}_2^0$ and/or $\tilde{\tau}_1 \rightarrow \nu_\tau \tilde{\chi}_1^-$ lead to additional jets and/or leptons. The parameter domains of the various stau decays in the (M, μ) plane are shown in Fig. 4.13 for $m_{\tilde{\tau}_1} = 90$ GeV and $\tan \beta = 40$.

In Fig. 4.14 we show the branching ratios of $\tilde{\tau}_1$ decays into $\tau \tilde{\chi}_1^0$, $\tau \tilde{\chi}_2^0$, and $\nu_\tau \tilde{\chi}_1^-$ as a function of $\cos \theta_{\tilde{\tau}}$ for $m_{\tilde{\tau}_1} = 90$ GeV and $\tan \beta = 40$ for the scenarios pt5, pt6, pt7, and pt8 of Tab. 4.1. As in the case of \tilde{b}_1 decays we have taken the same sign for $\cos \theta_{\tilde{\tau}}$ and μ in order to avoid unnatural large values for A_τ . The branching ratio $BR(\tilde{\tau}_1 \rightarrow \tau \tilde{\chi}_1^0)$ is always larger than 50% and it is nearly 100%

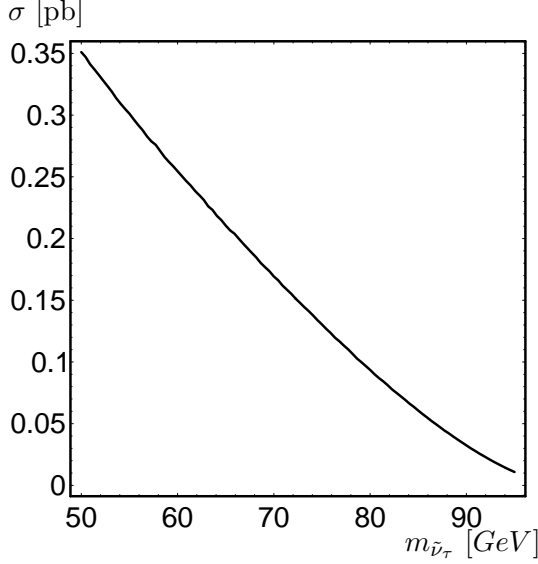


Fig. 4.15: Total cross section for $e^+e^- \rightarrow \tilde{\nu}_\tau \bar{\tilde{\nu}}_\tau$ in pb at $\sqrt{s} = 200$ GeV as a function of $m_{\tilde{\nu}_\tau}$. ISR-corrections are included.

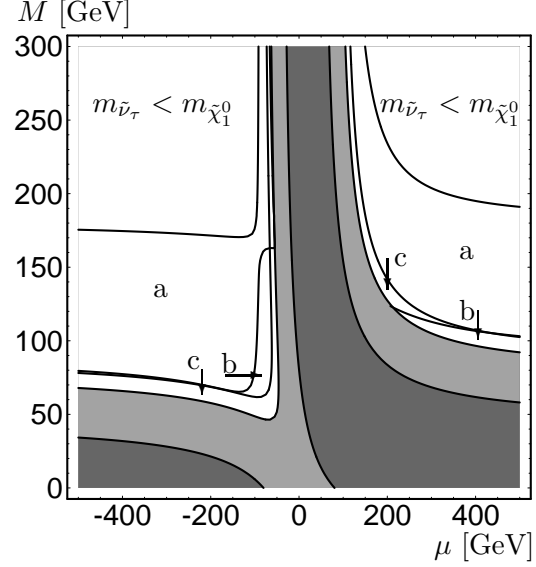


Fig. 4.16: Kinematically allowed parameter domains in the (M, μ) $m_{\tilde{\nu}_\tau} = 90$ GeV and $\tan \beta = 1.5$ for the decays: a) $\tilde{\nu}_\tau \rightarrow \nu_\tau \tilde{\chi}_1^0$, b) $\tilde{\nu}_\tau \rightarrow \nu_\tau \tilde{\chi}_2^0$ and c) $\tilde{\nu}_\tau \rightarrow \tau \tilde{\chi}_1^+$. The dark grey area is excluded by LEP1 and the bright grey area is excluded by LEP1.5 ($\sqrt{s} = 170$ GeV, $m_{\tilde{\nu}_e} = 90$ GeV).

for $\cos \theta_{\tilde{\tau}} \sim 0$ if the neutralinos and the lighter chargino are mainly gauginos (pt5). In contrast, $BR(\tilde{\tau}_1 \rightarrow \nu_\tau \tilde{\chi}_1^-)$ is larger for smaller $\cos \theta_{\tilde{\tau}}$ if the lighter chargino is mainly a higgsino (Fig. 4.14c). In the case that the gaugino- and the higgsino-content of the chargino are of the same order there is less dependence of the branching ratio on $\cos \theta_{\tilde{\tau}}$ (Fig. 4.14b and d).

OPAL has studied stau search at LEP2 for the case $m_{\tilde{\tau}_R} \ll m_{\tilde{\tau}_L}$ [56]. At $\sqrt{s} = 190$ GeV and for $\mathcal{L} = 300 \text{ pb}^{-1}$ they obtained a 5σ detectability for $m_{\tilde{\tau}_R} \simeq 70$ to 80 GeV for neutralino masses in the range between 20 and 72 GeV. However, they have not considered the interesting case of $\tilde{\tau}_R$ - $\tilde{\tau}_L$ mixing.

4.4 Tau Sneutrino

In Fig. 4.15 we show the production cross section $e^+e^- \rightarrow \tilde{\nu}_\tau \bar{\tilde{\nu}}_\tau$ as a function of $m_{\tilde{\nu}_\tau}$ for $\sqrt{s} = 200$ GeV (ISR corrections are included). For $m_{\tilde{\nu}_\tau} = 80$ (50) GeV the cross section is 0.094 (0.35) pb leading to 28 (105) events per year for an integrated luminosity of 300 pb^{-1} .

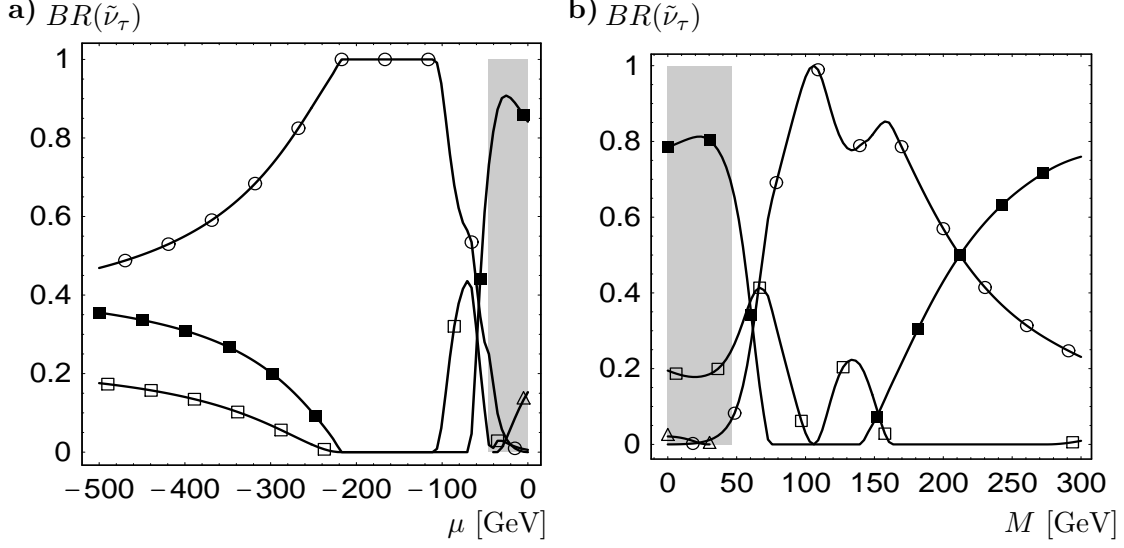


Fig. 4.17: Branching ratios for the decays of the tau sneutrino for $\tan\beta = 1.5$ and $m_{\tilde{\nu}_\tau} = 90$ GeV. In Fig. a we show the branching ratios as a function of μ for $M = 70$ GeV. In Fig. b we show the branching ratios as a function of M for $\mu = -64.9$ GeV. The curves correspond to the following transitions: $\circ \tilde{\nu}_\tau \rightarrow \nu_\tau \tilde{\chi}_1^0$, $\square \tilde{\nu}_\tau \rightarrow \nu_\tau \tilde{\chi}_2^0$ and $\blacksquare \tilde{\nu}_\tau \rightarrow \tau \tilde{\chi}_1^+$. The grey area is excluded by LEP1.5 ($\sqrt{s} = 170$ GeV, $m_{\tilde{\nu}_e} = 90$ GeV).

In the case that only the invisible decay $\tilde{\nu}_\tau \rightarrow \nu_\tau \tilde{\chi}_1^0$ is possible the signature is a single photon + \cancel{E} , the photon coming from the incoming electron or positron. The main background is single photon production stemming from $e^+e^- \rightarrow \nu\bar{\nu}\gamma$. The probability for this process is several magnitudes higher than that for sneutrino production. Therefore, it seems not to be clear if the signal for sneutrino production can be extracted in this case. If $\tilde{\nu}_\tau$ decays into $\nu_\tau \tilde{\chi}_2^0$ or $\tau \tilde{\chi}_1^+$ the signature is charged leptons and/or jets + \cancel{E} , a single τ + leptons and/or jets + \cancel{E} , or 2 τ + leptons and/or jets. Note, that these signatures are similar to that of neutralino production. However, a study of the differential cross sections should clarify the situation, because sneutrinos have a $\sin^2\theta$ angular distribution whereas neutralinos have a $E^2(1 + \cos^2\theta) + m_{\tilde{\chi}_i^0}^2 \sin^2\theta$ angular distribution due to their different spins. Here $\cos\theta$ is the angle between the e^- beam and the outgoing sneutrino or neutralino. In the case that $\tilde{\nu}_\tau \rightarrow \tau \tilde{\chi}_1^+$ is allowed, the breaking of lepton universality gives a clear distinction. As an example the domains of the various decays in the (M, μ) plane are shown in Fig. 4.16 for $m_{\tilde{\nu}_\tau} = 90$ GeV and $\tan\beta = 1.5$.

In Fig. 4.17 we show the branching ratios of the various sneutrino decays for $m_{\tilde{\nu}_\tau} = 90$ GeV and $\tan\beta = 1.5$. In Fig. 4.17a we show the branching ratios as a function of μ for $M = 70.0$ GeV. Here the invisible decay into $\nu_\tau \tilde{\chi}_1^0$ is the most important one. However for $\mu \lesssim -350$ GeV the sum of the cascade decays is at least as important as the invisible decay leading to $\sim 50\%$ one-sided events. In

the case that $M \sim |\mu|$ the branching ratios depend strongly on μ . With increasing $|\mu|$ the number of one-sided events increases until $\mu \lesssim -100$ GeV where $\tilde{\nu}_\tau$ decays completely invisibly. In Fig. 4.17b the branching ratios are shown as a function of M for $\mu = -64.9$ GeV. In the range $70 \text{ GeV} \lesssim M \lesssim 200 \text{ GeV}$ the sneutrino mainly decays invisibly. In the other parameter range the decay into $\tau \tilde{\chi}_1^+$ becomes important and even dominant while the decay into $\tilde{\chi}_2^0$ can be important for $M \lesssim 150$ GeV. Especially for $M \gg |\mu|$ the main signatures are one or two τ + additional leptons and/or jets + \cancel{E} .

Chapter 5

Production of sfermions at a Linear Collider

In this chapter we systematically present the production cross sections of the various sfermions. The formulae for these processes including ISR- and SUSY-QCD corrections are given in Appendix C [52, 53]. In the following examples these corrections will be included. A Linear Collider will most likely offer the possibility of polarized beams. As will be shown, beam polarization is an important tool for the determination of $\cos^2 \theta_{\tilde{f}}$ from the measurement of the production cross sections. Conservative assumptions for the expected luminosities are: 10 fb^{-1} for $\sqrt{s} = 0.5 \text{ TeV}$, 100 fb^{-1} for $\sqrt{s} = 1 \text{ TeV}$ and 2 TeV [59].

In Fig. 5.1 the total cross section for $e^+e^- \rightarrow \tilde{\nu}_\tau \bar{\tilde{\nu}}_\tau$ is shown as a function of $m_{\tilde{\nu}_\tau}$ for a) $\sqrt{s} = 500 \text{ GeV}$ and b) $\sqrt{s} = 2 \text{ TeV}$, for unpolarized, left polarized and right polarized e^- beams. The ratio $\sigma_L : \sigma_U : \sigma_R$ is given by $2L_e^2 : (L_e^2 + R_e^2) : 2R_e^2 \simeq 1.16 : 1 : 0.84$. Here L, U and R denote left-polarized, unpolarized and right-polarized respectively, $L_e = -1/2 + \sin^2 \theta_W$ and $R_e = \sin^2 \theta_W$. This ratio is independent of the underlying parameters at tree level (and even when ISR corrections are included), because the $\tilde{\nu}_\tau$ is a pure left state in the MSSM. Therefore, a deviation from this ratio is a clear hint for the existence of a right sneutrino and/or a mixing with other sneutrinos.

In Fig. 5.2a the total cross section $e^+e^- \rightarrow \tilde{\tau}_1 \bar{\tilde{\tau}}_1$ is shown as a function of $\cos \theta_{\tilde{\tau}}$ for $\sqrt{s} = 500 \text{ GeV}$ and several stau masses. For unpolarized beams and $m_{\tilde{\tau}_1} \gtrsim 150 \text{ GeV}$ the dependence on the mixing angle is rather weak. The dependence is much stronger if a polarized electron beam is available as can be seen in Fig. 5.2b. It is important to note that this dependence is opposite for left and right polarization. In particular the quantity

$$\sigma(\tilde{\tau}_1)_{LR} \equiv \sigma(e^+e^-_L \rightarrow \tilde{\tau}_1 \bar{\tilde{\tau}}_1) - \sigma(e^+e^-_R \rightarrow \tilde{\tau}_1 \bar{\tilde{\tau}}_1) \quad (5.1)$$

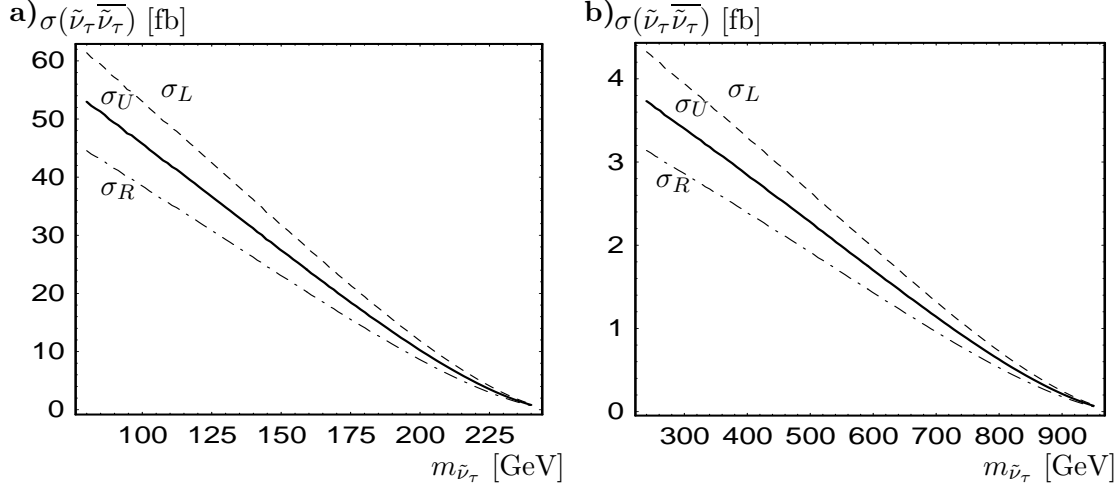


Fig. 5.1: Total cross section $\sigma(e^+e^- \rightarrow \tilde{\nu}_\tau \bar{\tilde{\nu}}_\tau)$ in fb as a function of $m_{\tilde{\nu}_\tau}$ for unpolarized e^- (σ_U , full line), left polarized e^- (σ_L , dashed line), right polarized e^- (σ_R , dashed dotted line), a) $\sqrt{s} = 500$ GeV; b) $\sqrt{s} = 2$ TeV. ISR-corrections are included.

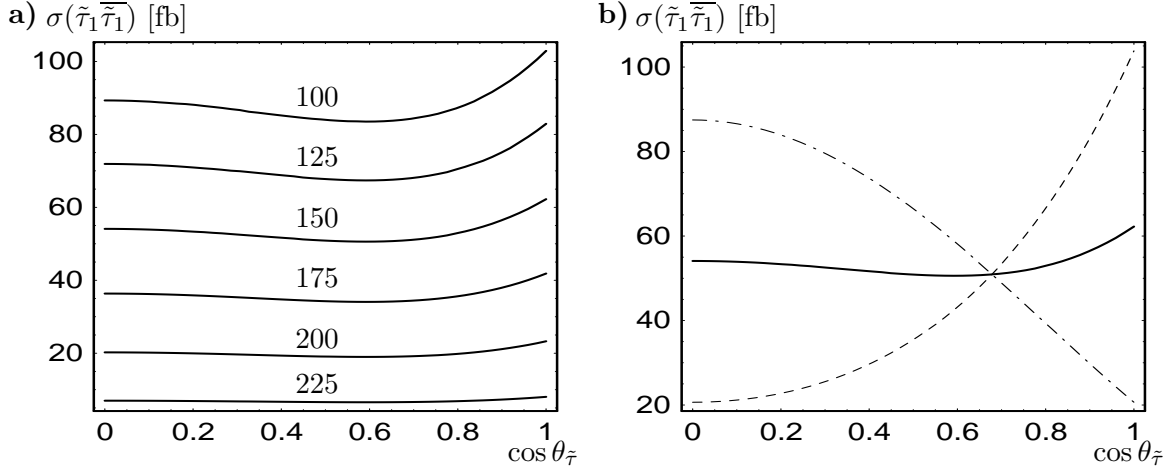


Fig. 5.2: Total cross section $\sigma(e^+e^- \rightarrow \tilde{\tau}_1 \bar{\tilde{\tau}}_1)$ in fb as a function of $\cos \theta_{\tilde{\tau}}$ for $\sqrt{s} = 500$ GeV; a) unpolarized e^- and various $m_{\tilde{\tau}_1}$: 100, 125, 150, 175, 200, and 225 GeV; b) unpolarized e^- (full line), left polarized e^- (dashed line), right polarized e^- (dashed dotted line), for $m_{\tilde{\tau}_1} = 150$ GeV. ISR-corrections are included.

shows a strong dependence on $\cos \theta_{\tilde{\tau}}$ (see also [60]). Here e_L^- (e_R^-) denotes a left-polarized (right-polarized) electron. Note, that the sign of $\cos \theta_{\tilde{\tau}}$ can not be determined, because the cross section depends on $\cos^2 \theta_{\tilde{\tau}}$ (see Eq. (C.1) and (C.5)).

In Fig. 5.3a the total cross section $\sigma(e^+e^- \rightarrow \tilde{\tau}_2 \bar{\tilde{\tau}}_2)$ is shown as a function of $\cos \theta_{\tilde{\tau}}$ for $\sqrt{s} = 2$ TeV and several stau masses. Concerning the dependence on the mixing angle the situation is obviously similar to the case of $\tilde{\tau}_1$ pair production: there is hardly any dependence on $\cos \theta_{\tilde{\tau}}$ for $m_{\tilde{\tau}_2} \gtrsim 700$ GeV and unpolarized electrons.

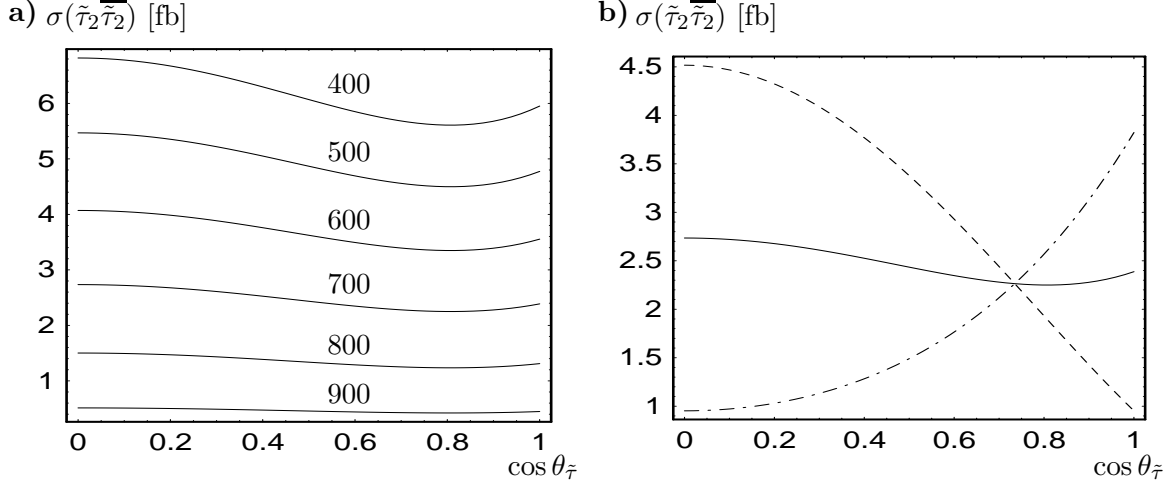


Fig. 5.3: Total cross section $\sigma(e^+e^- \rightarrow \tilde{\tau}_2 \bar{\tilde{\tau}}_2)$ in fb as a function of $\cos \theta_{\tilde{\tau}}$ for $\sqrt{s} = 2$ TeV; a) unpolarized e^- and various $m_{\tilde{\tau}_2}$: 400, 500, 600, 700, 800, and 900 GeV; b) unpolarized e^- (full line), left polarized e^- (dashed line), right polarized e^- (dashed dotted line), for $m_{\tilde{\tau}_2} = 700$ GeV. ISR-corrections are included.

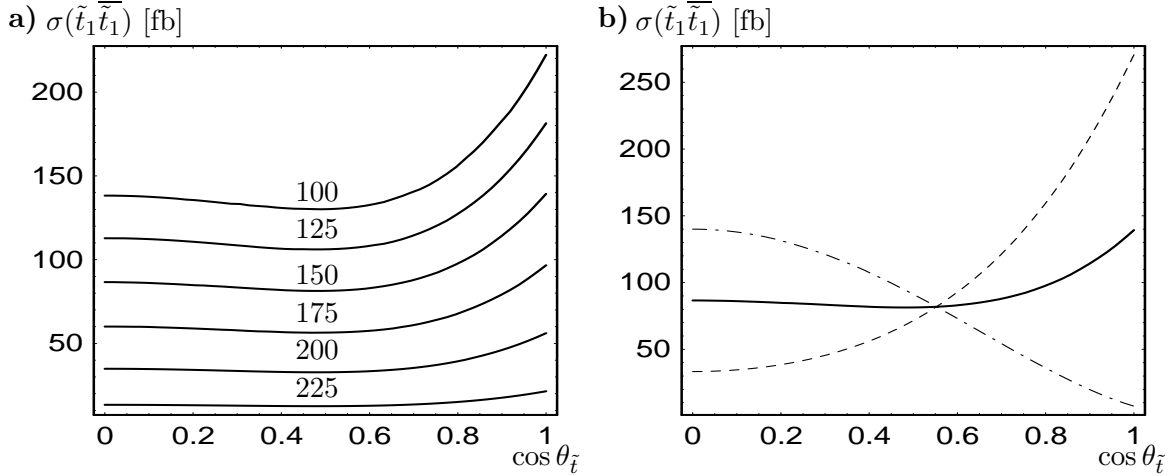


Fig. 5.4: Total cross section $\sigma(e^+e^- \rightarrow \tilde{t}_1 \bar{\tilde{t}}_1)$ in fb as a function of $\cos \theta_{\tilde{t}}$ for $\sqrt{s} = 500$ GeV; a) unpolarized e^- and various $m_{\tilde{t}_1}$: 100, 125, 150, 175, 200, and 225 GeV; b) unpolarized e^- (full line), left polarized e^- (dashed line), right polarized e^- (dashed dotted line), for $m_{\tilde{t}_1} = 150$ GeV. ISR- and SUSY-QCD corrections are included ($m_{\tilde{g}} = 825$ GeV, $m_{\tilde{t}_2} = 400$ GeV).

Again the dependence is much stronger if a polarized electron beam can be used as demonstrated in Fig. 5.3b. In principal also the processes $e^+e^- \rightarrow \tilde{\tau}_1 \bar{\tilde{\tau}}_2$, $\bar{\tilde{\tau}}_1 \tilde{\tau}_2$ are possible. It turns out that the corresponding cross sections are rather small. We get for

example $\sigma = 1.3$ fb for $\sqrt{s} = 1$ TeV, $m_{\tilde{\tau}_1} = 250$ GeV, $m_{\tilde{\tau}_2} = 400$ GeV and $\cos \theta_{\tilde{\tau}} = 1/\sqrt{2}$. Therefore, we do not show the cross section in an extra figure. However, one can take as a guideline $\sigma(e^+e^- \rightarrow \tilde{\tau}_1\tilde{\tau}_2 + \tilde{\tau}_1\tilde{\tau}_2) \simeq \sigma(e^+e^- \rightarrow \tilde{t}_1\tilde{t}_2 + \tilde{t}_1\tilde{t}_2)/3$ for the results presented in Fig. 5.5.

In Fig. 5.4a the total cross section for the process $e^+e^- \rightarrow \tilde{t}_1\tilde{t}_1$ at $\sqrt{s} = 500$ GeV is shown for various stop masses. For the calculation of the SUSY-QCD corrections we have assumed $m_{\tilde{t}_2} = 400$ GeV. The cross section can reach 220 fb for $m_{\tilde{t}_1} = 100$ GeV and $\cos \theta_{\tilde{t}} = 1$. There is a strong dependence on $\cos \theta_{\tilde{t}}$ if $\cos \theta_{\tilde{t}} \gtrsim 0.6$. As already mentioned in the case of stau production the dependence on $\cos \theta_{\tilde{t}}$ is stronger if polarized e^- -beams are used. This can be seen in Fig. 5.4b where the cross section is shown for various beam polarizations. The quantity $\sigma_{LR}(\tilde{t}_1)$ varies from -117 fb ($\cos \theta_{\tilde{t}} = 0$) to 250 fb ($\cos \theta_{\tilde{t}} = 1$).

In Fig. 5.5 the cross section $e^+e^- \rightarrow \tilde{t}_1\tilde{t}_2 + \tilde{t}_1\tilde{t}_2$ is shown as a function of $\cos \theta_{\tilde{t}}$ for $\sqrt{s} = 1$ TeV, $m_{\tilde{t}_1} = 250$ GeV and various \tilde{t}_2 masses. For the calculation of the SUSY-QCD corrections we have taken $m_{\tilde{g}} = 755$ GeV. For this process only the Z -exchange contributes at tree-level. The cross section has its maximum at $\cos \theta_{\tilde{t}} = 1/\sqrt{2} \simeq 0.71$ because the $Z\tilde{t}_1\tilde{t}_2$ coupling is proportional to $\sin 2\theta_{\tilde{t}}$. Note, that this cross section is rather small even at its maximum compared to $\tilde{t}_1\tilde{t}_1$ and $\tilde{t}_2\tilde{t}_2$ production: $\sigma(e^+e^- \rightarrow \tilde{t}_1\tilde{t}_1) = 29.3$ fb, $\sigma(e^+e^- \rightarrow \tilde{t}_1\tilde{t}_2 + \tilde{t}_1\tilde{t}_2) = 4.8$ fb and $\sigma(e^+e^- \rightarrow \tilde{t}_2\tilde{t}_2) = 8.9$ fb for $\sqrt{s} = 1$ TeV, $m_{\tilde{t}_1} = 250$ GeV, $m_{\tilde{t}_2} = 400$ GeV and $\cos \theta_{\tilde{t}} = 1/\sqrt{2}$. Therefore, this process is mainly of interest for the case that only $\tilde{t}_1\tilde{t}_1$ can be produced at a given energy but not $\tilde{t}_2\tilde{t}_2$. Assuming an integrated luminosity of 50 fb^{-1} and that ~ 100 stop pairs are needed for a successful detection, one can probe \tilde{t}_2 masses up to ~ 550 GeV in our example if the mixing is maximal. Beam polarization changes the cross section in the following way: $\sigma(e^+e_L^-) : \sigma(e^+e_U^-) : \sigma(e^+e_R^-) = (2L_e^2) : (L_e^2 + R_e^2) : (2R_e^2)$ as in the case of sneutrino production.

In Fig. 5.6a the total cross section $\sigma(e^+e^- \rightarrow \tilde{t}_2\tilde{t}_2)$ is shown as a function of $\cos \theta_{\tilde{t}}$ for $\sqrt{s} = 2$ TeV. For the calculation of the SUSY-QCD corrections we have assumed $m_{\tilde{t}_1} = 300$ GeV and $m_{\tilde{g}} = 693$ GeV. The total cross section goes up to ~ 14 fb

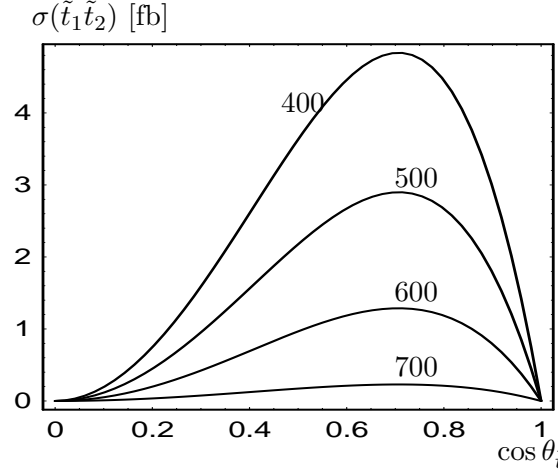


Fig. 5.5: Total cross section $e^+e^- \rightarrow \tilde{t}_1\tilde{t}_2$ in fb as a function of $\cos \theta_{\tilde{t}}$ for $\sqrt{s} = 1$ TeV, $m_{\tilde{t}_1} = 250$ GeV and various \tilde{t}_2 masses: 400 GeV, 500 GeV, 600 GeV and 700 GeV. ISR- and SUSY-QCD corrections are included ($m_{\tilde{g}} = 755$ GeV).

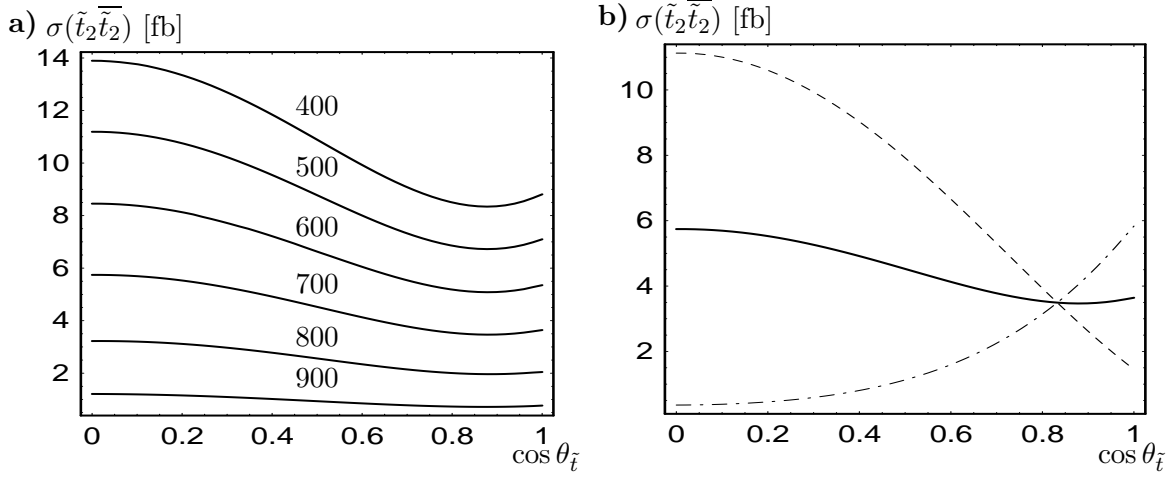


Fig. 5.6: Total cross section $\sigma(e^+e^- \rightarrow \tilde{t}_2 \bar{\tilde{t}}_2)$ in fb as a function of $\cos \theta_{\tilde{t}}$ for $\sqrt{s} = 2$ TeV; a) unpolarized e^- and various \tilde{t}_2 masses (in GeV): 400, 500, 600, 700, 800, and 900; b) unpolarized e^- (full line), left polarized e^- (dashed line), right polarized e^- (dashed dotted line), for $m_{\tilde{t}_2} = 700$ GeV. ISR- and SUSY-QCD corrections are included ($m_{\tilde{t}_1} = 300$ GeV and $m_{\tilde{g}} = 693$ GeV).

for $m_{\tilde{t}_2} = 400$ GeV and $\cos \theta_{\tilde{t}} = 0$. Even for $m_{\tilde{t}_2} = 900$ GeV it can reach 1.7 fb if $\cos \theta_{\tilde{t}} = 0$. This corresponds to 340 produced \tilde{t}_2 pairs for an integrated luminosity of 200 fb^{-1} . As in the case of $\tilde{t}_1 \bar{\tilde{t}}_1$ production the quantity $\sigma_{LR}(\tilde{t}_2)$ shows the strongest dependence on $\cos \theta_{\tilde{t}}$ as can be seen in Fig. 5.6b. Here the production cross section is shown for $m_{\tilde{t}_2} = 700$ GeV and polarized e^- beams.

In Fig. 5.7a we present the total cross section for the process $e^+e^- \rightarrow \tilde{b}_1 \bar{\tilde{b}}_1$ for $\sqrt{s} = 500$ GeV and various sbottom masses. For the SUSY-QCD corrections we have taken $m_{\tilde{b}_2} = 400$ GeV and $m_{\tilde{g}} = 825$ GeV. The cross section can reach 155 fb for $m_{\tilde{b}_1} = 100$ GeV and $\cos \theta_{\tilde{b}} = 1$. The dependence on $\cos \theta_{\tilde{b}}$ is similar to the \tilde{t}_1 and $\tilde{\tau}_1$ cases: i) there is hardly any dependence for $\cos \theta_{\tilde{b}} \lesssim 0.6$ and ii) there is a clear dependence for polarized beams (Fig. 5.7b).

In Fig. 5.8a the total cross section for $e^+e^- \rightarrow \tilde{b}_2 \bar{\tilde{b}}_2$ is shown as a function of $\cos \theta_{\tilde{b}}$ for $\sqrt{s} = 2$ TeV. For the calculation of the SUSY-QCD corrections we have taken $m_{\tilde{b}_1} = 300$ GeV and $m_{\tilde{g}} = 693$ GeV. The cross section can reach up to ~ 9.5 fb if $\tilde{b}_2 = \tilde{b}_R$ and $m_{\tilde{t}_2} = 400$ GeV. Even for $m_{\tilde{b}_2} = 900$ GeV it can reach 0.9 fb corresponding to 180 produced \tilde{b}_2 pairs for an integrated luminosity of 200 fb^{-1} . As in the previous cases the quantity $\sigma_{LR}(\tilde{b}_2)$ shows the strongest dependence on $\cos \theta_{\tilde{b}}$ as can be seen in Fig. 5.8b. Here the production cross section is shown for $m_{\tilde{b}_2} = 700$ GeV and polarized e^- beams.

As in the case of the stops the processes $e^+e^- \rightarrow \tilde{b}_1 \bar{\tilde{b}}_2, \bar{\tilde{b}}_1 \tilde{b}_2$ are possible. The results are very similar to the stop case (Fig. 5.5). The only differences come from SUSY-QCD corrections which are of $O(0.1\%)$.

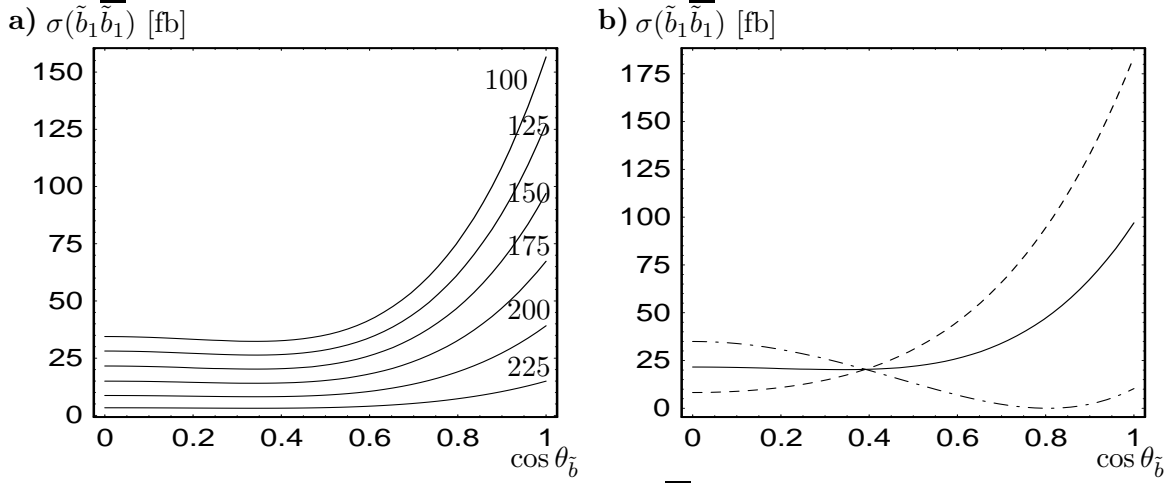


Fig. 5.7: Total cross section $\sigma(e^+e^- \rightarrow \tilde{b}_1 \bar{\tilde{b}}_1)$ in fb as a function of $\cos \theta_{\tilde{b}}$ for $\sqrt{s} = 500$ GeV; a) unpolarized e^- and various $m_{\tilde{b}_1}$: 100, 125, 150, 175, 200, and 225 GeV; b) unpolarized e^- (full line), left polarized e^- (dashed line), right polarized e^- (dashed dotted line), for $m_{\tilde{b}_1} = 150$ GeV. ISR- and SUSY-QCD corrections are included ($m_{\tilde{g}} = 825$ GeV, $m_{\tilde{b}_2} = 400$ GeV).

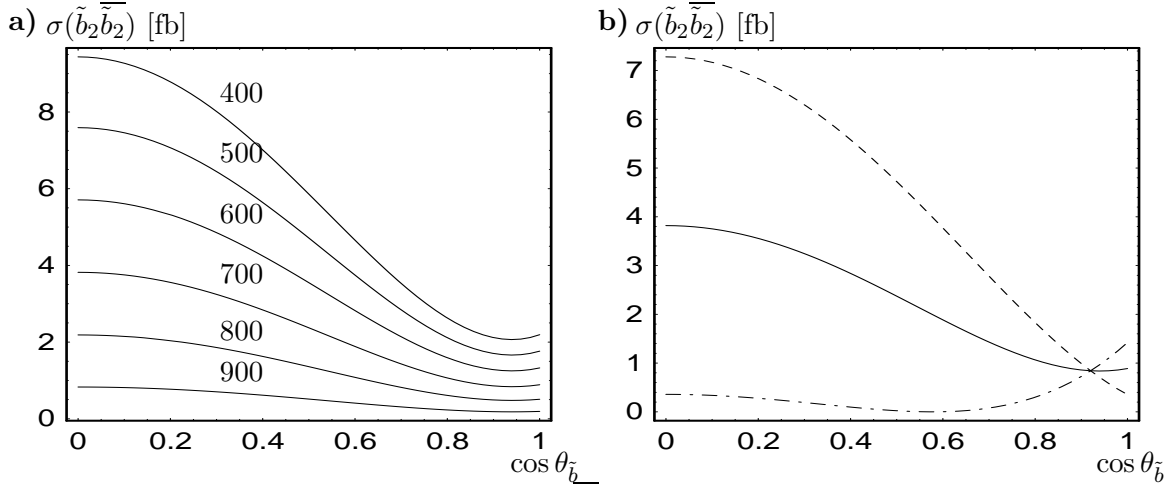


Fig. 5.8: Total cross section $\sigma(e^+e^- \rightarrow \tilde{b}_2 \bar{\tilde{b}}_2)$ in fb as a function of $\cos \theta_{\tilde{b}}$ for $\sqrt{s} = 2$ TeV; a) unpolarized e^- and various $m_{\tilde{b}_2}$: 400 GeV, 500 GeV, 600 GeV, 700 GeV, 800 GeV and 900 GeV; b) unpolarized e^- (full line), left polarized e^- (dashed line), right polarized e^- (dashed dotted line), for $m_{\tilde{b}_2} = 700$ GeV. ISR- and SUSY-QCD corrections are included ($m_{\tilde{b}_1} = 300$ GeV and $m_{\tilde{g}} = 693$ GeV).

Chapter 6

Masses and mixing angles

6.1 Outlook on the following chapters

In the following chapters we discuss the phenomenology of the various sfermions at colliders where sfermion masses can be probed up to the TeV range, for example the LHC or a future Linear Collider. Sfermions in that mass range cannot only decay into fermions but also in another sfermion plus either a gauge boson or a Higgs boson. We have seen in Chapter 4 that the mixing between left and right sfermions strongly influences the fermionic decay modes. As we will demonstrate in the next chapters this is also true for the bosonic decay modes.

As it is shown in Appendix B there are relations between sfermion masses and mixing angles. Therefore, we will change our strategy and use the soft SUSY breaking parameters as input for the discussion of the decays instead of the physical quantities. Let us shortly review underlying parameters for the masses and mixing angles:

- sleptons: $M_E, M_L, A_\tau, \tan \beta$ and μ
- squarks: $M_D, M_Q, M_U, A_b, A_t, \tan \beta$ and μ
- gluino: $m_{\tilde{g}}$
- charginos and neutralinos: M', M, μ and $\tan \beta$
- Higgs bosons: m_{A^0} and $\tan \beta$. The squark parameters also enter the mass matrix due to radiative corrections.

Even for a detailed discussion it is not necessary to study the dependence on all 14 parameters. Therefore, we fix $M = 350$ GeV and use the GUT relations to compute M' and $m_{\tilde{g}}$ as stated in Chapter 2. We choose $m_{A^0} = 150$ GeV so that the decays into Higgs bosons are kinematically possible. We further assume $A_b = A_t = A_\tau$.

Moreover, we have chosen three $(M_D, M_Q, M_U; M_E, M_L)$ sets: $(700, 700, 700; 700, 700)$, $(980, 350, 700; 350, 700)$ and $(500, 500, 700; 980, 700)$. At first glance one may ask how strongly the squark parameters influence the slepton phenomenology due to the radiative correction on the Higgs masses and the mixing angle. Here we want to note first, that also A_b , A_t , μ and $\tan\beta$ enter these corrections so that there are seven input parameters for the four physical quantities m_{h^0} , m_{H^0} , $\cos\alpha$, and m_{H^\pm} . Therefore, the resulting Higgs masses and Higgs mixing angle can be seen as typical examples independent of the specific input parameters if one studies the phenomenology of the sleptons. We have explicitly checked, that a variation of M_D , M_Q and/or M_U does not change the general features of slepton decays into Higgs bosons.

In the remaining sections of this chapter we present the results for the various masses and mixing angles as needed for the following chapters. In the next chapter we start with the discussion of slepton phenomenology. Here the situation is easier, because there are fewer parameters compared to the squark sector. Afterwards the results for stops and sbottoms will be presented. As implicitly mentioned above we study the cases $M_E < M_L$, $M_E = M_L$, $M_D = M_Q = M_U$, $M_U < M_Q < M_D$ and $M_D = M_U < M_Q$. Here results from the study of renormalization group equations in supergravity models [18, 22] and models with gauge mediated SUSY breaking [58] have served as guidelines for the ordering of the masses. The only exception is the case $M_E > M_L$. It has been included to study the phenomenology if SUSY is realized and broken in a different way than proposed in those models. Examples are models with additional gauge bosons [61].

6.2 Masses and mixing angles of staus and sbottoms

We treat the masses and the mixing angles of staus and sbottoms together because their mass matrices have the same structure including their $\tan\beta$ dependence (see Eq. (2.33)).

In Fig. 6.1 we show $m_{\tilde{\tau}_1}$, $m_{\tilde{\tau}_2}$, and $\cos\theta_{\tilde{\tau}}$ as function of μ . We fix $M_L = 700$ GeV and choose three different M_E values: 700 GeV (full line), 350 GeV (dashed line), and 980 GeV (dashed dotted line). In Fig. 6.1a $m_{\tilde{\tau}_{1,2}}$ are shown for $\tan\beta = 1.5$ and $A_\tau = 500$ GeV. Clearly the masses are mainly determined by M_E and M_L in this case, because the off-diagonal element $m_\tau(A_\tau - \mu \tan\beta)$ is rather small compared to $M_{E,L}^2$. Nevertheless this mixing term can lead to a strong mixing for $M_E \sim M_L$ as can be seen in Fig. 6.1b. The reason for this at first glance surprising effect is that $(M_{\tilde{\tau}_{11}}^2 - m_{\tilde{\tau}_1}^2)^2$ is of the same order as $m_\tau^2(A_\tau - \mu \tan\beta)^2$ (see Eq. (2.36)). Moreover, there is a rather strong dependence of $\cos\theta_{\tilde{\tau}}$ on μ if $\mu \sim A_\tau \cot\beta$ and $M_E \sim M_L$. In the case $M_E = 350$ GeV (980 GeV) $\tilde{\tau}_1$ is nearly $\tilde{\tau}_R$ ($\tilde{\tau}_L$).

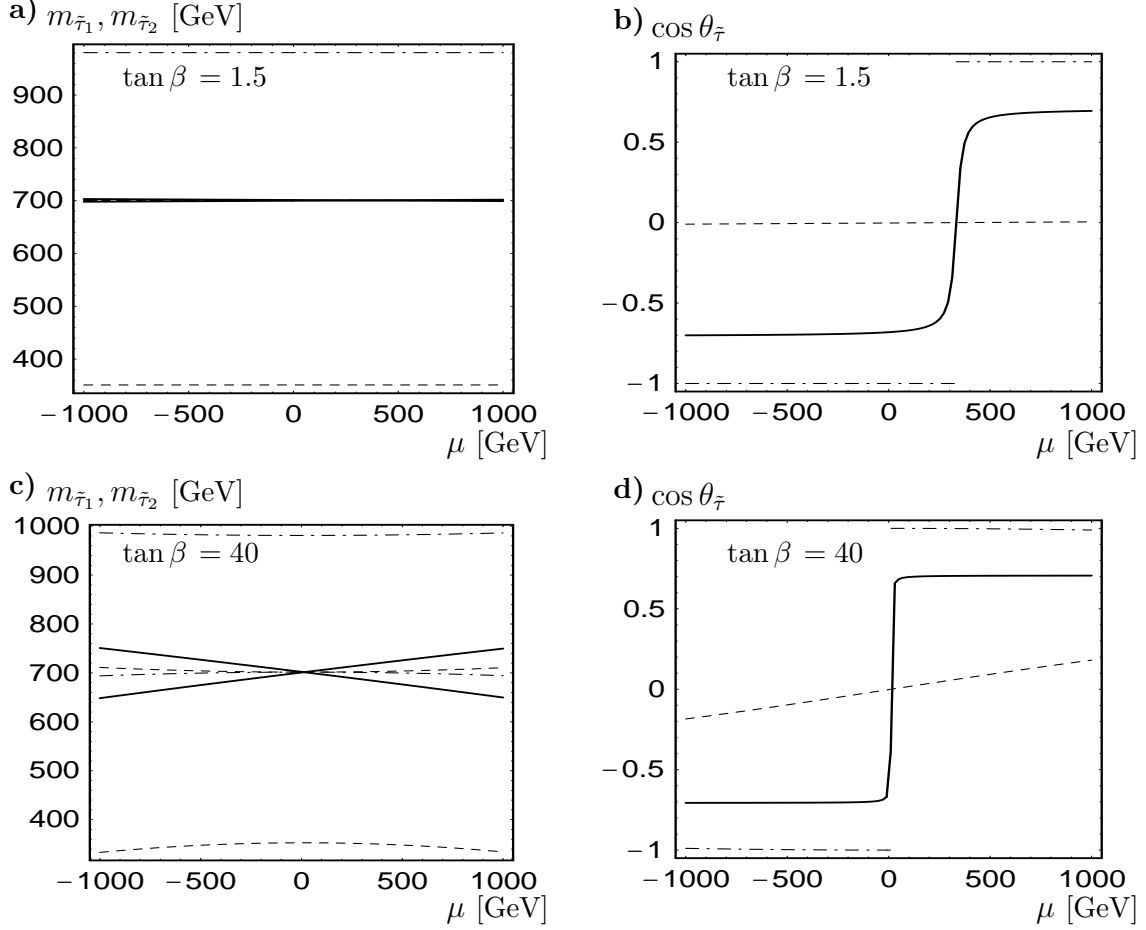


Fig. 6.1: Stau masses (a,c) and mixing angle (b,d) as a function of μ for $A_\tau = 500$ GeV, $\tan \beta = 1.5$ (a,b) and $\tan \beta = 40$ (c,d). The graphs correspond to the following parameter sets (M_E, M_L) (in GeV): (700,700) full line, (350,700) dashed line, and (980,700) dashed-dotted line.

In Fig. 6.1c and 6.1d the μ dependence is shown for $\tan \beta = 40$. The dependence on μ is the stronger the closer M_E and M_L are because then the mass splitting is mainly due to the off diagonal element. Concerning the mixing angle we have again a strong mixing for the case $M_E = M_L$. As in the case of small $\tan \beta$ the lighter mass eigenstate is nearly a right state (left state) if $M_E = 350$ GeV (980 GeV). We have found that the masses are nearly independent of A_τ . The same is true for the mixing angle except the case where $A_\tau \sim \mu \tan \beta$ and at the same time $M_E \sim M_L$.

In Fig. 6.2 we show the masses and mixing angle of the sbottoms. The differences to the stau case are only due to the fact that $m_b \simeq 3m_\tau$. For small $\tan \beta$ the situation is nearly the same except that for the case $M_D = M_Q$ there is a slight

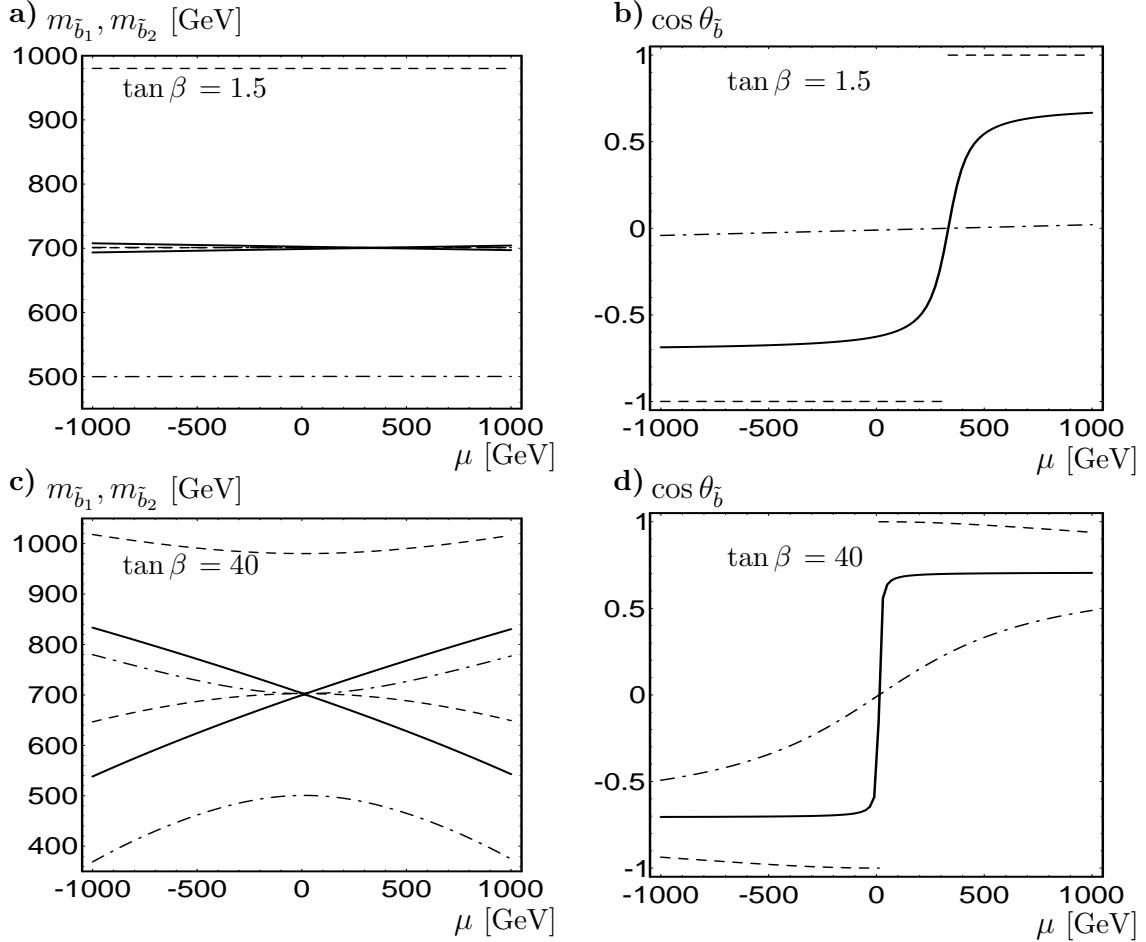


Fig. 6.2: Sbottom masses (a,c) and mixing angle (b,d) as a function of μ for $A_b = 500$ GeV and $\tan \beta = 1.5$ (a,b) ($\tan \beta = 40$ (c,d)). The graphs correspond to the following parameter sets (M_D, M_Q) (in GeV): (700,700) full line, (980,700) dashed line, and (500,700) dashed-dotted line.

visible dependence of μ on the masses. In case of large $\tan \beta$ the dependence on μ is much more pronounced than in the stau case.

6.3 Masses and mixing angles of the stops

The stops differ in two ways from the staus and sbottoms: Firstly, m_t is much larger than m_b or m_τ . Secondly, the off diagonal term in the mass matrix is given by $m_t(A_t - \mu \cot \beta)$. The combination of these two facts leads to a strong dependence of the masses on μ for the case $M_Q = M_U$ and small $\tan \beta$ as can be seen in Fig. 6.3. This is a case of maximal mixing ($\cos \theta_{\tilde{t}} \simeq \pm 1/\sqrt{2}$) except the range where $\mu \simeq A_t \tan \beta$. Clearly the dependence of the masses on μ becomes weaker for larger

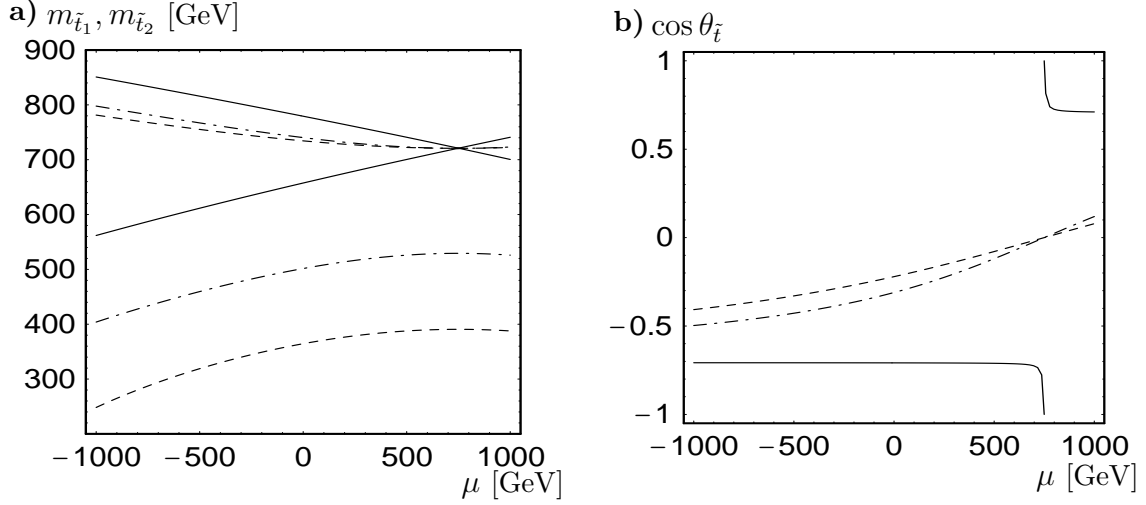


Fig. 6.3: Stop masses (a) and mixing angle (b) as a function of μ for $A_t = 500$ GeV and $\tan \beta = 1.5$. The graphs correspond to the following parameter sets (M_Q, M_U) (in GeV): (700,700) full line, (700,350) dashed line, and (700,500) dashed-dotted line.

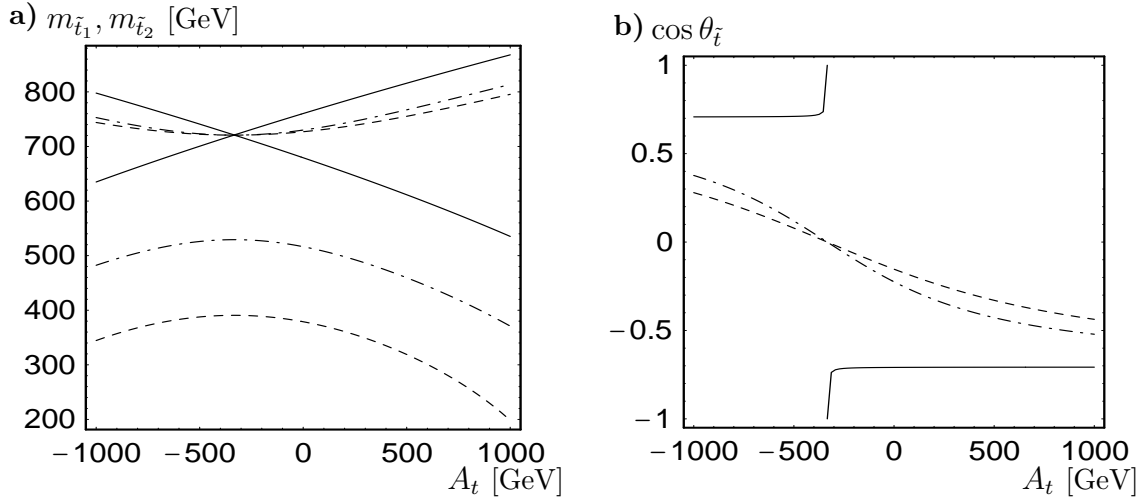


Fig. 6.4: Stop masses (a) and mixing angle (b) as a function of A_t for $\mu = -500$ GeV and $\tan \beta = 1.5$. The graphs correspond to the following parameter sets (M_Q, M_U) (in GeV): (700,700) full line, (700,350) dashed line, and (700,500) dashed-dotted line.

$|M_U^2 - M_Q^2|$. In this case $\cos \theta_{\tilde{t}}$ shows a stronger dependence on μ than in the previous case. Note, that the masses and $\cos \theta_{\tilde{t}}$ depend hardly on μ for large $\tan \beta$.

The masses show also a strong dependence on A_t as it is demonstrated in Fig. 6.4 for the different (M_Q, M_U) sets and small $\tan \beta$. This is also true for $\cos \theta_{\tilde{t}}$ except in the case $M_U \simeq M_Q$. There is still a strong dependence on A_t if $\tan \beta$ increases. The only difference is that the point where the stops are pure left or right eigenstates is shifted towards $A_t = 0$.

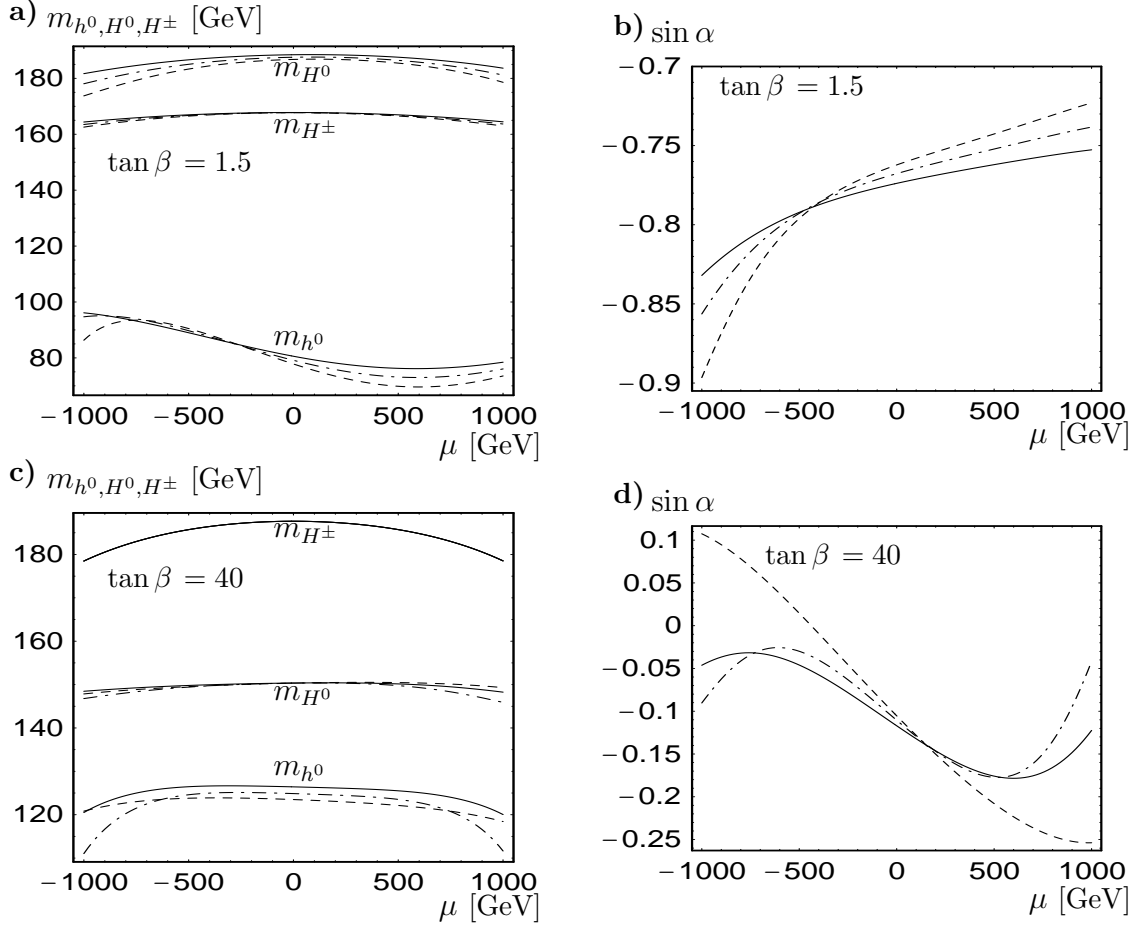


Fig. 6.5: Higgs masses and mixing angle as a function of μ for $A_t = A_b = 500$ GeV, $m_{A^0} = 150$ GeV, a) and c) $\tan \beta = 1.5$, b) and d) $\tan \beta = 40$. In (a,c) we show m_{h^0} , m_{H^0} and m_{H^\pm} , and in (b,d) $\sin \alpha$. Radiative corrections are included, the graphs correspond to the following (M_D, M_Q, M_U) sets (in GeV): (700,700,700) full line, (980,700,350) dashed line, and (500,700,500) dashed-dotted line.

6.4 Higgs masses and mixing angle

Last but not least we present the Higgs masses and the Higgs mixing angle. In Fig. 6.5 the μ dependence is shown. m_{H^\pm} is nearly independent of the ratio of the scalar squark masses as can be seen in Fig. 6.5a and c. In the small $\tan \beta$ case its mass varies between 160 and 166 GeV and is therefore somewhat smaller than its tree level value ($= 170$ GeV). For large $\tan \beta$ the corrections are positive and more important. In this case the mass can be as high as 183 GeV. The same features hold if one varies A_t for fixed μ (Fig. 6.6a and c).

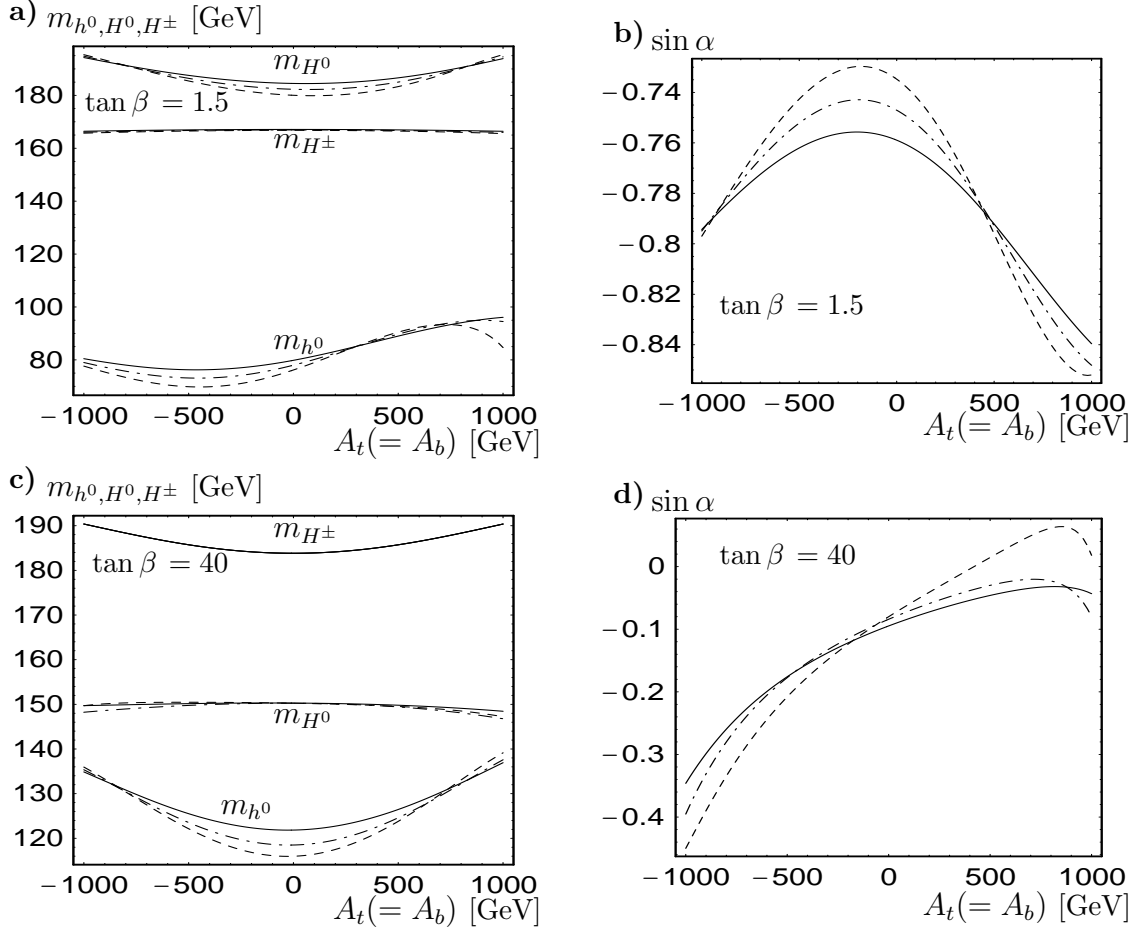


Fig. 6.6: Higgs masses as a function of $A_t = A_b$ for $\mu = -500$ GeV, $m_{A^0} = 150$ GeV, a) and c) $\tan \beta = 1.5$, b) and d) $\tan \beta = 40$. In (a,c) we show m_{h^0} , m_{H^0} and m_{H^\pm} , and in (b,d) $\sin \alpha$. Radiative corrections are included, the graphs correspond to the following (M_D, M_Q, M_U) sets (in GeV): (700,700,700) full line, (980,700,350) dashed line, and (500,700,500) dashed-dotted line.

The masses and the mixing angle of the neutral scalar Higgs bosons depend on the ratio of the scalar squark masses. One finds that with increasing $\tan \beta$ m_{h^0} increases whereas m_{H^0} decreases (Fig. 6.5c and d). m_{H^0} also decreases with increasing $|\mu|$. Note, that $|\sin \alpha|$ is rather small for large $\tan \beta$ implying $\cos \alpha \simeq 1$. These general features hold also if one studies the A_t dependence except for the fact that m_{H^0} is increasing with increasing $|A_t|$ for small $\tan \beta$ (Fig. 6.6a and c).

Chapter 7

Numerical results for sleptons

7.1 Decays of $\tilde{\nu}_\tau$

As mentioned in the previous chapter we start our discussion with the phenomenology of the tau sneutrino because here the fewest parameters enter. In Fig. 7.1 branching ratios for $\tilde{\nu}_\tau$ decays are shown as a function of μ for $M_L = 700$ GeV, $M = 350$ GeV, a) $\tan\beta = 1.5$ and b) $\tan\beta = 40$. Moreover, we have chosen $A_\tau = 500$ GeV and $M_E \geq M_L$ to ensure that the decays $\tilde{\nu}_\tau \rightarrow W^+ \tilde{\tau}_1$ and $\tilde{\nu}_\tau \rightarrow H^+ \tilde{\tau}_1$ are kinematically forbidden. The sneutrino mass is 689.9 GeV (697.0 GeV) if $\tan\beta = 1.5$ (40). In the case of $\tan\beta = 1.5$ the decays into $\tau \tilde{\chi}_1^+$ and $\nu_\tau \tilde{\chi}_2^0$ ($\tau \tilde{\chi}_2^+$ and $\nu_\tau \tilde{\chi}_4^0$) are the most important ones if $M < |\mu|$ ($M > |\mu|$). The reason is that the $\tilde{\nu}_\tau$ couples mainly to the zino and to the wino in such a scenario. The more $\tan\beta$ increases the more the coupling to the charged higgsino becomes important as can be seen in Fig. 7.1b. It is interesting to note that in these examples the branching ratio for the invisible mode $\tilde{\nu}_\tau \rightarrow \nu_\tau \tilde{\chi}_1^0$ is always smaller than 20%, leading to much fewer one side events compared to the examples we have studied for LEP2 (see Fig. 4.17 and the corresponding discussion).

In Fig. 7.2 we study examples where the decays $\tilde{\nu}_\tau \rightarrow W^+ \tilde{\tau}_1$ and $\tilde{\nu}_\tau \rightarrow H^+ \tilde{\tau}_1$ are kinematically allowed. We have fixed $M_E = 350$ GeV, $\tan\beta = 40$, and the other parameters as above. In Fig. 7.2a the branching ratios are shown as a function of μ for $A_\tau = 500$ GeV. The decay $\tilde{\nu}_\tau \rightarrow W^+ \tilde{\tau}_1$ can reach $\sim 34\%$ for $|\mu| \sim 1$ TeV. At first glance this is a surprising fact, because the lighter stau is mainly a right state and therefore the coupling to the W -boson is rather small ($\cos\theta_{\tilde{\tau}} \simeq 2 \cdot 10^{-4} * \mu$ in our example). To understand this, let us compare this decay with $\tilde{\nu}_\tau \rightarrow \tau \tilde{\chi}_1^+$ which is the most important one for $|\mu| = 1$ TeV:

$$\frac{\Gamma(\tilde{\nu}_\tau \rightarrow W^+ \tilde{\tau}_1)}{\Gamma(\tilde{\nu}_\tau \rightarrow \tau \tilde{\chi}_1^+)} \simeq \frac{\cos^2\theta_{\tilde{\tau}} \lambda^{\frac{3}{2}}(m_{\tilde{\nu}_\tau}^2, m_{m_W}^2, m_{m_{\tilde{\tau}_1}}^2)}{V_{11}^2 m_W^2 (m_{\tilde{\nu}_\tau}^2 - m_{\tilde{\chi}_1^+}^2)^2} = \frac{\cos^2\theta_{\tilde{\tau}}}{V_{11}^2} C_1 \quad (7.1)$$

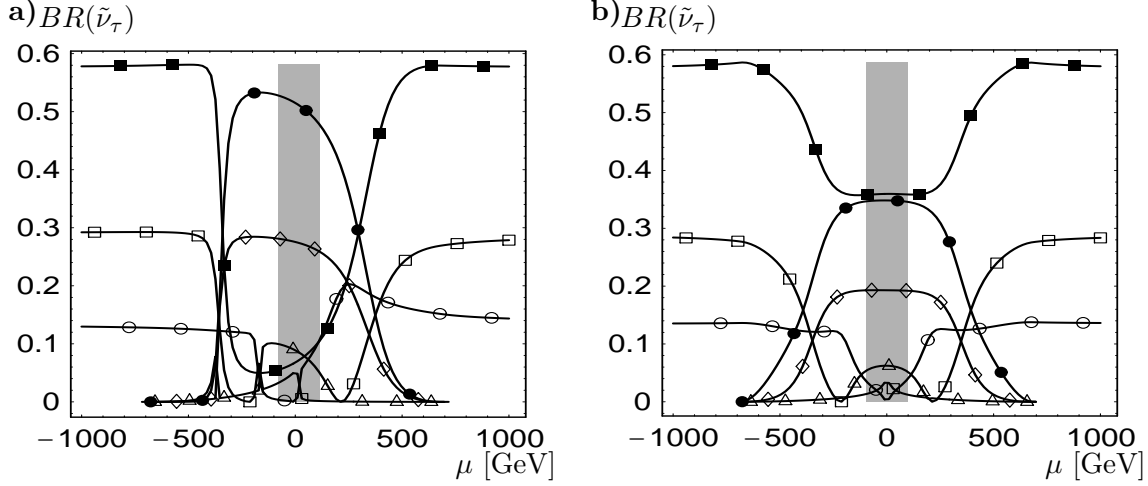


Fig. 7.1: Branching ratios for $\tilde{\nu}_\tau$ decays as a function of μ for $M_L = 700$ GeV, $M = 350$ GeV, a) $\tan \beta = 1.5$ and b) $\tan \beta = 40$. The curves correspond to the transitions: $\circ \tilde{\nu}_\tau \rightarrow \nu_\tau \tilde{\chi}_1^0$, $\square \tilde{\nu}_\tau \rightarrow \nu_\tau \tilde{\chi}_2^0$, $\triangle \tilde{\nu}_\tau \rightarrow \nu_\tau \tilde{\chi}_3^0$, $\diamond \tilde{\nu}_\tau \rightarrow \nu_\tau \tilde{\chi}_4^0$, $\blacksquare \tilde{\nu}_\tau \rightarrow \tau \tilde{\chi}_1^+$, and $\bullet \tilde{\nu}_\tau \rightarrow \tau \tilde{\chi}_2^+$. The grey area will be covered by LEP2 ($m_{\tilde{\chi}_1^\pm} \leq 95$ GeV).

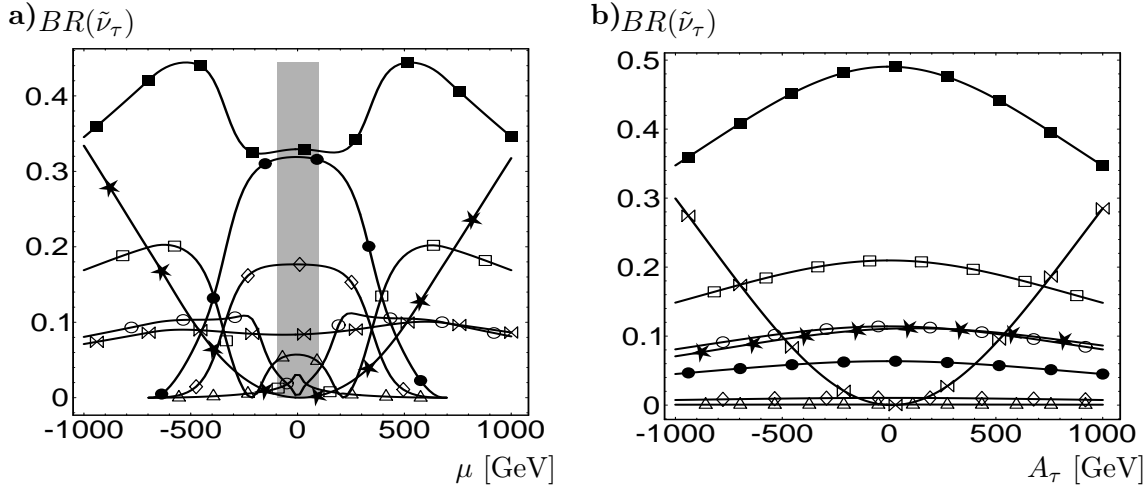


Fig. 7.2: Branching ratios for $\tilde{\nu}_\tau$ decays as a function a) of μ for $A_\tau = 500$ GeV, and b) of A_τ for $\mu = -500$ GeV. The other parameters are $\tan \beta = 40$, $M = 350$ GeV, $M_L = 700$ GeV and $M_E = 350$ GeV. The curves correspond to the transitions: $\circ \tilde{\nu}_\tau \rightarrow \nu_\tau \tilde{\chi}_1^0$, $\square \tilde{\nu}_\tau \rightarrow \nu_\tau \tilde{\chi}_2^0$, $\triangle \tilde{\nu}_\tau \rightarrow \nu_\tau \tilde{\chi}_3^0$, $\diamond \tilde{\nu}_\tau \rightarrow \nu_\tau \tilde{\chi}_4^0$, $\blacksquare \tilde{\nu}_\tau \rightarrow \tau \tilde{\chi}_1^+$, $\bullet \tilde{\nu}_\tau \rightarrow \tau \tilde{\chi}_2^+$, $\star \tilde{\nu}_\tau \rightarrow W^+ \tilde{\tau}_1$, and $\times \tilde{\nu}_\tau \rightarrow H^+ \tilde{\tau}_1$. The grey area will be covered by LEP2 ($m_{\tilde{\chi}_1^\pm} \leq 95$ GeV).

Note that C_1 is ~ 50 for $m_{\tilde{\chi}_1^+} \simeq M = 350$ GeV which is caused by the factor $\lambda(m_{\tilde{\nu}_\tau}^2, m_W^2, m_{\tilde{\tau}_1}^2)/m_W^2$. This factor arises from the derivative in the corresponding part of the interaction Lagrangian (see Eq. (3.1)). Here λ is the kinematic function $\lambda(x, y, z) = (x - y - z)^2 - 4yz$.

Let us now compare the decay into a W^+ with the decay into a H^+ . For $|A_\tau| \gtrsim 50$ GeV and $\cos^2 \theta_{\tilde{\tau}} < 1/2$ the ratio of the two decay widths is approximately given by

$$\begin{aligned} \frac{\Gamma(\tilde{\nu}_\tau \rightarrow W^+ \tilde{\tau}_1)}{\Gamma(\tilde{\nu}_\tau \rightarrow H^+ \tilde{\tau}_1)} &\simeq \frac{\lambda^{\frac{1}{2}}(m_{\tilde{\nu}_\tau}^2, m_{m_W}^2, m_{m_{\tilde{\tau}_1}}^2)}{\lambda^{\frac{1}{2}}(m_{\tilde{\nu}_\tau}^2, m_{m_{H^+}}^2, m_{m_{\tilde{\tau}_1}}^2)} \frac{\cot^2 \theta_{\tilde{\tau}} \lambda(m_{\tilde{\nu}_\tau}^2, m_W^2, m_{\tilde{\tau}_1}^2)}{m_\tau^2 A_\tau^2 \tan^2 \beta} \\ &= C_2 \frac{\cot^2 \theta_{\tilde{\tau}} \lambda(m_{\tilde{\nu}_\tau}^2, m_W^2, m_{\tilde{\tau}_1}^2)}{m_\tau^2 A_\tau^2 \tan^2 \beta} \simeq C_2 \frac{\mu^2 \lambda(m_{\tilde{\nu}_\tau}^2, m_W^2, m_{\tilde{\tau}_1}^2)}{A_\tau^2 (M_L^2 - m_{\tilde{\tau}_1}^2)^2} \quad (7.2) \end{aligned}$$

where $C_2 \simeq 1.07$ for the examples shown in Fig. 7.2. Especially the last relation of Eq. (7.2) explains the relative importance of $\tilde{\nu}_\tau \rightarrow W^+ \tilde{\tau}_1$ to $\tilde{\nu}_\tau \rightarrow H^+ \tilde{\tau}_1$ in Fig. 7.2. Note, that in Fig. 7.2b all partial decay widths are nearly independent of A_τ except the one into H^+ .

Let us now turn to the question, which cascade decays are induced by these decay modes. For most cases one has to keep in mind that a right stau decays mainly into a tau-lepton and the lightest neutralino (see Fig. 7.3d of the next section). Therefore, the decay chains are:

$$\tilde{\nu}_\tau \rightarrow W^+ \tilde{\tau}_1 \rightarrow W^+ \tau \tilde{\chi}_1^0 \rightarrow \begin{cases} q q' \tau \tilde{\chi}_1^0 & (\sim 70\%) \\ l^+ \tau \nu_l \tilde{\chi}_1^0 & (\sim 30\%) \end{cases} \quad (7.3)$$

$$\tilde{\nu}_\tau \rightarrow H^+ \tilde{\tau}_1 \rightarrow H^+ \tau \tilde{\chi}_1^0 \rightarrow \begin{cases} \tau^+ \tau \nu_\tau \tilde{\chi}_1^0 & (\sim 90\%) \\ c \bar{s} \tau \tilde{\chi}_1^0 & (\sim 10\%) \end{cases} \quad (7.4)$$

For the discussion of H^+ decays in this mass range see for example [62]. As can be seen in Fig. 7.3d the lighter stau can also decay into charginos and the other neutralinos if $|\mu| \lesssim M$ leading to additional quarks and/or leptons for these final states.

7.2 Decays of $\tilde{\tau}_1$

In Fig. 7.3 we show branching ratios for $\tilde{\tau}_1$ decays as a function of μ for various scenarios. We have seen in Chapter 6 that the nature of the staus is mainly determined by M_E , M_L and the product $\mu \tan \beta$. For the following discussion we have fixed $A_\tau = 500$ GeV. In Fig. 7.3a a maximal mixing scenario for $\tan \beta = 1.5$ is realized except a small range near $\mu \simeq 333$ GeV where $\tilde{\tau}_1 \simeq \tilde{\tau}_R$. We have chosen $M_L = M_E = 700$ GeV. For $|\mu| \gtrsim 200$ GeV the decay into $\tau \tilde{\chi}_1^0$ dominates. Note, that the decay into $\nu_\tau \tilde{\chi}_1^-$ has nearly the same branching ratio for a wide range of μ . For large $\tan \beta$ this decay becomes more important (Fig. 7.3b). This results from the increasing Yukawa coupling and the interferences between the gaugino and the higgsino components of the chargino in the corresponding decay widths.

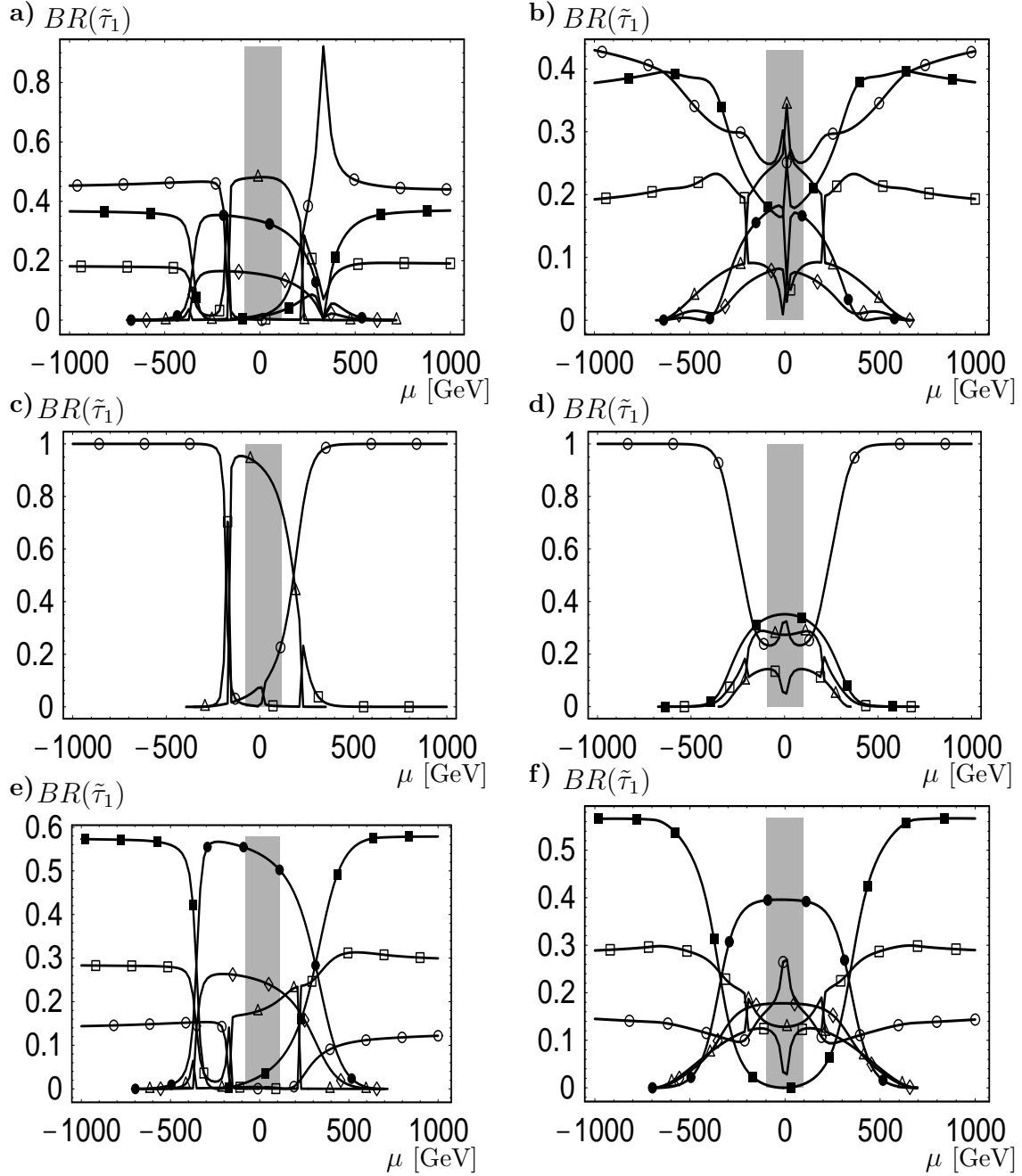


Fig. 7.3: Branching ratios for $\tilde{\tau}_1$ decays as a function of μ for $A_\tau = 500$ GeV, $M = 350$ GeV, $M_L = 700$ GeV, in a) and b) $M_E = 700$ GeV, in c) and d) $M_E = 350$ GeV, and in e) and f) $M_E = 980$ GeV. In a), c) and e) $\tan \beta = 1.5$ and in b), d) and f) $\tan \beta = 40$. The curves correspond to the following transitions: $\circ \tilde{\tau}_1 \rightarrow \tau \tilde{\chi}_1^0$, $\square \tilde{\tau}_1 \rightarrow \tau \tilde{\chi}_2^0$, $\triangle \tilde{\tau}_1 \rightarrow \tau \tilde{\chi}_3^0$, $\diamond \tilde{\tau}_1 \rightarrow \tau \tilde{\chi}_4^0$, $\blacksquare \tilde{\tau}_1 \rightarrow \nu_\tau \tilde{\chi}_1^-$, and $\bullet \tilde{\tau}_1 \rightarrow \nu_\tau \tilde{\chi}_2^-$. The grey area will be covered by LEP2 ($m_{\tilde{\chi}_1^\pm} \leq 95$ GeV).

In Fig. 7.3c ($\tan\beta = 1.5$) and Fig. 7.3d ($\tan\beta = 40$) we show the situation $\tilde{\tau}_1 \simeq \tilde{\tau}_R$. We have taken $M_E = 350$ GeV and the other parameters as above. The coupling to the bino is the dominating one for small $\tan\beta$. Therefore, the decay into $\tilde{\chi}_1^0$ ($\tilde{\chi}_3^0$) is the most important one for $|\mu| \gtrsim 200$ GeV ($|\mu| \lesssim 200$ GeV). Note, that for $200 \text{ GeV} \lesssim \mu \lesssim 350 \text{ GeV}$ also the decay into $\tilde{\chi}_2^0$ gains some importance. The results for small $\tan\beta$ are nearly independent of the flavour. Therefore, the branching ratios for \tilde{e}_R - and $\tilde{\mu}_R$ -decays are nearly the same (see e.g. [63]). The differences between small and large $\tan\beta$ scenarios (Fig. 7.3c and d) are again due to the different Yukawa couplings.

Let us now turn to the case $\tilde{\tau}_1 \simeq \tilde{\tau}_L$ (Fig. 7.3e and 7.3f). Here we have chosen $M_E = 980$ GeV and the other parameters as above. The couplings to the zino and the wino dominate if $\tan\beta = 1.5$. The most important decays are those into charginos followed by the decays into $\tilde{\chi}_2^0$ ($M \lesssim |\mu|$) and $\tilde{\chi}_4^0$ ($M \gtrsim |\mu|$). Similar as in the above example the couplings to the higgsino components become important for $\tan\beta = 40$ and $|\mu| \lesssim M$ (Fig. 7.3f).

7.3 Decays of $\tilde{\tau}_2$

In Fig. 7.4 the branching ratios for $\tilde{\tau}_2$ decays are shown as a function of μ for $M_E = M_L = 700$ GeV, $A_\tau = 500$ GeV, and $M = 350$ GeV. In Fig. 7.4a we have chosen $\tan\beta = 1.5$. Comparing Fig. 7.4a with Fig. 7.3a one notices that the branching ratio for the various decays of $\tilde{\tau}_1$ and $\tilde{\tau}_2$ are nearly the same for a wide range of μ . Here it is likely that very accurate measurements will be needed to separate the signals of the staus and to determine their properties. Only in the range where $\mu \simeq A_\tau \tan\beta$ does the heavier stau have completely different properties because the mass eigenstates are nearly identical with the weak eigenstates.

Let us now see how the phenomenology differs by changing the ratio $M_L : M_E$. In Fig. 7.5 the branching ratios are shown as function of μ for $M_L = 700$ GeV, $M_E = 350$ GeV, $m_{A^0} = 150$ GeV and $\tan\beta = 40$. As a qualitatively new feature the decays into the Z boson and neutral Higgs bosons are possible. In Fig. 7.5a the branching ratios for the decays into fermions are shown. For $|\mu| > M$ the decay into $\nu_\tau \tilde{\chi}_1^-$ dominates followed by $\tau \tilde{\chi}_2^0$ and $\tau \tilde{\chi}_1^0$. The decays into $\tilde{\chi}_2^-$, $\tilde{\chi}_{3,4}^0$ become kinematically possible if $|\mu| \lesssim M$. Especially the decay into the heavier chargino gets important in that range. The importance of these decays is expected because $\tilde{\tau}_2$ is mainly a left state. In Fig. 7.5b the branching ratios for the decays into bosons are shown. Their sum varies between $\sim 10\%$ and $\sim 40\%$. The decays into $Z \tilde{\tau}_1$ and $h^0 \tilde{\tau}_1$ are important for large μ where the branching ratios go up to $\sim 18\%$ and $\sim 14\%$ respectively. Their varying importance can be understood by having a look on the

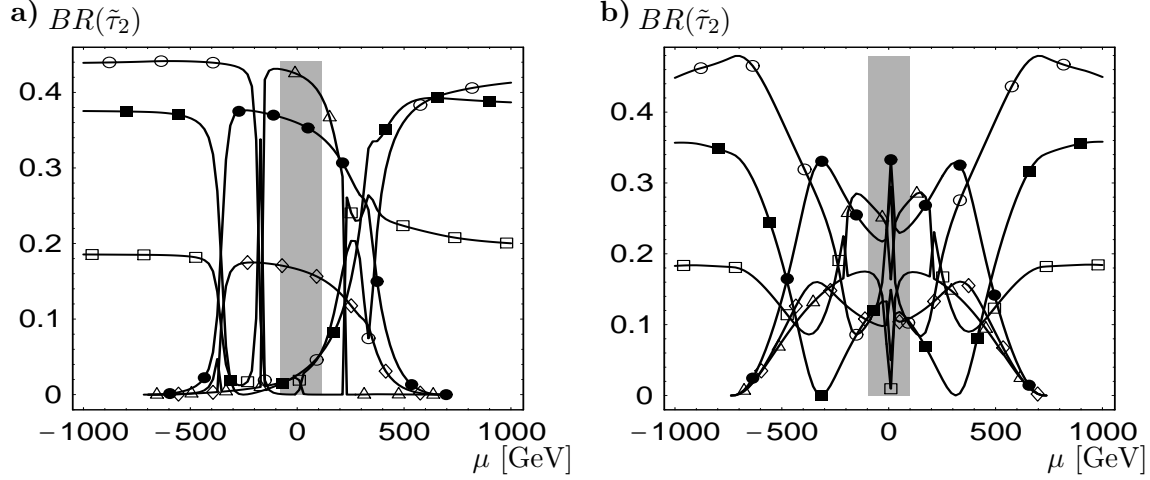


Fig. 7.4: Branching ratios for $\tilde{\tau}_2$ decays as a function of μ for $A_\tau = 500$ GeV, $M = 350$ GeV, $m_{A^0} = 150$ GeV, $M_L = M_E = 700$ GeV, a) $\tan \beta = 1.5$ and b) $\tan \beta = 40$. The curves correspond to the transitions: $\circ \tilde{\tau}_2 \rightarrow \tau \tilde{\chi}_1^0$, $\square \tilde{\tau}_2 \rightarrow \tau \tilde{\chi}_2^0$, $\triangle \tilde{\tau}_2 \rightarrow \tau \tilde{\chi}_3^0$, $\diamond \tilde{\tau}_2 \rightarrow \tau \tilde{\chi}_4^0$, $\blacksquare \tilde{\tau}_2 \rightarrow \nu_\tau \tilde{\chi}_1^-$, and $\bullet \tilde{\tau}_2 \rightarrow \nu_\tau \tilde{\chi}_2^-$. The grey area will be covered by LEP2 ($m_{\tilde{\chi}_1^\pm} \leq 95$ GeV).

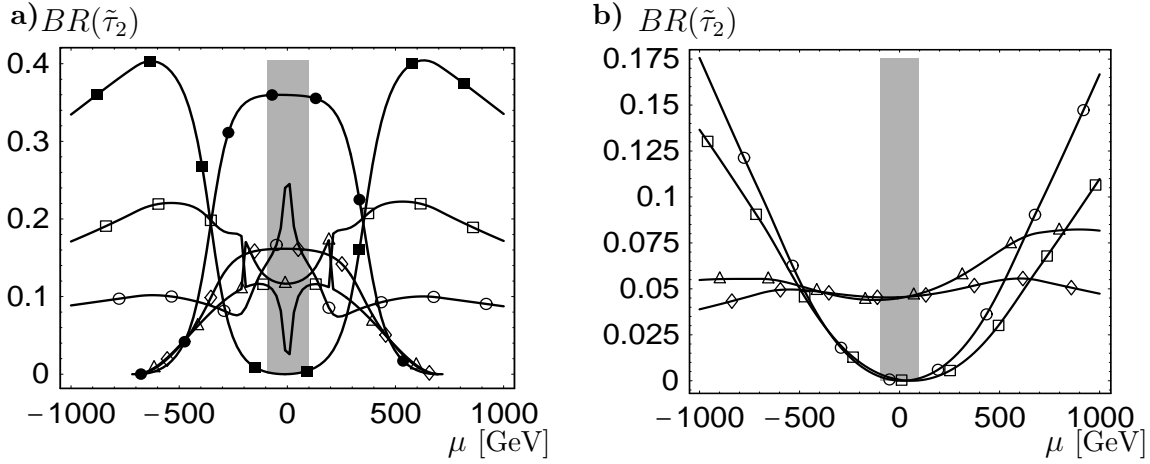


Fig. 7.5: Branching ratios for $\tilde{\tau}_2$ decays as a function of μ for $\tan \beta = 40$, $A_\tau = 500$ GeV, $M = 350$ GeV, $m_{A^0} = 150$ GeV, $M_L = 700$ GeV, and $M_E = 350$ GeV. The curves in a) correspond to: $\circ \tilde{\tau}_2 \rightarrow \tau \tilde{\chi}_1^0$, $\square \tilde{\tau}_2 \rightarrow \tau \tilde{\chi}_2^0$, $\triangle \tilde{\tau}_2 \rightarrow \tau \tilde{\chi}_3^0$, $\diamond \tilde{\tau}_2 \rightarrow \tau \tilde{\chi}_4^0$, $\blacksquare \tilde{\tau}_2 \rightarrow \nu_\tau \tilde{\chi}_1^-$, and $\bullet \tilde{\tau}_2 \rightarrow \nu_\tau \tilde{\chi}_2^-$. The curves in b) correspond to: $\circ \tilde{\tau}_2 \rightarrow Z^0 \tilde{\tau}_1$, $\square \tilde{\tau}_2 \rightarrow h^0 \tilde{\tau}_1$, $\triangle \tilde{\tau}_2 \rightarrow H^0 \tilde{\tau}_1$, and $\diamond \tilde{\tau}_2 \rightarrow A^0 \tilde{\tau}_1$. The grey area will be covered by LEP2 ($m_{\tilde{\chi}_1^\pm} \leq 95$ GeV).

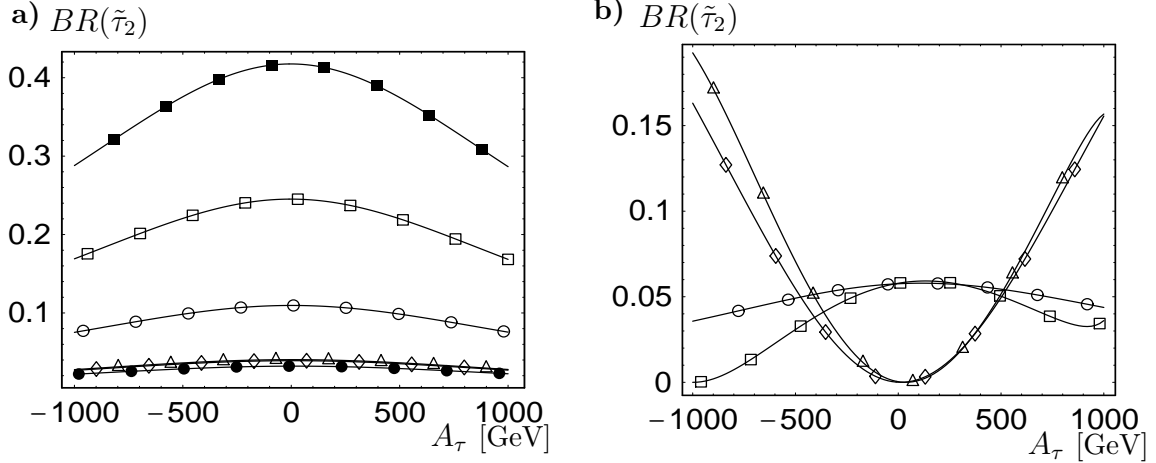


Fig. 7.6: Branching ratios for $\tilde{\tau}_2$ decays as a function of A_τ for $\tan\beta = 40$, $\mu = -500$ GeV, $M = 350$ GeV, $m_{A^0} = 150$ GeV, $M_L = 700$ GeV, and $M_E = 350$ GeV. The curves in a) correspond to: $\circ \tilde{\tau}_2 \rightarrow \tau \tilde{\chi}_1^0$, $\square \tilde{\tau}_2 \rightarrow \tau \tilde{\chi}_2^0$, $\triangle \tilde{\tau}_2 \rightarrow \tau \tilde{\chi}_3^0$, $\diamond \tilde{\tau}_2 \rightarrow \tau \tilde{\chi}_4^0$, $\blacksquare \tilde{\tau}_2 \rightarrow \nu_\tau \tilde{\chi}_1^-$, and $\bullet \tilde{\tau}_2 \rightarrow \nu_\tau \tilde{\chi}_2^-$. The curves in b) correspond to: $\circ \tilde{\tau}_2 \rightarrow Z^0 \tilde{\tau}_1$, $\square \tilde{\tau}_2 \rightarrow h^0 \tilde{\tau}_1$, $\triangle \tilde{\tau}_2 \rightarrow H^0 \tilde{\tau}_1$, $\diamond \tilde{\tau}_2 \rightarrow A^0 \tilde{\tau}_1$, $\blacksquare \tilde{\tau}_2 \rightarrow W^- \tilde{\nu}_\tau$, and $\bullet \tilde{\tau}_2 \rightarrow H^- \tilde{\nu}_\tau$.

μ dependence of the couplings (see also Eq. (3.15) and Eq. (3.27)):

$$\begin{aligned} Z\tilde{\tau}_2\tilde{\tau}_1 &\sim \sin 2\theta_{\tilde{\tau}} & h^0\tilde{\tau}_2\tilde{\tau}_1 &\sim \cos 2\theta_{\tilde{\tau}} (A_\tau \sin \alpha + \mu \cos \alpha) \\ A^0\tilde{\tau}_2\tilde{\tau}_1 &\sim (A_\tau \tan \beta + \mu) & H^0\tilde{\tau}_2\tilde{\tau}_1 &\sim \cos 2\theta_{\tilde{\tau}} (-A_\tau \cos \alpha + \mu \sin \alpha) \end{aligned} \quad (7.5)$$

Here we have only considered the most important parts of the couplings to the Higgs bosons. From Eq. (7.5) the "parabolic" form of the branching ratios into $Z \tilde{\tau}_1$ and $h^0 \tilde{\tau}_1$ follows ($\cos \alpha \simeq \pm 1$) whereas the branching ratios for the decays into $H^0 \tilde{\tau}_1$ and $A^0 \tilde{\tau}_1$ show only a mild dependence on μ . Note, that the appearance of $\sin 2\theta_{\tilde{\tau}}$ in the $Z \tilde{\tau}_2 \tilde{\tau}_1$ coupling corresponds to the fact that the $Z \tau \tau$ coupling preserves the chirality of the τ . In the same way $\cos 2\theta_{\tilde{\tau}}$ corresponds to the chirality change of the τ -lepton in the Higgs tau coupling. In Fig. 7.6b we show the branching ratios as a function of A_τ for $\mu = -500$ GeV and the other parameters as above. Here the decays into $H^0 \tilde{\tau}_1$ and $A^0 \tilde{\tau}_1$ become important for large $|A_\tau|$. Note that $BR(\tilde{\tau}_2 \rightarrow h^0 \tilde{\tau}_1)$ is very small for large negative A_τ whereas at the same time $BR(\tilde{\tau}_2 \rightarrow H^0 \tilde{\tau}_1)$ increases. This can be understood by having a look at Fig. 6.6d where we can see that $\sin \alpha \simeq -0.4$ for $A_\tau \lesssim -850$ GeV. Now the signs in front of A_τ in the couplings come into the play (Eq. (7.5)) leading to a reduction of the coupling in the case of h^0 and an increase in case of H^0 . Note, that the partial widths for the decays into charginos and neutralinos are nearly independent of A_τ . The variation of the corresponding branching ratios in Fig. 7.6a is mainly due to the variation of the partial widths for the decays into bosons.

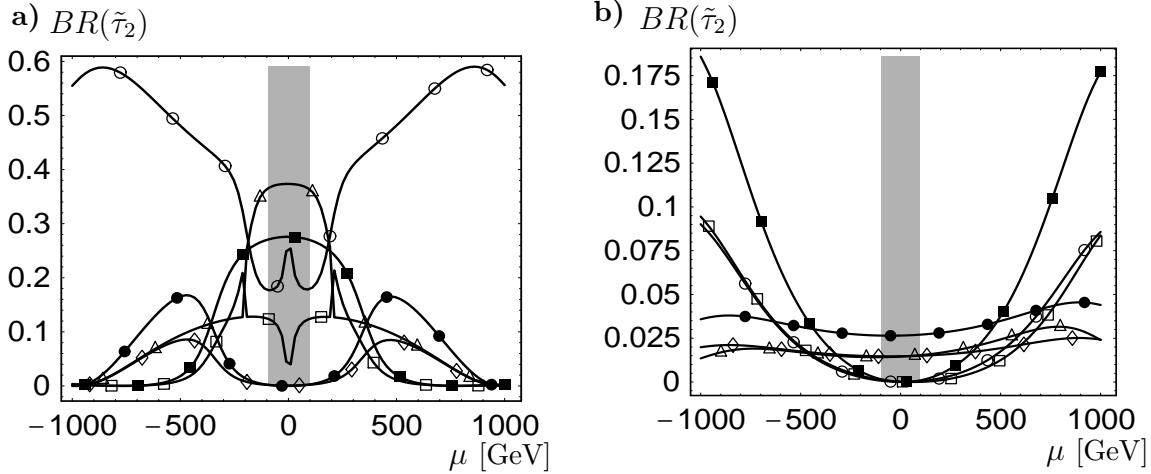


Fig. 7.7: Branching ratios for $\tilde{\tau}_2$ decays as a function of μ for $\tan\beta = 40$, $A_\tau = 500$ GeV, $M = 350$ GeV, $m_{A^0} = 150$ GeV, $M_L = 700$ GeV, and $M_E = 980$ GeV. The curves in a) correspond to: $\circ \tilde{\tau}_2 \rightarrow \tau \tilde{\chi}_1^0$, $\square \tilde{\tau}_2 \rightarrow \tau \tilde{\chi}_2^0$, $\triangle \tilde{\tau}_2 \rightarrow \tau \tilde{\chi}_3^0$, $\diamond \tilde{\tau}_2 \rightarrow \tau \tilde{\chi}_4^0$, $\blacksquare \tilde{\tau}_2 \rightarrow \nu_\tau \tilde{\chi}_1^-$, and $\bullet \tilde{\tau}_2 \rightarrow \nu_\tau \tilde{\chi}_2^-$. The curves in b) correspond to: $\circ \tilde{\tau}_2 \rightarrow Z^0 \tilde{\tau}_1$, $\square \tilde{\tau}_2 \rightarrow h^0 \tilde{\tau}_1$, $\triangle \tilde{\tau}_2 \rightarrow H^0 \tilde{\tau}_1$, $\diamond \tilde{\tau}_2 \rightarrow A^0 \tilde{\tau}_1$, $\blacksquare \tilde{\tau}_2 \rightarrow W^- \tilde{\nu}_\tau$, and $\bullet \tilde{\tau}_2 \rightarrow H^- \tilde{\nu}_\tau$. The grey area will be covered by LEP2 ($m_{\tilde{\chi}_1^\pm} \leq 95$ GeV).

Let us now turn to the question, which decay chains are induced by these decay modes:

$$\tilde{\tau}_2 \rightarrow Z \tilde{\tau}_1 \rightarrow Z \tau \tilde{\chi}_1^0 \rightarrow \begin{cases} q \bar{q} \tau \tilde{\chi}_1^0 & (\sim 70\%) \\ l^+ l^- \tau \tilde{\chi}_1^0 & (\sim 10\%) \\ \nu_l \bar{\nu}_l \tau \tilde{\chi}_1^0 & (\sim 20\%) \end{cases} \quad (7.6)$$

$$\tilde{\tau}_2 \rightarrow h^0 \tilde{\tau}_1 \rightarrow h^0 \tau \tilde{\chi}_1^0 \rightarrow \begin{cases} b \bar{b} \tau \tilde{\chi}_1^0 & (\sim 96\%) \\ \tau^+ \tau^- \tau \tilde{\chi}_1^0 & (\sim 4\%) \\ W W^* \tau \tilde{\chi}_1^0 & (\sim 90\%) \\ Z Z^* \tau \tilde{\chi}_1^0 & (\sim 10\%) \end{cases} \begin{cases} \text{if } |\sin\alpha| \gtrsim 0.05 \\ \text{if } |\sin\alpha| \lesssim 0.01 \end{cases} \quad (7.7)$$

$$\tilde{\tau}_2 \rightarrow H^0 \tilde{\tau}_1 \rightarrow H^0 \tau \tilde{\chi}_1^0 \rightarrow \begin{cases} b \bar{b} \tau \tilde{\chi}_1^0 & (\sim 96\%) \\ \tau^+ \tau^- \tau \tilde{\chi}_1^0 & (\sim 4\%) \end{cases} \quad (7.8)$$

$$\tilde{\tau}_2 \rightarrow A^0 \tilde{\tau}_1 \rightarrow A^0 \tau \tilde{\chi}_1^0 \rightarrow \begin{cases} b \bar{b} \tau \tilde{\chi}_1^0 & (\sim 96\%) \\ \tau^+ \tau^- \tau \tilde{\chi}_1^0 & (\sim 4\%) \end{cases} \quad (7.9)$$

As mentioned above the lighter stau can also decay into charginos and the other neutralinos if $|\mu| \lesssim M$ (Fig. 7.3d) leading to additional quarks and/or leptons for these final states.

In Fig. 7.7 the branching ratios are shown for the case $M_E > M_L$ as a function of μ . Here we fix $M_E = 980$ GeV, $M_L = 700$ GeV, $A_\tau = 500$ GeV and the other parameters as above. Therefore, $\tilde{\tau}_2$ is nearly a right state and the decay into the

lightest neutralino dominates except for a small range where $\tilde{\chi}_3^0$ is mainly a bino (Fig. 7.7a). The decays into higgsino-like particles also have sizable branching ratios due to the Yukawa couplings. Note, that in this case the influence of the Yukawa couplings is much stronger than in the case of $M_E < M_L$ because now they only compete with the gauge coupling to the bino. As a new feature the decays into $W^- \tilde{\nu}_\tau$ and $H^- \tilde{\nu}_\tau$ are possible (Fig. 7.7b). Especially the decay into $W^- \tilde{\nu}_\tau$ becomes important for large $|\mu|$ because $|\sin \theta_{\tilde{\tau}}|$ becomes larger. The sum of the branching ratios into bosons varies between $\sim 6\%$ ($|\mu| < 150$ GeV) and $\sim 54\%$ ($|\mu| = 1$ TeV). Beside the decay into W^+ , also the decays into $Z \tilde{\tau}_1$ and $h^0 \tilde{\tau}_1$ get sizable branching ratios for large μ .

Chapter 8

Numerical results for $\tilde{t}_{1,2}$

8.1 Decays of \tilde{t}_1

In Chapter 4 we have seen that in the mass range of LEP2 the lighter stop has only one two body decay mode at tree level, namely $\tilde{t}_1 \rightarrow b \tilde{\chi}_1^+$. For larger stop masses the decays into $t \tilde{\chi}_i^0$ are possible if $m_{\tilde{t}_1} \gtrsim \min(M/2, |\mu|) + m_t$. In Fig. 8.1a branching ratios are shown as a function of μ for $M_D = M_Q = M_U = 700$ GeV, $A_b = A_t = 500$ GeV, $M = 350$ GeV, $\tan \beta = 1.5$ and $m_{A^0} = 150$ GeV. For $|\mu| \gtrsim m_{\tilde{t}_1}$ only the decays into $\tilde{\chi}_1^+$ and $\tilde{\chi}_{1,2}^0$ are kinematically allowed, where the decay into $\tilde{\chi}_1^+$ is dominating. Note, that the kinks near $\mu = 750$ GeV are due to the fact that $\tilde{t}_1 = \tilde{t}_L$ for this specific value. Moreover, the sign of $\cos \theta_{\tilde{t}}$ changes at this point leading to an interchange between positive and negative interferences of the gaugino and higgsino couplings. For $|\mu| \lesssim m_{\tilde{t}_1}$ the other charginos and neutralinos also enter the game. Here complicated decay chains are expected. In this parameter range the different branching ratios depend strongly on μ as a result of various interferences between the gaugino and higgsino couplings. Moreover, kinematics changes from both sides: light stop and charginos/neutralinos. In addition the nature of the charginos and neutralinos depends strongly on the sign of μ for low $\tan \beta$.

In Fig. 8.1b the branching ratios are shown for $\tan \beta = 40$ and the other parameters as above. Here $m_{\tilde{t}_1}$ and $\cos \theta_{\tilde{t}}$ are nearly independent of μ . For the decays into charginos also the bottom Yukawa coupling becomes important leading to an enhancement of the sum of both partial decay widths. The branching ratio for $\tilde{t}_1 \rightarrow b \tilde{\chi}_1^+$ ($b \tilde{\chi}_2^+$) can reach 60% (55%). For large μ the decays into $t \tilde{\chi}_{1,2}^0$ have branching ratios of $\sim 20\%$. Note, that for $|\mu| \sim 350$ GeV the decay into $t \tilde{\chi}_4^0$ can reach 25% being the dominant one among the decays into neutralinos. As a new feature compared to the previous case, the decay $\tilde{t}_1 \rightarrow W^+ \tilde{b}_1$ becomes kinematically possible for large μ (Fig. 6.2). The branching ratio can reach 20% because there is a strong mixing in the stop sector as well as in the sbottom sector. The \tilde{b}_1 decays further into $t \tilde{\chi}_1^-$ ($\sim 30\%$), $b \tilde{\chi}_1^0$ ($\sim 25\%$) and $b \tilde{\chi}_2^0$ ($\sim 45\%$) (see Fig. 9.1b for details).

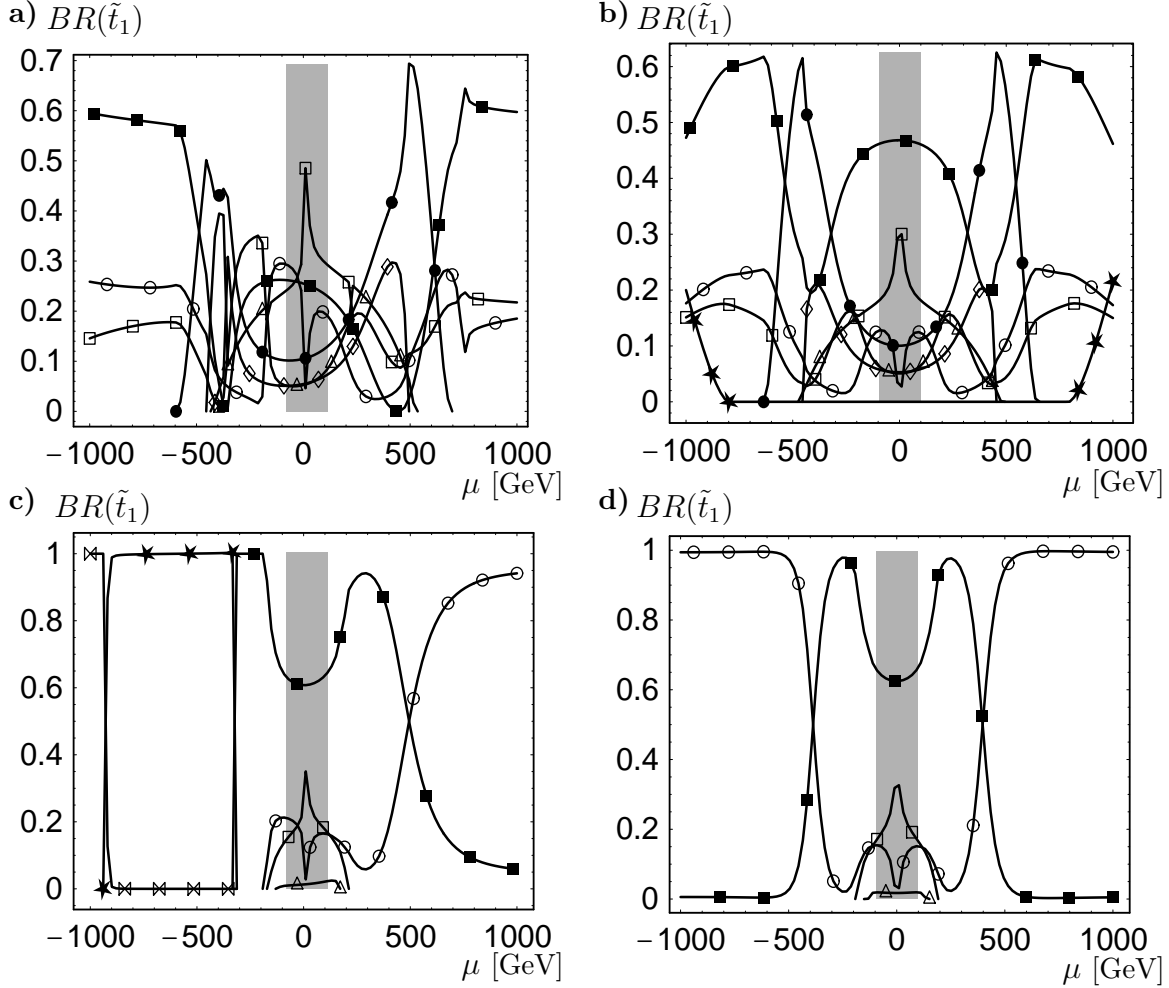


Fig. 8.1: Branching ratios for \tilde{t}_1 decays as a function of μ for $A_t = A_b = 500$ GeV, $M = 350$ GeV, $M_Q = 700$ GeV, in a) and b) $M_U = M_D = 700$ GeV, and in c) and d) $M_U = 350$ GeV, $M_D = 980$ GeV. In a), and c) $\tan\beta = 1.5$ and in b), and d) $\tan\beta = 40$. The curves correspond to the following transitions: $\circ \tilde{t}_1 \rightarrow t \tilde{\chi}_1^0$, $\square \tilde{t}_1 \rightarrow t \tilde{\chi}_2^0$, $\triangle \tilde{t}_1 \rightarrow t \tilde{\chi}_3^0$, $\diamond \tilde{t}_1 \rightarrow t \tilde{\chi}_4^0$, $\blacksquare \tilde{t}_1 \rightarrow b \tilde{\chi}_1^+$, and $\bullet \tilde{t}_1 \rightarrow b \tilde{\chi}_2^+$. In addition \star in b) denotes the transition $\tilde{t}_1 \rightarrow W^+ \tilde{b}_1$, and in c) \star the transition $\tilde{t}_1 \rightarrow W^+ b \tilde{\chi}_1^0$ whereas \bowtie denotes $\tilde{t}_1 \rightarrow c \tilde{\chi}_1^0$. The grey area will be covered by LEP2 ($m_{\tilde{\chi}_1^\pm} \leq 95$ GeV).

In Fig. 8.1c we show the branching ratios for $M_D = 980$ GeV, $M_U = 350$ GeV, $\tan\beta = 1.5$ and the other parameters as above. With this parameter choice \tilde{t}_1 is mainly \tilde{t}_R . For $\mu \lesssim -300$ GeV only higher order decays are possible. The dominant decay mode is $\tilde{t}_1 \rightarrow b W^+ \tilde{\chi}_1^0$ wherever it is kinematically possible. The decay mode $\tilde{t}_1 \rightarrow c \tilde{\chi}_1^0$ is dominant if all three body decay modes are kinematically forbidden. A more detailed discussion of these decays will be given in Chapter 10 to which we refer for further details. As can be seen in Fig. 8.2a the total decay width can be

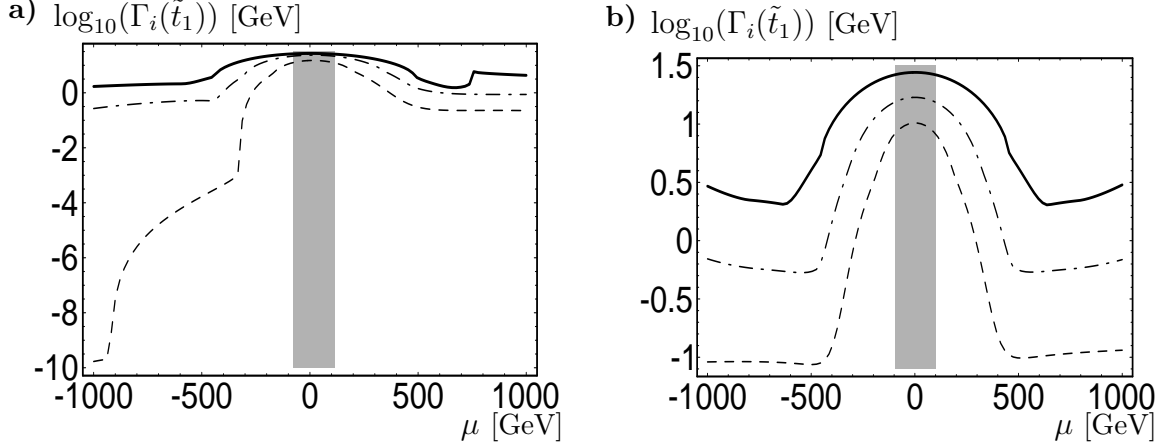


Fig. 8.2: Total decay widths of \tilde{t}_1 as function of μ for $A_t = A_b = 500$ GeV, $m_{A^0} = 150$ GeV, $M = 350$ GeV, a) $\tan \beta = 1.5$ and b) $\tan \beta = 40$. The graphs correspond to the following (M_D, M_Q, M_U) sets (in GeV): full line (700,700,700), dashed line (980,700,350), and dashed-dotted line (500,700,500).

much smaller than 0.2 GeV for this parameter range. Therefore, hadronization effects will become important. The remaining part of Fig. 8.1 can be understood by kinematics and the fact that a right stop couples only to the bino and the higgsinos. This leads to the dominance of $\tilde{t}_1 \rightarrow t \tilde{\chi}_1^0$ for $\mu \gtrsim 500$ GeV, because there the lightest neutralino is mainly a bino and the lighter chargino is mainly a wino. For $|\mu| \lesssim 500$ GeV the decay into $b \tilde{\chi}_1^+$ dominates due to the strong coupling to the charged higgsino and as a result of kinematics. The situation is similar for large $\tan \beta$ except that now tree level decays are kinematically allowed over the whole μ range considered (Fig. 8.1d).

Let us have a short look on the decay widths shown in Fig. 8.2. In general the decay width is too large for hadronization effects to become important. The obvious exception is that only higher order decays are allowed as mentioned above (Fig. 8.2a). For $M_U = 350$ GeV, $|\mu| \gtrsim 500$ GeV and $\tan \beta = 40$ (dashed line of Fig. 8.2b) the decay width is in the order of 0.1 GeV. Here remains of a hadronization process could be visible although tree level two body decays are allowed and $m_{\tilde{t}_1} \simeq 360$ GeV.

In Fig. 8.3a we study the dependence of the branching ratios on $A_t (= A_b)$ for $M_D = M_Q = M_U = 700$ GeV, $\mu = -500$ GeV and $\tan \beta = 1.5$. With this the chargino/neutralino sector is completely fixed and only the properties of the stop are varied. At $A_t = \mu \cot \beta = 1000/3$ GeV the lighter stop is a pure left state and here also the sign of $\cos \theta_{\tilde{t}}$ changes. The stop mass and the absolute value of $\cos \theta_{\tilde{t}}$ are symmetric with respect to this point (Fig. 6.4) but not the branching ratios. Therefore, it should be possible to determine the sign of $\cos \theta_{\tilde{t}}$ and A_t in such a scenario from the branching ratios once μ and $\tan \beta$ are known. The assumption $A_t = A_b$ is not restrictive in this case, because A_b does not enter in the two body

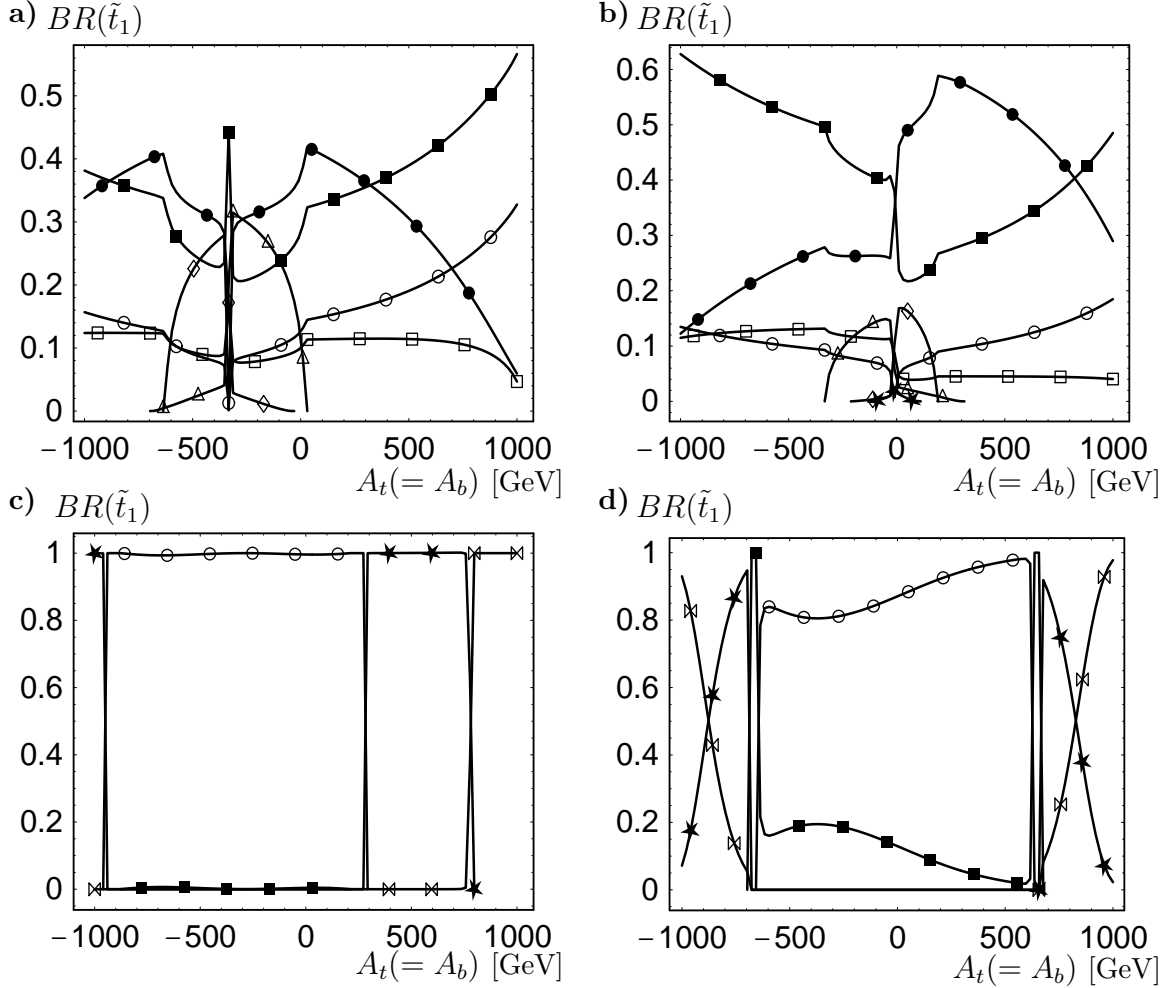


Fig. 8.3: Branching ratios for \tilde{t}_1 decays as a function of $A_t (= A_b)$ for $\mu = -500$ GeV, $M = 350$ GeV, $M_Q = 700$ GeV, in a) and b) $M_U = M_D = 700$ GeV, and in c) and d) $M_U = 350$ GeV, $M_D = 980$ GeV. In a), and c) $\tan\beta = 1.5$ and in b), and d) $\tan\beta = 40$. The curves in a), and b) correspond to the transitions: $\circ \tilde{t}_1 \rightarrow t \tilde{\chi}_1^0$, $\square \tilde{t}_1 \rightarrow t \tilde{\chi}_2^0$, $\triangle \tilde{t}_1 \rightarrow t \tilde{\chi}_3^0$, $\diamond \tilde{t}_1 \rightarrow t \tilde{\chi}_4^0$, $\blacksquare \tilde{t}_1 \rightarrow b \tilde{\chi}_1^+$, $\bullet \tilde{t}_1 \rightarrow b \tilde{\chi}_2^+$, and $\star \tilde{t}_1 \rightarrow W^+ \tilde{b}_1$. The curves in c) and d) correspond to the transitions: $\circ \tilde{t}_1 \rightarrow t \tilde{\chi}_1^0$, $\blacksquare \tilde{t}_1 \rightarrow b \tilde{\chi}_1^+$, $\bowtie \tilde{t}_1 \rightarrow c \tilde{\chi}_1^0$, and $\star \tilde{t}_1 \rightarrow W^+ b \tilde{\chi}_1^0$.

decay widths at tree level. Note, that the variation of the branching ratios with A_t starting from $A_t = \mu \cot\beta$ is mainly determined by kinematics and hardly by the couplings except near $A_t = \mu \cot\beta$. The change in the ordering of the branching ratios caused by the change of the sign of $\cos\theta_t$ is even more pronounced for large $\tan\beta$ as can be seen in Fig. 8.3b.

The case $M_U \ll M_Q$ is shown in Fig. 8.3c and d. If $\tan\beta$ is small (Fig. 8.3c) then there is hardly any dependence on A_t . As expected by the fact that the light

stop is mainly a right state the decay into $t \tilde{\chi}_1^0$ dominates if kinematically allowed. In the range of A_t where only higher order decays are possible again the decay into $b W^+ \tilde{\chi}_1^0$ dominates. For $A_t \gtrsim 800$ GeV only the decay into $c \tilde{\chi}_1^0$ is possible. For large $\tan \beta$ (Fig. 8.3d) the situation changes for the two body decays at tree level. Here the bottom Yukawa coupling becomes important for the decay into $b \tilde{\chi}_1^+$ leading to somewhat stronger dependence on A_t .

8.2 Decays of \tilde{t}_2

Before discussing the different scenarios for \tilde{t}_2 decays in detail we want to note that there is a wide parameter range where the decays into bosons dominate. In particular this holds for large values of μ and/or A_t .

In Fig. 8.4a and b the branching ratios are shown as a function of μ for $M_D = M_Q = M_U = 700$ GeV, $A_t = A_b = 500$ GeV, $\tan \beta = 1.5$, and $m_{A^0} = 150$ GeV. For positive μ only decays into fermions are kinematically allowed. Here the decay into $b \tilde{\chi}_1^+$ dominates with branching ratios up to $\sim 60\%$ followed by the decays into $t \tilde{\chi}_2^0$ and $t \tilde{\chi}_3^0$. For negative μ the decays into bosons become kinematically accessible (Fig. 8.4b). Before discussing them we want to note that in the range -500 GeV $< \mu < -300$ GeV the decay into $t \tilde{\chi}_4^0$ is the most important one followed by $b \tilde{\chi}_2^+$. This remarkable feature is again due to the positive interference between gaugino and higgsino components of $\tilde{\chi}_2^+$ and $\tilde{\chi}_4^0$. For the discussion of the bosonic decays it is useful to consider the most important parts of the relevant couplings:

$$\begin{aligned} Z^0 \tilde{t}_2 \tilde{t}_1 &\sim \sin 2\theta_{\tilde{t}} & h^0 \tilde{t}_2 \tilde{t}_1 &\sim \cos 2\theta_{\tilde{t}} (\mu \sin \alpha + A_t \cos \alpha) \\ A^0 \tilde{t}_2 \tilde{t}_1 &\sim (A_t \cot \beta + \mu) & H^0 \tilde{t}_2 \tilde{t}_1 &\sim \cos 2\theta_{\tilde{t}} (\mu \cos \alpha - A_t \sin \alpha) \end{aligned} \quad (8.1)$$

For $\mu \lesssim -600$ GeV the decay into $Z \tilde{t}_1$ dominates for two reasons: firstly, similar to the case $\tilde{\nu}_\tau \rightarrow W^+ \tilde{\tau}_1$ (Section 7.1), there is a large factor $\lambda(m_{\tilde{t}_2}^2, m_{\tilde{t}_1}^2, m_Z^2)/m_W^2$. Secondly, the coupling is proportional to $\sin 2\theta_{\tilde{t}}$ which is near its maximum. The branching ratio for $\tilde{t}_2 \rightarrow A^0 \tilde{t}_1$ increases for large $|\mu|$ because of kinematics and because the coupling is proportional to $(A_t \cot \beta + \mu)$. The occurrence of decays into both sbottoms is typical for scenarios where $\tan \beta$ is small and $M_D \simeq M_Q$ because here $m_{\tilde{b}_1} \simeq m_{\tilde{b}_2}$ and there is a strong mixing in the sbottom sector as explained in Chapter 6 (see especially Fig. 6.2). In this scenario the properties of the sbottoms are rather similar. Therefore, it could be difficult to distinguish between these two decay modes. The decays $\tilde{t}_2 \rightarrow \tilde{t}_1 h^0, \tilde{t}_1 H^0$ are also possible. However, $\cos 2\theta_{\tilde{t}}$ is rather small and therefore their branching ratios are so tiny that we won't show them.

In Fig. 8.4c and d we present the scenario where $M_U = 350$ GeV, $M_Q = 700$ GeV, and $M_D = 980$ GeV and the other parameters as above. Now decays into bosons are

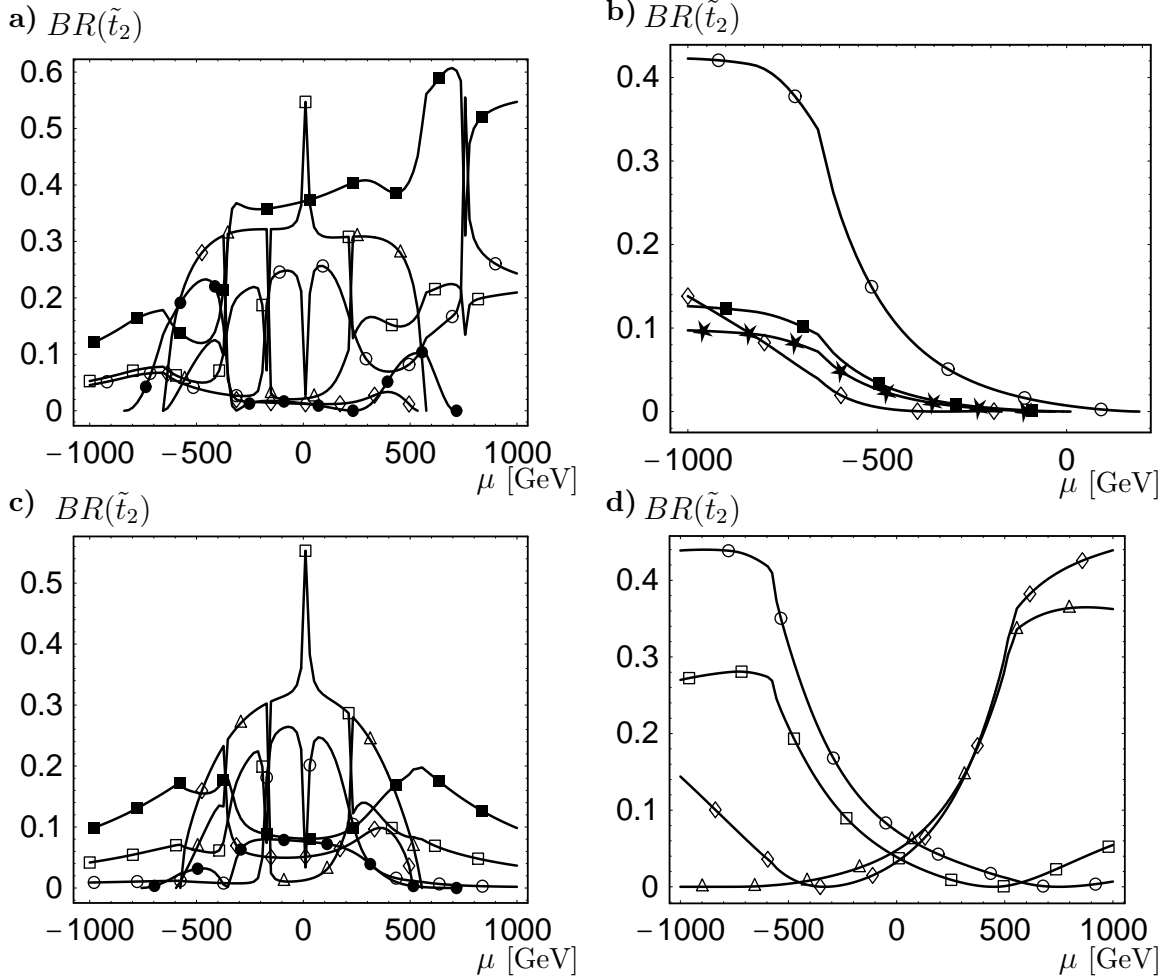


Fig. 8.4: Branching ratios for \tilde{t}_2 decays as a function of μ for $\tan\beta = 1.5$, $M = 350$ GeV, $m_{A^0} = 150$ GeV, $A_t = A_b = 500$ GeV, $M_Q = 700$ GeV, a) and b) $M_U = M_D = 700$ GeV, c) and d) $M_U = 350$ GeV, $M_D = 980$ GeV. The curves in a), and c) correspond to: $\circ \tilde{t}_2 \rightarrow t \tilde{\chi}_1^0$, $\square \tilde{t}_2 \rightarrow t \tilde{\chi}_2^0$, $\triangle \tilde{t}_2 \rightarrow t \tilde{\chi}_3^0$, $\diamond \tilde{t}_2 \rightarrow t \tilde{\chi}_4^0$, $\blacksquare \tilde{t}_2 \rightarrow b \tilde{\chi}_1^+$, and $\bullet \tilde{t}_2 \rightarrow b \tilde{\chi}_2^+$. The curves in b), and d) correspond to: $\circ \tilde{t}_2 \rightarrow Z^0 \tilde{t}_1$, $\square \tilde{t}_2 \rightarrow h^0 \tilde{t}_1$, $\triangle \tilde{t}_2 \rightarrow H^0 \tilde{t}_1$, $\diamond \tilde{t}_2 \rightarrow A^0 \tilde{t}_1$, $\blacksquare \tilde{t}_2 \rightarrow W^+ \tilde{b}_1$, and $\star \tilde{t}_2 \rightarrow W^+ \tilde{b}_2$. The grey area will be covered by LEP2 ($m_{\tilde{\chi}_1^\pm} \leq 95$ GeV).

allowed for the whole μ range. Note, that the decays into sbottoms are not shown because they are kinematically highly suppressed (therefore, they are not shown). For $|\mu| \lesssim 350$ GeV the decays into fermions are kinematically favoured. Here the decays into neutralinos dominate. For large positive μ the decays into $H^0 \tilde{t}_1$ and $A^0 \tilde{t}_1$ dominate whereas the branching ratios for $\tilde{t}_2 \rightarrow Z^0 \tilde{t}_1$, $h^0 \tilde{t}_1$ are very small, because $|\cos\theta_{\tilde{t}}|$ is rather small ($\lesssim 0.1$) and $\sin\alpha \simeq -0.75$. Note, that the sign in front of A_t in Eq. (8.1) leads to an increase of the $H^0 \tilde{t}_1$ channel and to a decrease

in the $h^0 \tilde{t}_1$ channel. On the other side for large negative μ we find $\cos \theta_{\tilde{t}} \simeq -0.4$ and $-0.9 \lesssim \cos \alpha \lesssim -0.8$. This and the kinematics lead to the dominance of $\tilde{t}_2 \rightarrow Z \tilde{t}_1$. For $\mu \lesssim -800$ GeV this branching ratio shows a slight decrease although the corresponding decay width is growing. The reason is that the decay width for $\tilde{t}_2 \rightarrow A^0 \tilde{t}_1$ increases much stronger. Note that in this parameter are hardly any decays into H^0 . The kink in $BR(\tilde{t}_2 \rightarrow h^0 \tilde{t}_1)$ arises because the coupling has a maximum near this point and because of the growth of the above mentioned decay widths. We want to stress that for large $|\mu|$ more than 80% of the \tilde{t}_2 decay into bosons.

In Fig. 8.5 the situation is shown for $\tan \beta = 40$. In the case $M_D = M_Q = M_U$ (Fig. 8.5a and b) we encounter the following differences compared to $\tan \beta = 1.5$. Among the decays into fermions the decay into $b \tilde{\chi}_1^+$ is the most important one for the whole μ range (in fact this is independent of the ratio $M_D : M_Q : M_U$ in the considered examples). For large $|\mu|$ the decays into $W^+ \tilde{b}_1$ and $H^+ \tilde{b}_1$ are the dominant ones. This is partly due to the fact that \tilde{b}_1 becomes relatively light for these values of μ . In case of $H^+ \tilde{b}_1$ also the term $(-\sin \theta_{\tilde{b}} \sin \theta_{\tilde{t}} m_b A_b \tan \beta + \cos \theta_{\tilde{b}} \cos \theta_{\tilde{t}} m_t \mu)/m_W$ becomes large (see also Eq. (3.17)). Moreover, the decays into b_2 are kinematically forbidden and also the decay $\tilde{t}_2 \rightarrow Z \tilde{t}_1$ is suppressed by kinematics.

Similar to the small $\tan \beta$ scenarios the situation changes in two important ways, if one turns to the case $M_U = 350$ GeV and $M_D = 980$ GeV (Fig. 8.5c and d). Firstly, the decays into \tilde{b}_1 are at least highly suppressed by kinematics if not forbidden. Secondly, the decays into $h^0 \tilde{t}_1$ and $H^0 \tilde{t}_1$ get sizable branching ratios. Besides this, there are some differences stemming mainly from the fact that $m_{\tilde{t}_1}$, $m_{\tilde{t}_2}$, $\cos \theta_{\tilde{t}}$, and $\cos \alpha$ are nearly independent of μ for large $\tan \beta$. The decay into $A^0 \tilde{t}_1$ becomes the most important one for large $|\mu|$ followed by $\tilde{t}_2 \rightarrow H^0 \tilde{t}_1$. The branching ratio for the decay into $Z \tilde{t}_1$ never exceeds 13% because $\cos \theta_{\tilde{t}}$ is small ($\simeq -0.2$ in this example).

In the case $M_U = M_D = 500$ GeV and $M_Q = 700$ GeV the decays into \tilde{b}_1 become important as can be seen in Fig. 8.5f. Especially for large $|\mu|$ they are the dominant decays and they are in general more important than the decays into \tilde{t}_1 because $m_{\tilde{b}_1} < m_{\tilde{t}_1}$. For small $|\mu|$ the decay into $W^+ \tilde{b}_1$ becomes less important because $|\cos \theta_{\tilde{b}}| \lesssim 0.1$ in this range. Note, that $BR(\tilde{t}_2 \rightarrow H^+ \tilde{b}_1)$ is always larger than 8% and can even reach 22%.

Let us now turn to the A_t dependence for fixed μ . In Fig. 8.6a and b the branching ratios are shown for $M_D = M_Q = M_U = 700$ GeV and $\tan \beta = 40$. Similar to the case of the light stop the branching ratios for the decays into fermions are sensitive to the sign of $\cos \theta_{\tilde{t}}$ which changes at $A_t = \mu \cot \beta$. This does not happen in the case of the decays into bosons as their decay widths are mainly determined by $\cos^2 \theta_{\tilde{t}}$ (see Section 3.2 and 3.3) except $\tilde{t}_2 \rightarrow H^+ \tilde{b}_1$. In this case the most important contribution

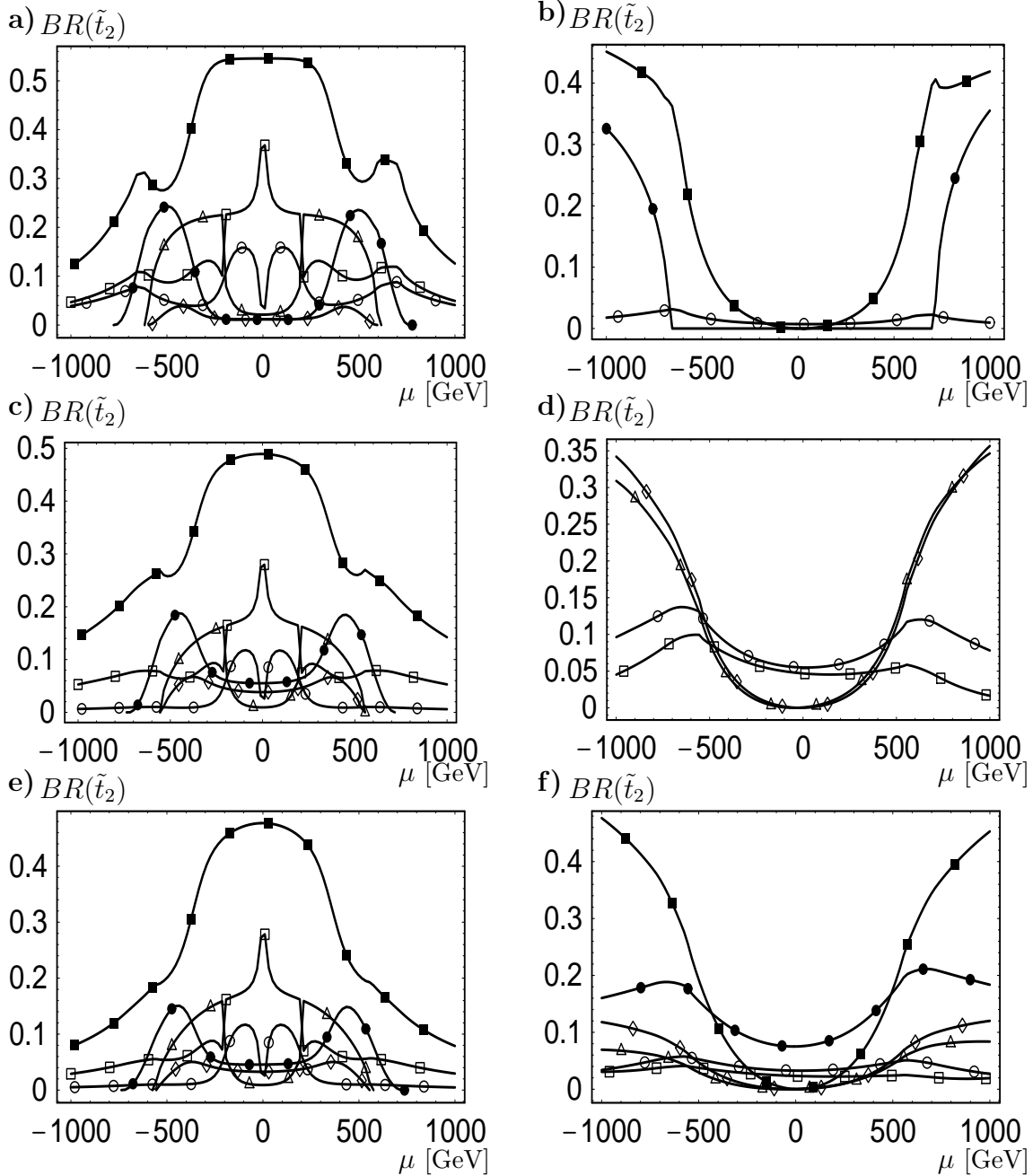


Fig. 8.5: Branching ratios for \tilde{t}_2 decays as a function of μ for $\tan\beta = 40$, $A_t = A_b = 500$ GeV, $M = 350$ GeV, $m_{A^0} = 150$ GeV, $M_Q = 700$ GeV, a) and b) $M_U = M_D = 700$ GeV, c) and d) $M_U = 350$ GeV, $M_D = 980$ GeV, e) and f) $M_U = M_D = 500$ GeV. The curves in a), c) and e) correspond to: $\circ \tilde{t}_2 \rightarrow t \tilde{\chi}_1^0$, $\square \tilde{t}_2 \rightarrow t \tilde{\chi}_2^0$, $\triangle \tilde{t}_2 \rightarrow t \tilde{\chi}_3^0$, $\diamond \tilde{t}_2 \rightarrow t \tilde{\chi}_4^0$, $\blacksquare \tilde{t}_2 \rightarrow b \tilde{\chi}_1^+$, and $\bullet \tilde{t}_2 \rightarrow b \tilde{\chi}_2^+$. The curves in b), d) and f) correspond to: $\circ \tilde{t}_2 \rightarrow Z^0 \tilde{t}_1$, $\square \tilde{t}_2 \rightarrow h^0 \tilde{t}_1$, $\triangle \tilde{t}_2 \rightarrow H^0 \tilde{t}_1$, $\diamond \tilde{t}_2 \rightarrow A^0 \tilde{t}_1$, $\blacksquare \tilde{t}_2 \rightarrow W^+ \tilde{b}_1$, and $\bullet \tilde{t}_2 \rightarrow H^+ \tilde{b}_1$. The grey area will be covered by LEP2 ($m_{\tilde{\chi}_1^\pm} \leq 95$ GeV).

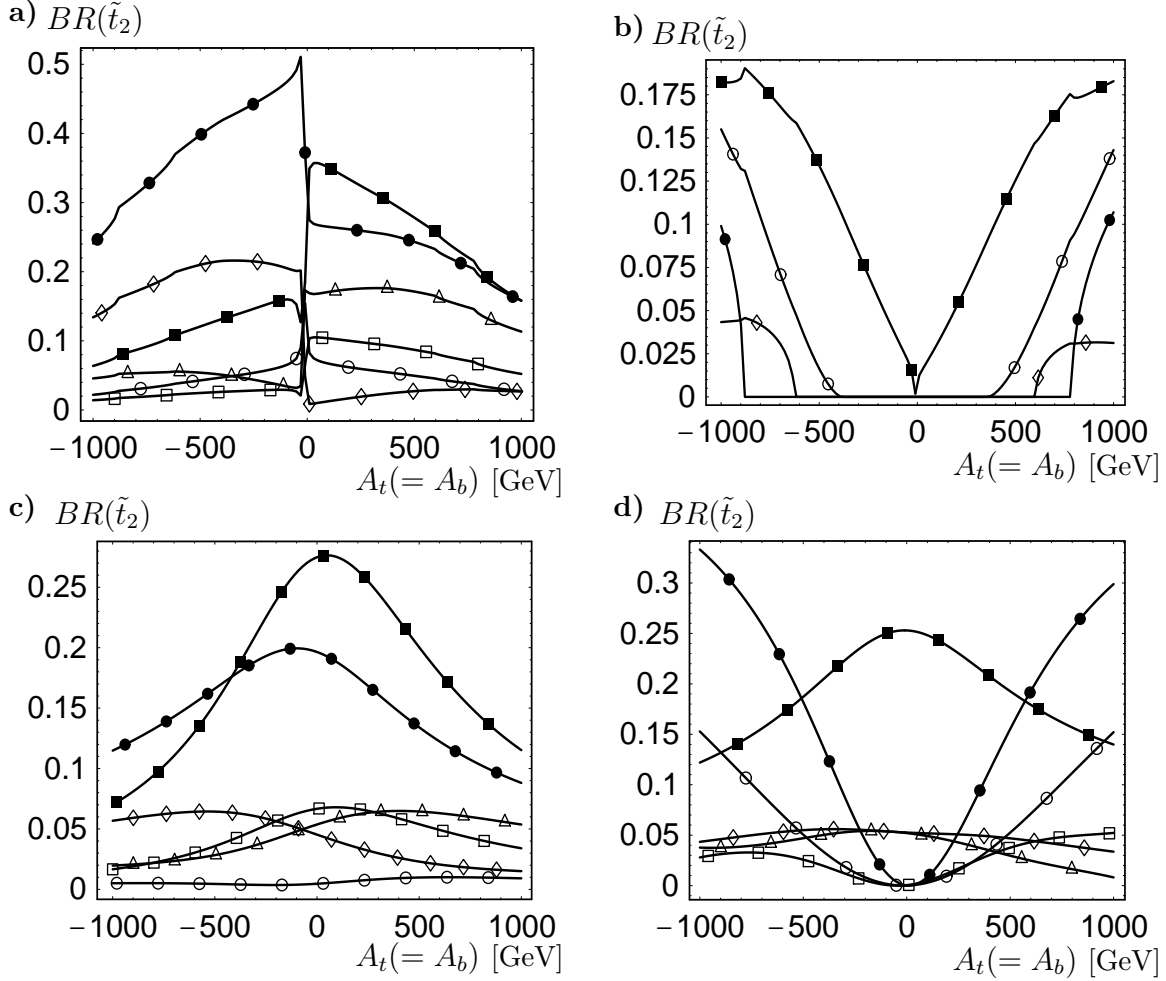


Fig. 8.6: Branching ratios for \tilde{t}_2 decays as a function of $A_t (= A_b)$ for $\tan \beta = 40$, $\mu = -500$ GeV, $M = 350$ GeV, $m_{A^0} = 100$ GeV, $M_Q = 700$ GeV, a) and b) $M_U = M_D = 700$ GeV, c) and d) $M_U = M_D = 500$ GeV. The curves in a) and c) correspond to: $\circ \tilde{t}_2 \rightarrow t \tilde{\chi}_1^0$, $\square \tilde{t}_2 \rightarrow t \tilde{\chi}_2^0$, $\triangle \tilde{t}_2 \rightarrow t \tilde{\chi}_3^0$, $\diamond \tilde{t}_2 \rightarrow t \tilde{\chi}_4^0$, $\blacksquare \tilde{t}_2 \rightarrow b \tilde{\chi}_1^+$, and $\bullet \tilde{t}_2 \rightarrow b \tilde{\chi}_2^+$. The curves in b) and d) correspond to: $\circ \tilde{t}_2 \rightarrow Z^0 \tilde{t}_1$, $\square \tilde{t}_2 \rightarrow h^0 \tilde{t}_1$, $\triangle \tilde{t}_2 \rightarrow H^0 \tilde{t}_1$, $\diamond \tilde{t}_2 \rightarrow A^0 \tilde{t}_1$, $\blacksquare \tilde{t}_2 \rightarrow W^+ \tilde{b}_1$, and $\bullet \tilde{t}_2 \rightarrow H^+ \tilde{b}_1$.

to the coupling is $(-\sin \theta_{\tilde{b}} \sin \theta_{\tilde{t}} m_b A_b \tan \beta + \cos \theta_{\tilde{b}} \cos \theta_{\tilde{t}} m_t \mu) / m_W$ as mentioned above. Here the sign of A_b is correlated to the sign of $\cos \theta_{\tilde{t}}$ due to the assumption $A_b = A_t$. The assumption $A_b = -A_t$ would lead to a reduction of this branching ratio. This is even true if one changes simultaneous the sign of μ as then, in general, $\cos \theta_{\tilde{b}}$ also changes its sign. Note, that all partial decay widths are growing with $|A_t|$ because of kinematics. This increase is stronger for the decays into bosons than for the decays into fermions except for the decay into $A^0 \tilde{t}_1$. In case of the vector bosons

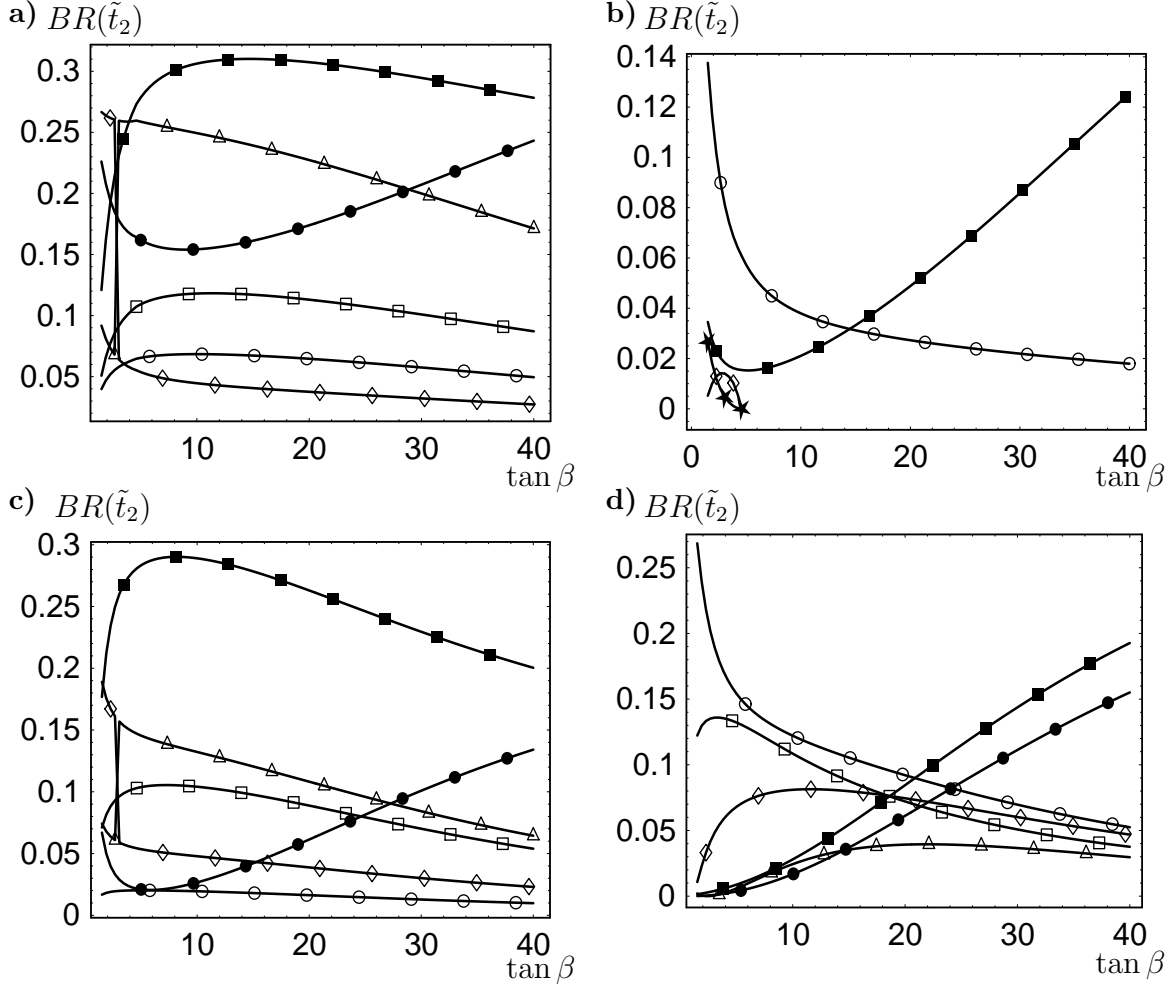


Fig. 8.7: Branching ratios for \tilde{t}_2 decays as a function of $\tan \beta$ for $A_t = A_b = 500$ GeV, $\mu = -500$ GeV, $M = 350$ GeV, $m_{A^0} = 100$ GeV, $M_Q = 700$ GeV, a) and b) $M_U = M_D = 700$ GeV, c) and d) $M_U = M_D = 500$ GeV. The curves in a) and c) correspond to: $\circ \tilde{t}_2 \rightarrow t \tilde{\chi}_1^0$, $\square \tilde{t}_2 \rightarrow t \tilde{\chi}_2^0$, $\triangle \tilde{t}_2 \rightarrow t \tilde{\chi}_3^0$, $\diamond \tilde{t}_2 \rightarrow t \tilde{\chi}_4^0$, $\blacksquare \tilde{t}_2 \rightarrow b \tilde{\chi}_1^+$, and $\bullet \tilde{t}_2 \rightarrow b \tilde{\chi}_2^+$. The curves in b) and d) correspond to: $\circ \tilde{t}_2 \rightarrow Z^0 \tilde{t}_1$, $\square \tilde{t}_2 \rightarrow h^0 \tilde{t}_1$, $\triangle \tilde{t}_2 \rightarrow H^0 \tilde{t}_1$, $\diamond \tilde{t}_2 \rightarrow A^0 \tilde{t}_1$, $\blacksquare \tilde{t}_2 \rightarrow W^+ \tilde{b}_1$, and $\star \tilde{t}_2 \rightarrow W^+ \tilde{b}_2$, $\bullet \tilde{t}_2 \rightarrow H^+ \tilde{b}_1$.

again the extra factor $\lambda(m_{\tilde{t}_2}^2, m_V^2, m_{f_1}^2)/m_V^2$ is the reason, whereas in case of H^+ it is the term proportional to A_b in the coupling.

Similar to the case of \tilde{t}_1 , the situation changes if $M_U \ll M_Q$. This can be seen in Fig. 8.6c and d where we have taken $M_U = M_D = 500$ GeV and the other parameters as above. The main reason is that $\cos \theta_{\tilde{t}}$ changes smoothly its sign at $A_t = \mu \cot \beta$ ($\tilde{t}_2 \simeq \tilde{t}_L$). Therefore, the asymmetry of the fermionic decays with respect to this point is less pronounced. The measurements of these decay modes could nevertheless

give a clear hint for the relative sign between A_t and μ . The decrease in the $W^+ \tilde{b}_1$ channel is due to the decrease of $\sin \theta_{\tilde{t}}$ for large $|\mu|$ which, on the contrary, leads to the increase of the $Z^0 \tilde{t}_1$ mode. Note, that $BR(\tilde{t}_2 \rightarrow H^0 \tilde{t}_1)$ nearly vanishes near $\mu = 1$ TeV.

In Fig. 8.7 we study the $\tan \beta$ dependence for $A_t = A_b = 500$ GeV, and $\mu = -500$ GeV. Again we compare the case $M_D = M_Q = M_U = 700$ GeV with $M_D = M_U = 500$ GeV and $M_Q = 700$ GeV. In Fig. 8.7a and c the fermionic decay modes are shown. As a general feature the decays into gaugino-like particles increase with $\tan \beta$ whereas the decays into higgsino-like particles decrease for $\tan \beta \lesssim 10$. The main reason is that for small $\tan \beta$ the mixture between gauginos and higgsinos is smaller than for large $\tan \beta$. The only exception is $\tilde{t}_2 \rightarrow t \tilde{\chi}_1^0$ for $M_U = 500$ GeV because here the \tilde{t}_L component of \tilde{t}_2 increases with $\tan \beta$. Near $\tan \beta = 2.72$ the two heaviest neutralinos have the same mass and change their (higgsino) nature (for a discussion of such degenerate points of the neutralino mass matrix see for example [31]). For large $\tan \beta$ the branching ratios decrease except for $BR(\tilde{t}_2 \rightarrow b \tilde{\chi}_2^+)$ which grows because of the bottom Yukawa coupling. The decay into $Z^0 \tilde{t}_1$ in both cases decreases with $\tan \beta$ because of phase space as can be seen in Fig. 8.7b and d. In case of $M_U = 500$ GeV the decrease of $\sin^2 2\theta_{\tilde{t}}$ also leads to a stronger decrease in this branching ratio. Note, that with increasing $\tan \beta$ $\cos \alpha$ and m_{h^0} also grow whereas m_{H^0} decreases leading to the shown dependence of the branching ratios. $BR(\tilde{t}_2 \rightarrow A^0 \tilde{t}_1)$ grows with $\tan \beta$ for small $\tan \beta$. Here, the decrease of phase space is compensated by the increase of $(A_t \cot \beta + \mu)$. The decays into sbottoms are mainly influenced by kinematics and the fact that $\cos^2 \theta_{\tilde{b}}$ grows with $\tan \beta$. It is important to note that various branching ratios have minima and maxima for $\tan \beta \lesssim 25$ making an easy interpolation between small and large $\tan \beta$ scenarios impossible.

Chapter 9

Numerical results for $\tilde{b}_{1,2}$

9.1 Decays of \tilde{b}_1

Many of the properties of the sbottoms can be understood from the discussions in the previous chapters. Therefore, we concentrate in this chapter mainly on the decays into bosons. In Fig. 9.1a we show the branching ratios as a function of μ for $M_D = M_Q = M_U = 700$ GeV and $\tan \beta = 1.5$. As explained in Section 6.2, $\cos \theta_{\tilde{b}}$ is ~ 0.7 for most of the μ range although $\tan \beta$ is small. This leads to the remarkable result that the decays into $t \tilde{\chi}_1^-$, $t \tilde{\chi}_2^-$ dominate in the whole μ range except near $\mu = A_b \cot \beta$ where $\cos \theta_{\tilde{b}}$ vanishes. Note, that the dominance of $\tilde{b}_1 \rightarrow t \tilde{\chi}_2^-$ ($t \tilde{\chi}_1^-$) for -450 GeV $\lesssim \mu \lesssim -350$ GeV ($|\mu| \lesssim 350$ GeV) is caused by the top Yukawa coupling. A second consequence of $\cos \theta_{\tilde{b}} \simeq 0.7$ is the appearance of $\tilde{b}_1 \rightarrow W^- \tilde{t}_1$ with a branching ratio up to 30%. In Fig. 9.1b the branching ratios are shown for $\tan \beta = 40$. Here the influence of the bottom Yukawa coupling leads to an enhancement of the decays into neutralinos. Moreover, there is less phase space compared to the small $\tan \beta$ case.

In Fig. 9.1c the situation is shown for $M_D = 980$ GeV, $M_Q = 700$ GeV, $M_U = 350$ GeV, and $\tan \beta = 1.5$. Here we do not show the branching ratios for the decays into $b \tilde{\chi}_1^0$, $b \tilde{\chi}_3^0$ which turn out to be rather small. For $\mu \lesssim -350$ GeV the decay into $W^- \tilde{t}_1$ dominates whereas for $\mu \gtrsim 350$ GeV the decay into $H^- \tilde{t}_1$ is the dominating one. For $|\mu| \lesssim 350$ GeV $\tilde{b}_1 \rightarrow t \tilde{\chi}_1^-$ is the most important decay. Qualitatively this can be understood by having a look on the most relevant parts of the couplings (see also Eq. (3.13) and (3.17)):

$$\begin{aligned} W^\pm \tilde{b}_1 \tilde{t}_1 &\sim \cos \theta_{\tilde{t}} \cos \theta_{\tilde{b}} \sim (A_t - \mu \cot \beta)(A_b - \mu \tan \beta) \\ H^\pm \tilde{b}_1 \tilde{t}_1 &\sim \sin \theta_{\tilde{t}} \cos \theta_{\tilde{b}} m_t (\mu + A_t \cot \beta) \end{aligned} \quad (9.1)$$

Here the relative sign between A_b and μ is important. Now $\cos \theta_{\tilde{t}}$ varies between -0.4 ($\mu = -1$ TeV) and 0.1 ($\mu = 1$ TeV) and $|\cos \theta_{\tilde{b}}| \simeq 1$ leading to the dominance of

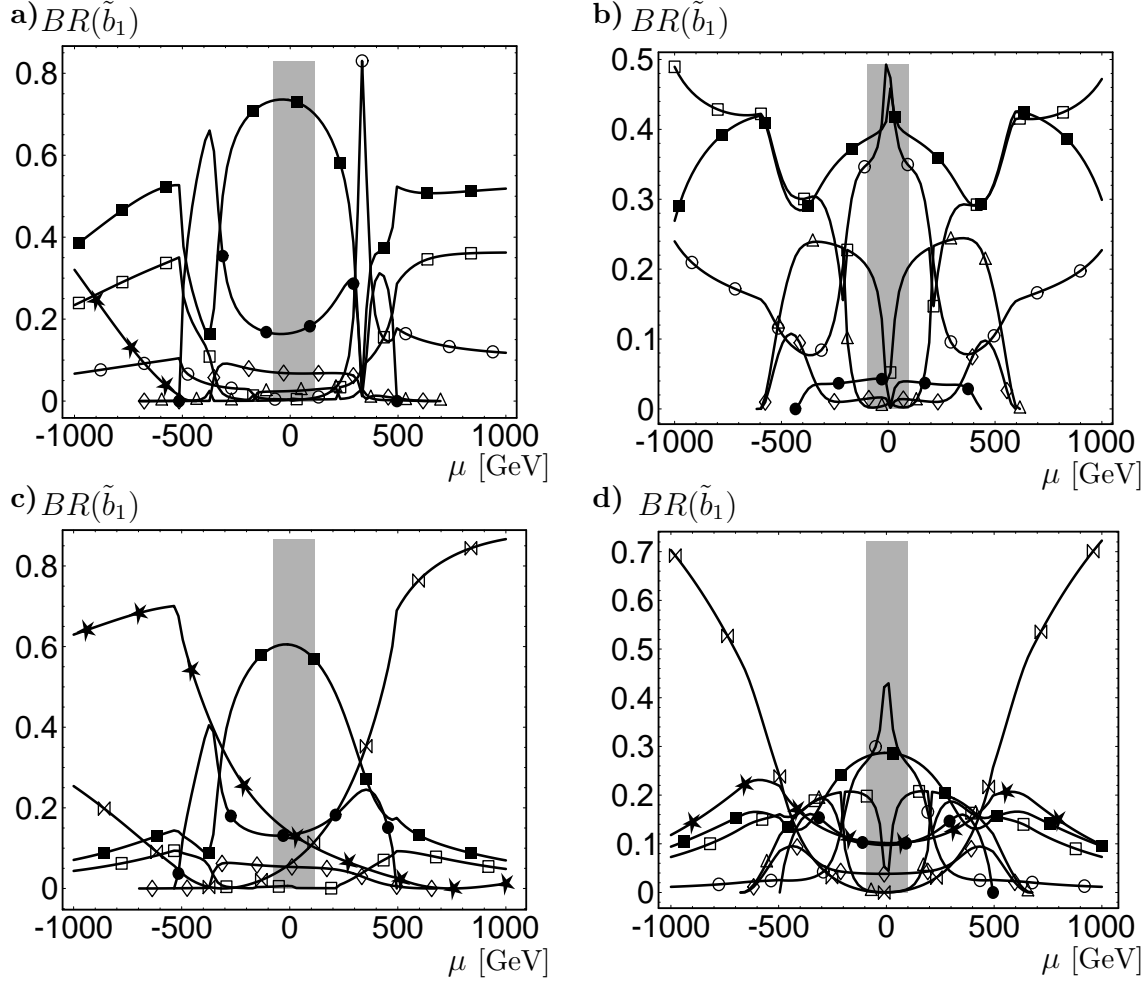


Fig. 9.1: Branching ratios for \tilde{b}_1 decays as a function of μ for $A_t = A_b = 500$ GeV, $M = 350$ GeV, $M_Q = 700$ GeV, in a) and b) $M_U = M_D = 700$ GeV, and in c) and d) $M_U = 350$ GeV, $M_D = 980$ GeV. In a), and c) $\tan\beta = 1.5$ and in b), and d) $\tan\beta = 40$. The curves correspond to the following transitions: $\circ \tilde{b}_1 \rightarrow b \tilde{\chi}_1^0$, $\square \tilde{b}_1 \rightarrow b \tilde{\chi}_2^0$, $\triangle \tilde{b}_1 \rightarrow b \tilde{\chi}_3^0$, $\diamond \tilde{b}_1 \rightarrow b \tilde{\chi}_4^0$, $\blacksquare \tilde{b}_1 \rightarrow t \tilde{\chi}_1^-$, $\bullet \tilde{b}_1 \rightarrow t \tilde{\chi}_2^-$, $\star \tilde{b}_1 \rightarrow W^- \tilde{t}_1$, and $\times \tilde{b}_1 \rightarrow H^- \tilde{t}_1$. The grey area will be covered by LEP2 ($m_{\tilde{\chi}_1^\pm} \leq 95$ GeV).

$\tilde{b}_1 \rightarrow W^- \tilde{t}_1$ ($\tilde{b}_1 \rightarrow H^- \tilde{t}_1$) for negative (positive) μ . The sum of both branching ratios constitutes at least 20% ($\mu \simeq 100$ GeV) and can reach up to 85% ($|\mu| \simeq 1$ TeV). Concerning the importance of the decays into charginos for $|\mu| \lesssim 500$ GeV we would like to note, that this is again due to the top Yukawa coupling. In Fig. 9.1d the branching ratios are shown for $\tan\beta = 40$ and the other parameters as above. Concerning the decays into fermions, the situation is similar to the case $M_D = M_Q = M_U$, the main differences arise due to kinematics since $m_{\tilde{b}_1}$ is now, in general, larger. Concerning

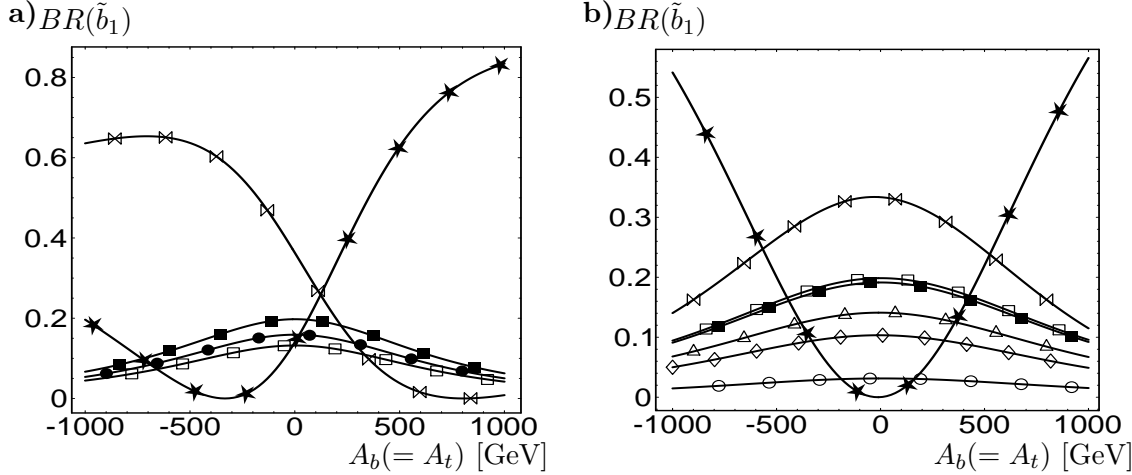


Fig. 9.2: Branching ratios for \tilde{b}_1 decays as a function of $A_b(= A_t)$ for $\mu = -500$ GeV, $M = 350$ GeV, $M_Q = 700$ GeV, $M_U = 350$ GeV, $M_D = 980$ GeV, a) $\tan \beta = 1.5$ and b) $\tan \beta = 40$. The curves correspond to the transitions: $\circ \tilde{b}_1 \rightarrow b \tilde{\chi}_1^0$, $\square \tilde{b}_1 \rightarrow b \tilde{\chi}_2^0$, $\triangle \tilde{b}_1 \rightarrow b \tilde{\chi}_3^0$, $\diamond \tilde{b}_1 \rightarrow b \tilde{\chi}_4^0$, $\blacksquare \tilde{b}_1 \rightarrow t \tilde{\chi}_1^-$, $\bullet \tilde{b}_1 \rightarrow t \tilde{\chi}_2^-$, $\star \tilde{b}_1 \rightarrow W^- \tilde{t}_1$, and $\bowtie \tilde{b}_1 \rightarrow H^- \tilde{t}_1$.

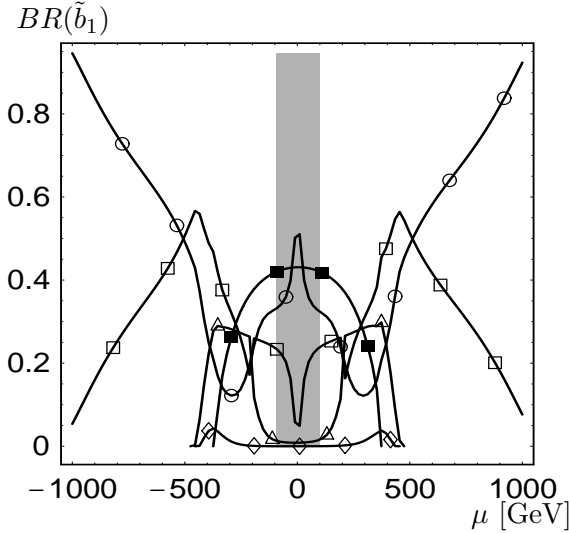


Fig. 9.3: Branching ratios for \tilde{b}_1 decays as a function of μ for $A_t = A_b = 500$ GeV, $M = 350$ GeV, $M_Q = 700$ GeV, $M_U = M_D = 500$ GeV, and $\tan \beta = 40$. The curves correspond to the following transitions: $\circ \tilde{b}_1 \rightarrow b \tilde{\chi}_1^0$, $\square \tilde{b}_1 \rightarrow b \tilde{\chi}_2^0$, $\triangle \tilde{b}_1 \rightarrow b \tilde{\chi}_3^0$, $\diamond \tilde{b}_1 \rightarrow b \tilde{\chi}_4^0$, and $\blacksquare \tilde{b}_1 \rightarrow t \tilde{\chi}_1^-$. The grey area will be covered by LEP2 ($m_{\tilde{\chi}_1^\pm} \leq 95$ GeV).

the decay into $H^- \tilde{t}_1$ we would like to note, that the term $\cos \theta_{\tilde{t}} \sin \theta_{\tilde{b}} m_b (\mu + A_b \tan \beta)$ is still suppressed because $\cos \theta_{\tilde{t}} \simeq -0.21$ and $|\cos \theta_{\tilde{b}}| \gtrsim 0.9$. This leads to the dominance of the above mentioned term in Eq. (9.1). For the same reason, $BR(\tilde{b}_1 \rightarrow W^- \tilde{t}_1)$ is larger than $BR(\tilde{b}_1 \rightarrow H^- \tilde{t}_1)$ for $|\mu| \gtrsim 500$ GeV.

Note, that a larger $|A_t|$ leads to an enhancement of the $W^- \tilde{t}_1$ mode. This is demonstrated in Fig. 9.2b where we show the branching ratios as a function of A_t for $\mu = -500$ GeV and the other parameters as above. Note, that $BR(\tilde{b}_1 \rightarrow W^- \tilde{t}_1)$ and $BR(\tilde{b}_1 \rightarrow H^- \tilde{t}_1)$ are of the same size if $|A_t| \simeq |\mu|$. This is a general result for large $\tan \beta$ scenarios if $M_U \ll M_Q \ll M_D$. In Fig. 9.2a the branching ratios are shown for $\tan \beta = 1.5$. The differences between positive and negative A_t are due the same reasons as between negative and positive μ .

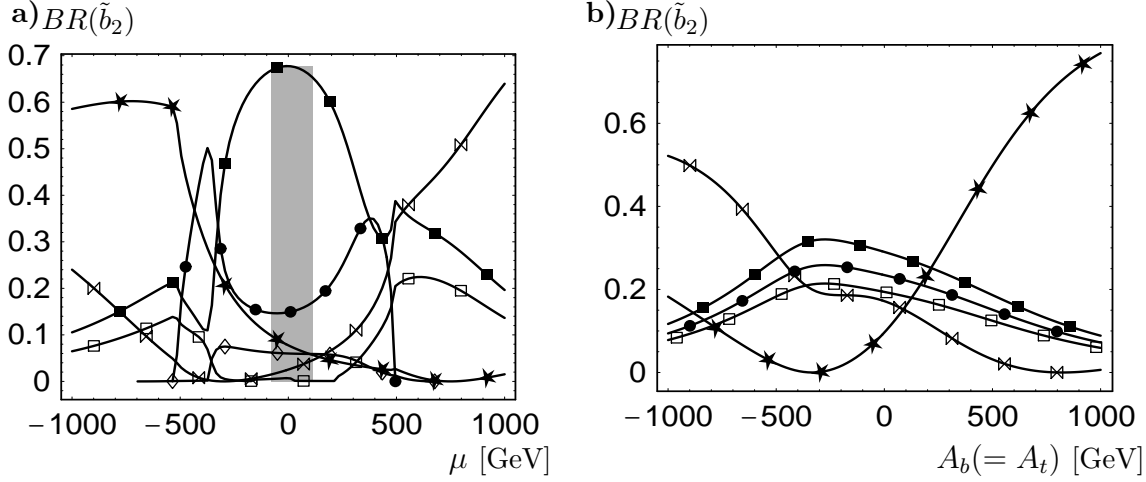


Fig. 9.4: Branching ratios for \tilde{b}_2 decays a) as a function of μ for $A_t = A_b = 500$ GeV and b) as a function of $A_b(= A_t)$ for $\mu = -500$ GeV. The other parameters are $\tan \beta = 1.5$, $M = 350$ GeV, $m_{A^0} = 150$ GeV, $M_Q = 700$ GeV, and $M_U = M_D = 500$ GeV. The curves correspond to: \square $\tilde{b}_2 \rightarrow b \tilde{\chi}_2^0$, \diamond $\tilde{b}_2 \rightarrow b \tilde{\chi}_4^0$, \blacksquare $\tilde{b}_2 \rightarrow t \tilde{\chi}_1^-$, \bullet $\tilde{b}_2 \rightarrow t \tilde{\chi}_2^-$, \star $\tilde{b}_2 \rightarrow W^- \tilde{t}_1$, and \bowtie $\tilde{b}_2 \rightarrow H^- \tilde{t}_1$. The grey area in a) will be covered by LEP2 ($m_{\tilde{\chi}_1^\pm} \leq 95$ GeV).

RGE studies favour the case $M_D \simeq M_U \ll M_Q$ if $\tan \beta$ is large. In such a case the decays into bosons will be kinematically forbidden and one has only decays into fermions as in the case $M_D \simeq M_U \simeq M_Q$. An example is presented in Fig. 9.3 where we have chosen $M_U = M_D = 500$ GeV, and $M_Q = 700$ GeV.

9.2 Decays of \tilde{b}_2

In the case that $\tan \beta$ is small it turns out that the decays of \tilde{b}_2 into bosons are negligible. The exceptions are the decays into $W^- \tilde{t}_1$, $H^- \tilde{t}_1$ if $M_U \simeq M_D \ll M_Q$ or in other words if $\tilde{b}_2 \simeq \tilde{b}_L$ and $m_{\tilde{b}_2} > m_{\tilde{t}_1} + m_W$, $m_{\tilde{t}_1} + m_{H^\pm}$. A typical example is shown in Fig. 9.4 where the branching ratios are shown as a function of μ and A_b for $M_D = M_U = 500$ GeV, $M_Q = 700$ GeV and $\tan \beta = 1.5$. Here, we do not show the decays into $b \tilde{\chi}_{1,3}^0$; $Z^0, h^0, H^0, A^0 \tilde{b}_1$ because the maximum of their branching ratios is less than 2%. Even their sum is always less than 5%. For the importance of the decays into $W^- \tilde{t}_1$ and $H^- \tilde{t}_1$ similar arguments hold as in the \tilde{b}_1 case if one replaces $\cos \theta_{\tilde{b}}$ by $-\sin \theta_{\tilde{b}}$ and $\sin \theta_{\tilde{b}}$ by $\cos \theta_{\tilde{b}}$. In the case $M_D \gg M_Q$ also $BR(\tilde{b}_2 \rightarrow W^- \tilde{t}_1)$ and $BR(\tilde{b}_2 \rightarrow H^- \tilde{t}_1)$ are small (1-5%). This can also be seen in Fig. 9.5 where we show the branching ratios as a function of $\tan \beta$ for $A_b = A_t = 500$ GeV and $\mu = -500$ GeV. Similar as in the case of \tilde{t}_2 it can be misleading if one simply interpolates the branching ratios between small and large $\tan \beta$ scenarios because of the minima and maxima in between. Note, that the smallness

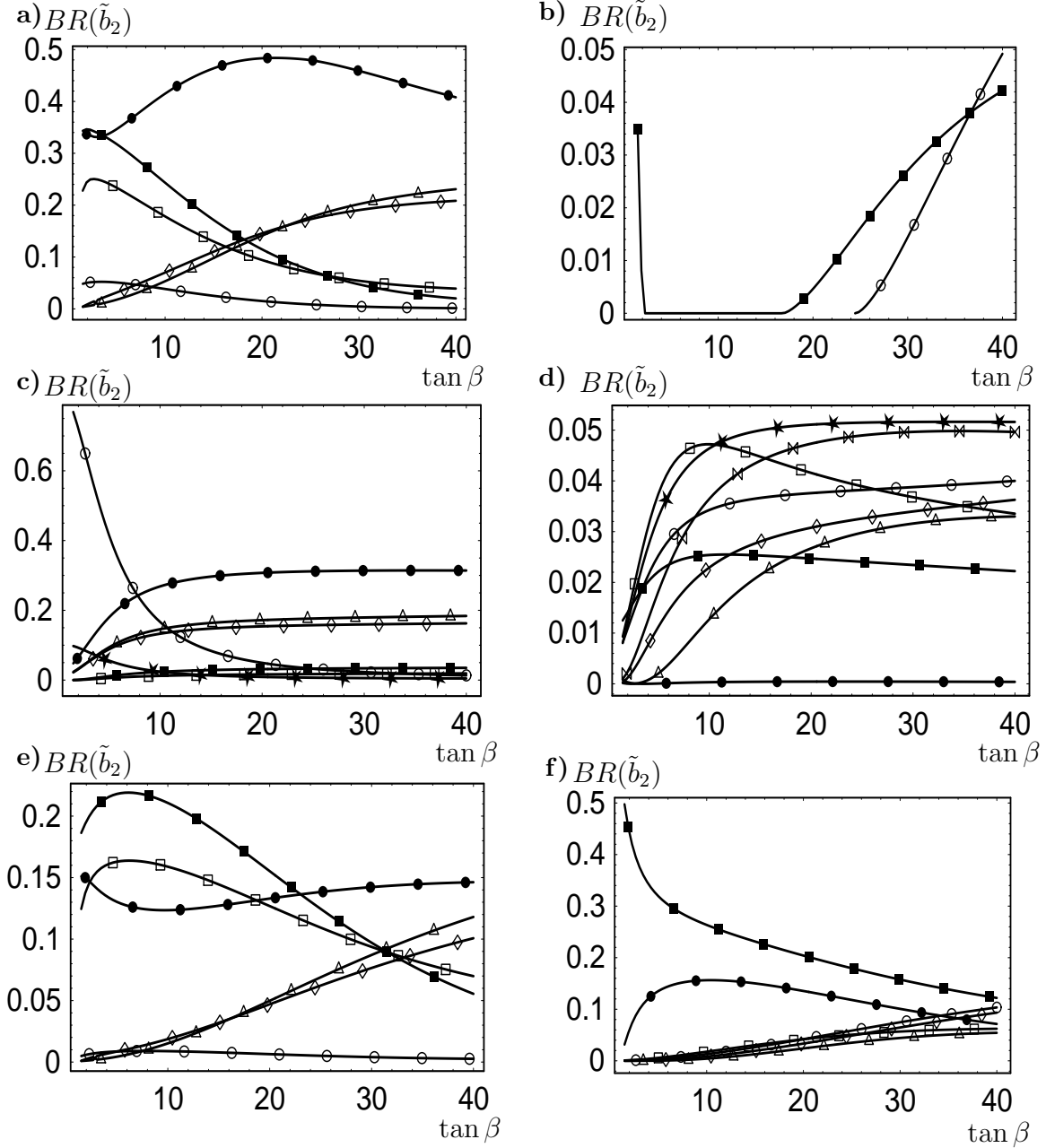


Fig. 9.5: Branching ratios for \tilde{b}_2 decays as a function of $\tan \beta$ for $\mu = -500$ GeV, $A_t = A_b = 500$ GeV, $M = 350$ GeV, $m_{A^0} = 150$ GeV, $M_Q = 700$ GeV, a) and b) $M_U = M_D = 700$ GeV, c) and d) $M_U = 350$ GeV, $M_D = 980$ GeV, e) and f) $M_U = M_D = 500$ GeV. The curves in a), c) and e) correspond to: $\circ \tilde{b}_2 \rightarrow b \tilde{\chi}_1^0$, $\square \tilde{b}_2 \rightarrow b \tilde{\chi}_2^0$, $\triangle \tilde{b}_2 \rightarrow b \tilde{\chi}_3^0$, $\diamond \tilde{b}_2 \rightarrow b \tilde{\chi}_4^0$, $\blacksquare \tilde{b}_2 \rightarrow t \tilde{\chi}_1^-$, $\bullet \tilde{b}_2 \rightarrow t \tilde{\chi}_2^-$, and $\star \tilde{b}_2 \rightarrow b \tilde{g}$. The curves in b), d) and f) correspond to: $\circ \tilde{b}_2 \rightarrow Z^0 \tilde{b}_1$, $\square \tilde{b}_2 \rightarrow h^0 \tilde{b}_1$, $\triangle \tilde{b}_2 \rightarrow H^0 \tilde{b}_1$, $\diamond \tilde{b}_2 \rightarrow A^0 \tilde{b}_1$, $\blacksquare \tilde{b}_2 \rightarrow W^- \tilde{t}_1$, $\star \tilde{b}_2 \rightarrow W^- \tilde{t}_2$, $\bullet \tilde{b}_2 \rightarrow H^- \tilde{t}_1$ and $\bowtie \tilde{b}_2 \rightarrow H^- \tilde{t}_2$.

of the branching ratios into bosonic states for $\tan\beta = 40$ in Fig. 9.5b and d is due to our choices of A_b, A_t and μ . The larger these parameters are the larger the branching ratios of the bosonic decay modes.

This is demonstrated in Fig. 9.6 where the branching ratios are shown as a function of μ for $\tan\beta = 40$. It is interesting to note that the sum of the branching ratios into bosonic modes is greater than 80% if $\max(M_D, M_Q) \lesssim |\mu|$. To explain their relative importance it is again useful to rewrite the most important parts of the couplings: (see also Eqs. (3.13), (3.15), (3.17) and (3.27)):

$$\begin{aligned}
Z\tilde{b}_2\tilde{b}_1 &\sim \sin 2\theta_{\tilde{b}} & h^0\tilde{b}_2\tilde{b}_1 &\sim \cos 2\theta_{\tilde{b}} (A_b \sin \alpha + \mu \cos \alpha) \\
A^0\tilde{b}_2\tilde{b}_1 &\sim (A_b \tan \beta + \mu) & H^0\tilde{b}_2\tilde{b}_1 &\sim \cos 2\theta_{\tilde{b}} (-A_b \cos \alpha + \mu \sin \alpha) \\
W^\pm\tilde{b}_2\tilde{t}_1 &\sim \cos \theta_{\tilde{t}} \sin \theta_{\tilde{b}} & W^\pm\tilde{b}_2\tilde{t}_2 &\sim \sin \theta_{\tilde{t}} \sin \theta_{\tilde{b}} \\
H^\pm\tilde{b}_2\tilde{t}_1 &\sim \sin \theta_{\tilde{t}} \sin \theta_{\tilde{b}} m_t (\mu + A_t \cot \beta) - \cos \theta_{\tilde{t}} \cos \theta_{\tilde{b}} m_b (\mu + A_b \tan \beta) \\
H^\pm\tilde{b}_2\tilde{t}_2 &\sim \cos \theta_{\tilde{t}} \sin \theta_{\tilde{b}} m_t (\mu + A_t \cot \beta) + \sin \theta_{\tilde{t}} \cos \theta_{\tilde{b}} m_b (\mu + A_b \tan \beta)
\end{aligned} \tag{9.2}$$

Let us start with the case $M_D = M_Q = M_U$ shown in Fig. 9.6a and b. The dominance of the decays into gauge bosons is again due to the factor λ/m_V^2 and because of the strong mixing in the sbottom and in the stop sector. The ordering of these two modes is caused by $m_{\tilde{b}_1} < m_{\tilde{t}_1}$. The decrease of $BR(\tilde{b}_2 \rightarrow A^0 \tilde{b}_1)$ occurs because $\Gamma(\tilde{b}_2 \rightarrow A^0 \tilde{b}_1)$ grows less with μ compared to the widths for the decays into gauge bosons.

In the case $M_D = 980$ GeV, $M_Q = 700$ GeV and $M_U = 350$ GeV all possible decays into gauge and Higgs bosons are kinematically allowed (Fig. 9.5c and d). For large $|\mu|$ the decay $\tilde{b}_2 \rightarrow W^- \tilde{t}_2$ is the most important one followed by $\tilde{b}_2 \rightarrow Z \tilde{b}_1$ and $\tilde{b}_2 \rightarrow h^0 \tilde{b}_1$. This can be understood by noticing that $|\cos \theta_{\tilde{t}}| \lesssim 0.3$, $|\cos \theta_{\tilde{b}}| \gtrsim 0.9$, and $\cos \alpha \simeq 1$. This leads to the remarkable result that $BR(\tilde{b}_2 \rightarrow W^- \tilde{t}_2) > BR(\tilde{b}_2 \rightarrow W^- \tilde{t}_1)$ and $BR(\tilde{b}_2 \rightarrow H^- \tilde{t}_2) > BR(\tilde{b}_2 \rightarrow H^- \tilde{t}_1)$ because \tilde{t}_2 is mainly a left state. Note, that the $H^\pm \tilde{q}_L \tilde{q}'_R$ coupling is in general larger than the $H^\pm \tilde{q}_R \tilde{q}'_R$ coupling and the $H^\pm \tilde{q}_L \tilde{q}'_L$ coupling. As in the case of the neutral Higgs this corresponds to the chirality change in the $H^\pm \bar{q} q'$ coupling. The decay $\tilde{b}_2 \rightarrow Z \tilde{b}_1$ is less important than $\tilde{b}_2 \rightarrow W^- \tilde{t}_2$ because there is only a small mixing in the sbottom sector. Especially in the range $|\mu| \lesssim M$, the smallness of $\sin \theta_{\tilde{b}}$ leads to the suppression of both branching ratios. In this range the most important bosonic decay modes are $\tilde{b}_2 \rightarrow H^- \tilde{t}_2$, $H^0 \tilde{b}_1$, $A^0 \tilde{b}_1$. Here their decay widths depend hardly on μ . The sum of their branching ratios does not exceed 12% and therefore they are less important than the fermionic decay modes. Here $\tilde{b}_2 \rightarrow t \tilde{\chi}_1^-$ is the most important decay because of the large top Yukawa coupling. Finally, we would like to note that the decay $\tilde{b}_2 \rightarrow b \tilde{g}$ also is possible in this example. However, its branching ratio is always smaller than 2% and thus it is now shown.

In the case $M_D = M_U = 500$ GeV and $M_Q = 700$ GeV $\tilde{b}_2 \rightarrow Z \tilde{b}_1$ is the most important decay for large $|\mu|$. The mixing in the sbottom sector is larger than in the

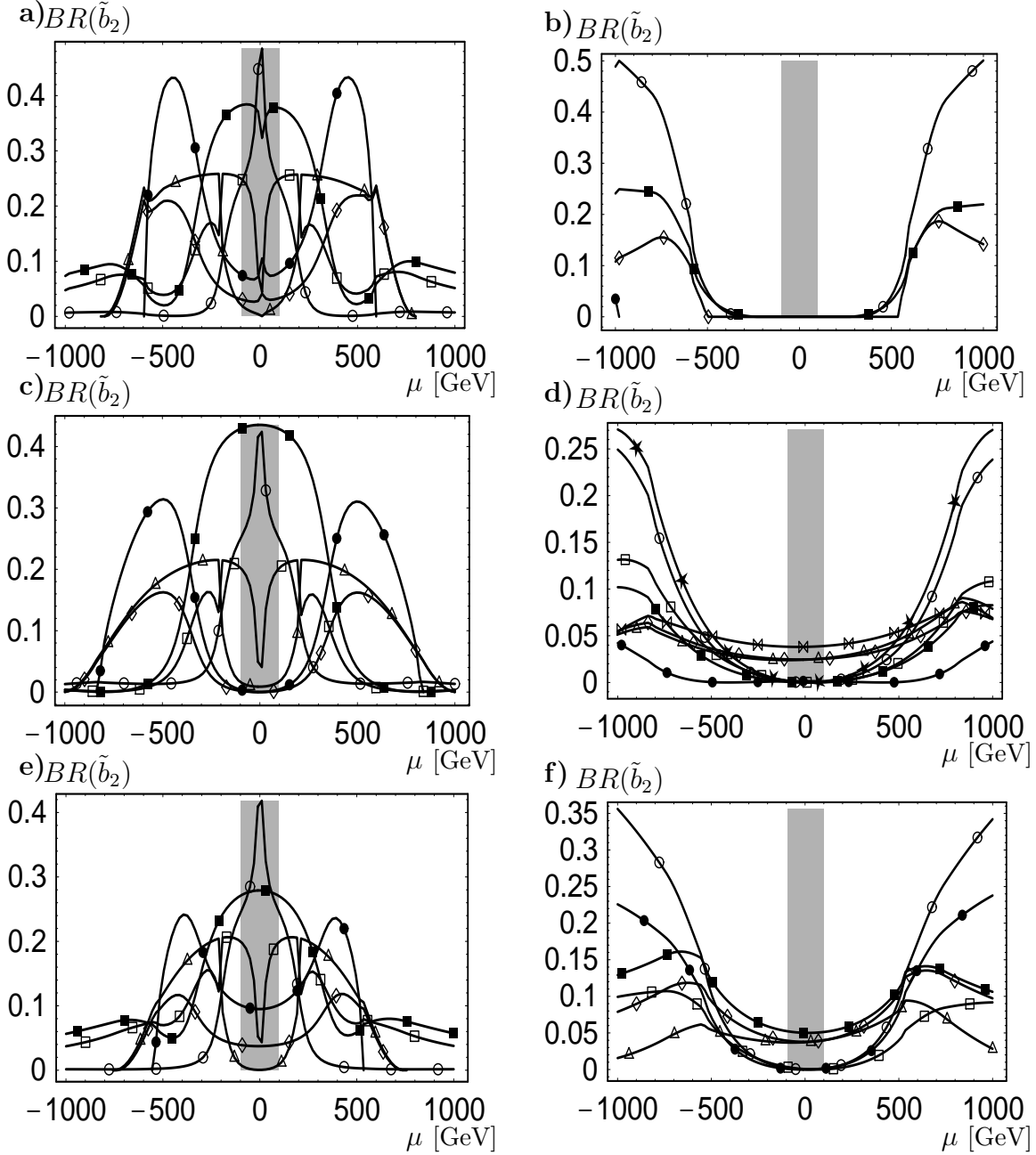


Fig. 9.6: Branching ratios for \tilde{b}_2 decays as a function of μ for $\tan\beta = 40$, $A_t = A_b = 500$ GeV, $M = 350$ GeV, $m_{A^0} = 150$ GeV, $M_Q = 700$ GeV, a) and b) $M_U = M_D = 700$ GeV, c) and d) $M_U = 350$ GeV, $M_D = 980$ GeV, e) and f) $M_U = M_D = 500$ GeV. The curves in a), c) and e) correspond to: $\circ \tilde{b}_2 \rightarrow b \tilde{\chi}_1^0$, $\square \tilde{b}_2 \rightarrow b \tilde{\chi}_2^0$, $\triangle \tilde{b}_2 \rightarrow b \tilde{\chi}_3^0$, $\diamond \tilde{b}_2 \rightarrow b \tilde{\chi}_4^0$, $\blacksquare \tilde{b}_2 \rightarrow t \tilde{\chi}_1^-$, and $\bullet \tilde{b}_2 \rightarrow t \tilde{\chi}_2^-$. The curves in b), d) and f) correspond to: $\circ \tilde{b}_2 \rightarrow Z^0 \tilde{b}_1$, $\square \tilde{b}_2 \rightarrow h^0 \tilde{b}_1$, $\triangle \tilde{b}_2 \rightarrow H^0 \tilde{b}_1$, $\diamond \tilde{b}_2 \rightarrow A^0 \tilde{b}_1$, $\blacksquare \tilde{b}_2 \rightarrow W^- \tilde{t}_1$, $\star \tilde{b}_2 \rightarrow W^- \tilde{t}_2$, $\bullet \tilde{b}_2 \rightarrow H^- \tilde{t}_1$, and $\bowtie \tilde{b}_2 \rightarrow H^- \tilde{t}_2$. The grey area will be covered by LEP2 ($m_{\tilde{\chi}_1^\pm} \leq 95$ GeV).

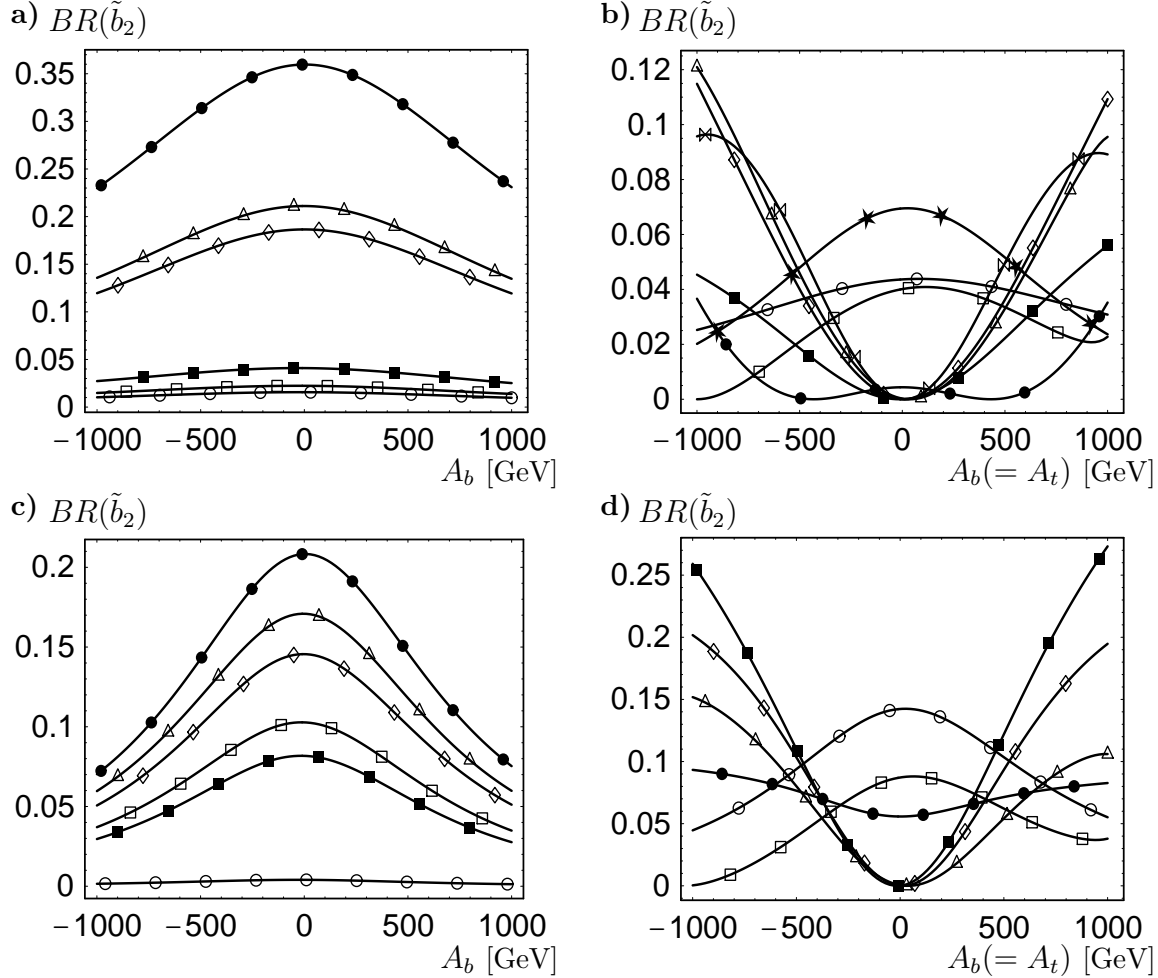


Fig. 9.7: Branching ratios for \tilde{b}_2 decays as a function of $A_b (= A_t)$ for $\tan \beta = 40$, $\mu = -500$ GeV, $M = 350$ GeV, $m_{A^0} = 150$ GeV, $M_Q = 700$ GeV, a) and b) $M_U = 350$ GeV, $M_D = 980$ GeV, c) and d) $M_U = M_D = 500$ GeV. The curves in a), and c) correspond to: $\circ \tilde{b}_2 \rightarrow b \tilde{\chi}_1^0$, $\square \tilde{b}_2 \rightarrow b \tilde{\chi}_2^0$, $\triangle \tilde{b}_2 \rightarrow b \tilde{\chi}_3^0$, $\diamond \tilde{b}_2 \rightarrow b \tilde{\chi}_4^0$, $\blacksquare \tilde{b}_2 \rightarrow t \tilde{\chi}_1^-$, $\bullet \tilde{b}_2 \rightarrow t \tilde{\chi}_2^-$, and $\star \tilde{b}_2 \rightarrow b \tilde{g}$. The curves in b), and d) correspond to: $\circ \tilde{b}_2 \rightarrow Z^0 \tilde{b}_1$, $\square \tilde{b}_2 \rightarrow h^0 \tilde{b}_1$, $\triangle \tilde{b}_2 \rightarrow H^0 \tilde{b}_1$, $\diamond \tilde{b}_2 \rightarrow A^0 \tilde{b}_1$, $\blacksquare \tilde{b}_2 \rightarrow W^- \tilde{t}_1$, $\star \tilde{b}_2 \rightarrow W^- \tilde{t}_2$, $\bullet \tilde{b}_2 \rightarrow H^- \tilde{t}_1$ and $\bowtie \tilde{b}_2 \rightarrow H^- \tilde{t}_2$.

previous case. Moreover, the decays into \tilde{t}_2 are kinematically not possible. In this example \tilde{t}_1 and \tilde{b}_1 are mainly right states leading to $BR(\tilde{b}_2 \rightarrow H^- \tilde{t}_1) > BR(\tilde{b}_2 \rightarrow W^- \tilde{t}_1)$ for large $|\mu|$ although $m_W < m_{H^\pm}$. $\Gamma(\tilde{b}_2 \rightarrow H^- \tilde{t}_1)$ vanishes for small μ because of kinematics (see also Chapter 6).

Let us have a short look on the fermionic decay modes. In general the most important ones among them are those into a chargino independent of $\cos \theta_{\tilde{b}}$. Whenever the decays into neutralinos are more important it turns out that they are higgsino

like. In each case the (relative) dominance is due to large Yukawa couplings.

Let us finally discuss the A_b dependence for the cases $M_D < M_Q$ and $M_D > M_Q$ Fig. 9.7. Here $m_{\tilde{b}_1}$, $m_{\tilde{b}_2}$, and $\cos \theta_{\tilde{b}}$ are nearly independent of A_b because $\tan \beta = 40$. This implies that the widths for the decays into charginos, into neutralinos, and into $Z \tilde{b}_1$ also are nearly independent of A_b . We start with the case $M_U < M_Q < M_D$ shown in Fig. 9.7a and b. The ordering of the various modes can be understood by noting that i) $\cos \theta_{\tilde{t}} \simeq 0$ for small μ , and for large μ $|\cos \theta_{\tilde{t}}| \simeq 1/2$, ii) m_{h^0} and m_{H^\pm} grow with $|A_b|$ whereas m_{H^0} decreases, iii) $\sin \alpha \simeq -0.45$ for $A_b \simeq -1$ TeV and $\sin \alpha \simeq 0.05$ for $A_b \simeq 1$ TeV. The first point leads to a decrease of $BR(\tilde{b}_2 \rightarrow W^- \tilde{t}_2)$ for large $|A_b|$ and at the same time to an increase in the $BR(\tilde{b}_2 \rightarrow W^- \tilde{t}_1)$. The second observation implies a slower increase of $\Gamma(\tilde{b}_2 \rightarrow H^- \tilde{t}_2)$ compared to $\Gamma(\tilde{b}_2 \rightarrow A^0 \tilde{b}_1)$ which grows as $A_b^2 \tan^2 \beta$ leading to the decrease in the $BR(\tilde{b}_2 \rightarrow H^- \tilde{t}_2)$ for $|A_b| \simeq 1$ TeV. The third observation explains the dependence of $BR(\tilde{b}_2 \rightarrow h^0 \tilde{b}_1)$ and $BR(\tilde{b}_2 \rightarrow H^0 \tilde{b}_1)$ on the sign of A_b . Similar arguments hold for the case $M_D = M_U < M_Q$ shown in Fig. 9.7c and d.

Chapter 10

Higher order decays of \tilde{t}_1 and \tilde{b}_1

10.1 Three body decays of \tilde{t}_1

In Section 4.1 scenarios have been presented where the main decays of \tilde{t}_1 are three body decays into sleptons. For larger stop masses also the decays into $b W^+ \tilde{\chi}_1^0$ and $b H^+ \tilde{\chi}_1^0$ become possible as we have seen in Section 8.1. There only scenarios have been considered where decays into sleptons are kinematically forbidden. In this section we are going to compare both possibilities.

For fixing the parameters we have chosen the following procedure: additional to $\tan \beta$ and μ we have used within the stop sector $m_{\tilde{t}_1}$ and $\cos \theta_{\tilde{t}}$ as input parameters. For the sbottom (stau) sector we have fixed M_Q, M_D and A_b (M_E, M_L, A_τ) as input parameters. We have used this mixed set of parameters in order to avoid unnatural parameters in the sbottom (stau) sector. Moreover, we have assumed for simplicity that the soft SUSY breaking parameters are equal for all generations. Note, that because of $SU(2)$ invariance M_Q also appears in the stop mass matrix (see Eq. (2.33) and also Appendix B). After some algebraic manipulation of the formulae in Appendix B it can be seen that by variation of μ or $\tan \beta$ for fixed $m_{\tilde{t}_1}$ and $\cos \theta_{\tilde{t}}$ one also varies A_t and M_U . Therefore, the mass of the heavier stop can be calculated from this set of input parameters:

$$m_{\tilde{t}_2}^2 = \frac{2M_Q^2 + 2m_Z^2 \cos 2\beta \left(\frac{1}{2} - \frac{2}{3} \sin^2 \theta_W \right) + 2m_t^2 - m_{\tilde{t}_1}^2 (1 + \cos 2\theta_{\tilde{t}})}{1 - \cos 2\theta_{\tilde{t}}} \quad (10.1)$$

In the sbottom (stau) sector obviously the physical quantities $m_{\tilde{b}_1}, m_{\tilde{b}_2}$, and $\cos \theta_{\tilde{b}}$ ($m_{\tilde{\tau}_1}, m_{\tilde{\tau}_2}, \cos \theta_{\tilde{\tau}}$) change with μ and $\tan \beta$.

A typical example is given in Fig. 10.1 where we show branching ratios as a function of $\cos \theta_{\tilde{t}}$. We have restricted the $\cos \theta_{\tilde{t}}$ range in such a way that $|A_t| \lesssim 1$ TeV to avoid color/charge breaking minima. The parameters and physical quantities are given in Tab. 10.1. The slepton parameters have been chosen in such a way that

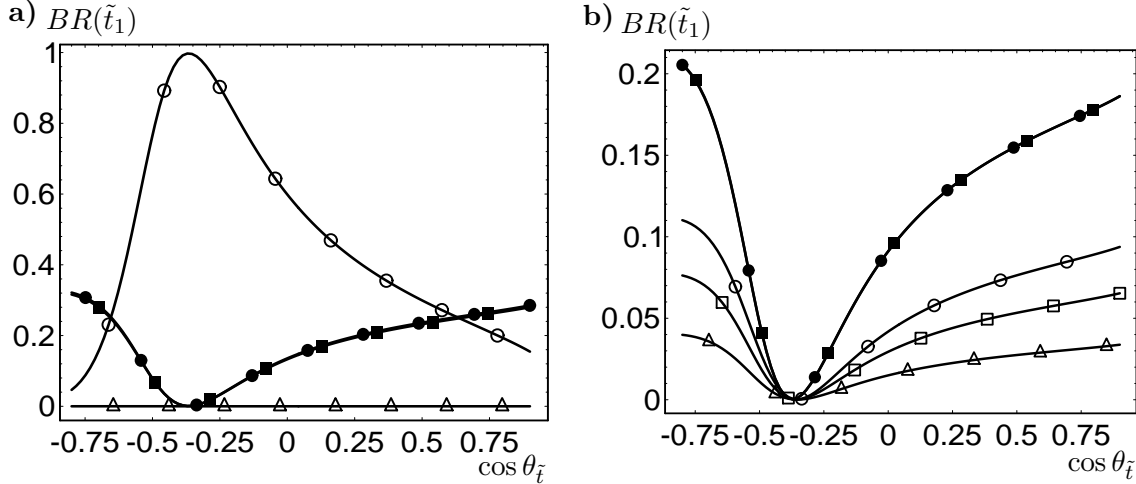


Fig. 10.1: Branching ratios for \tilde{t}_1 decays as a function of $\cos \theta_{\tilde{t}}$ for $m_{\tilde{t}_1} = 250$ GeV, $\tan \beta = 2$, $\mu = 530$ GeV, and $M = 270$ GeV. The other parameters are given in Tab. 10.1. The curves in a) correspond to the transitions: $\circ \tilde{t}_1 \rightarrow b W^+ \tilde{\chi}_1^0$, $\triangle \tilde{t}_1 \rightarrow c \tilde{\chi}_1^0$, $\blacksquare (\tilde{t}_1 \rightarrow b e^+ \tilde{\nu}_e) + (\tilde{t}_1 \rightarrow b \nu_e \tilde{e}_L^+)$, and $\bullet (\tilde{t}_1 \rightarrow b \tau^+ \tilde{\nu}_\tau) + (\tilde{t}_1 \rightarrow b \nu_\tau \tilde{\tau}_1) + (\tilde{t}_1 \rightarrow b \nu_\tau \tilde{\tau}_2)$. The curves in b) correspond to the transitions: $\circ \tilde{t}_1 \rightarrow b \nu_e \tilde{e}_L^+$, $\square \tilde{t}_1 \rightarrow b \nu_\tau \tilde{\tau}_1$, $\triangle \tilde{t}_1 \rightarrow b \nu_\tau \tilde{\tau}_2$, $\blacksquare \tilde{t}_1 \rightarrow b e^+ \tilde{\nu}_e$, and $\bullet \tilde{t}_1 \rightarrow b \tau^+ \tilde{\nu}_\tau$.

$\tan \beta$	μ	M	$m_{\tilde{\chi}_1^0}$	$m_{\tilde{\chi}_1^+}$	$m_{\tilde{\chi}_2^+}$
2	530	270	130	250	551
M_D	M_Q	A_b	$m_{\tilde{b}_1}$	$m_{\tilde{b}_2}$	$\cos \theta_{\tilde{b}}$
370	340	150	342	372	0.98
M_E	M_L	A_τ	$m_{\tilde{\tau}_1}$	$m_{\tilde{\tau}_2}$	$\cos \theta_{\tilde{\tau}}$
210	210	150	209	217	0.68
		$m_{\tilde{t}_1}$	$m_{\tilde{e}_L}$	$m_{\tilde{e}_R}$	$m_{\tilde{\nu}_\tau}$
		250	213	212	204

Table 10.1: Parameters and physical quantities used in Fig. 10.1. All masses are given in GeV.

the sum of the final state particles are 215 ± 5 GeV leading to comparable kinematics for each decay mode. In Fig. 10.1a we present $BR(\tilde{t}_1 \rightarrow b W^+ \tilde{\chi}_1^0)$, $BR(\tilde{t}_1 \rightarrow c \tilde{\chi}_1^0)$, $BR(\tilde{t}_1 \rightarrow b e^+ \tilde{\nu}_e) + BR(\tilde{t}_1 \rightarrow b \nu_e \tilde{e}_L^+)$, and $BR(\tilde{t}_1 \rightarrow b \tau^+ \tilde{\nu}_\tau) + BR(\tilde{t}_1 \rightarrow b \nu_\tau \tilde{\tau}_1) + BR(\tilde{t}_1 \rightarrow b \nu_\tau \tilde{\tau}_2)$. Here we have not included the possibility $BR(\tilde{t}_1 \rightarrow b H^+ \tilde{\chi}_1^0)$ because it was not possible to find a m_{A^0} which simultaneously allowed this decay and fulfilled the condition $m_{h^0} \gtrsim 70$ GeV. However, we will

discuss this decay later on. We have added those branching ratios for the decays into sleptons that give the same final state after the sleptons have decayed. For example:

$$\tilde{t}_1 \rightarrow b \nu_\tau \tilde{\tau}_1 \rightarrow b \tau \nu_\tau \tilde{\chi}_1^0; \quad \tilde{t}_1 \rightarrow b \tau \tilde{\nu}_\tau \rightarrow b \tau \nu_\tau \tilde{\chi}_1^0 \quad (10.2)$$

Note, that the requirement $m_{\tilde{t}_1} - m_b < m_{\tilde{\chi}_1^+}$ implies that the sleptons can only decay into the corresponding lepton plus the lightest neutralino except a small parameter

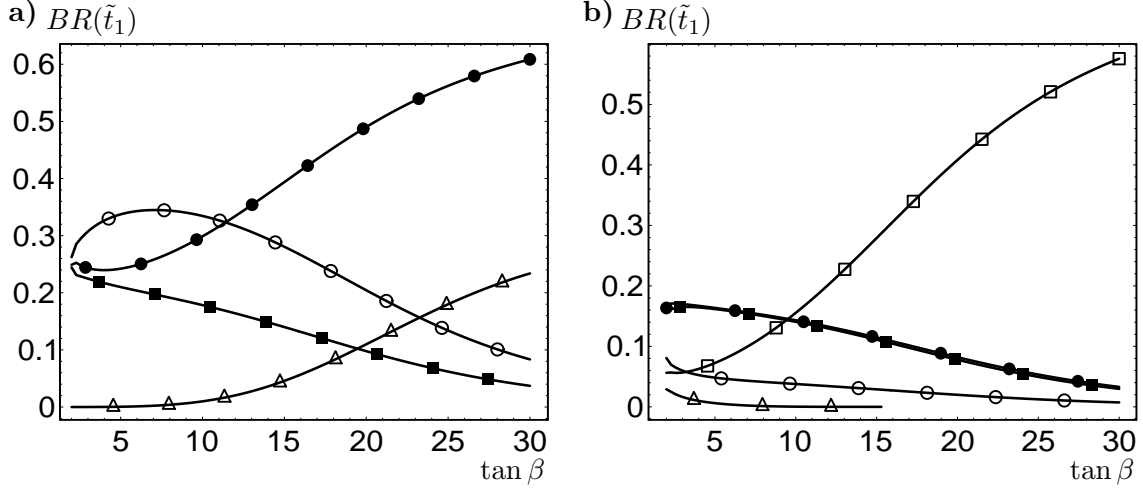


Fig. 10.2: Branching ratios for \tilde{t}_1 decays as a function of $\tan \beta$ for $m_{\tilde{t}_1} = 250$ GeV, $\cos \theta_{\tilde{t}} = 0.6$, $\mu = 530$ GeV, $M = 270$ GeV. The other parameters are given in Tab. 10.1. The curves in a) correspond to the transitions: $\circ \tilde{t}_1 \rightarrow b W^+ \tilde{\chi}_1^0$, $\triangle \tilde{t}_1 \rightarrow c \tilde{\chi}_1^0$, $\blacksquare (\tilde{t}_1 \rightarrow b e^+ \tilde{\nu}_e) + (\tilde{t}_1 \rightarrow b \nu_e \tilde{e}_L^+)$, and $\bullet (\tilde{t}_1 \rightarrow b \tau^+ \tilde{\nu}_\tau) + (\tilde{t}_1 \rightarrow b \nu_\tau \tilde{\tau}_1) + (\tilde{t}_1 \rightarrow b \nu_\tau \tilde{\tau}_2)$. The curves in b) correspond to the transitions: $\circ \tilde{t}_1 \rightarrow b \nu_e \tilde{e}_L^+$, $\square \tilde{t}_1 \rightarrow b \nu_\tau \tilde{\tau}_1$, $\triangle \tilde{t}_1 \rightarrow b \nu_\tau \tilde{\tau}_2$, $\blacksquare \tilde{t}_1 \rightarrow b e^+ \tilde{\nu}_e$, and $\bullet \tilde{t}_1 \rightarrow b \tau^+ \tilde{\nu}_\tau$.

region where the decay into $\tilde{\chi}_2^0$ is possible. However, there this decay will be negligible due to kinematics. The branching ratios for decays into $\tilde{\mu}_L$, $\tilde{\nu}_\mu$ are not shown because they are the same as in the case of \tilde{e}_L , $\tilde{\nu}_e$ up to very tiny mass effects. The sum of the branching ratios for the decays into $\tilde{\tau}_1$ and $\tilde{\tau}_2$ also has nearly the same size because of the small $\tan \beta$. The $BR(\tilde{t}_1 \rightarrow c \tilde{\chi}_1^0)$ is $O(10^{-4})$ independent of $\cos \theta_{\tilde{t}}$ and therefore is negligible. Near $\cos \theta_{\tilde{t}} = -0.3$ the decay into $b W^+ \tilde{\chi}_1^0$ has a branching ratio of $\sim 100\%$. Here $\tilde{l}_{11}^{\tilde{t}}$ vanishes leading to the reduction of the decays into sleptons (see also Section 4.1).

In Fig. 10.1b the branching ratios for the decays into the different sleptons are shown. As already mentioned in Section 4.1 the sleptons couple mainly to the gaugino components of $\tilde{\chi}_1^+$ if $\tan \beta$ is small. Therefore, the branching ratios for decays into the staus are reduced because they are strongly mixed. However, the sum of both branching ratios is nearly the same as $BR(\tilde{t}_1 \rightarrow b \nu_e \tilde{e}_L^+)$. The decays into sneutrinos are preferred by kinematics. Moreover, the matrix elements (Eq. (3.35) and (3.36)) for the decays into charged and neutral sleptons have a different structure in the limit $m_b, m_l \rightarrow 0$ leading to an additional difference:

$$T_{fi}(\tilde{t}_1 \rightarrow b l^+ \tilde{\nu}) \sim m_{\tilde{\chi}_i^\pm} \bar{u}(p_b) P_R v(p_l) \quad (10.3)$$

$$T_{fi}(\tilde{t}_1 \rightarrow b \nu_l \tilde{l}_k) \sim \bar{u}(p_b) P_R \not{p}_{\tilde{\chi}_i^\pm} v(p_{\nu_l}) \quad (10.4)$$

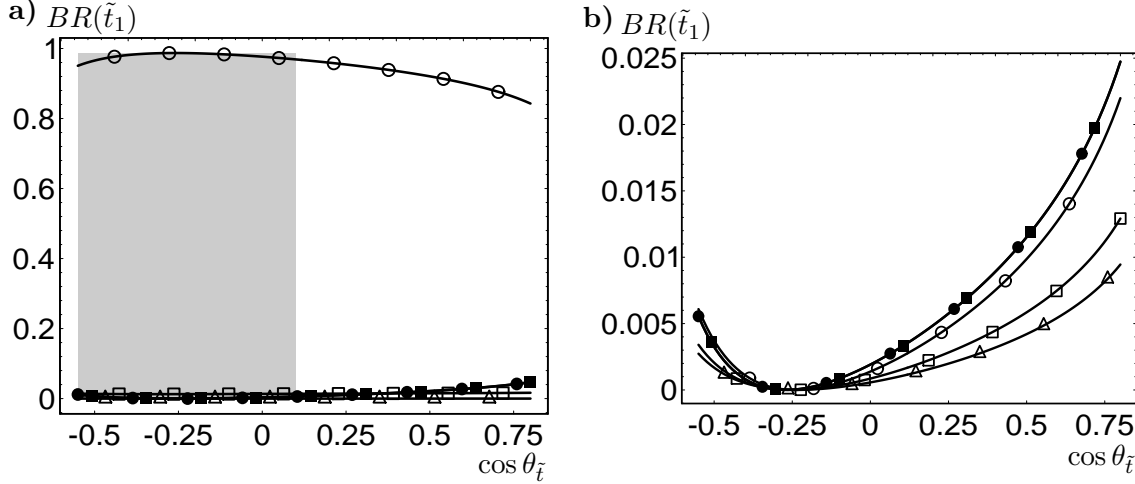


Fig. 10.3: Branching ratios for \tilde{t}_1 decays as a function of $\cos \theta_{\tilde{t}}$ for $m_{\tilde{t}_1} = 350$ GeV, $\tan \beta = 2$, $\mu = 750$ GeV, $M = 380$ GeV, and $m_{A^0} = 110$ GeV. The other parameters are given in the text. The curves in a) correspond to the transitions: $\circ \tilde{t}_1 \rightarrow b W^+ \tilde{\chi}_1^0$, $\square \tilde{t}_1 \rightarrow b H^+ \tilde{\chi}_1^0$, $\triangle \tilde{t}_1 \rightarrow c \tilde{\chi}_1^0$, $\blacksquare (\tilde{t}_1 \rightarrow b e^+ \tilde{\nu}_e) + (\tilde{t}_1 \rightarrow b \nu_e \tilde{e}_L^+)$, and $\bullet (\tilde{t}_1 \rightarrow b \tau^+ \tilde{\nu}_\tau) + (\tilde{t}_1 \rightarrow b \nu_\tau \tilde{\tau}_1) + (\tilde{t}_1 \rightarrow b \nu_\tau \tilde{\tau}_2)$. The curves in b) correspond to the transitions: $\circ \tilde{t}_1 \rightarrow b \nu_e \tilde{e}_L^+$, $\square \tilde{t}_1 \rightarrow b \nu_\tau \tilde{\tau}_1$, $\triangle \tilde{t}_1 \rightarrow b \nu_\tau \tilde{\tau}_2$, $\blacksquare \tilde{t}_1 \rightarrow b e^+ \tilde{\nu}_e$, and $\bullet \tilde{t}_1 \rightarrow b \tau^+ \tilde{\nu}_\tau$. In the grey area m_{h^0} is smaller than 70 GeV.

$\tan \beta$	μ	M	$m_{\tilde{\chi}_1^0}$	$m_{\tilde{\chi}_1^+}$	$m_{\tilde{\chi}_2^+}$
2	750	380	186	366	766
M_D	M_Q	A_b	$m_{\tilde{b}_1}$	$m_{\tilde{b}_2}$	$\cos \theta_{\tilde{b}}$
550	500	400	502	551	0.99
M_E	M_L	A_τ	$m_{\tilde{\tau}_1}$	$m_{\tilde{\tau}_2}$	$\cos \theta_{\tilde{\tau}}$
275	275	400	274	281	0.69
m_{H^+}	m_{A^0}	$m_{\tilde{t}_1}$	$m_{\tilde{e}_L}$	$m_{\tilde{e}_R}$	$m_{\tilde{\nu}_\tau}$
130 ± 1	110	350	278	277	270

Table 10.2: Parameters and physical quantities used in Fig. 10.3. All masses are given in GeV.

This leads to different decay widths even in the case where one assumes equal masses for all sleptons. The decay $\tilde{t}_1 \rightarrow b W^+ \tilde{\chi}_1^0$ is dominated by the t -quark contribution followed by the chargino contributions. In many cases the interference term between t and $\tilde{\chi}_{1,2}^+$ is more important than the $\tilde{\chi}_{1,2}^+$ part. Moreover, we have found that the contribution from the exchange of the sbottoms are in general negligible.

In Fig. 10.2 we show the branching ratios as a function of $\tan \beta$ for $\cos \theta_{\tilde{t}} = 0.6$ and the other parameters as above. For small $\tan \beta$ the decay into $\tilde{t}_1 \rightarrow b W^+ \tilde{\chi}_1^0$ is the most important one. The branching ratios for the decays into sleptons are reduced in the range $\tan \beta \lesssim 5$ because the gaugino component of $\tilde{\chi}_1^+$ decreases and its mass increases. For $\tan \beta \gtrsim 10$ the decays into the $b \tau \cancel{E}$ final state becomes more important because of the growing τ Yukawa coupling and because of kinematics ($m_{\tilde{\tau}_1}$ decreases if $\tan \beta$ increases and the other parameters are

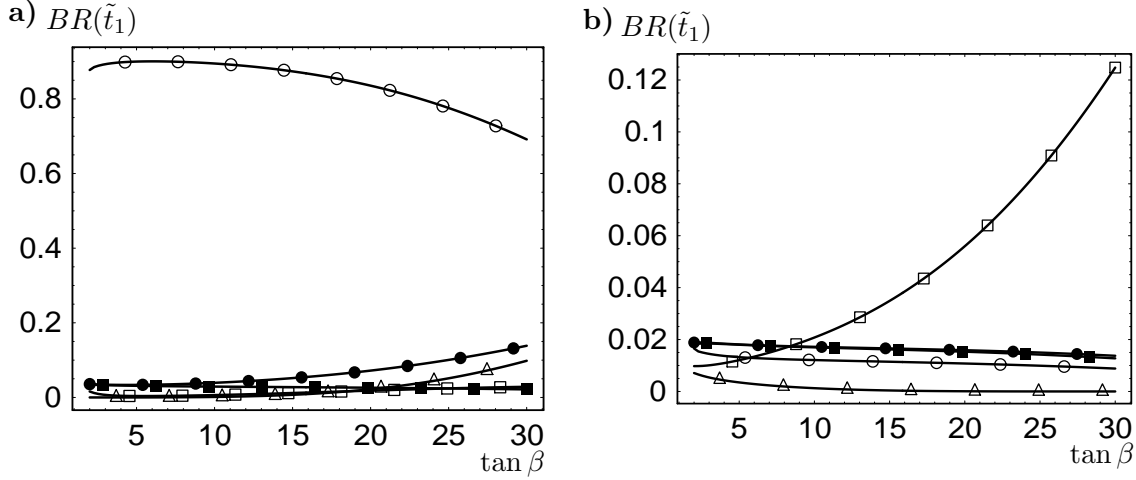


Fig. 10.4: Branching ratios for \tilde{t}_1 decays as a function of $\tan\beta$ for $m_{\tilde{t}_1} = 350$ GeV, $\cos\theta_{\tilde{t}} = 0.7$, $\mu = 750$ GeV, $M = 380$ GeV and $m_{A^0} = 110$ GeV. The other parameters are given in Tab. 10.2. The curves in a) correspond to the transitions: $\circ \tilde{t}_1 \rightarrow b W^+ \tilde{\chi}_1^0$, $\square \tilde{t}_1 \rightarrow b H^+ \tilde{\chi}_1^0$, $\triangle \tilde{t}_1 \rightarrow c \tilde{\chi}_1^0$, $\blacksquare (\tilde{t}_1 \rightarrow b e^+ \tilde{\nu}_e) + (\tilde{t}_1 \rightarrow b \nu_e \tilde{e}_L^+)$, and $\bullet (\tilde{t}_1 \rightarrow b \tau^+ \tilde{\nu}_\tau) + (\tilde{t}_1 \rightarrow b \nu_\tau \tilde{\tau}_1) + (\tilde{t}_1 \rightarrow b \nu_\tau \tilde{\tau}_2)$. The curves in b) correspond to the transitions: $\circ \tilde{t}_1 \rightarrow b \nu_e \tilde{e}_L^+$, $\square \tilde{t}_1 \rightarrow b \nu_\tau \tilde{\tau}_1$, $\triangle \tilde{t}_1 \rightarrow b \nu_\tau \tilde{\tau}_2$, $\blacksquare \tilde{t}_1 \rightarrow b e^+ \tilde{\nu}_e$, and $\bullet \tilde{t}_1 \rightarrow b \tau^+ \tilde{\nu}_\tau$.

fixed. See also the discussion at the end of Section 4.1). Here $\tilde{t}_1 \rightarrow b \nu_\tau \tilde{\tau}_1$ is the most important contribution as can be seen in Fig. 10.2b. For large $\tan\beta$ the decay into $c \tilde{\chi}_1^0$ also gains some importance because the width is proportional to the bottom Yukawa coupling in the approximation used (Eq. (3.41) and (3.42)).

From the requirement that no two body decays are allowed at tree level follows that $m_{\tilde{\chi}_1^+} > m_{\tilde{t}_1} - m_b$. Therefore, one expects an increase of $BR(\tilde{t}_1 \rightarrow b W^+ \tilde{\chi}_1^0)$ if $m_{\tilde{t}_1}$ increases, because the decay into $b W^+ \tilde{\chi}_1^0$ is dominated by the t exchange whereas for the decays into sleptons the $\tilde{\chi}_1^\pm$ contribution is the dominating one. This is demonstrated in Fig. 10.3 where we have fixed $m_{\tilde{t}_1} = 350$ GeV. Here we have also found scenarios where the decay into $b H^+ \tilde{\chi}_1^0$ is possible. It turns out that this channel is in general negligible because of kinematics. We have not found any case where $m_{H^+} \lesssim 120$ GeV if we use the mass formulae for the Higgs bosons in the MSSM and at the same time include the experimental bound $m_{h^0} < 70$ GeV [64].

These general features hold even if $\tan\beta$ increases as can be seen in Fig. 10.4. Here we have fixed $\cos\theta_{\tilde{t}} = 0.7$. As expected by the discussion above, the decay into $\tilde{t}_1 \rightarrow b \nu_\tau \tilde{\tau}_1$ gains some importance for large $\tan\beta$. Note, that for large $\tan\beta$ $BR(\tilde{t}_1 \rightarrow b H^+ \tilde{\chi}_1^0)$ decreases since m_{H^+} increases due to radiative corrections. However, there are scenarios where this decay can become important as demonstrated in Fig. 10.5. Here we show the branching ratios as a function of M_D for $m_{A^0} = 90$ GeV, $\tan\beta = 30$ and the other parameters as in Tab. 10.2. At the lower

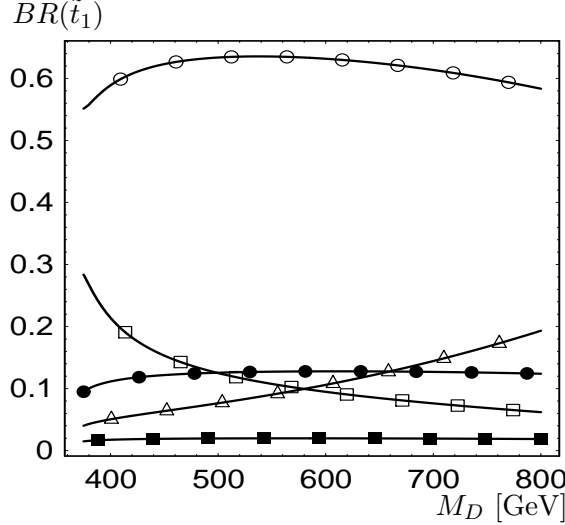


Fig. 10.5: Branching ratios for \tilde{t}_1 decays as a function of M_D for $m_{\tilde{t}_1} = 350$ GeV, $\cos\theta_{\tilde{t}} = 0.7$, $\tan\beta = 30$, $\mu = 750$ GeV, $M = 380$ GeV and $m_{A^0} = 90$ GeV. The other parameters are given in Tab. 10.2. The curves in a) correspond to the transitions: $\circ \tilde{t}_1 \rightarrow b W^+ \tilde{\chi}_1^0$, $\square \tilde{t}_1 \rightarrow b H^+ \tilde{\chi}_1^0$, $\triangle \tilde{t}_1 \rightarrow c \tilde{\chi}_1^0$, $\blacksquare (\tilde{t}_1 \rightarrow b e^+ \tilde{\nu}_e) + (\tilde{t}_1 \rightarrow b \nu_e \tilde{e}_L^+)$, and $\bullet (\tilde{t}_1 \rightarrow b \tau^+ \tilde{\nu}_\tau) + (\tilde{t}_1 \rightarrow b \nu_\tau \tilde{\tau}_1) + (\tilde{t}_1 \rightarrow b \nu_\tau \tilde{\tau}_2)$.

end of the M_D range we get $m_{H^+} = 114$ GeV. Moreover, $m_{\tilde{b}_1}$ is approximately $m_{\tilde{t}_1} - m_W$ leading to an enhancement of this width. We have found that the relative importance of the sbottom exchange is larger in the case of $\tilde{t}_1 \rightarrow b H^+ \tilde{\chi}_1^0$ than in the case of $\tilde{t}_1 \rightarrow b W^+ \tilde{\chi}_1^0$. This is a consequence of the different spin structure of the corresponding matrix elements (Eq. (3.31) and (3.33)). Note, that the decrease in the $BR(\tilde{t}_1 \rightarrow b H^+ \tilde{\chi}_1^0)$ for $M_D \gtrsim 450$ GeV is mainly due to the growth in m_{H^+} .

10.2 The decay $\tilde{b}_1 \rightarrow c \tilde{\chi}_1^-$

In the following we assume that SUSY is realized in nature in such a way that i) $\tilde{\chi}_1^0$, $\tilde{\chi}_2^0$, and $\tilde{\chi}_1^\pm$ are mainly higgsinos, ii) $m_{\tilde{b}_1} < \min(m_{\tilde{\chi}_1^\pm} + m_t, m_{\tilde{\chi}_3^0} + m_b)$ and iii) $\tan\beta$ is small. Under these conditions the decay widths $\Gamma(\tilde{b}_1 \rightarrow b \tilde{\chi}_1^0)$ and $\Gamma(\tilde{b}_1 \rightarrow b \tilde{\chi}_2^0)$ will be small. Now the mixing between the squark generations and between the the c -quark and the t -quark leads to the decay $\tilde{b}_1 \rightarrow c \tilde{\chi}_1^-$. In the following we will assume for simplicity that the mixing in the squark sector is the same as in the quark sector. In this case the decay width is given by:

$$\Gamma(\tilde{b}_1 \rightarrow c + \tilde{\chi}_1^-) = \frac{g^2 |K_{cb}^2| \lambda^{\frac{1}{2}} (m_{\tilde{b}_1}^2, m_c^2, m_{\tilde{\chi}_1^\pm}^2)}{16\pi m_{\tilde{b}_1}^3} \times \left[(k_{11}^{\tilde{b}^2} i k + l_{11}^{\tilde{b}^2} i k) (m_{\tilde{b}_1}^2 - m_c^2 - m_{\tilde{\chi}_1^\pm}^2) - 4 k_{11}^{\tilde{b}} l_{11}^{\tilde{b}} m_c m_{\tilde{\chi}_1^\pm} \right] \quad (10.5)$$

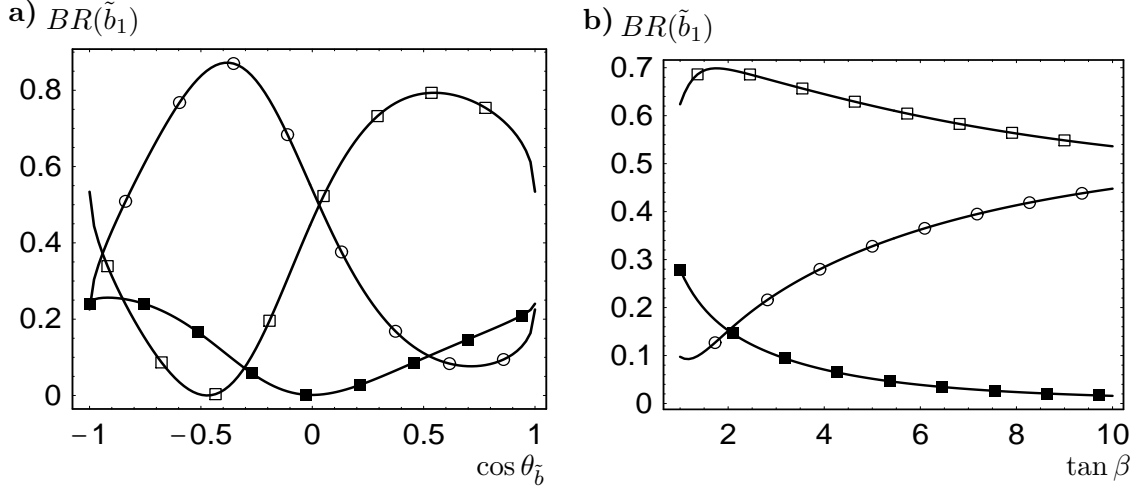


Fig. 10.6: Branching ratios for \tilde{b}_1 decays a) as a function of $\cos \theta_{\tilde{b}}$ for $\tan \beta = 1.5$ and b) as a function of $\tan \beta$ for $\cos \beta = -0.9$. The other parameters are $m_{\tilde{b}_1} = 200$ GeV, $M = 500$ GeV, and $\mu = -110$ GeV. The curves correspond to the transitions: $\circ \tilde{b}_1 \rightarrow b \tilde{\chi}_1^0$, $\square \tilde{b}_1 \rightarrow b \tilde{\chi}_2^0$, and $\blacksquare \tilde{b}_1 \rightarrow c \tilde{\chi}_1^-$.

where K_{cb} is the corresponding CKM matrix element. Note, that the decay width is approximately proportional to m_t^2 if we neglect m_c and the couplings to the gaugino component of $\tilde{\chi}_1^-$:

$$\Gamma(\tilde{b}_1 \rightarrow c + \tilde{\chi}_1^-) \simeq \frac{g^2 |K_{cb}^2| V_{12}^2 \cos^2 \theta_{\tilde{b}} m_t^2}{32 \pi \sin^2 \beta m_W^2 m_{b_1}^3} (m_{b_1}^2 - m_{\tilde{\chi}_1^\pm}^2)^2 \quad (10.6)$$

As a typical example we have taken $M = 500$ GeV, $\mu = -110$ GeV, $\tan \beta = 1.5$, and $m_{\tilde{b}_1} = 200$ GeV. This corresponds to $m_{\tilde{\chi}_1^0} \simeq 110$ GeV, $m_{\tilde{\chi}_2^0} \simeq 126$ GeV, and $m_{\tilde{\chi}_1^\pm} \simeq 120$ GeV. In Fig. 10.6a we show the branching ratios as a function of $\cos \theta_{\tilde{b}}$. As expected by the approximation formula in Eq. (10.6) $BR(\tilde{b}_1 \rightarrow c \tilde{\chi}_1^-)$ has its maximum near $|\cos \theta_{\tilde{b}}| = 1$ where it is of $\sim 20\%$. The reason for this, at first glance, large branching ratio is that N_{11}^2 and N_{12}^2 are of the same order as $|K_{cb}|^2 m_t^2 / m_W^2$. The signatures will be combinations of the following final states:

$$\begin{aligned} \tilde{b}_1 \rightarrow c \tilde{\chi}_1^- &\rightarrow c l^- \bar{\nu}_l \tilde{\chi}_1^0 \\ &\rightarrow c q \bar{q}' \tilde{\chi}_1^0 \\ \tilde{b}_1 &\rightarrow b \tilde{\chi}_1^0 \\ \tilde{b}_1 \rightarrow b \tilde{\chi}_2^0 &\rightarrow b l^- l^+ \tilde{\chi}_1^0 \\ &\rightarrow b \nu_l \bar{\nu}_l \tilde{\chi}_1^0 \\ &\rightarrow b q \bar{q} \tilde{\chi}_1^0 \end{aligned} \quad (10.7)$$

with $q = u, d, c, s, b$ and $l = e, \mu, \tau$.

To get a feeling for the term 'small $\tan \beta$ ' we show in Fig. 10.6b the branching ratios as a function of $\tan \beta$ for $\cos \theta_{\tilde{b}} = -0.9$. One sees that it rapidly decreases with the increasing of $\tan \beta$. For example we get that $BR(\tilde{b}_1 \rightarrow c \tilde{\chi}_1^-) \simeq 0.1$ (0.02) for $\tan \beta = 3$ (10). In every case we have found that the total decay width $\Gamma(\tilde{b}_1)$ is of $O(10 \text{ MeV})$. Therefore, we expect hadronization to play a rôle in such a scenario.

Chapter 11

Summary

We have studied the phenomenology of third generation sfermions paying particular attention to the implications of the Yukawa couplings and to the left-right mixing. Analytical formulae have been given for the sfermion mixing, the production cross sections, and for all possible two body decay widths that can occur at tree level.

In respect to the masses and the mixing angles of the sfermions we have found that a large mass splitting between sfermions of the same flavour occurs if either the off diagonal term $m_f(A_f - \mu\Theta(\beta))$ and/or $|M_{LL}^2 - M_{RR}^2|$ is large ($\Theta(\beta) = \cot \beta$ for $f = t$ and $\tan \beta$ for $f = b, \tau$). The size of the mixing is determined by the ratio $m_f(A_f - \mu\Theta(\beta))/(M_{LL}^2 - m_{\tilde{f}_1}^2)$. This can lead to a rather large mixing for sbottoms and staus even if $\tan \beta$ is small. The production cross sections of stops, sbottoms and staus in e^+e^- annihilation depend on the mixing angle in a characteristic way. This dependence is more pronounced if polarized e^- are available.

Large Yukawa couplings and left-right mixing strongly influences the decays of $\tilde{t}_{1,2}$, $\tilde{b}_{1,2}$, $\tilde{\tau}_{1,2}$, and $\tilde{\nu}_\tau$. In the case of the decays into charginos and neutralinos there occur interferences between gaugino and higgsino components. These interferences can be either positive or negative depending on the parameters. In particular we have found scenarios where the decays into the heaviest neutralino and chargino are the most important ones.

In the case that the mass splitting of the sfermions is large, decays into gauge bosons and Higgs bosons also have large branching ratios. Here we have found that the following facts are important: An extra λ/m_V^2 factor strengthens kinematical effects in case of decays into gauge bosons. The decay width into a Z boson is enlarged if there is a strong mixing of the sfermions whereas in case of a W boson the width is enhanced if both sfermions are left states. Both cases can be explained through the chirality preservation of the gauge boson couplings to the corresponding fermions. By contrast, Higgs bosons change the chirality of fermions. Corresponding to this we have found that decays of sfermions into Higgs bosons are important if one of the sfermions is a left state and the other is a right state. The only

exception is the pseudoscalar Higgs because its couplings are independent of the mixing angles. Moreover, the decay widths are strongly influenced by the magnitude of A_i ($i = b, t, \tau$) and μ , the relative sign between these parameters, and the Higgs mixing angle.

In case of the light stop it is possible that all two body decays are forbidden at tree level. In such a scenario three body decays will be important followed by the one loop decay into a charm quark and the lightest neutralino. Additionally, in case of the light sbottom we have found scenarios where the flavour changing decay into a charm-quark and the lightest chargino gains some importance. In both cases we expect hadronization effects to be important.

We have seen that stops, sbottoms, staus and the tau sneutrino have a rich phenomenology. A precise determination of their properties will give us insight into the SUSY breaking parameters and hopefully also into the mechanism of SUSY breaking.

Appendix A

Formulae for the three body decay widths

In the subsequent the formulae for the three body decay widths of the light stop are collected which have been omitted in Section 3.4.

A.1 The Decay of the Light Stop into a W-Boson, a Bottom Quark and the Lightest Neutralino

The decay width is given by

$$\begin{aligned} \Gamma(\tilde{t}_1 \rightarrow W^+ + b + \tilde{\chi}_1^0) &= \\ &= \frac{\alpha^2}{16 \pi m_{\tilde{t}_1}^3 \sin^4 \theta_W} \int_{(m_b + m_{\tilde{\chi}_1^0})^2}^{(m_{\tilde{t}_1} - m_W)^2} ds \left(F_{\tilde{\chi}^+ \tilde{\chi}^+} + F_{\tilde{\chi}^+ t} + F_{\tilde{\chi}^+ \bar{b}} + F_{t t} + F_{t \bar{b}} + F_{\bar{b} \bar{b}} \right) \end{aligned} \quad (\text{A.1})$$

with

$$\begin{aligned} F_{\tilde{\chi}^+ \tilde{\chi}^+} &= \sum_{i=1}^2 \left[(ca_{i1} + ca_{i2}s + ca_{i3}s^2 + ca_{i4}s^3) \right. \\ &\quad * J_t^0(m_{\tilde{t}_1}^2 + m_W^2 + m_b^2 + m_{\tilde{\chi}_1^0}^2 - m_{\tilde{\chi}_i^+}^2 - s, \Gamma_{\tilde{\chi}_i^+} m_{\tilde{\chi}_i^+}) \\ &\quad + (ca_{i5} + ca_{i6}s + 2ca_{i4}s^2) \\ &\quad * J_t^1(m_{\tilde{t}_1}^2 + m_W^2 + m_b^2 + m_{\tilde{\chi}_1^0}^2 - m_{\tilde{\chi}_i^+}^2 - s, \Gamma_{\tilde{\chi}_i^+} m_{\tilde{\chi}_i^+}) \\ &\quad \left. + (ca_{i7} + ca_{i4}s) J_t^2(m_{\tilde{t}_1}^2 + m_W^2 + m_b^2 + m_{\tilde{\chi}_1^0}^2 - m_{\tilde{\chi}_i^+}^2 - s, \Gamma_{\tilde{\chi}_i^+} m_{\tilde{\chi}_i^+}) \right] \\ &\quad + (ca_{31} + ca_{32}s + ca_{33}s^2 + ca_{34}s^3) \end{aligned}$$

$$\begin{aligned}
& *J_{tt}^0(m_{\tilde{t}_1}^2 + m_W^2 + m_b^2 + m_{\tilde{\chi}_1^0}^2 - m_{\tilde{\chi}_1^+}^2 - s, \Gamma_{\tilde{\chi}_1^+} m_{\tilde{\chi}_1^+} \\
& \quad , m_{\tilde{t}_1}^2 + m_W^2 + m_b^2 + m_{\tilde{\chi}_1^0}^2 - m_{\tilde{\chi}_2^+}^2 - s, \Gamma_{\tilde{\chi}_2^+} m_{\tilde{\chi}_2^+}) \\
& + (ca_{35} + ca_{36}s + 2ca_{34}s^2) \\
& *J_{tt}^1(m_{\tilde{t}_1}^2 + m_W^2 + m_b^2 + m_{\tilde{\chi}_1^0}^2 - m_{\tilde{\chi}_1^+}^2 - s, \Gamma_{\tilde{\chi}_1^+} m_{\tilde{\chi}_1^+} \\
& \quad , m_{\tilde{t}_1}^2 + m_W^2 + m_b^2 + m_{\tilde{\chi}_1^0}^2 - m_{\tilde{\chi}_2^+}^2 - s, \Gamma_{\tilde{\chi}_2^+} m_{\tilde{\chi}_2^+}) \\
& + (ca_{37} + ca_{34}s) \\
& *J_{tt}^2(m_{\tilde{t}_1}^2 + m_W^2 + m_b^2 + m_{\tilde{\chi}_1^0}^2 - m_{\tilde{\chi}_1^+}^2 - s, \Gamma_{\tilde{\chi}_1^+} m_{\tilde{\chi}_1^+} \\
& \quad , m_{\tilde{t}_1}^2 + m_W^2 + m_b^2 + m_{\tilde{\chi}_1^0}^2 - m_{\tilde{\chi}_2^+}^2 - s, \Gamma_{\tilde{\chi}_2^+} m_{\tilde{\chi}_2^+}) \tag{A.2}
\end{aligned}$$

$$\begin{aligned}
F_{\tilde{\chi}^+ t} = & \sum_{i=1}^2 \left[(cb_{i1} + cb_{i2}s + cb_{i3}s^2) \right. \\
& *J_{tt}^0(m_{\tilde{t}_1}^2 + m_W^2 + m_b^2 + m_{\tilde{\chi}_1^0}^2 - m_{\tilde{\chi}_1^+}^2 - s, -\Gamma_{\tilde{\chi}_1^+} m_{\tilde{\chi}_1^+}, m_t^2, \Gamma_t m_t) \\
& + (cb_{i4} + cb_{i5}s + cb_{i6}s^2) \\
& *J_{tt}^1(m_{\tilde{t}_1}^2 + m_W^2 + m_b^2 + m_{\tilde{\chi}_1^0}^2 - m_{\tilde{\chi}_1^+}^2 - s, -\Gamma_{\tilde{\chi}_1^+} m_{\tilde{\chi}_1^+}, m_t^2, \Gamma_t m_t) \\
& + (cb_{i7} + cb_{i6}s) \\
& \left. *J_{tt}^2(m_{\tilde{t}_1}^2 + m_W^2 + m_b^2 + m_{\tilde{\chi}_1^0}^2 - m_{\tilde{\chi}_1^+}^2 - s, -\Gamma_{\tilde{\chi}_1^+} m_{\tilde{\chi}_1^+}, m_t^2, \Gamma_t m_t) \right] \tag{A.3}
\end{aligned}$$

$$\begin{aligned}
F_{\tilde{\chi}^+ \tilde{b}} = & \sum_{k,i=1}^2 \left[(cc_{ik1} + cc_{ik2}s + cc_{ik3}s^2 + cc_{ik4}s^3) \right. \\
& *J_{st}^0(m_{\tilde{b}_k}^2, \Gamma_{\tilde{b}_k} m_{\tilde{b}_k}, m_{\tilde{t}_1}^2 + m_W^2 + m_b^2 + m_{\tilde{\chi}_1^0}^2 - m_{\tilde{\chi}_1^+}^2 - s, -\Gamma_{\tilde{\chi}_1^+} m_{\tilde{\chi}_1^+}) \\
& + (cc_{ik5} + cc_{ik6}s + cc_{ik4}s^2) \\
& \left. *J_{st}^1(m_{\tilde{b}_k}^2, \Gamma_{\tilde{b}_k} m_{\tilde{b}_k}, m_{\tilde{t}_1}^2 + m_W^2 + m_b^2 + m_{\tilde{\chi}_1^0}^2 - m_{\tilde{\chi}_1^+}^2 - s, -\Gamma_{\tilde{\chi}_1^+} m_{\tilde{\chi}_1^+}) \right] \tag{A.4}
\end{aligned}$$

$$\begin{aligned}
F_{tt} = & (cd_1 + cd_2s)J_t^0(m_t^2, \Gamma_t m_t) + (cd_3 + cd_4s)J_t^1(m_t^2, \Gamma_t m_t) \\
& + (cd_5 + cd_6s)J_t^2(m_t^2, \Gamma_t m_t) \tag{A.5}
\end{aligned}$$

$$\begin{aligned}
F_{t\tilde{b}} = & \sum_{k=1}^2 \left[(ce_{k1} + ce_{k2}s + ce_{k3}s^2)J_{st}^0(m_{\tilde{b}_k}^2, \Gamma_{\tilde{b}_k} m_{\tilde{b}_k}, m_t^2, \Gamma_t m_t) \right. \\
& \left. + (ce_{k4} + ce_{k5}s + ce_{k6}s^2)J_{st}^1(m_{\tilde{b}_k}^2, \Gamma_{\tilde{b}_k} m_{\tilde{b}_k}, m_t^2, \Gamma_t m_t) \right] \tag{A.6}
\end{aligned}$$

$$\begin{aligned}
F_{\tilde{b}\tilde{b}} = & \left\{ \sum_{k=1}^2 \frac{(cf_{k1} + cf_{k2}s)}{m_W^2[(s - m_{\tilde{b}_k}^2)^2 + \Gamma_{\tilde{b}_k}^2 m_{\tilde{b}_k}^2]} \right. \\
& + Re \left[\frac{(cf_{31} + cf_{32}s)}{m_W^2[(s - m_{\tilde{b}_1}^2) + i\Gamma_{\tilde{b}_1} m_{\tilde{b}_1}][(s - m_{\tilde{b}_2}^2) - i\Gamma_{\tilde{b}_2} m_{\tilde{b}_2}]} \right] \Big\} \\
& * \frac{\lambda(s, m_{\tilde{t}_1}^2, m_W^2) \sqrt{\lambda(s, m_{\tilde{t}_1}^2, m_W^2)} \lambda(s, m_{\tilde{\chi}_1^0}^2, m_b^2)}{s}
\end{aligned} \tag{A.7}$$

The integrals $J_{t,tt,st}^{0,1,2}$ are defined in Section A.4.1. Their integration range is given by

$$\begin{aligned}
t_{min}^{max} = & \frac{m_{\tilde{t}_1}^2 + m_b^2 + m_W^2 + m_{\tilde{\chi}_1^0}^2 - s}{2} - \frac{(m_{\tilde{t}_1}^2 - m_W^2)(m_{\tilde{\chi}_1^0}^2 - m_b^2)}{2s} \\
& \pm \frac{\sqrt{\lambda(s, m_{\tilde{t}_1}^2, m_W^2) \lambda(s, m_{\tilde{\chi}_1^0}^2, m_b^2)}}{2s}
\end{aligned} \tag{A.8}$$

and $s = (p_{\tilde{t}_1} - p_W)^2$. Note, that $-\Gamma_{\tilde{\chi}_1^+} m_{\tilde{\chi}_1^+}$ appears in the entries of the integrals $F_{\tilde{\chi}^+ \tilde{b}_j}$ and $F_{\tilde{\chi}^+ t}$ because the chargino exchange is the u -channel in our convention. The coefficients are given by:

$$\begin{aligned}
ca_{11} = & 6 O'_{L11} O'_{R11} \left[((k_{11}^{\tilde{t}})^2 + (l_{11}^{\tilde{t}})^2) m_{\tilde{\chi}_1^+} m_{\tilde{\chi}_1^0} (2m_b^2 + m_{\tilde{\chi}_1^0}^2 + m_W^2) \right. \\
& \left. + 2 k_{11}^{\tilde{t}} l_{11}^{\tilde{t}} m_b m_{\tilde{\chi}_1^0} (m_b^2 + m_{\tilde{\chi}_1^0}^2 + m_{\tilde{t}_1}^2 + m_{\tilde{\chi}_1^+}^2 + m_W^2) \right] \\
& - \left((l_{11}^{\tilde{t}})^2 (O'_{L11})^2 + (k_{11}^{\tilde{t}})^2 (O'_{R11})^2 \right) \left[(4m_b^2 + m_W^2)(m_{\tilde{\chi}_1^0}^2 + m_b^2) + m_{\tilde{\chi}_1^0}^4 \right. \\
& \left. + m_{\tilde{t}_1}^2 (2m_W^2 + 4m_b^2 + m_{\tilde{\chi}_1^0}^2) + \frac{(m_b^2 + m_{\tilde{t}_1}^2)(m_b^4 + m_b^2 m_{\tilde{t}_1}^2 + m_{\tilde{\chi}_1^0}^2 m_{\tilde{t}_1}^2)}{m_W^2} \right] \\
& - \left((k_{11}^{\tilde{t}})^2 (O'_{L11})^2 + (l_{11}^{\tilde{t}})^2 (O'_{R11})^2 \right) m_{\tilde{\chi}_1^+}^2 \left(m_{\tilde{\chi}_1^0}^2 + m_{\tilde{t}_1}^2 + 2m_b^2 + \frac{m_b^4 + m_b^2 m_{\tilde{t}_1}^2}{m_W^2} \right) \\
& - 2 k_{11}^{\tilde{t}} l_{11}^{\tilde{t}} \left((O'_{L11})^2 + (O'_{R11})^2 \right) m_b m_{\tilde{\chi}_1^+} \\
& * \left(3m_b^2 + 2m_{\tilde{\chi}_1^0}^2 + 3m_{\tilde{t}_1}^2 + \frac{(m_{\tilde{t}_1}^2 + m_b^2)^2}{m_W^2} \right) \\
ca_{12} = & -12 k_{11}^{\tilde{t}} l_{11}^{\tilde{t}} O'_{L11} O'_{R11} m_b m_{\tilde{\chi}_1^0} - 6 \left((k_{11}^{\tilde{t}})^2 + (l_{11}^{\tilde{t}})^2 \right) O'_{L11} O'_{R11} m_{\tilde{\chi}_1^+} m_{\tilde{\chi}_1^0} \\
& + 2 k_{11}^{\tilde{t}} l_{11}^{\tilde{t}} \left((O'_{L11})^2 + (O'_{R11})^2 \right) m_b m_{\tilde{\chi}_1^+} \left(3 + \frac{2(m_b^2 + m_{\tilde{t}_1}^2)}{m_W^2} \right) \\
& + \left((l_{11}^{\tilde{t}})^2 (O'_{L11})^2 + (k_{11}^{\tilde{t}})^2 (O'_{R11})^2 \right) \left(6m_b^2 + 2m_{\tilde{\chi}_1^0}^2 + 2m_{\tilde{t}_1}^2 + m_W^2 \right. \\
& \left. + \frac{3m_b^4 + m_b^2 m_{\tilde{\chi}_1^0}^2 + 4m_b^2 m_{\tilde{t}_1}^2 + 2m_{\tilde{\chi}_1^0}^2 m_{\tilde{t}_1}^2 + m_{\tilde{t}_1}^4}{m_W^2} \right)
\end{aligned} \tag{A.9}$$

$$+ \left((k_{11}^{\tilde{t}})^2 (O'_{L11})^2 + (l_{11}^{\tilde{t}})^2 (O'_{R11})^2 \right) m_{\tilde{\chi}_1^+}^2 \left(2 + \frac{m_b^2}{m_W^2} \right) \quad (\text{A.10})$$

$$\begin{aligned} ca_{13} = & -2 k_{11}^{\tilde{t}} l_{11}^{\tilde{t}} \left((O'_{L11})^2 + (O'_{R11})^2 \right) \frac{m_b m_{\tilde{\chi}_1^+}}{m_W^2} \\ & - \left((l_{11}^{\tilde{t}})^2 (O'_{L11})^2 + (k_{11}^{\tilde{t}})^2 (O'_{R11})^2 \right) \left(2 + \frac{m_{\tilde{\chi}_1^0}^2 + 3 m_b^2 + 2 m_{t_1}^2}{m_W^2} \right) \end{aligned} \quad (\text{A.11})$$

$$ca_{14} = \frac{(l_{11}^{\tilde{t}})^2 (O'_{L11})^2 + (k_{11}^{\tilde{t}})^2 (O'_{R11})^2}{m_W^2} \quad (\text{A.12})$$

$$\begin{aligned} ca_{15} = & -12 k_{11}^{\tilde{t}} l_{11}^{\tilde{t}} O'_{L11} O'_{R11} m_b m_{\tilde{\chi}_1^0} - 6 \left((k_{11}^{\tilde{t}})^2 + (l_{11}^{\tilde{t}})^2 \right) O'_{L11} O'_{R11} m_{\tilde{\chi}_1^+} m_{\tilde{\chi}_1^0} \\ & + 2 k_{11}^{\tilde{t}} l_{11}^{\tilde{t}} \left((O'_{L11})^2 + (O'_{R11})^2 \right) m_b m_{\tilde{\chi}_1^+} \left(3 + 2 \frac{m_b^2 + m_{t_1}^2}{m_W^2} \right) \\ & + \left((l_{11}^{\tilde{t}})^2 (O'_{L11})^2 + (k_{11}^{\tilde{t}})^2 (O'_{R11})^2 \right) \left(6 m_b^2 + 3 m_{\tilde{\chi}_1^0}^2 + 2 m_{t_1}^2 + 2 m_W^2 \right. \\ & \quad \left. + \frac{2 m_b^4 + 2 m_b^2 m_{t_1}^2 + m_{\tilde{\chi}_1^0}^2 m_{t_1}^2}{m_W^2} \right) \\ & + \left((k_{11}^{\tilde{t}})^2 (O'_{L11})^2 + (l_{11}^{\tilde{t}})^2 (O'_{R11})^2 \right) m_{\tilde{\chi}_1^+}^2 \left(1 + \frac{2 m_b^2 + m_{t_1}^2}{m_W^2} \right) \end{aligned} \quad (\text{A.13})$$

$$\begin{aligned} ca_{16} = & -4 k_{11}^{\tilde{t}} l_{11}^{\tilde{t}} \left((O'_{L11})^2 + (O'_{R11})^2 \right) \frac{m_b m_{\tilde{\chi}_1^+}}{m_W^2} \\ & - \left((k_{11}^{\tilde{t}})^2 (O'_{L11})^2 + (l_{11}^{\tilde{t}})^2 (O'_{R11})^2 \right) \frac{m_{\tilde{\chi}_1^+}^2}{m_W^2} \\ & - \left((l_{11}^{\tilde{t}})^2 (O'_{L11})^2 + (k_{11}^{\tilde{t}})^2 (O'_{R11})^2 \right) \left(4 + \frac{m_{\tilde{\chi}_1^0}^2 + 4 m_b^2 + 2 m_{t_1}^2}{m_W^2} \right) \end{aligned} \quad (\text{A.14})$$

$$\begin{aligned} ca_{17} = & -2 k_{11}^{\tilde{t}} l_{11}^{\tilde{t}} \left((O'_{L11})^2 + (O'_{R11})^2 \right) \frac{m_b m_{\tilde{\chi}_1^+}}{m_W^2} \\ & - \left((l_{11}^{\tilde{t}})^2 (O'_{L11})^2 + (k_{11}^{\tilde{t}})^2 (O'_{R11})^2 \right) \left(2 + \frac{m_b^2}{m_W^2} \right) \\ & - \left((k_{11}^{\tilde{t}})^2 (O'_{L11})^2 + (l_{11}^{\tilde{t}})^2 (O'_{R11})^2 \right) \frac{m_{\tilde{\chi}_1^+}^2}{m_W^2} \end{aligned} \quad (\text{A.15})$$

$$\begin{aligned} ca_{31} = & 12 \left(k_{12}^{\tilde{t}} l_{11}^{\tilde{t}} O'_{L12} O'_{R11} + k_{11}^{\tilde{t}} l_{12}^{\tilde{t}} O'_{L11} O'_{R12} \right) m_b m_{\tilde{\chi}_1^0} m_{\tilde{\chi}_1^+} m_{\tilde{\chi}_2^+} \\ & + 12 \left(k_{11}^{\tilde{t}} l_{12}^{\tilde{t}} O'_{L12} O'_{R11} + k_{12}^{\tilde{t}} l_{11}^{\tilde{t}} O'_{L11} O'_{R12} \right) m_b m_{\tilde{\chi}_1^0} \\ & \quad * (m_b^2 + m_{\tilde{\chi}_1^0}^2 + m_{t_1}^2 + m_W^2) \end{aligned}$$

$$\begin{aligned}
& + 6 \left(l_{11}^{\tilde{t}} l_{12}^{\tilde{t}} O'_{L_{12}} O'_{R_{11}} + k_{11}^{\tilde{t}} k_{12}^{\tilde{t}} O'_{L_{11}} O'_{R_{12}} \right) m_{\tilde{\chi}_1^0} m_{\tilde{\chi}_1^+} (2m_b^2 + m_{\tilde{\chi}_1^0}^2 + m_W^2) \\
& + 6 \left(k_{11}^{\tilde{t}} k_{12}^{\tilde{t}} O'_{L_{12}} O'_{R_{11}} + l_{11}^{\tilde{t}} l_{12}^{\tilde{t}} O'_{L_{11}} O'_{R_{12}} \right) m_{\tilde{\chi}_1^0} m_{\tilde{\chi}_2^+} (2m_b^2 + m_{\tilde{\chi}_1^0}^2 + m_W^2) \\
& - 2 \left(l_{11}^{\tilde{t}} l_{12}^{\tilde{t}} O'_{L_{11}} O'_{L_{12}} + k_{11}^{\tilde{t}} k_{12}^{\tilde{t}} O'_{R_{11}} O'_{R_{12}} \right) \\
& \quad * \left[(m_{\tilde{\chi}_1^0}^2 + m_b^2) (m_{\tilde{\chi}_1^0}^2 + m_{\tilde{t}_1}^2 + m_W^2 + m_b^2) + 2m_{\tilde{t}_1}^2 m_W^2 \right. \\
& \quad \left. + m_b^2 (3m_b^2 + 2m_{\tilde{\chi}_1^0}^2 + 3m_{\tilde{t}_1}^2) + (m_b^4 + m_{\tilde{t}_1}^2 (m_{\tilde{\chi}_1^0}^2 + m_b^2)) \frac{m_b^2 + m_{\tilde{t}_1}^2}{m_W^2} \right] \\
& - 2 \left(k_{11}^{\tilde{t}} l_{12}^{\tilde{t}} O'_{L_{11}} O'_{L_{12}} + k_{12}^{\tilde{t}} l_{11}^{\tilde{t}} O'_{R_{11}} O'_{R_{12}} \right) m_b m_{\tilde{\chi}_1^+} \\
& \quad * \left[3m_b^2 + 2m_{\tilde{\chi}_1^0}^2 + 3m_{\tilde{t}_1}^2 + \frac{(m_b^2 + m_{\tilde{t}_1}^2)(m_b^2 + m_{\tilde{t}_1}^2)}{m_W^2} \right] \\
& - 2 \left(k_{12}^{\tilde{t}} l_{11}^{\tilde{t}} O'_{L_{11}} O'_{L_{12}} + k_{11}^{\tilde{t}} l_{12}^{\tilde{t}} O'_{R_{11}} O'_{R_{12}} \right) m_b m_{\tilde{\chi}_2^+} \\
& \quad * \left[3m_b^2 + 2m_{\tilde{\chi}_1^0}^2 + 3m_{\tilde{t}_1}^2 + \frac{(m_b^2 + m_{\tilde{t}_1}^2)(m_b^2 + m_{\tilde{t}_1}^2)}{m_W^2} \right] \\
& - 2 \left(k_{11}^{\tilde{t}} k_{12}^{\tilde{t}} O'_{L_{11}} O'_{L_{12}} + l_{11}^{\tilde{t}} l_{12}^{\tilde{t}} O'_{R_{11}} O'_{R_{12}} \right) m_{\tilde{\chi}_1^+} m_{\tilde{\chi}_2^+} \\
& \quad * \left[2m_b^2 + m_{\tilde{\chi}_1^0}^2 + m_{\tilde{t}_1}^2 + \frac{(m_b^2 + m_{\tilde{t}_1}^2)m_b^2}{m_W^2} \right] \tag{A.16}
\end{aligned}$$

$$\begin{aligned}
ca_{32} = & -6 \left(l_{11}^{\tilde{t}} l_{12}^{\tilde{t}} O'_{L_{12}} O'_{R_{11}} + k_{11}^{\tilde{t}} k_{12}^{\tilde{t}} O'_{L_{11}} O'_{R_{12}} \right) m_{\tilde{\chi}_1^0} m_{\tilde{\chi}_1^+} \\
& -12 \left(k_{11}^{\tilde{t}} l_{12}^{\tilde{t}} O'_{L_{12}} O'_{R_{11}} + k_{12}^{\tilde{t}} l_{11}^{\tilde{t}} O'_{L_{11}} O'_{R_{12}} \right) m_b m_{\tilde{\chi}_1^0} \\
& -6 \left(k_{11}^{\tilde{t}} k_{12}^{\tilde{t}} O'_{L_{12}} O'_{R_{11}} + l_{11}^{\tilde{t}} l_{12}^{\tilde{t}} O'_{L_{11}} O'_{R_{12}} \right) m_{\tilde{\chi}_1^0} m_{\tilde{\chi}_2^+} \\
& +2 \left(l_{11}^{\tilde{t}} l_{12}^{\tilde{t}} O'_{L_{11}} O'_{L_{12}} + k_{11}^{\tilde{t}} k_{12}^{\tilde{t}} O'_{R_{11}} O'_{R_{12}} \right) \\
& \quad * \left[6m_b^2 + 2m_{\tilde{\chi}_1^0}^2 + 2m_{\tilde{t}_1}^2 + m_W^2 + \frac{(2m_b^2 + m_{\tilde{\chi}_1^0}^2)(m_b^2 + 2m_{\tilde{t}_1}^2) + m_b^4 + m_{\tilde{t}_1}^4}{m_W^2} \right] \\
& +2 \left(k_{11}^{\tilde{t}} l_{12}^{\tilde{t}} O'_{L_{11}} O'_{L_{12}} + k_{12}^{\tilde{t}} l_{11}^{\tilde{t}} O'_{R_{11}} O'_{R_{12}} \right) m_b m_{\tilde{\chi}_1^+} \frac{3 + 2(m_b^2 + m_{\tilde{t}_1}^2)}{m_W^2} \\
& +2 \left(k_{12}^{\tilde{t}} l_{11}^{\tilde{t}} O'_{L_{11}} O'_{L_{12}} + k_{11}^{\tilde{t}} l_{12}^{\tilde{t}} O'_{R_{11}} O'_{R_{12}} \right) m_b m_{\tilde{\chi}_2^+} \frac{3 + 2(m_b^2 + m_{\tilde{t}_1}^2)}{m_W^2} \\
& +2 \left(k_{11}^{\tilde{t}} k_{12}^{\tilde{t}} O'_{L_{11}} O'_{L_{12}} + l_{11}^{\tilde{t}} l_{12}^{\tilde{t}} O'_{R_{11}} O'_{R_{12}} \right) m_{\tilde{\chi}_1^+} m_{\tilde{\chi}_2^+} \left(2 + \frac{m_b^2}{m_W^2} \right) \tag{A.17} \\
ca_{33} = & -2 \left(k_{11}^{\tilde{t}} l_{12}^{\tilde{t}} O'_{L_{11}} O'_{L_{12}} + k_{12}^{\tilde{t}} l_{11}^{\tilde{t}} O'_{R_{11}} O'_{R_{12}} \right) \frac{m_b m_{\tilde{\chi}_1^+}}{m_W^2} \\
& -2 \left(k_{12}^{\tilde{t}} l_{11}^{\tilde{t}} O'_{L_{11}} O'_{L_{12}} + k_{11}^{\tilde{t}} l_{12}^{\tilde{t}} O'_{R_{11}} O'_{R_{12}} \right) \frac{m_b m_{\tilde{\chi}_2^+}}{m_W^2}
\end{aligned}$$

$$-2 \left(l_{11}^{\tilde{t}} l_{12}^{\tilde{t}} O'_{L_{11}} O'_{L_{12}} + k_{11}^{\tilde{t}} k_{12}^{\tilde{t}} O'_{R_{11}} O'_{R_{12}} \right) \left(2 + \frac{m_{\tilde{\chi}_1^0}^2 + 3m_b^2 + 2m_{\tilde{t}_1}^2}{m_W^2} \right) \quad (\text{A.18})$$

$$ca_{34} = \frac{2 \left(l_{11}^{\tilde{t}} l_{12}^{\tilde{t}} O'_{L_{11}} O'_{L_{12}} + k_{11}^{\tilde{t}} k_{12}^{\tilde{t}} O'_{R_{11}} O'_{R_{12}} \right)}{m_W^2} \quad (\text{A.19})$$

$$\begin{aligned} ca_{35} = & -6 \left(l_{11}^{\tilde{t}} l_{12}^{\tilde{t}} O'_{L_{12}} O'_{R_{11}} + k_{11}^{\tilde{t}} k_{12}^{\tilde{t}} O'_{L_{11}} O'_{R_{12}} \right) m_{\tilde{\chi}_1^0} m_{\tilde{\chi}_1^+} \\ & -12 \left(k_{11}^{\tilde{t}} l_{12}^{\tilde{t}} O'_{L_{12}} O'_{R_{11}} + k_{12}^{\tilde{t}} l_{11}^{\tilde{t}} O'_{L_{11}} O'_{R_{12}} \right) m_b m_{\tilde{\chi}_1^0} \\ & -6 \left(k_{11}^{\tilde{t}} k_{12}^{\tilde{t}} O'_{L_{12}} O'_{R_{11}} + l_{11}^{\tilde{t}} l_{12}^{\tilde{t}} O'_{L_{11}} O'_{R_{12}} \right) m_{\tilde{\chi}_1^0} m_{\tilde{\chi}_2^+} \\ & +2 \left(l_{11}^{\tilde{t}} l_{12}^{\tilde{t}} O'_{L_{11}} O'_{L_{12}} + k_{11}^{\tilde{t}} k_{12}^{\tilde{t}} O'_{R_{11}} O'_{R_{12}} \right) \\ & \quad * \left[6m_b^2 + 3m_{\tilde{\chi}_1^0}^2 + 2m_{\tilde{t}_1}^2 + 2m_W^2 + \frac{2m_b^4 + m_{\tilde{t}_1}^2 (m_{\tilde{\chi}_1^0}^2 + 2m_b^2)}{m_W^2} \right] \\ & +2 \left(k_{11}^{\tilde{t}} l_{12}^{\tilde{t}} O'_{L_{11}} O'_{L_{12}} + k_{12}^{\tilde{t}} l_{11}^{\tilde{t}} O'_{R_{11}} O'_{R_{12}} \right) m_b m_{\tilde{\chi}_1^+} \left(3 + \frac{2(m_b^2 + m_{\tilde{t}_1}^2)}{m_W^2} \right) \\ & +2 \left(k_{12}^{\tilde{t}} l_{11}^{\tilde{t}} O'_{L_{11}} O'_{L_{12}} + k_{11}^{\tilde{t}} l_{12}^{\tilde{t}} O'_{R_{11}} O'_{R_{12}} \right) m_b m_{\tilde{\chi}_2^+} \left(3 + \frac{2(m_b^2 + m_{\tilde{t}_1}^2)}{m_W^2} \right) \\ & +2 \left(k_{11}^{\tilde{t}} k_{12}^{\tilde{t}} O'_{L_{11}} O'_{L_{12}} + l_{11}^{\tilde{t}} l_{12}^{\tilde{t}} O'_{R_{11}} O'_{R_{12}} \right) m_{\tilde{\chi}_1^+} m_{\tilde{\chi}_2^+} \left(1 + \frac{2m_b^2 + m_{\tilde{t}_1}^2}{m_W^2} \right) \quad (\text{A.20}) \end{aligned}$$

$$\begin{aligned} ca_{36} = & -2 \left(k_{11}^{\tilde{t}} k_{12}^{\tilde{t}} O'_{L_{11}} O'_{L_{12}} + l_{11}^{\tilde{t}} l_{12}^{\tilde{t}} O'_{R_{11}} O'_{R_{12}} \right) \frac{m_{\tilde{\chi}_1^+} m_{\tilde{\chi}_2^+}}{m_W^2} \\ & -4 \left(k_{11}^{\tilde{t}} l_{12}^{\tilde{t}} O'_{L_{11}} O'_{L_{12}} + k_{12}^{\tilde{t}} l_{11}^{\tilde{t}} O'_{R_{11}} O'_{R_{12}} \right) \frac{m_b m_{\tilde{\chi}_1^+}}{m_W^2} \\ & -4 \left(k_{12}^{\tilde{t}} l_{11}^{\tilde{t}} O'_{L_{11}} O'_{L_{12}} + k_{11}^{\tilde{t}} l_{12}^{\tilde{t}} O'_{R_{11}} O'_{R_{12}} \right) \frac{m_b m_{\tilde{\chi}_2^+}}{m_W^2} \\ & -2 \left(l_{11}^{\tilde{t}} l_{12}^{\tilde{t}} O'_{L_{11}} O'_{L_{12}} + k_{11}^{\tilde{t}} k_{12}^{\tilde{t}} O'_{R_{11}} O'_{R_{12}} \right) \left(4 + \frac{m_{\tilde{\chi}_1^0}^2 + 4m_b^2 + 2m_{\tilde{t}_1}^2}{m_W^2} \right) \quad (\text{A.21}) \end{aligned}$$

$$\begin{aligned} ca_{37} = & -2 \left(l_{11}^{\tilde{t}} l_{12}^{\tilde{t}} O'_{L_{11}} O'_{L_{12}} + k_{11}^{\tilde{t}} k_{12}^{\tilde{t}} O'_{R_{11}} O'_{R_{12}} \right) \left(2 + \frac{m_b^2}{m_W^2} \right) \\ & -2 \left(k_{11}^{\tilde{t}} l_{12}^{\tilde{t}} O'_{L_{11}} O'_{L_{12}} + k_{12}^{\tilde{t}} l_{11}^{\tilde{t}} O'_{R_{11}} O'_{R_{12}} \right) \frac{m_b m_{\tilde{\chi}_1^+}}{m_W^2} \\ & -2 \left(k_{12}^{\tilde{t}} l_{11}^{\tilde{t}} O'_{L_{11}} O'_{L_{12}} + k_{11}^{\tilde{t}} l_{12}^{\tilde{t}} O'_{R_{11}} O'_{R_{12}} \right) \frac{m_b m_{\tilde{\chi}_2^+}}{m_W^2} \\ & -2 \left(k_{11}^{\tilde{t}} k_{12}^{\tilde{t}} O'_{L_{11}} O'_{L_{12}} + l_{11}^{\tilde{t}} l_{12}^{\tilde{t}} O'_{R_{11}} O'_{R_{12}} \right) \frac{m_{\tilde{\chi}_1^+} m_{\tilde{\chi}_2^+}}{m_W^2} \quad (\text{A.22}) \end{aligned}$$

$$\begin{aligned}
cb_{11} = & -\sqrt{2} \left\{ 3 b_{11}^{\tilde{t}} l_{11}^{\tilde{t}} O'_{L_{11}} m_t m_{\tilde{\chi}_1^0} (2 m_b^2 + m_{\tilde{\chi}_1^0}^2 + m_W^2) \right. \\
& + 6 b_{11}^{\tilde{t}} k_{11}^{\tilde{t}} O'_{L_{11}} m_t m_{\tilde{\chi}_1^0} m_b m_{\tilde{\chi}_1^+} + 3 a_{11}^{\tilde{t}} k_{11}^{\tilde{t}} O'_{L_{11}} m_b m_{\tilde{\chi}_1^+} (m_{\tilde{\chi}_1^0}^2 - m_{\tilde{t}_1}^2) \\
& + a_{11}^{\tilde{t}} l_{11}^{\tilde{t}} O'_{L_{11}} \\
& \quad \left. * \left[2 (m_{\tilde{\chi}_1^0}^2 - m_{\tilde{t}_1}^2) (m_W^2 + m_{\tilde{\chi}_1^0}^2 + m_b^2) - m_b^2 m_{\tilde{t}_1}^2 \left(1 + \frac{m_{\tilde{\chi}_1^0}^2 - m_b^2 - m_{\tilde{t}_1}^2}{m_W^2} \right) \right] \right. \\
& + a_{11}^{\tilde{t}} l_{11}^{\tilde{t}} O'_{R_{11}} m_{\tilde{\chi}_1^0} m_{\tilde{\chi}_1^+} \left[2 m_W^2 - m_b^2 \left(1 + \frac{m_b^2}{m_W^2} \right) \right] \\
& + a_{11}^{\tilde{t}} k_{11}^{\tilde{t}} O'_{R_{11}} m_b m_{\tilde{\chi}_1^0} \left[3 m_W^2 + m_{\tilde{t}_1}^2 \left(2 - \frac{m_b^2}{m_W^2} \right) - m_b^2 \left(2 + \frac{m_b^2}{m_W^2} \right) - m_{\tilde{\chi}_1^0}^2 \right] \\
& - b_{11}^{\tilde{t}} l_{11}^{\tilde{t}} O'_{R_{11}} m_t m_{\tilde{\chi}_1^+} \left[m_{\tilde{\chi}_1^0}^2 + m_{\tilde{t}_1}^2 \left(1 + \frac{m_b^2}{m_W^2} \right) + m_b^2 \left(2 + \frac{m_b^2}{m_W^2} \right) \right] \\
& \left. - b_{11}^{\tilde{t}} k_{11}^{\tilde{t}} O'_{R_{11}} m_b m_t \left[2 m_{\tilde{\chi}_1^0}^2 + (m_b^2 + m_{\tilde{t}_1}^2) \left(3 + \frac{m_b^2 + m_{\tilde{t}_1}^2}{m_W^2} \right) \right] \right\} \quad (A.23)
\end{aligned}$$

$$\begin{aligned}
cb_{12} = & -\sqrt{2} \left\{ a_{11}^{\tilde{t}} l_{11}^{\tilde{t}} O'_{L_{11}} (m_{\tilde{t}_1}^2 - m_{\tilde{\chi}_1^0}^2) \left(2 - \frac{m_b^2}{m_W^2} \right) - 3 b_{11}^{\tilde{t}} l_{11}^{\tilde{t}} O'_{L_{11}} m_t m_{\tilde{\chi}_1^0} \right. \\
& + a_{11}^{\tilde{t}} k_{11}^{\tilde{t}} O'_{R_{11}} m_b m_{\tilde{\chi}_1^0} \left(\frac{m_b^2}{m_W^2} - 1 \right) + b_{11}^{\tilde{t}} l_{11}^{\tilde{t}} O'_{R_{11}} m_t m_{\tilde{\chi}_1^+} \left(2 + \frac{m_b^2}{m_W^2} \right) \\
& \left. + b_{11}^{\tilde{t}} k_{11}^{\tilde{t}} O'_{R_{11}} m_b m_t \left(3 + 2 \frac{m_b^2 + m_{\tilde{t}_1}^2}{m_W^2} \right) \right\} \quad (A.24)
\end{aligned}$$

$$cb_{13} = \sqrt{2} b_{11}^{\tilde{t}} k_{11}^{\tilde{t}} O'_{R_{11}} \frac{m_b m_t}{m_W^2} \quad (A.25)$$

$$\begin{aligned}
cb_{14} = & -\sqrt{2} \left\{ 3 a_{11}^{\tilde{t}} k_{11}^{\tilde{t}} O'_{L_{11}} m_b m_{\tilde{\chi}_1^+} - 3 b_{11}^{\tilde{t}} l_{11}^{\tilde{t}} O'_{L_{11}} m_t m_{\tilde{\chi}_1^0} \right. \\
& - a_{11}^{\tilde{t}} l_{11}^{\tilde{t}} O'_{R_{11}} m_{\tilde{\chi}_1^0} m_{\tilde{\chi}_1^+} \left(1 - 2 \frac{m_b^2}{m_W^2} \right) + a_{11}^{\tilde{t}} k_{11}^{\tilde{t}} O'_{R_{11}} m_b m_{\tilde{\chi}_1^0} \left(1 + \frac{2 m_b^2 + m_{\tilde{t}_1}^2}{m_W^2} \right) \\
& + b_{11}^{\tilde{t}} l_{11}^{\tilde{t}} O'_{R_{11}} m_t m_{\tilde{\chi}_1^+} \left(1 + \frac{2 m_b^2 + m_{\tilde{t}_1}^2}{m_W^2} \right) + b_{11}^{\tilde{t}} k_{11}^{\tilde{t}} O'_{R_{11}} m_b m_t \left(3 + 2 \frac{m_b^2 + m_{\tilde{t}_1}^2}{m_W^2} \right) \\
& \left. + a_{11}^{\tilde{t}} l_{11}^{\tilde{t}} O'_{L_{11}} \left[4 m_b^2 + 2 m_W^2 + m_{\tilde{t}_1}^2 \left(2 + \frac{m_{\tilde{\chi}_1^0}^2 - m_b^2}{m_W^2} \right) \right] \right\} \quad (A.26)
\end{aligned}$$

$$\begin{aligned}
 cb_{15} = & \sqrt{2} \left\{ a_{11}^{\tilde{t}} k_{11}^{\tilde{t}} O'_{R_{11}} \frac{m_b m_{\tilde{\chi}_1^0}}{m_W^2} + b_{11}^{\tilde{t}} l_{11}^{\tilde{t}} O'_{R_{11}} \frac{m_t m_{\tilde{\chi}_1^+}}{m_W^2} \right. \\
 & \left. + a_{11}^{\tilde{t}} l_{11}^{\tilde{t}} O'_{L_{11}} \left(3 + \frac{m_b^2 + m_{\tilde{t}_1}^2 + m_{\tilde{\chi}_1^0}^2}{m_W^2} \right) + 2 b_{11}^{\tilde{t}} k_{11}^{\tilde{t}} O'_{R_{11}} \frac{m_b m_t}{m_W^2} \right\} \quad (A.27)
 \end{aligned}$$

$$cb_{16} = -\frac{\sqrt{2} a_{11}^{\tilde{t}} l_{11}^{\tilde{t}} O'_{L_{11}}}{m_W^2} \quad (A.28)$$

$$\begin{aligned}
 cb_{17} = & \sqrt{2} \left\{ 2 a_{11}^{\tilde{t}} l_{11}^{\tilde{t}} O'_{L_{11}} + a_{11}^{\tilde{t}} l_{11}^{\tilde{t}} O'_{R_{11}} \frac{m_{\tilde{\chi}_1^0} m_{\tilde{\chi}_1^+}}{m_W^2} + a_{11}^{\tilde{t}} k_{11}^{\tilde{t}} O'_{R_{11}} \frac{m_b m_{\tilde{\chi}_1^0}}{m_W^2} \right. \\
 & \left. + b_{11}^{\tilde{t}} l_{11}^{\tilde{t}} O'_{R_{11}} \frac{m_t m_{\tilde{\chi}_1^+}}{m_W^2} + b_{11}^{\tilde{t}} k_{11}^{\tilde{t}} O'_{R_{11}} \frac{m_b m_t}{m_W^2} \right\} \quad (A.29)
 \end{aligned}$$

$$\begin{aligned}
 cc_{ki1} = & -\sqrt{2} \cos \theta_{\tilde{t}} \cos \theta_{\tilde{b}} \left\{ \left(a_{11}^{\tilde{b}} l_{11}^{\tilde{t}} O'_{L_{11}} + b_{11}^{\tilde{b}} k_{11}^{\tilde{t}} O'_{R_{11}} \right) \left[m_b^2 m_W^2 + m_b^4 \right. \right. \\
 & \left. \left. - 2 m_b^2 m_{\tilde{\chi}_1^0}^2 + m_{\tilde{\chi}_1^0}^2 m_{\tilde{t}_1}^2 \left(\frac{m_{\tilde{t}_1}^2}{m_W^2} - 1 \right) + m_b^2 m_{\tilde{t}_1}^2 \left(\frac{m_b^2}{m_W^2} - 2 \right) + \frac{m_b^2 m_{\tilde{t}_1}^4}{m_W^2} \right] \right. \\
 & + \left(b_{11}^{\tilde{b}} l_{11}^{\tilde{t}} O'_{L_{11}} + a_{11}^{\tilde{b}} k_{11}^{\tilde{t}} O'_{R_{11}} \right) m_b m_{\tilde{\chi}_1^0} \left(m_b^2 - m_{\tilde{t}_1}^2 - 2 m_{\tilde{\chi}_1^0}^2 + m_{\tilde{t}_1}^2 \frac{m_b^2 + m_{\tilde{t}_1}^2}{m_W^2} \right) \\
 & + \left(b_{11}^{\tilde{b}} k_{11}^{\tilde{t}} O'_{L_{11}} + a_{11}^{\tilde{b}} l_{11}^{\tilde{t}} O'_{R_{11}} \right) m_{\tilde{\chi}_1^0} m_{\tilde{\chi}_1^+} \left[m_b^2 - m_W^2 - 2 m_{\tilde{\chi}_1^0}^2 + m_{\tilde{t}_1}^2 \left(1 + \frac{m_b^2}{m_W^2} \right) \right] \\
 & \left. + \left(a_{11}^{\tilde{b}} k_{11}^{\tilde{t}} O'_{L_{11}} + b_{11}^{\tilde{b}} l_{11}^{\tilde{t}} O'_{R_{11}} \right) m_b m_{\tilde{\chi}_1^+} \left[m_b^2 - 2 m_{\tilde{\chi}_1^0}^2 + m_{\tilde{t}_1}^2 \left(\frac{m_b^2 + m_{\tilde{t}_1}^2}{m_W^2} - 1 \right) \right] \right\} \quad (A.30)
 \end{aligned}$$

$$\begin{aligned}
 cc_{ki2} = & \sqrt{2} \cos \theta_{\tilde{t}} \cos \theta_{\tilde{b}} \left\{ \left(a_{11}^{\tilde{b}} l_{11}^{\tilde{t}} O'_{L_{11}} + b_{11}^{\tilde{b}} k_{11}^{\tilde{t}} O'_{R_{11}} \right) \right. \\
 & * \left[m_{\tilde{\chi}_1^0}^2 \left(1 + 2 \frac{m_{\tilde{t}_1}^2}{m_W^2} \right) + \frac{m_{\tilde{t}_1}^4}{m_W^2} + m_W^2 + m_b^2 \left(3 + \frac{m_b^2 + 3 m_{\tilde{t}_1}^2}{m_W^2} \right) \right] \\
 & + \left(b_{11}^{\tilde{b}} l_{11}^{\tilde{t}} O'_{L_{11}} + a_{11}^{\tilde{b}} k_{11}^{\tilde{t}} O'_{R_{11}} \right) m_b m_{\tilde{\chi}_1^0} \left(1 + \frac{m_b^2 + 2 m_{\tilde{t}_1}^2}{m_W^2} \right) \\
 & + \left(b_{11}^{\tilde{b}} k_{11}^{\tilde{t}} O'_{L_{11}} + a_{11}^{\tilde{b}} l_{11}^{\tilde{t}} O'_{R_{11}} \right) m_{\tilde{\chi}_1^0} m_{\tilde{\chi}_1^+} \left(\frac{m_b^2}{m_W^2} - 1 \right) \\
 & \left. + \left(a_{11}^{\tilde{b}} k_{11}^{\tilde{t}} O'_{L_{11}} + b_{11}^{\tilde{b}} l_{11}^{\tilde{t}} O'_{R_{11}} \right) m_b m_{\tilde{\chi}_1^+} \left(1 + \frac{m_b^2 + 2 m_{\tilde{t}_1}^2}{m_W^2} \right) \right\} \quad (A.31)
 \end{aligned}$$

$$\begin{aligned}
 cC_{ki3} = & -\sqrt{2} \cos \theta_{\tilde{t}} \cos \theta_{\tilde{b}} \left\{ \left(a_{11}^{\tilde{b}} k_{11}^{\tilde{t}} O'_{L_{11}} + b_{11}^{\tilde{b}} l_{11}^{\tilde{t}} O'_{R_{11}} \right) \frac{m_b m_{\tilde{\chi}_1^+}}{m_W^2} \right. \\
 & + \left(b_{11}^{\tilde{b}} l_{11}^{\tilde{t}} O'_{L_{11}} + a_{11}^{\tilde{b}} k_{11}^{\tilde{t}} O'_{R_{11}} \right) \frac{m_b m_{\tilde{\chi}_1^0}}{m_W^2} \\
 & \left. + \left(a_{11}^{\tilde{b}} l_{11}^{\tilde{t}} O'_{L_{11}} + b_{11}^{\tilde{b}} k_{11}^{\tilde{t}} O'_{R_{11}} \right) \left(2 + \frac{2 m_b^2 + m_{\tilde{\chi}_1^0}^2 + 2 m_{\tilde{t}_1}^2}{m_W^2} \right) \right\} \quad (A.32)
 \end{aligned}$$

$$cC_{ki4} = \sqrt{2} \cos \theta_{\tilde{t}} \cos \theta_{\tilde{b}} \frac{\left(a_{11}^{\tilde{b}} l_{11}^{\tilde{t}} O'_{L_{11}} + b_{11}^{\tilde{b}} k_{11}^{\tilde{t}} O'_{R_{11}} \right)}{m_W^2} \quad (A.33)$$

$$\begin{aligned}
 cC_{ki5} = & -\sqrt{2} \cos \theta_{\tilde{t}} \cos \theta_{\tilde{b}} \left(1 - \frac{m_{\tilde{t}_1}^2}{m_W^2} \right) \\
 & * \left[\left(b_{11}^{\tilde{b}} k_{11}^{\tilde{t}} O'_{L_{11}} + a_{11}^{\tilde{b}} l_{11}^{\tilde{t}} O'_{R_{11}} \right) m_{\tilde{\chi}_1^0} m_{\tilde{\chi}_1^+} + \left(a_{11}^{\tilde{b}} k_{11}^{\tilde{t}} O'_{L_{11}} + b_{11}^{\tilde{b}} l_{11}^{\tilde{t}} O'_{R_{11}} \right) m_b m_{\tilde{\chi}_1^+} \right. \\
 & \left. + \left(b_{11}^{\tilde{b}} l_{11}^{\tilde{t}} O'_{L_{11}} + a_{11}^{\tilde{b}} k_{11}^{\tilde{t}} O'_{R_{11}} \right) m_b m_{\tilde{\chi}_1^0} + \left(a_{11}^{\tilde{b}} l_{11}^{\tilde{t}} O'_{L_{11}} + b_{11}^{\tilde{b}} k_{11}^{\tilde{t}} O'_{R_{11}} \right) m_b^2 \right] \quad (A.34)
 \end{aligned}$$

$$\begin{aligned}
 cC_{ki6} = & -\sqrt{2} \cos \theta_{\tilde{t}} \cos \theta_{\tilde{b}} \left\{ \left(b_{11}^{\tilde{b}} l_{11}^{\tilde{t}} O'_{L_{11}} + a_{11}^{\tilde{b}} k_{11}^{\tilde{t}} O'_{R_{11}} \right) \frac{m_b m_{\tilde{\chi}_1^0}}{m_W^2} \right. \\
 & + \left(b_{11}^{\tilde{b}} k_{11}^{\tilde{t}} O'_{L_{11}} + a_{11}^{\tilde{b}} l_{11}^{\tilde{t}} O'_{R_{11}} \right) \frac{m_{\tilde{\chi}_1^0} m_{\tilde{\chi}_1^+}}{m_W^2} + \left(a_{11}^{\tilde{b}} k_{11}^{\tilde{t}} O'_{L_{11}} + b_{11}^{\tilde{b}} l_{11}^{\tilde{t}} O'_{R_{11}} \right) \frac{m_b m_{\tilde{\chi}_1^+}}{m_W^2} \\
 & \left. + \left(a_{11}^{\tilde{b}} l_{11}^{\tilde{t}} O'_{L_{11}} + b_{11}^{\tilde{b}} k_{11}^{\tilde{t}} O'_{R_{11}} \right) \left(1 + \frac{m_b^2 + m_{\tilde{t}_1}^2}{m_W^2} \right) \right\} \quad (A.35)
 \end{aligned}$$

$$\begin{aligned}
 cd_1 = & (a_{11}^{\tilde{t}})^2 \frac{(m_{\tilde{\chi}_1^0}^2 - m_{\tilde{t}_1}^2)}{2} \left[2 m_W^2 - m_b^2 \left(1 + \frac{m_b^2}{m_W^2} \right) \right] \\
 & - (b_{11}^{\tilde{t}})^2 \frac{m_{\tilde{t}}^2}{2} \left[m_{\tilde{\chi}_1^0}^2 + m_{\tilde{t}_1}^2 + m_b^2 \left(2 + \frac{m_b^2 + m_{\tilde{t}_1}^2}{m_W^2} \right) \right] \\
 & + a_{11}^{\tilde{t}} b_{11}^{\tilde{t}} m_t m_{\tilde{\chi}_1^0} \left[2 m_W^2 - m_b^2 \left(1 + \frac{m_b^2}{m_W^2} \right) \right] \quad (A.36)
 \end{aligned}$$

$$cd_2 = (b_{11}^{\tilde{t}})^2 m_t^2 \left(1 + \frac{m_b^2}{2 m_W^2} \right) \quad (A.37)$$

$$\begin{aligned}
 cd_3 = & (a_{11}^{\tilde{t}})^2 \left(\frac{m_b^2}{2} + m_{\tilde{t}_1}^2 + m_W^2 + (2 m_{\tilde{\chi}_1^0}^2 - m_{\tilde{t}_1}^2) \frac{m_b^2}{2 m_W^2} \right) \\
 & + (b_{11}^{\tilde{t}})^2 m_t^2 \frac{(m_W^2 + 2 m_b^2 + m_{\tilde{t}_1}^2)}{2 m_W^2} - a_{11}^{\tilde{t}} b_{11}^{\tilde{t}} m_t m_{\tilde{\chi}_1^0} \left(1 - 2 \frac{m_b^2}{m_W^2} \right) \quad (A.38)
 \end{aligned}$$

$$cd_4 = -(a_{11}^{\tilde{t}})^2 \left(1 + \frac{m_b^2}{2m_W^2} \right) - (b_{11}^{\tilde{t}})^2 \frac{m_t^2}{2m_W^2} \quad (\text{A.39})$$

$$cd_5 = -(a_{11}^{\tilde{t}})^2 \left(1 + \frac{m_{\tilde{\chi}_1^0}^2}{2m_W^2} \right) - a_{11}^{\tilde{t}} b_{11}^{\tilde{t}} \frac{m_t m_{\tilde{\chi}_1^0}}{m_W^2} - (b_{11}^{\tilde{t}})^2 \frac{m_t^2}{2m_W^2} \quad (\text{A.40})$$

$$cd_6 = \frac{(a_{11}^{\tilde{t}})^2}{2m_W^2} \quad (\text{A.41})$$

$$\begin{aligned} ce_{11} = & \cos \theta_{\tilde{t}} \cos \theta_{\tilde{b}} \left\{ \left(a_{11}^{\tilde{b}} b_{11}^{\tilde{t}} m_t m_{\tilde{\chi}_1^0} + b_{11}^{\tilde{b}} a_{11}^{\tilde{t}} m_b m_{\tilde{\chi}_1^0} \right) \right. \\ & * \left(m_b^2 + m_{\tilde{t}_1}^2 - 2m_{\tilde{\chi}_1^0}^2 - m_W^2 + \frac{m_b^2 m_{\tilde{t}_1}^2}{m_W^2} \right) \\ & + a_{11}^{\tilde{b}} a_{11}^{\tilde{t}} \left[m_b^2 (m_{\tilde{\chi}_1^0}^2 + m_{\tilde{t}_1}^2) + 2m_{\tilde{\chi}_1^0}^2 (m_{\tilde{t}_1}^2 - m_{\tilde{\chi}_1^0}^2 - m_W^2) + (m_{\tilde{\chi}_1^0}^2 - m_{\tilde{t}_1}^2) \frac{m_b^2 m_{\tilde{t}_1}^2}{m_W^2} \right] \\ & \left. + b_{11}^{\tilde{b}} b_{11}^{\tilde{t}} m_b m_t \left(m_b^2 - 2m_{\tilde{\chi}_1^0}^2 - m_{\tilde{t}_1}^2 + \frac{m_{\tilde{t}_1}^2 (m_b^2 + m_{\tilde{t}_1}^2)}{m_W^2} \right) \right\} \quad (\text{A.42}) \end{aligned}$$

$$\begin{aligned} ce_{12} = & \cos \theta_{\tilde{t}} \cos \theta_{\tilde{b}} \left\{ \left(a_{11}^{\tilde{b}} b_{11}^{\tilde{t}} m_t m_{\tilde{\chi}_1^0} + b_{11}^{\tilde{b}} a_{11}^{\tilde{t}} m_b m_{\tilde{\chi}_1^0} \right) \left(1 - \frac{m_b^2}{m_W^2} \right) \right. \\ & \left. + a_{11}^{\tilde{b}} a_{11}^{\tilde{t}} (m_{\tilde{\chi}_1^0}^2 - m_{\tilde{t}_1}^2) \left(2 - \frac{m_b^2}{m_W^2} \right) - b_{11}^{\tilde{b}} b_{11}^{\tilde{t}} m_b m_t \left(1 + \frac{m_b^2 + 2m_{\tilde{t}_1}^2}{m_W^2} \right) \right\} \quad (\text{A.43}) \end{aligned}$$

$$ce_{13} = \cos \theta_{\tilde{t}} \cos \theta_{\tilde{b}} b_{11}^{\tilde{b}} b_{11}^{\tilde{t}} \frac{m_b m_t}{m_W^2} \quad (\text{A.44})$$

$$\begin{aligned} ce_{14} = & \cos \theta_{\tilde{t}} \cos \theta_{\tilde{b}} \left(1 - \frac{m_{\tilde{t}_1}^2}{m_W^2} \right) \\ & * \left(a_{11}^{\tilde{b}} a_{11}^{\tilde{t}} m_{\tilde{\chi}_1^0}^2 + a_{11}^{\tilde{b}} b_{11}^{\tilde{t}} m_t m_{\tilde{\chi}_1^0} + b_{11}^{\tilde{b}} a_{11}^{\tilde{t}} m_b m_{\tilde{\chi}_1^0} + b_{11}^{\tilde{b}} b_{11}^{\tilde{t}} m_b m_t \right) \quad (\text{A.45}) \end{aligned}$$

$$\begin{aligned} ce_{15} = & \cos \theta_{\tilde{t}} \cos \theta_{\tilde{b}} \left\{ a_{11}^{\tilde{b}} a_{11}^{\tilde{t}} \left(1 + \frac{m_{\tilde{\chi}_1^0}^2 + m_{\tilde{t}_1}^2}{m_W^2} \right) + a_{11}^{\tilde{b}} b_{11}^{\tilde{t}} \frac{m_t m_{\tilde{\chi}_1^0}}{m_W^2} \right. \\ & \left. + b_{11}^{\tilde{b}} a_{11}^{\tilde{t}} \frac{m_b m_{\tilde{\chi}_1^0}}{m_W^2} + \cos \theta_{\tilde{b}} b_{11}^{\tilde{b}} b_{11}^{\tilde{t}} \frac{m_b m_t}{m_W^2} \right\} \quad (\text{A.46}) \end{aligned}$$

$$ce_{16} = -\frac{\cos \theta_{\tilde{t}} \cos \theta_{\tilde{b}} a_{11}^{\tilde{b}} a_{11}^{\tilde{t}}}{m_W^2} \quad (\text{A.47})$$

$$cf_{11} = -\frac{1}{2} \cos^2 \theta_{\tilde{t}} \cos^2 \theta_{\tilde{b}} \left[\left((a_{11}^{\tilde{b}})^2 + (b_{11}^{\tilde{b}})^2 \right) (m_b^2 + m_{\tilde{\chi}_1^0}^2) + 4 a_{11}^{\tilde{b}} b_{11}^{\tilde{b}} m_b m_{\tilde{\chi}_1^0} \right] \quad (\text{A.48})$$

$$cf_{12} = \frac{1}{2} \cos^2 \theta_{\tilde{t}} \cos^2 \theta_{\tilde{b}} \left((a_{11}^{\tilde{b}})^2 + (b_{11}^{\tilde{b}})^2 \right) \quad (\text{A.49})$$

$$cf_{31} = \cos^2 \theta_{\tilde{t}} \cos \theta_{\tilde{b}} \sin \theta_{\tilde{b}} \\ * \left[(a_{11}^{\tilde{b}} a_{12}^{\tilde{b}} + b_{11}^{\tilde{b}} b_{12}^{\tilde{b}}) (m_b^2 + m_{\tilde{\chi}_1^0}^2) + 2 (a_{11}^{\tilde{b}} b_{12}^{\tilde{b}} + b_{11}^{\tilde{b}} a_{12}^{\tilde{b}}) m_b m_{\tilde{\chi}_1^0} \right] \quad (\text{A.50})$$

$$cf_{32} = -\cos^2 \theta_{\tilde{t}} \cos \theta_{\tilde{b}} \sin \theta_{\tilde{b}} (a_{11}^{\tilde{b}} a_{12}^{\tilde{b}} + b_{11}^{\tilde{b}} b_{12}^{\tilde{b}}) \quad (\text{A.51})$$

To get the remaining coefficients one has to make the following replacements:

$$\begin{aligned} ca_{1i} \rightarrow ca_{2i}: & \quad l_{11}^{\tilde{t}} \rightarrow l_{12}^{\tilde{t}}, k_{11}^{\tilde{t}} \rightarrow k_{12}^{\tilde{t}}, O'_{L11} \rightarrow O'_{L12}, O'_{L11} \rightarrow O'_{L12}, m_{\tilde{\chi}_1^+} \rightarrow m_{\tilde{\chi}_2^+} \\ cb_{1i} \rightarrow cb_{2i}: & \quad l_{11}^{\tilde{t}} \rightarrow l_{12}^{\tilde{t}}, k_{11}^{\tilde{t}} \rightarrow k_{12}^{\tilde{t}}, O'_{L11} \rightarrow O'_{L12}, O'_{R11} \rightarrow O'_{R12}, m_{\tilde{\chi}_1^+} \rightarrow m_{\tilde{\chi}_2^+} \\ cc_{11i} \rightarrow cc_{12i}: & \quad l_{11}^{\tilde{t}} \rightarrow l_{12}^{\tilde{t}}, k_{11}^{\tilde{t}} \rightarrow k_{12}^{\tilde{t}}, O'_{L11} \rightarrow O'_{L12}, O'_{R11} \rightarrow O'_{R12}, m_{\tilde{\chi}_1^+} \rightarrow m_{\tilde{\chi}_2^+} \\ cc_{11i} \rightarrow cc_{21i}: & \quad a_{11}^{\tilde{b}} \rightarrow a_{12}^{\tilde{b}}, b_{11}^{\tilde{b}} \rightarrow b_{12}^{\tilde{b}}, m_{\tilde{b}_1} \rightarrow m_{\tilde{b}_2}, \cos \theta_{\tilde{b}} \rightarrow -\sin \theta_{\tilde{b}} \\ cc_{11i} \rightarrow cc_{22i}: & \quad l_{11}^{\tilde{t}} \rightarrow l_{12}^{\tilde{t}}, k_{11}^{\tilde{t}} \rightarrow k_{12}^{\tilde{t}}, O'_{L11} \rightarrow O'_{L12}, O'_{R11} \rightarrow O'_{R12}, m_{\tilde{\chi}_1^+} \rightarrow m_{\tilde{\chi}_2^+}, \\ & \quad a_{11}^{\tilde{b}} \rightarrow a_{12}^{\tilde{b}}, b_{11}^{\tilde{b}} \rightarrow b_{12}^{\tilde{b}}, m_{\tilde{b}_1} \rightarrow m_{\tilde{b}_2}, \cos \theta_{\tilde{b}} \rightarrow -\sin \theta_{\tilde{b}} \\ ce_{1i} \rightarrow ce_{2i}: & \quad a_{11}^{\tilde{b}} \rightarrow a_{12}^{\tilde{b}}, b_{11}^{\tilde{b}} \rightarrow b_{12}^{\tilde{b}}, m_{\tilde{b}_1} \rightarrow m_{\tilde{b}_2}, \cos \theta_{\tilde{b}} \rightarrow -\sin \theta_{\tilde{b}} \\ cf_{1i} \rightarrow cf_{2i}: & \quad a_{11}^{\tilde{b}} \rightarrow a_{12}^{\tilde{b}}, b_{11}^{\tilde{b}} \rightarrow b_{12}^{\tilde{b}}, m_{\tilde{b}_1} \rightarrow m_{\tilde{b}_2}, \cos \theta_{\tilde{b}} \rightarrow -\sin \theta_{\tilde{b}} \end{aligned}$$

A.2 The Decay of the Light Stop into a charged Higgs Boson, a Bottom Quark and the Lightest Neutralino

The decay width is given by

$$\begin{aligned} \Gamma(\tilde{t}_1 \rightarrow H^+ + b + \tilde{\chi}_1^0) &= \\ &= \frac{\alpha^2}{16 \pi m_{\tilde{t}_1}^3 \sin^4 \theta_W} \int_{(m_b + m_{\tilde{\chi}_1^0})^2}^{(m_{\tilde{t}_1} - m_{H^\pm})^2} ds \left(G_{\tilde{\chi}^+ \tilde{\chi}^+} + G_{\tilde{\chi}^+ t} + G_{\tilde{\chi}^+ \tilde{b}} + G_{tt} + G_{t\tilde{b}} + G_{\tilde{b}\tilde{b}} \right) \end{aligned} \quad (\text{A.52})$$

with

$$\begin{aligned} G_{\tilde{\chi}^+ \tilde{\chi}^+} &= \sum_{i=1}^2 \left[(da_{i1} + da_{i2}s) J_t^0(m_{\tilde{t}_1}^2 + m_{H^\pm}^2 + m_b^2 + m_{\tilde{\chi}_1^0}^2 - m_{\tilde{\chi}_i^+}^2 - s, \Gamma_{\tilde{\chi}_i^+} m_{\tilde{\chi}_i^+}) \right. \\ &\quad + (da_{i3} + da_{i4}s) J_t^1(m_{\tilde{t}_1}^2 + m_{H^\pm}^2 + m_b^2 + m_{\tilde{\chi}_1^0}^2 - m_{\tilde{\chi}_i^+}^2 - s, \Gamma_{\tilde{\chi}_i^+} m_{\tilde{\chi}_i^+}) \\ &\quad \left. + da_{i4} J_t^2(m_{\tilde{t}_1}^2 + m_{H^\pm}^2 + m_b^2 + m_{\tilde{\chi}_1^0}^2 - m_{\tilde{\chi}_i^+}^2 - s, \Gamma_{\tilde{\chi}_i^+} m_{\tilde{\chi}_i^+}) \right] \\ &\quad + (da_{31} + da_{32}s) J_{tt}^0(m_{\tilde{t}_1}^2 + m_{H^\pm}^2 + m_b^2 + m_{\tilde{\chi}_1^0}^2 - m_{\tilde{\chi}_1^+}^2 - s, \Gamma_{\tilde{\chi}_1^+} m_{\tilde{\chi}_1^+} \\ &\quad \quad \quad , m_{\tilde{t}_1}^2 + m_{H^\pm}^2 + m_b^2 + m_{\tilde{\chi}_1^0}^2 - m_{\tilde{\chi}_2^+}^2 - s, \Gamma_{\tilde{\chi}_2^+} m_{\tilde{\chi}_2^+}) \\ &\quad + (da_{33} + da_{34}s) J_{tt}^1(m_{\tilde{t}_1}^2 + m_{H^\pm}^2 + m_b^2 + m_{\tilde{\chi}_1^0}^2 - m_{\tilde{\chi}_1^+}^2 - s, \Gamma_{\tilde{\chi}_1^+} m_{\tilde{\chi}_1^+} \\ &\quad \quad \quad , m_{\tilde{t}_1}^2 + m_{H^\pm}^2 + m_b^2 + m_{\tilde{\chi}_1^0}^2 - m_{\tilde{\chi}_2^+}^2 - s, \Gamma_{\tilde{\chi}_2^+} m_{\tilde{\chi}_2^+}) \end{aligned}$$

$$\begin{aligned}
 & + da_{34} J_{tt}^2(m_{t_1}^2 + m_{H^\pm}^2 + m_b^2 + m_{\tilde{\chi}_1^0}^2 - m_{\tilde{\chi}_1^+}^2 - s, \Gamma_{\tilde{\chi}_1^+} m_{\tilde{\chi}_1^+} \\
 & \quad , m_{t_1}^2 + m_{H^\pm}^2 + m_b^2 + m_{\tilde{\chi}_1^0}^2 - m_{\tilde{\chi}_2^+}^2 - s, \Gamma_{\tilde{\chi}_2^+} m_{\tilde{\chi}_2^+}) \quad (A.53)
 \end{aligned}$$

$$\begin{aligned}
 G_{\tilde{\chi}^+ t} = & \sum_{i=1}^2 \left[(db_{i1} + db_{i2} s) \right. \\
 & * J_{tt}^0(m_{t_1}^2 + m_{H^\pm}^2 + m_b^2 + m_{\tilde{\chi}_1^0}^2 - m_{\tilde{\chi}_1^+}^2 - s, -\Gamma_{\tilde{\chi}_1^+} m_{\tilde{\chi}_1^+}, m_t^2, \Gamma_t m_t) \\
 & + (db_{i3} + db_{i4} s) \\
 & * J_{tt}^1(m_{t_1}^2 + m_{H^\pm}^2 + m_b^2 + m_{\tilde{\chi}_1^0}^2 - m_{\tilde{\chi}_1^+}^2 - s, -\Gamma_{\tilde{\chi}_1^+} m_{\tilde{\chi}_1^+}, m_t^2, \Gamma_t m_t) \\
 & \left. + db_{i4} J_{tt}^2(m_{t_1}^2 + m_{H^\pm}^2 + m_b^2 + m_{\tilde{\chi}_1^0}^2 - m_{\tilde{\chi}_1^+}^2 - s, -\Gamma_{\tilde{\chi}_1^+} m_{\tilde{\chi}_1^+}, m_t^2, \Gamma_t m_t) \right] \quad (A.54)
 \end{aligned}$$

$$\begin{aligned}
 G_{\tilde{\chi}^+ \tilde{b}} = & \sum_{k,i=1}^2 \left[(cc_{ik1} + cc_{ik2} s) \right. \\
 & * J_{st}^0(m_{b_k}^2, \Gamma_{\tilde{b}_k} m_{\tilde{b}_k}, m_{t_1}^2 + m_{H^\pm}^2 + m_b^2 + m_{\tilde{\chi}_1^0}^2 - m_{\tilde{\chi}_1^+}^2 - s, -\Gamma_{\tilde{\chi}_1^+} m_{\tilde{\chi}_1^+}) \\
 & \left. + cc_{ik3} J_{st}^1(m_{b_k}^2, \Gamma_{\tilde{b}_k} m_{\tilde{b}_k}, m_{t_1}^2 + m_{H^\pm}^2 + m_b^2 + m_{\tilde{\chi}_1^0}^2 - m_{\tilde{\chi}_1^+}^2 - s, -\Gamma_{\tilde{\chi}_1^+} m_{\tilde{\chi}_1^+}) \right] \quad (A.55)
 \end{aligned}$$

$$\begin{aligned}
 G_{tt} = & (dd_1 + dd_2 s) J_t^0(m_t^2, \Gamma_t m_t) + (dd_3 + dd_4 s) J_t^1(m_t^2, \Gamma_t m_t) \\
 & + dd_4 J_t^2(m_t^2, \Gamma_t m_t) \quad (A.56)
 \end{aligned}$$

$$\begin{aligned}
 G_{t\tilde{b}} = & \sum_{k=1}^2 \left[(de_{k1} + de_{k2} s) J_{st}^0(m_{b_k}^2, \Gamma_{\tilde{b}_k} m_{\tilde{b}_k}, m_t^2, \Gamma_t m_t) \right. \\
 & \left. + de_{k3} J_{st}^1(m_{b_k}^2, \Gamma_{\tilde{b}_k} m_{\tilde{b}_k}, m_t^2, \Gamma_t m_t) \right] \quad (A.57)
 \end{aligned}$$

$$\begin{aligned}
 G_{\tilde{b}\tilde{b}} = & \frac{\sqrt{\lambda(s, m_{t_1}^2, m_{H^\pm}^2) \lambda(s, m_{\tilde{\chi}_1^0}^2, m_b^2)}}{s} \\
 & * \left\{ \sum_{k=1}^2 \frac{(df_{k1} + df_{k2} s)}{(s - m_{b_k}^2)^2 + \Gamma_{b_k}^2 m_{b_k}^2} + Re \left[\frac{(df_{31} + df_{32} s)}{(s - m_{b_1}^2 + i\Gamma_{\tilde{b}_1} m_{\tilde{b}_1})(s - m_{b_2}^2 - i\Gamma_{\tilde{b}_2} m_{\tilde{b}_2})} \right] \right\} \quad (A.58)
 \end{aligned}$$

The integrals $J_{t,tt,st}^{0,1,2}$ are defined in Section A.4.1. Their integration range is given by

$$\begin{aligned}
 t_{min}^{max} = & \frac{m_{t_1}^2 + m_b^2 + m_{H^\pm}^2 + m_{\tilde{\chi}_1^0}^2 - s}{2} - \frac{(m_{t_1}^2 - m_{H^\pm}^2)(m_{\tilde{\chi}_1^0}^2 - m_b^2)}{2s} \\
 & \pm \frac{\sqrt{\lambda(s, m_{t_1}^2, m_{H^\pm}^2) \lambda(s, m_{\tilde{\chi}_1^0}^2, m_b^2)}}{2s} \quad (A.59)
 \end{aligned}$$

and $s = (p_{\tilde{t}_1} - p_{H^\pm})^2$. Note, that $-\Gamma_{\tilde{\chi}_1^+ m_{\tilde{\chi}_1^+}}$ appears in the entries of the integrals $G_{\tilde{\chi}^+ \tilde{b}_j}$ and $G_{\tilde{\chi}^+ t}$ because the chargino exchange is the u -channel in our convention. The coefficients are given by:

$$\begin{aligned}
da_{11} = & -4 k_{11}^{\tilde{t}} l_{11}^{\tilde{t}} Q'_{L11} Q'_{R11} m_b m_{\tilde{\chi}_1^0} \left(m_b^2 + m_{\tilde{\chi}_1^\pm}^2 + m_{\tilde{\chi}_1^0}^2 + m_{\tilde{t}_1}^2 + m_{H^\pm}^2 \right) \\
& -2 Q'_{L11} Q'_{R11} \left((k_{11}^{\tilde{t}})^2 + (l_{11}^{\tilde{t}})^2 \right) m_{\tilde{\chi}_1^0} m_{\tilde{\chi}_1^\pm} \left(2 m_b^2 + m_{\tilde{\chi}_1^0}^2 + m_{H^\pm}^2 \right) \\
& -2 k_{11}^{\tilde{t}} l_{11}^{\tilde{t}} \left((Q'_{L11})^2 + (Q'_{R11})^2 \right) m_b m_{\tilde{\chi}_1^\pm} \left(m_b^2 + 2 m_{\tilde{\chi}_1^0}^2 + m_{\tilde{t}_1}^2 \right) \\
& - \left((k_{11}^{\tilde{t}})^2 (Q'_{R11})^2 + (l_{11}^{\tilde{t}})^2 (Q'_{L11})^2 \right) \\
& \quad * \left[\left(m_b^2 + m_{\tilde{\chi}_1^0}^2 \right)^2 + \left(m_b^2 + m_{H^\pm}^2 \right) \left(m_{\tilde{\chi}_1^0}^2 + m_{\tilde{t}_1}^2 \right) \right] \\
& - \left((k_{11}^{\tilde{t}})^2 (Q'_{L11})^2 + (l_{11}^{\tilde{t}})^2 (Q'_{R11})^2 \right) m_{\tilde{\chi}_1^\pm}^2 \left(m_b^2 + m_{\tilde{\chi}_1^0}^2 \right) \tag{A.60}
\end{aligned}$$

$$\begin{aligned}
da_{12} = & 4 k_{11}^{\tilde{t}} l_{11}^{\tilde{t}} Q'_{L11} Q'_{R11} m_b m_{\tilde{\chi}_1^0} \\
& + \left((k_{11}^{\tilde{t}})^2 (Q'_{R11})^2 + (l_{11}^{\tilde{t}})^2 (Q'_{L11})^2 \right) \left(m_b^2 + m_{\tilde{\chi}_1^0}^2 \right) \\
& + 2 k_{11}^{\tilde{t}} l_{11}^{\tilde{t}} \left((Q'_{L11})^2 + (Q'_{R11})^2 \right) m_b m_{\tilde{\chi}_1^\pm} \\
& + 2 Q'_{L11} Q'_{R11} \left((k_{11}^{\tilde{t}})^2 + (l_{11}^{\tilde{t}})^2 \right) m_{\tilde{\chi}_1^0} m_{\tilde{\chi}_1^\pm} \\
& + \left((k_{11}^{\tilde{t}})^2 (Q'_{L11})^2 + (l_{11}^{\tilde{t}})^2 (Q'_{R11})^2 \right) m_{\tilde{\chi}_1^\pm}^2 \tag{A.61}
\end{aligned}$$

$$\begin{aligned}
da_{13} = & 4 k_{11}^{\tilde{t}} l_{11}^{\tilde{t}} Q'_{L11} Q'_{R11} m_b m_{\tilde{\chi}_1^0} + 2 Q'_{L11} Q'_{R11} \left((k_{11}^{\tilde{t}})^2 + (l_{11}^{\tilde{t}})^2 \right) m_{\tilde{\chi}_1^0} m_{\tilde{\chi}_1^\pm} \\
& + \left((k_{11}^{\tilde{t}})^2 (Q'_{R11})^2 + (l_{11}^{\tilde{t}})^2 (Q'_{L11})^2 \right) \left(2 m_b^2 + 2 m_{\tilde{\chi}_1^0}^2 + m_{H^\pm}^2 + m_{\tilde{t}_1}^2 \right) \\
& + 2 k_{11}^{\tilde{t}} l_{11}^{\tilde{t}} \left((Q'_{L11})^2 + (Q'_{R11})^2 \right) m_b m_{\tilde{\chi}_1^\pm} \tag{A.62}
\end{aligned}$$

$$da_{14} = -(k_{11}^{\tilde{t}})^2 (Q'_{R11})^2 - (l_{11}^{\tilde{t}})^2 (Q'_{L11})^2 \tag{A.63}$$

$$\begin{aligned}
da_{31} = & -2 \left(l_{11}^{\tilde{t}} l_{12}^{\tilde{t}} Q'_{L12} Q'_{R11} + k_{11}^{\tilde{t}} k_{12}^{\tilde{t}} Q'_{L11} Q'_{R12} \right) m_{\tilde{\chi}_1^0} m_{\tilde{\chi}_1^\pm} \left(m_{\tilde{\chi}_1^0}^2 + m_{H^\pm}^2 + 2 m_b^2 \right) \\
& -4 \left(k_{11}^{\tilde{t}} l_{12}^{\tilde{t}} Q'_{L12} Q'_{R11} + k_{12}^{\tilde{t}} l_{11}^{\tilde{t}} Q'_{L11} Q'_{R12} \right) m_b m_{\tilde{\chi}_1^0} \left(m_{\tilde{\chi}_1^0}^2 + m_{H^\pm}^2 + m_b^2 + m_{\tilde{t}_1}^2 \right) \\
& -4 \left(k_{12}^{\tilde{t}} l_{11}^{\tilde{t}} Q'_{L12} Q'_{R11} + k_{11}^{\tilde{t}} l_{12}^{\tilde{t}} Q'_{L11} Q'_{R12} \right) m_b m_{\tilde{\chi}_1^0} m_{\tilde{\chi}_1^\pm} m_{\tilde{\chi}_2^\pm} \\
& -2 \left(k_{11}^{\tilde{t}} k_{12}^{\tilde{t}} Q'_{L12} Q'_{R11} + l_{11}^{\tilde{t}} l_{12}^{\tilde{t}} Q'_{L11} Q'_{R12} \right) m_{\tilde{\chi}_1^0} m_{\tilde{\chi}_2^\pm} \left(m_{\tilde{\chi}_1^0}^2 + m_{H^\pm}^2 + 2 m_b^2 \right) \\
& -2 \left(l_{11}^{\tilde{t}} l_{12}^{\tilde{t}} Q'_{L11} Q'_{L12} + k_{11}^{\tilde{t}} k_{12}^{\tilde{t}} Q'_{R11} Q'_{R12} \right) \\
& \quad * \left[\left(m_b^2 + m_{\tilde{\chi}_1^0}^2 \right)^2 + \left(m_{\tilde{\chi}_1^0}^2 + m_{\tilde{t}_1}^2 \right) \left(m_b^2 + m_{H^\pm}^2 \right) \right] \\
& -2 \left(k_{11}^{\tilde{t}} l_{12}^{\tilde{t}} Q'_{L11} Q'_{L12} + k_{12}^{\tilde{t}} l_{11}^{\tilde{t}} Q'_{R11} Q'_{R12} \right) m_b m_{\tilde{\chi}_1^\pm} \left(m_b^2 + m_{\tilde{t}_1}^2 + 2 m_{\tilde{\chi}_1^0}^2 \right) \\
& -2 \left(k_{12}^{\tilde{t}} l_{11}^{\tilde{t}} Q'_{L11} Q'_{L12} + k_{11}^{\tilde{t}} l_{12}^{\tilde{t}} Q'_{R11} Q'_{R12} \right) m_b m_{\tilde{\chi}_2^\pm} \left(m_b^2 + m_{\tilde{t}_1}^2 + 2 m_{\tilde{\chi}_1^0}^2 \right) \\
& -2 \left(k_{11}^{\tilde{t}} k_{12}^{\tilde{t}} Q'_{L11} Q'_{L12} + l_{11}^{\tilde{t}} l_{12}^{\tilde{t}} Q'_{R11} Q'_{R12} \right) m_{\tilde{\chi}_1^\pm} m_{\tilde{\chi}_2^\pm} \left(m_{\tilde{\chi}_1^0}^2 + m_b^2 \right) \tag{A.64}
\end{aligned}$$

$$\begin{aligned}
 da_{32} = & 2 \left(l_{11}^{\tilde{t}} l_{12}^{\tilde{t}} Q'_{L_{12}} Q'_{R_{11}} + k_{11}^{\tilde{t}} k_{12}^{\tilde{t}} Q'_{L_{11}} Q'_{R_{12}} \right) m_{\tilde{\chi}_1^0} m_{\tilde{\chi}_1^\pm} \\
 & + 4 \left(k_{11}^{\tilde{t}} l_{12}^{\tilde{t}} Q'_{L_{12}} Q'_{R_{11}} + k_{12}^{\tilde{t}} l_{11}^{\tilde{t}} Q'_{L_{11}} Q'_{R_{12}} \right) m_b m_{\tilde{\chi}_1^0} \\
 & + 2 \left(k_{11}^{\tilde{t}} k_{12}^{\tilde{t}} Q'_{L_{12}} Q'_{R_{11}} + l_{11}^{\tilde{t}} l_{12}^{\tilde{t}} Q'_{L_{11}} Q'_{R_{12}} \right) m_{\tilde{\chi}_1^0} m_{\tilde{\chi}_2^\pm} \\
 & + 2 \left(l_{11}^{\tilde{t}} l_{12}^{\tilde{t}} Q'_{L_{11}} Q'_{L_{12}} + k_{11}^{\tilde{t}} k_{12}^{\tilde{t}} Q'_{R_{11}} Q'_{R_{12}} \right) (m_b^2 + m_{\tilde{\chi}_1^0}^2) \\
 & + 2 \left(k_{11}^{\tilde{t}} l_{12}^{\tilde{t}} Q'_{L_{11}} Q'_{L_{12}} + k_{12}^{\tilde{t}} l_{11}^{\tilde{t}} Q'_{R_{11}} Q'_{R_{12}} \right) m_b m_{\tilde{\chi}_1^\pm} \\
 & + 2 \left(k_{12}^{\tilde{t}} l_{11}^{\tilde{t}} Q'_{L_{11}} Q'_{L_{12}} + k_{11}^{\tilde{t}} l_{12}^{\tilde{t}} Q'_{R_{11}} Q'_{R_{12}} \right) m_b m_{\tilde{\chi}_2^\pm} \\
 & + 2 \left(k_{11}^{\tilde{t}} k_{12}^{\tilde{t}} Q'_{L_{11}} Q'_{L_{12}} + l_{11}^{\tilde{t}} l_{12}^{\tilde{t}} Q'_{R_{11}} Q'_{R_{12}} \right) m_{\tilde{\chi}_1^\pm} m_{\tilde{\chi}_2^\pm} \tag{A.65}
 \end{aligned}$$

$$\begin{aligned}
 da_{33} = & 2 \left(l_{11}^{\tilde{t}} l_{12}^{\tilde{t}} Q'_{L_{12}} Q'_{R_{11}} + k_{11}^{\tilde{t}} k_{12}^{\tilde{t}} Q'_{L_{11}} Q'_{R_{12}} \right) m_{\tilde{\chi}_1^0} m_{\tilde{\chi}_1^\pm} \\
 & + 4 \left(k_{11}^{\tilde{t}} l_{12}^{\tilde{t}} Q'_{L_{12}} Q'_{R_{11}} + k_{12}^{\tilde{t}} l_{11}^{\tilde{t}} Q'_{L_{11}} Q'_{R_{12}} \right) m_b m_{\tilde{\chi}_1^0} \\
 & + 2 \left(k_{11}^{\tilde{t}} k_{12}^{\tilde{t}} Q'_{L_{12}} Q'_{R_{11}} + l_{11}^{\tilde{t}} l_{12}^{\tilde{t}} Q'_{L_{11}} Q'_{R_{12}} \right) m_{\tilde{\chi}_1^0} m_{\tilde{\chi}_2^\pm} \\
 & + 2 \left(l_{11}^{\tilde{t}} l_{12}^{\tilde{t}} Q'_{L_{11}} Q'_{L_{12}} + k_{11}^{\tilde{t}} k_{12}^{\tilde{t}} Q'_{R_{11}} Q'_{R_{12}} \right) (2 m_b^2 + 2 m_{\tilde{\chi}_1^0}^2 + m_{H^\pm}^2 + m_{\tilde{t}_1}^2) \\
 & + 2 \left(k_{11}^{\tilde{t}} l_{12}^{\tilde{t}} Q'_{L_{11}} Q'_{L_{12}} + k_{12}^{\tilde{t}} l_{11}^{\tilde{t}} Q'_{R_{11}} Q'_{R_{12}} \right) m_b m_{\tilde{\chi}_1^\pm} \\
 & + 2 \left(k_{12}^{\tilde{t}} l_{11}^{\tilde{t}} Q'_{L_{11}} Q'_{L_{12}} + k_{11}^{\tilde{t}} l_{12}^{\tilde{t}} Q'_{R_{11}} Q'_{R_{12}} \right) m_b m_{\tilde{\chi}_2^\pm} \tag{A.66}
 \end{aligned}$$

$$da_{34} = -2 \left(l_{11}^{\tilde{t}} l_{12}^{\tilde{t}} Q'_{L_{11}} Q'_{L_{12}} + k_{11}^{\tilde{t}} k_{12}^{\tilde{t}} Q'_{R_{11}} Q'_{R_{12}} \right) \tag{A.67}$$

$$\begin{aligned}
 db_{11} = & \frac{\sqrt{2}}{m_W} \left\{ b_{11}^{\tilde{t}} k_{11}^{\tilde{t}} Q'_{L_{11}} m_{\tilde{\chi}_1^\pm} m_b m_t \left[(m_{\tilde{t}_1}^2 - m_{\tilde{\chi}_1^0}^2) \cot \beta - (m_b^2 + m_{\tilde{\chi}_1^0}^2) \tan \beta \right] \right. \\
 & + b_{11}^{\tilde{t}} l_{11}^{\tilde{t}} Q'_{L_{11}} m_t \left[(m_{H^\pm}^2 m_{\tilde{t}_1}^2 - m_b^2 m_{\tilde{\chi}_1^0}^2) \cot \beta - m_b^2 (m_b^2 + m_{\tilde{t}_1}^2 + 2 m_{\tilde{\chi}_1^0}^2) \tan \beta \right] \\
 & + a_{11}^{\tilde{t}} l_{11}^{\tilde{t}} Q'_{L_{11}} m_{\tilde{\chi}_1^0} \\
 & \quad * \left[m_b^2 (m_{H^\pm}^2 + m_{\tilde{t}_1}^2 - m_{\tilde{\chi}_1^0}^2 - m_b^2) \tan \beta - m_t^2 (2 m_b^2 + m_{\tilde{\chi}_1^0}^2 + m_{H^\pm}^2) \cot \beta \right] \\
 & + a_{11}^{\tilde{t}} k_{11}^{\tilde{t}} Q'_{L_{11}} m_{\tilde{\chi}_1^\pm} m_b m_{\tilde{\chi}_1^0} \left[(m_{H^\pm}^2 - m_b^2) \tan \beta - 2 m_t^2 \cot \beta \right] \\
 & + b_{11}^{\tilde{t}} k_{11}^{\tilde{t}} Q'_{R_{11}} m_{\tilde{\chi}_1^0} m_b m_t \\
 & \quad * \left[(m_{\tilde{t}_1}^2 + m_{H^\pm}^2 - m_b^2 - m_{\tilde{\chi}_1^0}^2) \cot \beta - (m_{H^\pm}^2 + 2 m_b^2 + m_{\tilde{\chi}_1^0}^2) \tan \beta \right] \\
 & + b_{11}^{\tilde{t}} l_{11}^{\tilde{t}} Q'_{R_{11}} m_t m_{\tilde{\chi}_1^0} m_{\tilde{\chi}_1^\pm} \left[(m_{H^\pm}^2 - m_b^2) \cot \beta - 2 m_b^2 \tan \beta \right] \\
 & - a_{11}^{\tilde{t}} k_{11}^{\tilde{t}} Q'_{R_{11}} m_b \\
 & \quad \left[(m_b^2 m_{\tilde{\chi}_1^0}^2 - m_{\tilde{t}_1}^2 m_{H^\pm}^2) \tan \beta + m_t^2 (m_b^2 + m_{\tilde{t}_1}^2 + 2 m_{\tilde{\chi}_1^0}^2) \cot \beta \right] \\
 & \left. - a_{11}^{\tilde{t}} l_{11}^{\tilde{t}} Q'_{R_{11}} m_{\tilde{\chi}_1^\pm} \left[m_b^2 (m_{\tilde{\chi}_1^0}^2 - m_{\tilde{t}_1}^2) \tan \beta + m_t^2 (m_b^2 + m_{\tilde{\chi}_1^0}^2) \cot \beta \right] \right\} \tag{A.68}
 \end{aligned}$$

$$\begin{aligned}
db_{12} = & \frac{\sqrt{2}}{m_W} \left\{ b_{11}^{\tilde{t}} k_{11}^{\tilde{t}} Q'_{L_{11}} m_{\tilde{\chi}_1^\pm} m_b m_t \tan \beta + b_{11}^{\tilde{t}} l_{11}^{\tilde{t}} Q'_{L_{11}} m_b^2 m_t \tan \beta \right. \\
& + a_{11}^{\tilde{t}} l_{11}^{\tilde{t}} Q'_{L_{11}} m_t^2 m_{\tilde{\chi}_1^0} \cot \beta + b_{11}^{\tilde{t}} k_{11}^{\tilde{t}} Q'_{R_{11}} m_{\tilde{\chi}_1^0} m_b m_t \tan \beta \\
& \left. + a_{11}^{\tilde{t}} l_{11}^{\tilde{t}} Q'_{R_{11}} m_{\tilde{\chi}_1^\pm} m_t^2 \cot \beta + a_{11}^{\tilde{t}} k_{11}^{\tilde{t}} Q'_{R_{11}} m_b m_t^2 \cot \beta \right\} \quad (\text{A.69})
\end{aligned}$$

$$\begin{aligned}
db_{13} = & -\frac{\sqrt{2}}{m_W} \left\{ b_{11}^{\tilde{t}} k_{11}^{\tilde{t}} Q'_{L_{11}} m_{\tilde{\chi}_1^\pm} m_b m_t \cot \beta - a_{11}^{\tilde{t}} l_{11}^{\tilde{t}} Q'_{L_{11}} m_t^2 m_{\tilde{\chi}_1^0} \cot \beta \right. \\
& + b_{11}^{\tilde{t}} l_{11}^{\tilde{t}} Q'_{L_{11}} m_t \left[(m_{\tilde{\chi}_1^0}^2 + m_{H^\pm}^2 + m_{t_1}^2 + m_b^2) \cot \beta - m_b^2 \tan \beta \right] \\
& + a_{11}^{\tilde{t}} k_{11}^{\tilde{t}} Q'_{L_{11}} m_{\tilde{\chi}_1^\pm} m_b m_{\tilde{\chi}_1^0} \tan \beta - b_{11}^{\tilde{t}} k_{11}^{\tilde{t}} Q'_{R_{11}} m_{\tilde{\chi}_1^0} m_b m_t \tan \beta \\
& + b_{11}^{\tilde{t}} l_{11}^{\tilde{t}} Q'_{R_{11}} m_{\tilde{\chi}_1^\pm} m_t m_{\tilde{\chi}_1^0} \cot \beta + a_{11}^{\tilde{t}} l_{11}^{\tilde{t}} Q'_{R_{11}} m_b^2 m_{\tilde{\chi}_1^\pm} \tan \beta \\
& \left. + a_{11}^{\tilde{t}} k_{11}^{\tilde{t}} Q'_{R_{11}} m_b \left[(m_b^2 + m_{\tilde{\chi}_1^0}^2 + m_{H^\pm}^2 + m_{t_1}^2) \tan \beta - m_t^2 \cot \beta \right] \right\} \quad (\text{A.70})
\end{aligned}$$

$$db_{14} = \frac{\sqrt{2}}{m_W} \left(b_{11}^{\tilde{t}} l_{11}^{\tilde{t}} Q'_{L_{11}} m_t \cot \beta + a_{11}^{\tilde{t}} k_{11}^{\tilde{t}} Q'_{R_{11}} m_b \tan \beta \right) \quad (\text{A.71})$$

$$\begin{aligned}
dc_{111} = & 2 C_{\tilde{t}_1 \tilde{b}_1}^H \left\{ \left(b_{11}^{\tilde{b}} l_{11}^{\tilde{t}} Q'_{L_{11}} + a_{11}^{\tilde{b}} k_{11}^{\tilde{t}} Q'_{R_{11}} \right) m_b (m_b^2 + m_{t_1}^2 + 2 m_{\tilde{\chi}_1^0}^2) \right. \\
& + \left(a_{11}^{\tilde{b}} l_{11}^{\tilde{t}} Q'_{L_{11}} + b_{11}^{\tilde{b}} k_{11}^{\tilde{t}} Q'_{R_{11}} \right) m_{\tilde{\chi}_1^0} (m_{\tilde{\chi}_1^0}^2 + m_{H^\pm}^2 + 2 m_b^2) \\
& + \left(b_{11}^{\tilde{b}} k_{11}^{\tilde{t}} Q'_{L_{11}} + a_{11}^{\tilde{b}} l_{11}^{\tilde{t}} Q'_{R_{11}} \right) m_{\tilde{\chi}_1^\pm} (m_b^2 + m_{\tilde{\chi}_1^0}^2) \\
& \left. + \left(a_{11}^{\tilde{b}} k_{11}^{\tilde{t}} Q'_{L_{11}} + b_{11}^{\tilde{b}} l_{11}^{\tilde{t}} Q'_{R_{11}} \right) 2 m_b m_{\tilde{\chi}_1^0} m_{\tilde{\chi}_1^\pm} \right\} \quad (\text{A.72})
\end{aligned}$$

$$\begin{aligned}
dc_{112} = & -2 C_{\tilde{t}_1 \tilde{b}_1}^H \left\{ \left(b_{11}^{\tilde{b}} l_{11}^{\tilde{t}} Q'_{L_{11}} + a_{11}^{\tilde{b}} k_{11}^{\tilde{t}} Q'_{R_{11}} \right) m_b \right. \\
& + \left(a_{11}^{\tilde{b}} l_{11}^{\tilde{t}} Q'_{L_{11}} + b_{11}^{\tilde{b}} k_{11}^{\tilde{t}} Q'_{R_{11}} \right) m_{\tilde{\chi}_1^0} \\
& \left. + \left(b_{11}^{\tilde{b}} k_{11}^{\tilde{t}} Q'_{L_{11}} + a_{11}^{\tilde{b}} l_{11}^{\tilde{t}} Q'_{R_{11}} \right) m_{\tilde{\chi}_1^\pm} \right\} \quad (\text{A.73})
\end{aligned}$$

$$\begin{aligned}
dc_{113} = & -2 C_{\tilde{t}_1 \tilde{b}_1}^H \left\{ \left(b_{11}^{\tilde{b}} l_{11}^{\tilde{t}} Q'_{L_{11}} + a_{11}^{\tilde{b}} k_{11}^{\tilde{t}} Q'_{R_{11}} \right) m_b \right. \\
& \left. + \left(a_{11}^{\tilde{b}} l_{11}^{\tilde{t}} Q'_{L_{11}} + b_{11}^{\tilde{b}} k_{11}^{\tilde{t}} Q'_{R_{11}} \right) m_{\tilde{\chi}_1^0} \right\} \quad (\text{A.74})
\end{aligned}$$

$$\begin{aligned}
dd_1 = & \frac{1}{2m_W^2} \left\{ - \left((a_{11}^{\tilde{t}})^2 m_t^2 \cot^2 \beta + (b_{11}^{\tilde{t}})^2 m_b^2 \tan^2 \beta \right) m_t^2 (m_b^2 + m_{\tilde{\chi}_1^0}^2) \right. \\
& + \left((a_{11}^{\tilde{t}})^2 m_b^2 \tan^2 \beta + (b_{11}^{\tilde{t}})^2 m_t^2 \cot^2 \beta \right) (m_{\tilde{\chi}_1^0}^2 - m_{\tilde{t}_1}^2) (m_{H^\pm}^2 - m_b^2) \\
& + 2 a_{11}^{\tilde{t}} b_{11}^{\tilde{t}} m_t m_{\tilde{\chi}_1^0} \left[(m_{H^\pm}^2 - m_b^2) (m_b^2 \tan^2 \beta + m_t^2 \cot^2 \beta) - 2 m_b^2 m_t^2 \right] \\
& \left. + 2 \left((a_{11}^{\tilde{t}})^2 + (b_{11}^{\tilde{t}})^2 \right) m_b^2 m_t^2 (m_{\tilde{t}_1}^2 - m_{\tilde{\chi}_1^0}^2) \right\} \quad (\text{A.75})
\end{aligned}$$

$$dd_2 = \frac{m_t^2}{2m_W^2} \left((a_{11}^{\tilde{t}})^2 m_t^2 \cot^2 \beta + (b_{11}^{\tilde{t}})^2 m_b^2 \tan^2 \beta \right) \quad (\text{A.76})$$

$$\begin{aligned}
dd_3 = & -\frac{1}{2m_W^2} \left\{ 2 \left((a_{11}^{\tilde{t}})^2 + (b_{11}^{\tilde{t}})^2 \right) m_b^2 m_t^2 \right. \\
& - \left((a_{11}^{\tilde{t}})^2 m_b^2 \tan^2 \beta + (b_{11}^{\tilde{t}})^2 m_t^2 \cot^2 \beta \right) (m_{H^\pm}^2 + m_{\tilde{t}_1}^2) \\
& \left. + 2 a_{11}^{\tilde{t}} b_{11}^{\tilde{t}} m_t m_{\tilde{\chi}_1^0} \left(m_b^2 (2 + \tan^2 \beta) + m_t^2 \cot^2 \beta \right) \right\} \quad (\text{A.77})
\end{aligned}$$

$$dd_4 = -\frac{(a_{11}^{\tilde{t}})^2 m_b^2 \tan^2 \beta + (b_{11}^{\tilde{t}})^2 m_t^2 \cot^2 \beta}{2m_W^2} \quad (\text{A.78})$$

$$\begin{aligned}
de_{11} = & -\frac{\sqrt{2} C_{\tilde{t}_1 \tilde{b}_1}^H}{m_W} \left\{ a_{11}^{\tilde{b}} b_{11}^{\tilde{t}} m_t m_{\tilde{\chi}_1^0} \left[(m_{H^\pm}^2 - m_b^2) \cot \beta - 2 m_b^2 \tan \beta \right] \right. \\
& + b_{11}^{\tilde{b}} b_{11}^{\tilde{t}} m_b m_t \left[(m_{\tilde{t}_1}^2 - m_{\tilde{\chi}_1^0}^2) \cot \beta - (m_b^2 + m_{\tilde{\chi}_1^0}^2) \tan \beta \right] \\
& - a_{11}^{\tilde{b}} a_{11}^{\tilde{t}} \left[m_t^2 (m_b^2 + m_{\tilde{\chi}_1^0}^2) \cot \beta + m_b^2 (m_{\tilde{\chi}_1^0}^2 - m_{\tilde{t}_1}^2) \tan \beta \right] \\
& \left. - b_{11}^{\tilde{b}} a_{11}^{\tilde{t}} m_b m_{\tilde{\chi}_1^0} \left[2 m_t^2 \cot \beta + (m_b^2 - m_{H^\pm}^2) \tan \beta \right] \right\} \quad (\text{A.79})
\end{aligned}$$

$$de_{12} = -\frac{\sqrt{2} C_{\tilde{t}_1 \tilde{b}_1}^H}{m_W} \left\{ a_{11}^{\tilde{b}} a_{11}^{\tilde{t}} m_t^2 \cot \beta + b_{11}^{\tilde{b}} b_{11}^{\tilde{t}} m_b m_t \tan \beta \right\} \quad (\text{A.80})$$

$$\begin{aligned}
de_{13} = & \frac{\sqrt{2} C_{\tilde{t}_1 \tilde{b}_1}^H}{m_W} \left\{ a_{11}^{\tilde{b}} b_{11}^{\tilde{t}} m_t m_{\tilde{\chi}_1^0} \cot \beta + b_{11}^{\tilde{b}} b_{11}^{\tilde{t}} m_b m_t \cot \beta \right. \\
& \left. + a_{11}^{\tilde{b}} a_{11}^{\tilde{t}} m_b^2 \tan \beta + b_{11}^{\tilde{b}} a_{11}^{\tilde{t}} m_b m_{\tilde{\chi}_1^0} \tan \beta \right\} \quad (\text{A.81})
\end{aligned}$$

$$df_{11} = -(C_{\tilde{t}_1 \tilde{b}_1}^H)^2 \left[\left((a_{11}^{\tilde{b}})^2 + (b_{11}^{\tilde{b}})^2 \right) (m_b^2 + m_{\tilde{\chi}_1^0}^2) + 4 a_{11}^{\tilde{b}} b_{11}^{\tilde{b}} m_b m_{\tilde{\chi}_1^0} \right] \quad (\text{A.82})$$

$$df_{12} = (C_{\tilde{t}_1 \tilde{b}_1}^H)^2 \left((a_{11}^{\tilde{b}})^2 + (b_{11}^{\tilde{b}})^2 \right) \quad (\text{A.83})$$

$$df_{31} = -2 C_{\tilde{t}_1 \tilde{b}_1}^H C_{\tilde{t}_1 \tilde{b}_2}^H \left[\left(a_{11}^{\tilde{b}} a_{12}^{\tilde{b}} + b_{11}^{\tilde{b}} b_{12}^{\tilde{b}} \right) \left(m_b^2 + m_{\tilde{\chi}_1^0}^2 \right) + 2 \left(a_{11}^{\tilde{b}} b_{12}^{\tilde{b}} + b_{11}^{\tilde{b}} a_{12}^{\tilde{b}} \right) m_b m_{\tilde{\chi}_1^0} \right] \quad (\text{A.84})$$

$$df_{32} = 2 C_{\tilde{t}_1 \tilde{b}_1}^H C_{\tilde{t}_1 \tilde{b}_2}^H \left(a_{11}^{\tilde{b}} a_{12}^{\tilde{b}} + b_{11}^{\tilde{b}} b_{12}^{\tilde{b}} \right) \quad (\text{A.85})$$

To get the remaining coefficients one has to make the following replacements:

$$\begin{aligned} da_{1i} \rightarrow da_{2i}: & \quad \tilde{l}_{11}^{\tilde{t}} \rightarrow \tilde{l}_{12}^{\tilde{t}}, \quad \tilde{k}_{11}^{\tilde{t}} \rightarrow \tilde{k}_{12}^{\tilde{t}}, \quad Q'_{L11} \rightarrow Q'_{L12}, \quad Q'_{R11} \rightarrow Q'_{R12}, \quad m_{\tilde{\chi}_1^+} \rightarrow m_{\tilde{\chi}_2^+} \\ db_{1i} \rightarrow db_{2i}: & \quad \tilde{l}_{11}^{\tilde{t}} \rightarrow \tilde{l}_{12}^{\tilde{t}}, \quad \tilde{k}_{11}^{\tilde{t}} \rightarrow \tilde{k}_{12}^{\tilde{t}}, \quad Q'_{L11} \rightarrow Q'_{L12}, \quad Q'_{R11} \rightarrow Q'_{R12}, \quad m_{\tilde{\chi}_1^+} \rightarrow m_{\tilde{\chi}_2^+} \\ dc_{11i} \rightarrow dc_{12i}: & \quad \tilde{l}_{11}^{\tilde{t}} \rightarrow \tilde{l}_{12}^{\tilde{t}}, \quad \tilde{k}_{11}^{\tilde{t}} \rightarrow \tilde{k}_{12}^{\tilde{t}}, \quad Q'_{L11} \rightarrow Q'_{L12}, \quad Q'_{R11} \rightarrow Q'_{R12}, \quad m_{\tilde{\chi}_1^+} \rightarrow m_{\tilde{\chi}_2^+} \\ dc_{11i} \rightarrow dc_{21i}: & \quad a_{11}^{\tilde{b}} \rightarrow a_{12}^{\tilde{b}}, \quad b_{11}^{\tilde{b}} \rightarrow b_{12}^{\tilde{b}}, \quad m_{\tilde{b}_1} \rightarrow m_{\tilde{b}_2}, \quad C_{\tilde{t}_1 \tilde{b}_1}^H \rightarrow C_{\tilde{t}_1 \tilde{b}_2}^H \\ dc_{11i} \rightarrow dc_{22i}: & \quad \tilde{l}_{11}^{\tilde{t}} \rightarrow \tilde{l}_{12}^{\tilde{t}}, \quad \tilde{k}_{11}^{\tilde{t}} \rightarrow \tilde{k}_{12}^{\tilde{t}}, \quad Q'_{L11} \rightarrow Q'_{L12}, \quad Q'_{R11} \rightarrow Q'_{R12}, \quad m_{\tilde{\chi}_1^+} \rightarrow m_{\tilde{\chi}_2^+}, \\ & \quad a_{11}^{\tilde{b}} \rightarrow a_{12}^{\tilde{b}}, \quad b_{11}^{\tilde{b}} \rightarrow b_{12}^{\tilde{b}}, \quad m_{\tilde{b}_1} \rightarrow m_{\tilde{b}_2}, \quad C_{\tilde{t}_1 \tilde{b}_1}^H \rightarrow C_{\tilde{t}_1 \tilde{b}_2}^H \\ de_{1i} \rightarrow de_{2i}: & \quad a_{11}^{\tilde{b}} \rightarrow a_{12}^{\tilde{b}}, \quad b_{11}^{\tilde{b}} \rightarrow b_{12}^{\tilde{b}}, \quad m_{\tilde{b}_1} \rightarrow m_{\tilde{b}_2}, \quad C_{\tilde{t}_1 \tilde{b}_1}^H \rightarrow C_{\tilde{t}_1 \tilde{b}_2}^H \\ df_{1i} \rightarrow df_{2i}: & \quad a_{11}^{\tilde{b}} \rightarrow a_{12}^{\tilde{b}}, \quad b_{11}^{\tilde{b}} \rightarrow b_{12}^{\tilde{b}}, \quad m_{\tilde{b}_1} \rightarrow m_{\tilde{b}_2}, \quad C_{\tilde{t}_1 \tilde{b}_1}^H \rightarrow C_{\tilde{t}_1 \tilde{b}_2}^H \end{aligned}$$

A.3 The Decay of the Light Stop into a Bottom Quark, a Slepton and a Lepton

Here the decay width is given by

$$\begin{aligned} \Gamma(\tilde{t}_1 \rightarrow b + \tilde{l} + l') &= \\ &= \frac{\alpha^2}{16 \pi m_{\tilde{t}_1}^3 \sin^4 \theta_W} \int_{(m_{l'} + m_{\tilde{l}})^2}^{(m_{\tilde{t}_1} - m_b)^2} ds \, W_{l'\tilde{l}}(s) \sum_{i=1}^3 \left(\sum_{j=1}^5 c_{ij} s^{(j-4)} \right) D_i(s) \end{aligned} \quad (\text{A.86})$$

with

$$D_{1,2}(s) = \frac{1}{(s - m_{\tilde{\chi}_{1,2}^\pm}^2)^2 + m_{\tilde{\chi}_{1,2}^\pm}^2 \Gamma_{\tilde{\chi}_{1,2}^\pm}^2} \quad (\text{A.87})$$

$$D_3(s) = \text{Re} \left(\frac{1}{(s - m_{\tilde{\chi}_1^\pm}^2 + i m_{\tilde{\chi}_1^\pm} \Gamma_{\tilde{\chi}_1^\pm})(s - m_{\tilde{\chi}_2^\pm}^2 - i m_{\tilde{\chi}_2^\pm} \Gamma_{\tilde{\chi}_2^\pm})} \right). \quad (\text{A.88})$$

In the case of $\tilde{t}_1 \rightarrow b + \tilde{\nu}_e + e^-$ one finds in the limit $m_e \rightarrow 0$ that

$$W_{e\tilde{\nu}_e}(s) = \lambda^{\frac{1}{2}}(s, m_{\tilde{t}_1}^2, m_b^2) (s - m_{\tilde{\nu}_e}^2) \quad (\text{A.89})$$

$$c_{11} = \frac{1}{2} (k_{11}^{\tilde{t}})^2 V_{11}^2 m_{\tilde{\chi}_1^\pm}^2 m_{\tilde{\nu}_e}^2 (m_b^2 - m_{\tilde{t}_1}^2) \quad (\text{A.90})$$

$$c_{12} = V_{11}^2 \left[\frac{1}{2} (l_{11}^{\tilde{t}})^2 m_{\tilde{\nu}_e}^2 (m_b^2 - m_{\tilde{t}_1}^2) + \frac{1}{2} (k_{11}^{\tilde{t}})^2 m_{\tilde{\chi}_1^\pm}^2 (m_{\tilde{t}_1}^2 + m_{\tilde{\nu}_e}^2 - m_b^2) + 2 k_{11}^{\tilde{t}} l_{11}^{\tilde{t}} m_b m_{\tilde{\chi}_1^\pm} m_{\tilde{\nu}_e}^2 \right] \quad (\text{A.91})$$

$$c_{13} = V_{11}^2 \left[\frac{1}{2} (l_{11}^{\tilde{t}})^2 (m_{\tilde{t}_1}^2 + m_{\tilde{\nu}_e}^2 - m_b^2) - 2 k_{11}^{\tilde{t}} l_{11}^{\tilde{t}} m_b m_{\tilde{\chi}_1^\pm} - \frac{1}{2} (k_{11}^{\tilde{t}})^2 m_{\tilde{\chi}_1^\pm}^2 \right] \quad (\text{A.92})$$

$$c_{14} = -\frac{(l_{11}^{\tilde{t}})^2 V_{11}^2}{2} \quad (\text{A.93})$$

c_{2i} is obtained from c_{1i} by the following replacements: $k_{11}^{\tilde{t}} \rightarrow k_{12}^{\tilde{t}}$, $l_{11}^{\tilde{t}} \rightarrow l_{12}^{\tilde{t}}$, $V_{11} \rightarrow V_{12}$ and $m_{\tilde{\chi}_1^\pm} \rightarrow m_{\tilde{\chi}_2^\pm}$.

$$c_{31} = k_{11}^{\tilde{t}} k_{12}^{\tilde{t}} V_{11} V_{12} m_{\tilde{\chi}_1^\pm} m_{\tilde{\chi}_2^\pm} (m_b^2 - m_{\tilde{t}_1}^2) m_{\tilde{\nu}_e}^2 \quad (\text{A.94})$$

$$c_{32} = V_{11} V_{12} \left[l_{11}^{\tilde{t}} l_{12}^{\tilde{t}} m_{\tilde{\nu}_e}^2 (m_b^2 - m_{\tilde{t}_1}^2) + k_{11}^{\tilde{t}} k_{12}^{\tilde{t}} m_{\tilde{\chi}_1^\pm} m_{\tilde{\chi}_2^\pm} (m_{\tilde{t}_1}^2 + m_{\tilde{\nu}_e}^2 - m_b^2) + 2 k_{11}^{\tilde{t}} l_{12}^{\tilde{t}} m_b m_{\tilde{\chi}_1^\pm} m_{\tilde{\nu}_e}^2 + 2 k_{12}^{\tilde{t}} l_{11}^{\tilde{t}} m_b m_{\tilde{\chi}_2^\pm} m_{\tilde{\nu}_e}^2 \right] \quad (\text{A.95})$$

$$c_{33} = V_{11} V_{12} \left[l_{11}^{\tilde{t}} l_{12}^{\tilde{t}} (m_{\tilde{t}_1}^2 + m_{\tilde{\nu}_e}^2 - m_b^2) - 2 k_{11}^{\tilde{t}} l_{12}^{\tilde{t}} m_b m_{\tilde{\chi}_1^\pm} - 2 k_{12}^{\tilde{t}} l_{11}^{\tilde{t}} m_b m_{\tilde{\chi}_2^\pm} - k_{11}^{\tilde{t}} k_{12}^{\tilde{t}} m_{\tilde{\chi}_1^\pm} m_{\tilde{\chi}_2^\pm} \right] \quad (\text{A.96})$$

$$c_{34} = -l_{11}^{\tilde{t}} l_{12}^{\tilde{t}} V_{11} V_{12} \quad (\text{A.97})$$

$$c_{15} = c_{25} = c_{35} = 0 \quad (\text{A.98})$$

In the case of $\tilde{t}_1 \rightarrow b + \tilde{\nu}_\tau + \tau^-$ one finds that

$$W_{\tau\tilde{\nu}_\tau}(s) = \lambda^{\frac{1}{2}}(s, m_{\tilde{t}_1}^2, m_b^2) \lambda^{\frac{1}{2}}(s, m_{\tilde{\nu}_\tau}^2, m_\tau^2) \quad (\text{A.99})$$

$$c_{11} = \frac{1}{2} \left((k_1^{\tilde{\nu}_\tau})^2 (l_{11}^{\tilde{t}})^2 + (l_1^{\tilde{\nu}_\tau})^2 (k_{11}^{\tilde{t}})^2 \right) m_{\tilde{\chi}_1^\pm}^2 (m_b^2 - m_{\tilde{t}_1}^2) (m_{\tilde{\nu}_\tau}^2 - m_\tau^2) \quad (\text{A.100})$$

$$c_{12} = \left[\frac{1}{2} \left((k_1^{\tilde{\nu}_\tau})^2 (k_{11}^{\tilde{t}})^2 + (l_1^{\tilde{\nu}_\tau})^2 (l_{11}^{\tilde{t}})^2 \right) (m_{\tilde{t}_1}^2 - m_b^2) (m_\tau^2 - m_{\tilde{\nu}_\tau}^2) + \frac{1}{2} \left((k_1^{\tilde{\nu}_\tau})^2 (l_{11}^{\tilde{t}})^2 + (l_1^{\tilde{\nu}_\tau})^2 (k_{11}^{\tilde{t}})^2 \right) m_{\tilde{\chi}_1^\pm}^2 (m_{\tilde{t}_1}^2 + m_{\tilde{\nu}_\tau}^2 - m_b^2 - m_\tau^2) + 2 k_1^{\tilde{\nu}_\tau} l_1^{\tilde{\nu}_\tau} \left((k_{11}^{\tilde{t}})^2 + (l_{11}^{\tilde{t}})^2 \right) m_\tau m_{\tilde{\chi}_1^\pm} (m_{\tilde{t}_1}^2 - m_b^2) + 2 k_{11}^{\tilde{t}} l_{11}^{\tilde{t}} \left((k_1^{\tilde{\nu}_\tau})^2 + (l_1^{\tilde{\nu}_\tau})^2 \right) m_b m_{\tilde{\chi}_1^\pm} (m_{\tilde{\nu}_\tau}^2 - m_\tau^2) - 4 k_1^{\tilde{\nu}_\tau} l_1^{\tilde{\nu}_\tau} k_{11}^{\tilde{t}} l_{11}^{\tilde{t}} m_b m_\tau m_{\tilde{\chi}_1^\pm}^2 \right] \quad (\text{A.101})$$

$$\begin{aligned}
 c_{13} = & \left[\frac{1}{2} \left((k_1^{\tilde{\nu}_\tau})^2 (k_{11}^{\tilde{t}})^2 + (l_1^{\tilde{\nu}_\tau})^2 (l_{11}^{\tilde{t}})^2 \right) (m_{\tilde{t}_1}^2 + m_{\tilde{\nu}_\tau}^2 - m_b^2 - m_\tau^2) \right. \\
 & - 2 k_{11}^{\tilde{t}} l_{11}^{\tilde{t}} \left((k_1^{\tilde{\nu}_\tau})^2 + (l_1^{\tilde{\nu}_\tau})^2 \right) m_b m_{\tilde{\chi}_1^\pm} \\
 & - \frac{1}{2} \left((k_1^{\tilde{\nu}_\tau})^2 (l_{11}^{\tilde{t}})^2 + (l_1^{\tilde{\nu}_\tau})^2 (k_{11}^{\tilde{t}})^2 \right) m_{\tilde{\chi}_1^\pm}^2 \\
 & \left. - 4 k_1^{\tilde{\nu}_\tau} l_1^{\tilde{\nu}_\tau} k_{11}^{\tilde{t}} l_{11}^{\tilde{t}} m_b m_\tau - 2 k_1^{\tilde{\nu}_\tau} l_1^{\tilde{\nu}_\tau} \left((k_{11}^{\tilde{t}})^2 + (l_{11}^{\tilde{t}})^2 \right) m_\tau m_{\tilde{\chi}_1^\pm} \right] \quad (\text{A.102})
 \end{aligned}$$

$$c_{14} = -\frac{1}{2} \left((k_1^{\tilde{\nu}_\tau})^2 (k_{11}^{\tilde{t}})^2 + (l_1^{\tilde{\nu}_\tau})^2 (l_{11}^{\tilde{t}})^2 \right) \quad (\text{A.103})$$

c_{2i} is obtained from c_{1i} by the following replacements: $k_{11}^{\tilde{t}} \rightarrow k_{12}^{\tilde{t}}, l_{11}^{\tilde{t}} \rightarrow l_{12}^{\tilde{t}}, k_1^{\tilde{\nu}_\tau} \rightarrow k_2^{\tilde{\nu}_\tau}, l_1^{\tilde{\nu}_\tau} \rightarrow l_2^{\tilde{\nu}_\tau}$ and $m_{\tilde{\chi}_1^\pm} \rightarrow m_{\tilde{\chi}_2^\pm}$.

$$c_{31} = \left(k_1^{\tilde{\nu}_\tau} k_2^{\tilde{\nu}_\tau} l_{11}^{\tilde{t}} l_{12}^{\tilde{t}} + k_{11}^{\tilde{t}} k_{12}^{\tilde{t}} l_1^{\tilde{\nu}_\tau} l_2^{\tilde{\nu}_\tau} \right) m_{\tilde{\chi}_1^\pm} m_{\tilde{\chi}_2^\pm} (m_b^2 - m_{\tilde{t}_1}^2) (m_{\tilde{\nu}_\tau}^2 - m_\tau^2) \quad (\text{A.104})$$

$$\begin{aligned}
 c_{32} = & \left[\left(k_1^{\tilde{\nu}_\tau} k_2^{\tilde{\nu}_\tau} k_{11}^{\tilde{t}} k_{12}^{\tilde{t}} + l_1^{\tilde{\nu}_\tau} l_2^{\tilde{\nu}_\tau} l_{11}^{\tilde{t}} l_{12}^{\tilde{t}} \right) (m_{\tilde{t}_1}^2 - m_b^2) (m_\tau^2 - m_{\tilde{\nu}_\tau}^2) \right. \\
 & + \left(k_1^{\tilde{\nu}_\tau} k_2^{\tilde{\nu}_\tau} l_{11}^{\tilde{t}} l_{12}^{\tilde{t}} + k_{11}^{\tilde{t}} k_{12}^{\tilde{t}} l_1^{\tilde{\nu}_\tau} l_2^{\tilde{\nu}_\tau} \right) m_{\tilde{\chi}_1^\pm} m_{\tilde{\chi}_2^\pm} (m_{\tilde{t}_1}^2 + m_{\tilde{\nu}_\tau}^2 - m_b^2 - m_\tau^2) \\
 & + 2 \left(k_1^{\tilde{\nu}_\tau} l_2^{\tilde{\nu}_\tau} l_{11}^{\tilde{t}} l_{12}^{\tilde{t}} + k_2^{\tilde{\nu}_\tau} k_{11}^{\tilde{t}} k_{12}^{\tilde{t}} l_1^{\tilde{\nu}_\tau} \right) m_\tau m_{\tilde{\chi}_1^\pm} (m_{\tilde{t}_1}^2 - m_b^2) \\
 & + 2 \left(k_1^{\tilde{\nu}_\tau} k_{11}^{\tilde{t}} k_{12}^{\tilde{t}} l_2^{\tilde{\nu}_\tau} + k_2^{\tilde{\nu}_\tau} l_1^{\tilde{\nu}_\tau} l_{11}^{\tilde{t}} l_{12}^{\tilde{t}} \right) m_\tau m_{\tilde{\chi}_2^\pm} (m_{\tilde{t}_1}^2 - m_b^2) \\
 & + 2 \left(k_1^{\tilde{\nu}_\tau} k_2^{\tilde{\nu}_\tau} k_{12}^{\tilde{t}} l_{11}^{\tilde{t}} + k_{11}^{\tilde{t}} l_1^{\tilde{\nu}_\tau} l_2^{\tilde{\nu}_\tau} l_{12}^{\tilde{t}} \right) m_b m_{\tilde{\chi}_1^\pm} (m_{\tilde{\nu}_\tau}^2 - m_\tau^2) \\
 & + 2 \left(k_1^{\tilde{\nu}_\tau} k_2^{\tilde{\nu}_\tau} k_{11}^{\tilde{t}} l_{12}^{\tilde{t}} + k_{12}^{\tilde{t}} l_1^{\tilde{\nu}_\tau} l_2^{\tilde{\nu}_\tau} l_{11}^{\tilde{t}} \right) m_b m_{\tilde{\chi}_2^\pm} (m_{\tilde{\nu}_\tau}^2 - m_\tau^2) \\
 & \left. - 4 \left(k_1^{\tilde{\nu}_\tau} k_{12}^{\tilde{t}} l_2^{\tilde{\nu}_\tau} l_{11}^{\tilde{t}} + k_2^{\tilde{\nu}_\tau} k_{11}^{\tilde{t}} l_1^{\tilde{\nu}_\tau} l_{12}^{\tilde{t}} \right) m_b m_\tau m_{\tilde{\chi}_1^\pm} m_{\tilde{\chi}_2^\pm} \right] \quad (\text{A.105})
 \end{aligned}$$

$$\begin{aligned}
 c_{33} = & \left[\left(k_1^{\tilde{\nu}_\tau} k_2^{\tilde{\nu}_\tau} k_{11}^{\tilde{t}} k_{12}^{\tilde{t}} + l_1^{\tilde{\nu}_\tau} l_2^{\tilde{\nu}_\tau} l_{11}^{\tilde{t}} l_{12}^{\tilde{t}} \right) (m_{\tilde{t}_1}^2 + m_{\tilde{\nu}_\tau}^2 - m_b^2 - m_\tau^2) \right. \\
 & - 2 \left(k_1^{\tilde{\nu}_\tau} k_2^{\tilde{\nu}_\tau} k_{12}^{\tilde{t}} l_{11}^{\tilde{t}} + k_{11}^{\tilde{t}} l_1^{\tilde{\nu}_\tau} l_2^{\tilde{\nu}_\tau} l_{12}^{\tilde{t}} \right) m_b m_{\tilde{\chi}_1^\pm} \\
 & - 2 \left(k_1^{\tilde{\nu}_\tau} k_2^{\tilde{\nu}_\tau} k_{11}^{\tilde{t}} l_{12}^{\tilde{t}} + k_{12}^{\tilde{t}} l_1^{\tilde{\nu}_\tau} l_2^{\tilde{\nu}_\tau} l_{11}^{\tilde{t}} \right) m_b m_{\tilde{\chi}_2^\pm} \\
 & - \left(k_1^{\tilde{\nu}_\tau} k_2^{\tilde{\nu}_\tau} l_{11}^{\tilde{t}} l_{12}^{\tilde{t}} + k_{11}^{\tilde{t}} k_{12}^{\tilde{t}} l_1^{\tilde{\nu}_\tau} l_2^{\tilde{\nu}_\tau} \right) m_{\tilde{\chi}_1^\pm} m_{\tilde{\chi}_2^\pm} \\
 & - 4 \left(k_1^{\tilde{\nu}_\tau} k_{11}^{\tilde{t}} l_2^{\tilde{\nu}_\tau} l_{12}^{\tilde{t}} + k_2^{\tilde{\nu}_\tau} k_{12}^{\tilde{t}} l_1^{\tilde{\nu}_\tau} l_{11}^{\tilde{t}} \right) m_b m_\tau \\
 & - 2 \left(k_1^{\tilde{\nu}_\tau} l_2^{\tilde{\nu}_\tau} l_{11}^{\tilde{t}} l_{12}^{\tilde{t}} + k_2^{\tilde{\nu}_\tau} k_{11}^{\tilde{t}} k_{12}^{\tilde{t}} l_1^{\tilde{\nu}_\tau} \right) m_\tau m_{\tilde{\chi}_1^\pm} \\
 & \left. - 2 \left(k_1^{\tilde{\nu}_\tau} k_{11}^{\tilde{t}} k_{12}^{\tilde{t}} l_2^{\tilde{\nu}_\tau} + k_2^{\tilde{\nu}_\tau} l_1^{\tilde{\nu}_\tau} l_{11}^{\tilde{t}} l_{12}^{\tilde{t}} \right) m_\tau m_{\tilde{\chi}_2^\pm} \right] \quad (\text{A.106})
 \end{aligned}$$

$$c_{34} = - \left(k_1^{\tilde{\nu}_\tau} k_2^{\tilde{\nu}_\tau} k_{11}^{\tilde{t}} k_{12}^{\tilde{t}} + l_1^{\tilde{\nu}_\tau} l_2^{\tilde{\nu}_\tau} l_{11}^{\tilde{t}} l_{12}^{\tilde{t}} \right) \quad (\text{A.107})$$

$$c_{15} = c_{25} = c_{35} = 0 \quad (\text{A.108})$$

In the case of $\tilde{t}_1 \rightarrow b + \tilde{\tau}_1 + \nu_\tau$ one finds that

$$W_{\nu_\tau \tilde{\tau}_1}(s) = \lambda^{\frac{1}{2}}(s, m_{\tilde{t}_1}^2, m_b^2) \quad (\text{A.109})$$

$$c_{11} = \frac{1}{2}(l_{11}^{\tilde{\tau}})^2(l_{11}^{\tilde{t}})^2 m_{\tilde{\chi}_1^\pm}^2 m_{\tilde{\tau}_1}^4 (m_{\tilde{t}_1}^2 - m_b^2) \quad (\text{A.110})$$

$$c_{12} = (l_{11}^{\tilde{\tau}})^2 \left[(l_{11}^{\tilde{t}})^2 m_{\tilde{\tau}_1}^2 m_{\tilde{\chi}_1^\pm}^2 (m_b^2 - m_{\tilde{t}_1}^2 - \frac{1}{2}m_{\tilde{\tau}_1}^2) + \frac{1}{2}(k_{11}^{\tilde{t}})^2 m_{\tilde{\tau}_1}^4 (m_{\tilde{t}_1}^2 - m_b^2) - 2k_{11}^{\tilde{t}} l_{11}^{\tilde{t}} m_b m_{\tilde{\chi}_1^\pm} m_{\tilde{\tau}_1}^4 \right] \quad (\text{A.111})$$

$$c_{13} = (l_{11}^{\tilde{\tau}})^2 \left[\frac{1}{2}(l_{11}^{\tilde{t}})^2 m_{\tilde{\chi}_1^\pm}^2 (m_{\tilde{t}_1}^2 + 2m_{\tilde{\tau}_1}^2 - m_b^2) + 4k_{11}^{\tilde{t}} l_{11}^{\tilde{t}} m_b m_{\tilde{\chi}_1^\pm} m_{\tilde{\tau}_1}^2 + (k_{11}^{\tilde{t}})^2 m_{\tilde{\tau}_1}^2 (m_b^2 - m_{\tilde{t}_1}^2 - \frac{1}{2}m_{\tilde{\tau}_1}^2) \right] \quad (\text{A.112})$$

$$c_{14} = (l_{11}^{\tilde{\tau}})^2 \left[\frac{1}{2}(k_{11}^{\tilde{t}})^2 (2m_{\tilde{\tau}_1}^2 + m_{\tilde{t}_1}^2 - m_b^2) - \frac{1}{2}(l_{11}^{\tilde{t}})^2 m_{\tilde{\chi}_1^\pm}^2 - 2k_{11}^{\tilde{t}} l_{11}^{\tilde{t}} m_b m_{\tilde{\chi}_1^\pm} \right] \quad (\text{A.113})$$

$$c_{15} = -\frac{1}{2}(l_{11}^{\tilde{\tau}})^2 (k_{11}^{\tilde{t}})^2 \quad (\text{A.114})$$

c_{2i} are obtained from c_{1i} by the following replacements: $k_{11}^{\tilde{t}} \rightarrow k_{12}^{\tilde{t}}, l_{11}^{\tilde{t}} \rightarrow l_{12}^{\tilde{t}}, l_{11}^{\tilde{\tau}} \rightarrow l_{12}^{\tilde{\tau}}$ and $m_{\tilde{\chi}_1^\pm} \rightarrow m_{\tilde{\chi}_2^\pm}$.

$$c_{31} = l_{11}^{\tilde{\tau}} l_{12}^{\tilde{\tau}} l_{11}^{\tilde{t}} l_{12}^{\tilde{t}} m_{\tilde{\chi}_1^\pm} m_{\tilde{\chi}_2^\pm} m_{\tilde{\tau}_1}^4 (m_{\tilde{t}_1}^2 - m_b^2) \quad (\text{A.115})$$

$$c_{32} = l_{11}^{\tilde{\tau}} l_{12}^{\tilde{\tau}} \left[k_{11}^{\tilde{t}} k_{12}^{\tilde{t}} m_{\tilde{\tau}_1}^4 (m_{\tilde{t}_1}^2 - m_b^2) + 2l_{11}^{\tilde{t}} l_{12}^{\tilde{t}} m_{\tilde{\chi}_1^\pm} m_{\tilde{\chi}_2^\pm} m_{\tilde{\tau}_1}^2 (m_b^2 - \frac{1}{2}m_{\tilde{\tau}_1}^2 - m_{\tilde{t}_1}^2) - 2l_{11}^{\tilde{t}} k_{12}^{\tilde{t}} m_b m_{\tilde{\chi}_1^\pm} m_{\tilde{\tau}_1}^4 - 2l_{12}^{\tilde{t}} k_{11}^{\tilde{t}} m_b m_{\tilde{\chi}_2^\pm} m_{\tilde{\tau}_1}^4 \right] \quad (\text{A.116})$$

$$c_{33} = l_{11}^{\tilde{\tau}} l_{12}^{\tilde{\tau}} \left[l_{11}^{\tilde{t}} l_{12}^{\tilde{t}} m_{\tilde{\chi}_1^\pm} m_{\tilde{\chi}_2^\pm} (2m_{\tilde{\tau}_1}^2 + m_{\tilde{t}_1}^2 - m_b^2) + 4l_{11}^{\tilde{t}} k_{12}^{\tilde{t}} m_b m_{\tilde{\chi}_1^\pm} m_{\tilde{\tau}_1}^2 + 4l_{12}^{\tilde{t}} k_{11}^{\tilde{t}} m_b m_{\tilde{\chi}_2^\pm} m_{\tilde{\tau}_1}^2 - 2k_{11}^{\tilde{t}} k_{12}^{\tilde{t}} m_{\tilde{\tau}_1}^2 (m_{\tilde{t}_1}^2 + \frac{1}{2}m_{\tilde{\tau}_1}^2 - m_b^2) \right] \quad (\text{A.117})$$

$$c_{34} = l_{11}^{\tilde{\tau}} l_{12}^{\tilde{\tau}} \left[k_{11}^{\tilde{t}} k_{12}^{\tilde{t}} (2m_{\tilde{\tau}_1}^2 + m_{\tilde{t}_1}^2 - m_b^2) - 2l_{11}^{\tilde{t}} k_{12}^{\tilde{t}} m_b m_{\tilde{\chi}_1^\pm} - 2l_{12}^{\tilde{t}} k_{11}^{\tilde{t}} m_b m_{\tilde{\chi}_2^\pm} - l_{11}^{\tilde{t}} l_{12}^{\tilde{t}} m_{\tilde{\chi}_1^\pm} m_{\tilde{\chi}_2^\pm} \right] \quad (\text{A.118})$$

$$c_{35} = -l_{11}^{\tilde{\tau}} l_{12}^{\tilde{\tau}} k_{11}^{\tilde{t}} k_{12}^{\tilde{t}} \quad (\text{A.119})$$

To get the coefficients for $\tilde{t}_1 \rightarrow b + \tilde{\tau}_2 + \nu_\tau$ one has to make the following replacements: $l_{1i}^{\tilde{\tau}} \rightarrow l_{2i}^{\tilde{\tau}}$ and $m_{\tilde{\tau}_1} \rightarrow m_{\tilde{\tau}_2}$. For $\tilde{t}_1 \rightarrow b + \tilde{e}_L + \nu_e$ one gets the corresponding coefficients by the replacements: $l_{1i}^{\tilde{\tau}} \rightarrow u_{1i}$ and $m_{\tilde{\tau}_1} \rightarrow m_{\tilde{e}_L}$.

A.4 Some analytical solutions of integrals

A.4.1 The integrals J_i

The following integrals appear in the formulae for the three body decays:

1.

$$J_t^0(m_1) = \int_{t_{min}}^{t_{max}} dt \frac{1}{(t - m_1^2)^2 + m_1^2 \Gamma_1^2}$$

2.

$$J_t^1(m_1) = \int_{t_{min}}^{t_{max}} dt \frac{t}{(t - m_1^2)^2 + m_1^2 \Gamma_1^2}$$

3.

$$J_t^2(m_1) = \int_{t_{min}}^{t_{max}} dt \frac{t^2}{(t - m_1^2)^2 + m_1^2 \Gamma_1^2}$$

4.

$$J_{tt}^0(m_1, m_2) = Re \int_{t_{min}}^{t_{max}} dt \frac{1}{(t - m_1^2 + im_1 \Gamma_1)(t - m_2^2 - im_2 \Gamma_2)}$$

5.

$$J_{tt}^1(m_1, m_2) = Re \int_{t_{min}}^{t_{max}} dt \frac{t}{(t - m_1^2 + im_1 \Gamma_1)(t - m_2^2 - im_2 \Gamma_2)}$$

6.

$$J_{tt}^2(m_1, m_2) = Re \int_{t_{min}}^{t_{max}} dt \frac{t^2}{(t - m_1^2 + im_1 \Gamma_1)(t - m_2^2 - im_2 \Gamma_2)}$$

7.

$$J_{st}^0(s, m_1, m_2) = \text{Re} \frac{1}{s - m_1^2 + im_1\Gamma_1} \int_{t_{min}}^{t_{max}} dt \frac{1}{t - m_2^2 - im_2\Gamma_2}$$

8.

$$J_{st}^1(s, m_1, m_2) = \text{Re} \frac{1}{s - m_1^2 + im_1\Gamma_1} \int_{t_{min}}^{t_{max}} dt \frac{t}{t - m_2^2 - im_2\Gamma_2}$$

A.4.2 The solution of $J_t^0(m_1)$

If $\Gamma_1 = 0$ then

$$J_t^0(m_1) = \frac{1}{t_{min} - m_1^2} - \frac{1}{t_{max} - m_1^2} \quad (\text{A.120})$$

else

$$J_t^0(m_1) = \frac{1}{m_1\Gamma_1} \left[\arctan \left(\frac{t_{max} - m_1^2}{m_1\Gamma_1} \right) - \arctan \left(\frac{t_{min} - m_1^2}{m_1\Gamma_1} \right) \right] \quad (\text{A.121})$$

A.4.3 The solution of $J_t^1(m_1)$

If $\Gamma_1 = 0$ then

$$J_t^1(m_1) = \frac{m_1^2}{t_{min} - m_1^2} - \frac{m_1^2}{t_{max} - m_1^2} + \log \left| \frac{t_{max} - m_1^2}{t_{min} - m_1^2} \right| \quad (\text{A.122})$$

else

$$\begin{aligned} J_t^1(m_1) = & \frac{m_1}{\Gamma_1} \left[\arctan \left(\frac{t_{max} - m_1^2}{m_1\Gamma_1} \right) - \arctan \left(\frac{t_{min} - m_1^2}{m_1\Gamma_1} \right) \right] \\ & + \frac{1}{2} \log \left| \frac{(t_{max} - m_1^2)^2 + m_1^2\Gamma_1^2}{(t_{min} - m_1^2)^2 + m_1^2\Gamma_1^2} \right| \end{aligned} \quad (\text{A.123})$$

A.4.4 The solution of $J_t^2(m_1)$

If $\Gamma_1 = 0$ then

$$J_t^2(m_1) = \frac{m_1^4}{t_{min} - m_1^2} - \frac{m_1^4}{t_{max} - m_1^2} + 2m_1^2 \log \left| \frac{t_{max} - m_1^2}{t_{min} - m_1^2} \right| + t_{max} - t_{min} \quad (\text{A.124})$$

else

$$\begin{aligned} J_t^2(m_1) = & \frac{m_1^4 - m_1^2 \Gamma_1^2}{m_1 \Gamma_1} \left[\arctan \left(\frac{t_{max} - m_1^2}{m_1 \Gamma_1} \right) - \arctan \left(\frac{t_{min} - m_1^2}{m_1 \Gamma_1} \right) \right] \\ & + m_1^2 \log \left| \frac{(t_{max} - m_1^2)^2 + m_1^2 \Gamma_1^2}{(t_{min} - m_1^2)^2 + m_1^2 \Gamma_1^2} \right| + t_{max} - t_{min} \end{aligned} \quad (\text{A.125})$$

A.4.5 The solution of $J_{tt}^0(m_1, m_2)$

If $\Gamma_1 = 0$ and $\Gamma_2 = 0$ then

$$J_{tt}^0(m_1, m_2) = \frac{1}{m_1^2 - m_2^2} \left[\log \left| \frac{t_{max} - m_1^2}{t_{min} - m_1^2} \right| - \log \left| \frac{t_{max} - m_2^2}{t_{min} - m_2^2} \right| \right] \quad (\text{A.126})$$

else

$$\begin{aligned} J_{tt}^0(m_1, m_2) = & \frac{m_1^2 - m_2^2}{2[(m_1^2 - m_2^2)^2 + (m_1 \Gamma_1 + m_2 \Gamma_2)^2]} \\ & * \left[\log \left| \frac{(t_{max} - m_1^2)^2 + m_1^2 \Gamma_1^2}{(t_{min} - m_1^2)^2 + m_1^2 \Gamma_1^2} \right| - \log \left| \frac{(t_{max} - m_2^2)^2 + m_2^2 \Gamma_2^2}{(t_{min} - m_2^2)^2 + m_2^2 \Gamma_2^2} \right| \right] \\ & + \frac{m_1 \Gamma_1 + m_2 \Gamma_2}{(m_1^2 - m_2^2)^2 + (m_1 \Gamma_1 + m_2 \Gamma_2)^2} \\ & * \left[\arctan \left(\frac{m_1 \Gamma_1}{t_{max} - m_1^2} \right) - \arctan \left(\frac{m_1 \Gamma_1}{t_{min} - m_1^2} \right) \right. \\ & \left. + \arctan \left(\frac{m_2 \Gamma_2}{t_{max} - m_2^2} \right) - \arctan \left(\frac{m_2 \Gamma_2}{t_{min} - m_2^2} \right) \right] \end{aligned} \quad (\text{A.127})$$

A.4.6 The solution of $J_{tt}^1(m_1, m_2)$

If $\Gamma_1 = 0$ and $\Gamma_2 = 0$ then

$$J_{tt}^1(m_1, m_2) = \frac{1}{m_1^2 - m_2^2} \left[m_1^2 \log \left| \frac{t_{max} - m_1^2}{t_{min} - m_1^2} \right| - m_2^2 \log \left| \frac{t_{max} - m_2^2}{t_{min} - m_2^2} \right| \right] \quad (\text{A.128})$$

else

$$\begin{aligned}
J_{tt}^1(m_1, m_2) = & \frac{m_1^2(m_1^2 - m_2^2) + m_1\Gamma_1(m_1\Gamma_1 + m_2\Gamma_2)}{2[(m_1^2 - m_2^2)^2 + (m_1\Gamma_1 + m_2\Gamma_2)^2]} \log \left| \frac{(t_{max} - m_1^2)^2 + m_1^2\Gamma_1^2}{(t_{min} - m_1^2)^2 + m_1^2\Gamma_1^2} \right| \\
& + \frac{m_2^2(m_2^2 - m_1^2) + m_2\Gamma_2(m_1\Gamma_1 + m_2\Gamma_2)}{2[(m_1^2 - m_2^2)^2 + (m_1\Gamma_1 + m_2\Gamma_2)^2]} \log \left| \frac{(t_{max} - m_2^2)^2 + m_2^2\Gamma_2^2}{(t_{min} - m_2^2)^2 + m_2^2\Gamma_2^2} \right| \\
& - \frac{m_2^2m_1\Gamma_1 + m_1^2m_2\Gamma_2}{(m_1^2 - m_2^2)^2 + (m_1\Gamma_1 + m_2\Gamma_2)^2} \\
& * \left[\arctan \left(\frac{m_1\Gamma_1}{t_{max} - m_1^2} \right) - \arctan \left(\frac{m_1\Gamma_1}{t_{min} - m_1^2} \right) \right. \\
& \left. + \arctan \left(\frac{m_2\Gamma_2}{t_{max} - m_2^2} \right) - \arctan \left(\frac{m_2\Gamma_2}{t_{min} - m_2^2} \right) \right] \quad (A.129)
\end{aligned}$$

A.4.7 The solution of $J_{tt}^2(m_1, m_2)$

If $\Gamma_1 = 0$ and $\Gamma_2 = 0$ then

$$\begin{aligned}
J_{tt}^2(m_1, m_2) = & t_{max} - t_{min} \\
& + \frac{1}{m_1^2 - m_2^2} \left[m_1^4 \log \left| \frac{t_{max} - m_1^2}{t_{min} - m_1^2} \right| - m_2^4 \log \left| \frac{t_{max} - m_2^2}{t_{min} - m_2^2} \right| \right] \quad (A.130)
\end{aligned}$$

else

$$\begin{aligned}
J_{tt}^2(m_1, m_2) = & t_{max} - t_{min} \\
& + \frac{(m_1^4 - m_1^2\Gamma_1^2)(m_1^2 - m_2^2) + 2m_1^3\Gamma_1(m_1\Gamma_1 + m_2\Gamma_2)}{2[(m_1^2 - m_2^2)^2 + (m_1\Gamma_1 + m_2\Gamma_2)^2]} \\
& * \log \left| \frac{(t_{max} - m_1^2)^2 + m_1^2\Gamma_1^2}{(t_{min} - m_1^2)^2 + m_1^2\Gamma_1^2} \right| \\
& + \frac{(m_2^4 - m_2^2\Gamma_2^2)(m_2^2 - m_1^2) + 2m_2^3\Gamma_2(m_1\Gamma_1 + m_2\Gamma_2)}{2[(m_1^2 - m_2^2)^2 + (m_1\Gamma_1 + m_2\Gamma_2)^2]} \\
& * \log \left| \frac{(t_{max} - m_2^2)^2 + m_2^2\Gamma_2^2}{(t_{min} - m_2^2)^2 + m_2^2\Gamma_2^2} \right| \\
& - \frac{(m_1^4 - m_1^2\Gamma_1^2)(m_1\Gamma_1 + m_2\Gamma_2) - 2m_1^3\Gamma_1(m_1^2 - m_2^2)}{(m_1^2 - m_2^2)^2 + (m_1\Gamma_1 + m_2\Gamma_2)^2} \\
& * \left[\arctan \left(\frac{m_1\Gamma_1}{t_{max} - m_1^2} \right) - \arctan \left(\frac{m_1\Gamma_1}{t_{min} - m_1^2} \right) \right] \\
& - \frac{(m_2^4 - m_2^2\Gamma_2^2)(m_1\Gamma_1 + m_2\Gamma_2) - 2m_2^3\Gamma_2(m_2^2 - m_1^2)}{(m_1^2 - m_2^2)^2 + (m_1\Gamma_1 + m_2\Gamma_2)^2}
\end{aligned}$$

$$* \left[\arctan \left(\frac{m_2 \Gamma_2}{t_{max} - m_2^2} \right) - \arctan \left(\frac{m_2 \Gamma_2}{t_{min} - m_2^2} \right) \right] \quad (\text{A.131})$$

A.4.8 The solution of $J_{st}^0(s, m_1, m_2)$

If $\Gamma_1 = 0$ and $\Gamma_2 = 0$ then

$$J_{st}^0(s, m_1, m_2) = \frac{1}{s - m_1^2} \log \left| \frac{t_{max} - m_2^2}{t_{min} - m_2^2} \right| \quad (\text{A.132})$$

else

$$\begin{aligned} J_{st}^0(s, m_1, m_2) &= \frac{s - m_1^2}{2[(s - m_1^2)^2 + m_1^2 \Gamma_1^2]} \log \left| \frac{(t_{max} - m_2^2)^2 + m_2^2 \Gamma_2^2}{(t_{min} - m_2^2)^2 + m_2^2 \Gamma_2^2} \right| \\ &\quad - \frac{m_1 \Gamma_1}{(s - m_1^2)^2 + m_1^2 \Gamma_1^2} \\ &\quad * \left[\arctan \left(\frac{m_2 \Gamma_2}{t_{max} - m_2^2} \right) - \arctan \left(\frac{m_2 \Gamma_2}{t_{min} - m_2^2} \right) \right] \end{aligned} \quad (\text{A.133})$$

A.4.9 The solution of $J_{st}^1(s, m_1, m_2)$

If $\Gamma_1 = 0$ and $\Gamma_2 = 0$ then

$$J_{st}^1(s, m_1, m_2) = \frac{1}{s - m_1^2} \left(t_{max} - t_{min} + m_2^2 \log \left| \frac{t_{max} - m_2^2}{t_{min} - m_2^2} \right| \right) \quad (\text{A.134})$$

else

$$\begin{aligned} J_{st}^1(s, m_1, m_2) &= \frac{s - m_1^2}{(s - m_1^2)^2 + m_1^2 \Gamma_1^2} (t_{max} - t_{min}) \\ &\quad + \frac{m_2^2(s - m_1^2) + m_1 \Gamma_1 m_2 \Gamma_2}{2[(s - m_1^2)^2 + m_1^2 \Gamma_1^2]} \log \left| \frac{(t_{max} - m_2^2)^2 + m_2^2 \Gamma_2^2}{(t_{min} - m_2^2)^2 + m_2^2 \Gamma_2^2} \right| \\ &\quad - \frac{m_2 \Gamma_2(s - m_1^2) - m_2^2 m_1 \Gamma_1}{(s - m_1^2)^2 + m_1^2 \Gamma_1^2} \\ &\quad * \left[\arctan \left(\frac{m_2 \Gamma_2}{t_{max} - m_2^2} \right) - \arctan \left(\frac{m_2 \Gamma_2}{t_{min} - m_2^2} \right) \right] \end{aligned} \quad (\text{A.135})$$

Appendix B

Calculation of sfermion parameters

Here we present the formulae for the computation of the soft SUSY parameters from sfermion masses and mixing angles. The following assumptions are made:

- μ and $\tan \beta$ are known from other experiments (Higgs, chargino and neutralino sector)
- there is hardly any mixing between the generations.

From the inversion of the eigenvalue-problem for the squark-masses one obtains:

$$M_{\tilde{Q}}^2 = -m_Z^2 \cos 2\beta \left(\frac{1}{2} - \frac{2}{3} \sin^2 \theta_W \right) - m_t^2 + \frac{1}{2} \left(m_{\tilde{t}_1}^2 + m_{\tilde{t}_2}^2 + (m_{\tilde{t}_1}^2 - m_{\tilde{t}_2}^2) \cos 2\theta_{\tilde{t}} \right) \quad (\text{B.1})$$

$$= m_Z^2 \cos 2\beta \left(\frac{1}{2} - \frac{1}{3} \sin^2 \theta_W \right) - m_b^2 + \frac{1}{2} \left(m_{\tilde{b}_1}^2 + m_{\tilde{b}_2}^2 + (m_{\tilde{b}_1}^2 - m_{\tilde{b}_2}^2) \cos 2\theta_{\tilde{b}} \right) \quad (\text{B.2})$$

$$M_{\tilde{U}}^2 = -m_Z^2 \cos 2\beta \frac{2}{3} \sin^2 \theta_W - m_t^2 + \frac{1}{2} \left(m_{\tilde{t}_1}^2 + m_{\tilde{t}_2}^2 + (m_{\tilde{t}_2}^2 - m_{\tilde{t}_1}^2) \cos 2\theta_{\tilde{t}} \right) \quad (\text{B.3})$$

$$M_{\tilde{D}}^2 = -m_Z^2 \cos 2\beta \frac{1}{3} \sin^2 \theta_W - m_b^2 + \frac{1}{2} \left(m_{\tilde{b}_1}^2 + m_{\tilde{b}_2}^2 + (m_{\tilde{b}_2}^2 - m_{\tilde{b}_1}^2) \cos 2\theta_{\tilde{b}} \right) \quad (\text{B.4})$$

$$A_t = \mu \cot \beta + \frac{(m_{\tilde{t}_1}^2 - m_{\tilde{t}_2}^2) \sin 2\theta_{\tilde{t}}}{2m_t} \quad (\text{B.5})$$

$$A_b = \mu \tan \beta + \frac{(m_{\tilde{b}_1}^2 - m_{\tilde{b}_2}^2) \sin 2\theta_{\tilde{b}}}{2m_b} \quad (\text{B.6})$$

As one can see, there are two equations to determine M_Q^2 . Therefore, one gets at tree-level the condition:

$$m_W^2 \cos 2\beta = m_{\tilde{t}_1}^2 \cos^2 \theta_{\tilde{t}} + m_{\tilde{t}_2}^2 \sin^2 \theta_{\tilde{t}} - m_t^2 - m_{\tilde{b}_1}^2 \cos^2 \theta_{\tilde{b}} - m_{\tilde{b}_2}^2 \sin^2 \theta_{\tilde{b}} + m_b^2 \quad (\text{B.7})$$

This condition implies that one of the six quantities $m_{\tilde{t}_1}$, $m_{\tilde{t}_2}$, $\cos^2 \theta_{\tilde{t}}$, $m_{\tilde{b}_1}$, $m_{\tilde{b}_2}$, $\cos^2 \theta_{\tilde{b}}$ can be predicted by the other five, if the above assumptions are fulfilled. However, the above relations are only valid at tree-level. For a precise calculation one needs also the inclusion of one-loop corrections [65].

For the sleptons the corresponding results are:

$$M_L^2 = m_{\tilde{\nu}_\tau}^2 - \frac{1}{2} m_Z^2 \cos 2\beta \quad (\text{B.8})$$

$$= m_Z^2 \cos 2\beta \left(\frac{1}{2} - \sin^2 \theta_W \right) - m_\tau^2 + \frac{1}{2} \left(m_{\tilde{\tau}_1}^2 + m_{\tilde{\tau}_2}^2 + (m_{\tilde{\tau}_1}^2 - m_{\tilde{\tau}_2}^2) \cos 2\theta_{\tilde{\tau}} \right) \quad (\text{B.9})$$

$$M_{\tilde{E}}^2 = -m_Z^2 \cos 2\beta \sin^2 \theta_W - m_\tau^2 + \frac{1}{2} \left(m_{\tilde{\tau}_1}^2 + m_{\tilde{\tau}_2}^2 + (m_{\tilde{\tau}_2}^2 - m_{\tilde{\tau}_1}^2) \cos 2\theta_{\tilde{\tau}} \right) \quad (\text{B.10})$$

$$A_b = \mu \tan \beta + \frac{(m_{\tilde{\tau}_1}^2 - m_{\tilde{\tau}_2}^2) \sin 2\theta_{\tilde{\tau}}}{2m_\tau} \quad (\text{B.11})$$

Again, there are two equations for $M_{\tilde{L}}^2$ giving the following condition:

$$m_W^2 \cos 2\beta = m_{\tilde{\nu}_\tau}^2 - m_{\tilde{\tau}_1}^2 \cos^2 \theta_{\tilde{\tau}} - m_{\tilde{\tau}_2}^2 \sin^2 \theta_{\tilde{\tau}} + m_\tau^2 \quad (\text{B.12})$$

Therefore, one of the four quantities $m_{\tilde{\nu}_\tau}$, $m_{\tilde{\tau}_1}$, $m_{\tilde{\tau}_2}$, $\cos^2 \theta_{\tilde{\tau}}$ can be predicted by the other three under the above assumptions.

Appendix C

Production cross sections

C.1 Tree Level

The reaction $e^+e^- \rightarrow \tilde{f}_i \tilde{f}_j^*$ proceeds via γ and Z^0 exchange (see Fig. C.1). The tree level cross section at a center-of-mass energy of \sqrt{s} is given by (no summation over i and j):

$$\sigma^{tree}(e^+e^- \rightarrow \tilde{f}_i \tilde{f}_j^*) = c_{ij} \left[e_f^2 \delta_{ij} - T_{\gamma Z} e_f a_{ij} \delta_{ij} + T_{ZZ} a_{ij}^2 \right], \quad (\text{C.1})$$

with

$$c_{ij} = \frac{\pi N_C \alpha^2}{3s} \lambda_{ij}^{3/2}, \quad (\text{C.2})$$

$$T_{\gamma Z} = \frac{(L_e + R_e)}{\sin^2 \theta_W \cos^2 \theta_W} \frac{s(s - m_Z^2)}{(s - m_Z^2)^2 + \Gamma_Z^2 m_Z^2}, \quad (\text{C.3})$$

$$T_{ZZ} = \frac{(L_e^2 + R_e^2)}{2 \sin^4 \theta_W \cos^4 \theta_W} \frac{s^2}{(s - m_Z^2)^2 + \Gamma_Z^2 m_Z^2}. \quad (\text{C.4})$$

Here N_C is a colour factor which is 3 for squarks and 1 for sleptons; $\lambda_{ij} = (1 - \mu_i^2 - \mu_j^2)^2 - 4\mu_i^2 \mu_j^2$, $\mu_{i,j}^2 = m_{\tilde{f}_{i,j}}^2/s$; e_f is the charge of the sfermions ($e_t = 2/3, e_b = -1/3, e_\tau = -1$) in units of $e (= \sqrt{4\pi\alpha})$. L_e (R_e) is the coupling of the left-handed (right-handed) electron to the Z boson: $L_e = -\frac{1}{2} + \sin^2 \theta_W$ ($R_e = \sin^2 \theta_W$), and a_{ij} are the corresponding couplings $Z \tilde{f}_i \tilde{f}_j^*$:

$$\begin{aligned} a_{11} &= 4(I_f^{3L} \cos^2 \theta_{\tilde{f}} - \sin^2 \theta_W e_f), \\ a_{22} &= 4(I_f^{3L} \sin^2 \theta_{\tilde{f}} - \sin^2 \theta_W e_f), \\ a_{12} &= a_{21} = -2I_q^{3L} \sin^2 \theta_{\tilde{f}}, \end{aligned} \quad (\text{C.5})$$

where I_f^{3L} is the third component of the weak isospin of the fermion f .

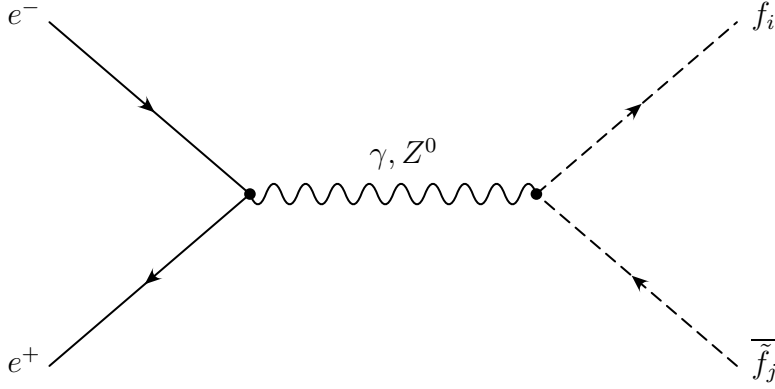


Fig. C.1: Feynman diagrams for the process $e^+e^- \rightarrow \tilde{f}_i \overline{\tilde{f}}_j$ ($f \neq e, \nu_e$).

σ^{tree} shows the typical $\lambda^{3/2}$ suppression. The interference of the γ and Z^0 exchange contributions leads to a characteristic minimum of the cross section at

$$\cos^2 \theta_{\tilde{f}}|_{min} = \frac{Q_f}{I_f^3} \sin^2 \theta_W \left[1 + \left(1 - \frac{m_Z^2}{s}\right) \cos^2 \theta_W \frac{L_e + R_e}{L_e^2 + R_e^2} \right] \quad (\text{C.6})$$

in case of $\tilde{f}_1 \overline{\tilde{f}}_1$ production. In the case of $\tilde{f}_2 \overline{\tilde{f}}_2$ production $\cos^2 \theta_{\tilde{f}}$ has to be replaced by $\sin^2 \theta_{\tilde{f}}$. The angular distribution has the familiar $\sin^2 \vartheta$ shape, with ϑ the scattering angle:

$$\frac{d\sigma^{tree}}{d\cos\vartheta} = \frac{3}{4} \sin^2 \vartheta \sigma^{tree}. \quad (\text{C.7})$$

These formulae for the production cross sections are valid for the case of unpolarized electrons. In the case of left-polarized electrons one has to make the substitutions $(L_e + R_e) \rightarrow 2L_e$ and $(L_e^2 + R_e^2) \rightarrow 2L_e^2$ and in case of right-polarized electrons: $(L_e + R_e) \rightarrow 2R_e$ and $(L_e^2 + R_e^2) \rightarrow 2R_e^2$. The cross section for a certain e^- beam polarization $\xi \in [-1, 1]$, where $\xi = (-1, 0, 1) \equiv (\text{left-polarized, unpolarized, right-polarized})$ e^- beam, has the form

$$\begin{aligned} \sigma(\xi) &= (\Theta(\xi) - \xi) \sigma_L + (\Theta(-\xi) + \xi) \sigma_R \\ \text{with} \quad \Theta(\xi) &= \begin{cases} 1 & \xi > 0 \\ 1/2 & \xi = 0 \\ 0 & \xi < 0 \end{cases} \end{aligned} \quad (\text{C.8})$$

C.2 SUSY-QCD Corrections

The supersymmetric QCD corrected cross section in $O(\alpha_s)$ can be written as [53]:

$$\sigma^{QCD} = \sigma^{tree} + \delta\sigma^g + \delta\sigma^{\tilde{g}} + \delta\sigma^{\tilde{q}}. \quad (\text{C.9})$$

$\delta\sigma^g$ gives the standard gluonic correction, $\delta\sigma^{\tilde{g}}$ is the correction due to the gluino exchange, and $\delta\sigma^{\tilde{q}}$ is the correction due to squark exchange. $\delta\sigma^{\tilde{q}}$ is 0 in the renormalization prescription used.

$\delta\sigma^g$ is given by

$$\delta\sigma^g = \sigma^{tree} \left[\frac{4\alpha_s}{3\pi} \Delta_{ij} \right] \quad (C.10)$$

with

$$\begin{aligned} \Delta_{ij} = & \log(\mu_i \mu_j) + 2 + \frac{2 + \mu_i^2 + \mu_j^2}{\lambda_{ij}^{1/2}} \log \lambda_0 + \frac{1 + 2\mu_i^2}{\lambda_{ij}^{1/2}} \log \lambda_1 + \frac{1 + 2\mu_j^2}{\lambda_{ij}^{1/2}} \log \lambda_2 \\ & + \frac{1 - \mu_i^2 - \mu_j^2}{\lambda_{ij}^{1/2}} \log \frac{1 - \mu_i^2 - \mu_j^2 + \lambda_{ij}^{1/2}}{1 - \mu_i^2 - \mu_j^2 - \lambda_{ij}^{1/2}} \\ & + \left[\frac{(1 - \mu_i^2 - \mu_j^2)}{\lambda_{ij}^{1/2}} \log \lambda_0 - 1 \right] \log \frac{\lambda_{ij}^2}{\mu_i^2 \mu_j^2} \\ & + \frac{4}{\lambda_{ij}^{3/2}} \left[\frac{1}{4} \lambda_{ij}^{1/2} (1 + \mu_i^2 + \mu_j^2) + \mu_i^2 \log \lambda_2 + \mu_j^2 \log \lambda_1 + \mu_i^2 \mu_j^2 \log \lambda_0 \right] \\ & + \frac{1 - \mu_i^2 - \mu_j^2}{\lambda_{ij}^{1/2}} \left[\frac{2\pi^2}{3} + 2\text{Li}_2(1 - \lambda_0^2) + \text{Li}_2(\lambda_1^2) - \text{Li}_2(1 - \lambda_1^2) + \text{Li}_2(\lambda_2^2) \right. \\ & \quad \left. - \text{Li}_2(1 - \lambda_2^2) + 2 \log^2 \lambda_0 - \log \lambda_{ij} \log \lambda_0 \right], \end{aligned} \quad (C.11)$$

$$\lambda_0 = \frac{1}{2\mu_i \mu_j} (1 - \mu_i^2 - \mu_j^2 + \lambda_{ij}^{1/2}) \quad , \quad \lambda_{1,2} = \frac{1}{2\mu_{j,i}} (1 \mp \mu_i^2 \pm \mu_j^2 - \lambda_{ij}^{1/2}), \quad (C.12)$$

and $\text{Li}_2(x) = -\int_0^1 \log(1 - xt)/t dt$. In Eq. (C.11) soft and hard gluon radiation is included.

The gluino correction can be written as:

$$\delta\sigma^{\tilde{g}} = c_{ij} \left[2e_q \Delta(e_q)_{ij}^{(\tilde{g})} \delta_{ij} - T_{\gamma Z}(e_q \delta_{ij} \Delta a_{ij}^{(\tilde{g})} + \Delta(e_q)_{ij}^{(\tilde{g})} a_{ij}) + 2T_{ZZ} a_{ij} \Delta a_{ij}^{(\tilde{g})} \right] \quad (C.13)$$

Here $\Delta a_{ij}^{(\tilde{g})}$ and $\Delta a_{ij}^{(\tilde{q})}$ are given by:

$$\begin{aligned} \Delta a_{ij}^{(\tilde{g})} = & \frac{2\alpha_s}{3\pi} \left\{ 2m_{\tilde{g}} m_q v_q (S^{\tilde{q}})_{ij} \left(2C_{ij}^+ + C_{ij}^0 \right) \right. \\ & + v_q \delta_{ij} \left[\left(2m_{\tilde{g}}^2 + 2m_q^2 + m_{\tilde{q}_i}^2 + m_{\tilde{q}_j}^2 \right) C_{ij}^+ + 2m_{\tilde{g}}^2 C_{ij}^0 + B^0(s, m_q^2, m_q^2) \right] \\ & \left. + a_q (A^{\tilde{q}})_{ij} \left[\left(2m_{\tilde{g}}^2 - 2m_q^2 + m_{\tilde{q}_i}^2 + m_{\tilde{q}_j}^2 \right) C_{ij}^+ \right. \right. \end{aligned}$$

$$\begin{aligned}
& + (m_{\tilde{q}_i}^2 - m_{\tilde{q}_j}^2) C_{ij}^- + 2 m_{\tilde{g}}^2 C_{ij}^0 + B^0(s, m_q^2, m_q^2) \Big] \\
& - \frac{a_{ij}}{2} \Big[B_0(m_{\tilde{q}_i}^2, m_{\tilde{g}}^2, m_q^2) + B_0(m_{\tilde{q}_j}^2, m_{\tilde{g}}^2, m_q^2) \\
& + (m_{\tilde{q}_i}^2 - m_q^2 - m_{\tilde{g}}^2 - 2m_q m_{\tilde{g}} (-1)^i \sin 2\theta_{\tilde{q}}) B'_0(m_{\tilde{q}_i}^2, m_{\tilde{g}}^2, m_q^2) \\
& + (m_{\tilde{q}_j}^2 - m_q^2 - m_{\tilde{g}}^2 - 2m_q m_{\tilde{g}} (-1)^j \sin 2\theta_{\tilde{q}}) B'_0(m_{\tilde{q}_j}^2, m_{\tilde{g}}^2, m_q^2) \Big] \\
& - \frac{2 m_{\tilde{g}} m_q}{m_{\tilde{q}_1}^2 - m_{\tilde{q}_2}^2} \delta_{ij} \Big[B^0(m_{\tilde{q}_i}^2, m_{\tilde{g}}^2, m_q^2) \left((-1)^{i+1} 2a_{ii'} \cos 2\theta_{\tilde{q}} - a_{i'i'} \sin 2\theta_{\tilde{q}} \right) \\
& + B^0(m_{\tilde{q}_{i'}}^2, m_{\tilde{g}}^2, m_q^2) a_{ii} \sin 2\theta_{\tilde{q}} \Big] \Big\}, \quad i' \neq i, j' \neq j, \quad (C.14)
\end{aligned}$$

and, if $i = j$,

$$\begin{aligned}
\Delta(e_q)_{ij}^{(\tilde{g})} &= \frac{2 e_q \alpha_s}{3 \pi} \Big\{ (2 m_{\tilde{g}}^2 + 2 m_q^2 + m_{\tilde{q}_i}^2 + m_{\tilde{q}_j}^2 + 4 m_{\tilde{g}} m_q (S^{\tilde{q}})_{ii}) C_{ij}^+ \\
& + 2 (m_{\tilde{g}}^2 + m_{\tilde{g}} m_q (S^{\tilde{q}})_{ii}) C_{ij}^0 + B^0(s, m_q^2, m_q^2) - B_0(m_{\tilde{q}_i}^2, m_{\tilde{g}}^2, m_q^2) \\
& - (m_{\tilde{q}_i}^2 - m_q^2 - m_{\tilde{g}}^2 - 2m_q m_{\tilde{g}} (-1)^i \sin 2\theta_{\tilde{q}}) B'_0(m_{\tilde{q}_i}^2, m_{\tilde{g}}^2, m_q^2) \Big\}, \quad (C.15)
\end{aligned}$$

and, if $i \neq j$,

$$\begin{aligned}
\Delta(e_q)_{ij}^{(\tilde{g})} &= \frac{2 e_q \alpha_s}{3 \pi} \Big\{ 2 m_{\tilde{g}} m_q (S^{\tilde{q}})_{ij} (2 C_{ij}^+ + C_{ij}^0) \\
& + \frac{2 m_{\tilde{g}} m_q \cos 2\theta_{\tilde{q}}}{m_{\tilde{q}_1}^2 - m_{\tilde{q}_2}^2} (B_0(m_{\tilde{q}_2}^2, m_{\tilde{g}}^2, m_q^2) - B_0(m_{\tilde{q}_1}^2, m_{\tilde{g}}^2, m_q^2)) \Big\}, \quad (C.16)
\end{aligned}$$

where δ_{ij} is the identity matrix, $v_q = 2I_q^{3L} - 4 \sin^2 \theta_W e_q$, $a_q = 2I_q^{3L}$,

$$A^{\tilde{q}} = \begin{pmatrix} \cos 2\theta_{\tilde{q}} & -\sin 2\theta_{\tilde{q}} \\ -\sin 2\theta_{\tilde{q}} & -\cos 2\theta_{\tilde{q}} \end{pmatrix}, \quad S^{\tilde{q}} = \begin{pmatrix} -\sin 2\theta_{\tilde{q}} & -\cos 2\theta_{\tilde{q}} \\ -\cos 2\theta_{\tilde{q}} & \sin 2\theta_{\tilde{q}} \end{pmatrix}. \quad (C.17)$$

The functions C_{ij}^{\pm} are defined by

$$C^+ = \frac{C^1 + C^2}{2}, \quad C^- = \frac{C^1 - C^2}{2}. \quad (C.18)$$

The arguments of all C-functions are $(m_{\tilde{q}_i}^2, s, m_{\tilde{q}_j}^2, m_{\tilde{g}}^2, m_q^2, m_q^2)$. B^0, C^0, C^1 , and C^2 are the usual two- and three-point functions [66]. Here we use the conventions of [67]:

$$\begin{aligned}
B^0(k^2, m_1^2, m_2^2) &= \int \frac{d^D q}{i\pi^2} \frac{1}{(q^2 - m_1^2)((q+k)^2 - m_2^2)}, \\
[C^0, k^\mu C^1 - \bar{k}^\mu C^2] &= \int \frac{d^D q}{i\pi^2} \frac{[1, q^\mu]}{(q^2 - m_{\tilde{g}}^2)((q+k)^2 - m_q^2)((q-\bar{k})^2 - m_q^2)}.
\end{aligned}$$

C.3 Initial-State Radiation

The effect of initial-state radiation is most easily included by introducing an energy-dependent e^+e^- luminosity function L_{ee} . For our purpose it is sufficient to use the $O(\alpha)$ expression, which reads after summing up the leading logarithms [52, 68] (Here we use the notation of [52]):

$$\sigma^{total} = \left(1 + \alpha(s) \left(\frac{\pi}{3} - \frac{1}{2\pi}\right)\right) \int_{x_{min}}^1 dx L_{ee}(x) \sigma^{QCD}(xs) \quad (C.19)$$

with (Obviously there are no QCD corrections in case of sleptons)

$$x_{min} = \frac{(m_{\tilde{f}_i} + m_{\tilde{f}_j})^2}{s}, \quad (C.20)$$

$$L_{ee}(x) = \beta_{em}(1-x)^{\beta_{em}-1} \left(1 + \frac{3}{4}\beta_{em}\right) - \frac{1}{2}\beta_{em}(1+x) \quad (C.21)$$

and

$$\beta_{em} = \frac{2\alpha_{em}}{\pi} \left(\log \left(\frac{s}{m_e^2} \right) - 1 \right). \quad (C.22)$$

For a discussion on $O(\alpha^2)$ corrections in various schemes see for instance [69].

Bibliography

- [1] C. Itzykson and J.-B. Zuber. *Quantum Field Theory*. McGraw-Hill, 1980;
C. Quigg. *Gauge Theories of Strong, Weak, and Electroweak Interactions*. Oxford University, Frontiers in Physics, Vol. 56, 1983;
D. Balin and A. Love. *Introduction to Gauge Field Theories*. Bristol: Institute of Physics Publishing, 1993.
- [2] O. Nachtmann. *Elementarteilchenphysik, Phänomene und Konzepte*. Vieweg, 1986.
- [3] G.G. Ross. *Grand Unified Theories*. Oxford University, Frontiers in Physics, Vol. 60, 1984.
- [4] Particle Data Group, Phys. Rev. D**54**, 1 (1996).
- [5] J.C. Pati and A. Salam, Phys. Rev. D**8**, 1240 (1973);
H. Georgi and S.L. Glashow, Phys. Rev. Lett. **32**, 438 (1974).
- [6] U. Amaldi, W. de Boer, and H. Fürstenau, Phys. Lett. B **260**, 447 (1991);
P. Langacker and M. Luo, Phys. Rev. D**44**, 817 (1991);
J. Ellis, S. Kelley, and D.V. Nanopoulos, Phys. Lett. B **260**, 161 (1991).
- [7] S. Weinberg, Phys. Rev. D**13**, 974 (1976); Phys. Rev. D**19**, 1277 (1979);
L. Susskind, Phys. Rev. D**20**, 2619 (1979);
G. t’Hooft, in “Recent developments in gauge theories”, Proceedings of the NATO Advanced Summer Institute, Chargese 1979, ed. G. t’Hooft et al. (Plenum, New York 1980).
- [8] E. Witten, Nucl. Phys. **B188**, 513 (1981);
N. Sakai, Z. Phys. C–Particles and Fields **11**, 153 (1981);
S. Dimopoulos and H. Georgi, Nucl. Phys. **B193**, 150 (1981);
R.K. Kaul and P. Majumdar, Nucl. Phys. **B199**, 36 (1982) .
- [9] P. Ramond, Phys. Rev. D**3**, 2415 (1971);
A. Neveu and J. Schwartz, Nucl. Phys. **B31**, 86 (1971);

- Yu. Gol'fand and E.P. Likhtman, JETP Lett. **13**, 323 (1971);
D.V. Volkov and V.P. Akulov, Phys. Lett. **468**, 109 (1973).
- [10] J. Wess and B. Zumino, Nucl. Phys. **B70**, 39 (1974);
J. Wess and B. Zumino, Phys. Lett. **493**, 52 (1974).
- [11] J. Wess and J. Bagger. *Supersymmetry and Supergravity*. Princeton University press, 2nd edition, 1991.
- [12] S. Coleman and J. Mandula, Phys. Rev. **159**, 1251 (1967);
R. Haag, J.T. Lopuszański, and M. Sohnius, Nucl. Phys. **B88**, 257 (1975).
- [13] L. Ibáñez and G.G. Ross, Phys. Lett. B **110**, 215 (1982).
- [14] J. Ellis et al., Nucl. Phys. **B238**, 453 (1984);
A. Gabutti et al., Astropart. Phys. **6**, 1 (1996);
H. Baer and M. Brhlik, Phys. Rev. D **53**, 597 (1996).
- [15] H.E. Haber and G.L. Kane, Phys. Rep. **117**, 75 (1984);
H.P. Nilles, Phys. Rep. **110**, 1 (1984);
A.B. Lahanas and D.V. Nanopoulos, Phys. Rep. **145**, 1 (1987).
- [16] P. Nath, R. Arnowitt, and A.H. Chamseddine, ICTP series in Theo. Phys. **1**, 1 (1984).
- [17] J.F. Gunion and H.E. Haber, Nucl. Phys. **B272**, 1 (1986).
- [18] M. Drees and S.P. Martin, **hep-ph/9504324**, MAD-PH-95-879, UM-TH-95-02.
- [19] D. Balin and A. Love. *Supersymmetric Gauge Field Theory and String Theory*. Bristol: Institute of Physics Publishing, 1995.
- [20] J. Amundson et al., Proceedings of the 1996 DPF/DPB Summer Study on High-Energy Physics, Snowmass, Colorado, June 25 – July 12, 1996, eds. D.G. Cassel, L. Trindle Gennari, R.H. Siemann, p. 655.
- [21] L. Girardello and M. T. Grisaru, Nucl. Phys. **B194**, 65 (1982).
- [22] V. Barger, M.S. Berger, and P. Ohmann, Phys. Rev. D **49**, 4908 (1994);
D.J. Castaño, E.J. Piard, and P. Ramond, Phys. Rev. D **49**, 4882 (1994);
W. de Boer, R. Ehret, and D.I. Kazakov, Z. Phys. C–Particles and Fields **67**, 647 (1995).
- [23] J. Ellis and S. Rudaz, Phys. Lett. B **128**, 248 (1983);
G. Altarelli and R. Rückl, Phys. Lett. B **144**, 126 (1984);
I. Bigi and S. Rudaz, Phys. Lett. B **153**, 335 (1985).

- [24] S. Coleman and E. Weinberg, Phys. Rev. **D7**, 1888 (1973).
- [25] P.H. Chankowski, S. Pokorski, and J. Rosiek, Nucl. Phys. **B423**, 437 (1994).
- [26] H. Eberl, diplom thesis at the “Technische Universität Wien”, (1993).
- [27] J. Ellis, G. Ridolfi, and F. Zwirner, Phys. Lett. B **257**, 83 (1991); Phys. Lett. B **262**, 477 (1991).
- [28] A. Brignole, Phys. Lett. B **277**, 313 (1992).
- [29] A. Bartl, H. Fraas, W. Majerotto, and B. Mösslacher, Z. Phys. C–Particles and Fields **55**, 257 (1992).
- [30] H.E. Haber and G.L. Kane, in [15].
- [31] A. Bartl, H. Fraas, W. Majerotto, and N. Oshimo, Phys. Rev. **D40**, 1594 (1989).
- [32] S.M. Bilenky, N.P. Nedelcheva, and S.T. Petcov, Nucl. Phys. **B247**, 61 (1984).
- [33] D. Pierce and A. Papadopoulos, Nucl. Phys. **B430**, 278 (1994).
- [34] S.L. Glashow, J. Illiopoulos, and L. Maiani, Phys. Rev. **D2**, 1285 (1970).
- [35] N. Cabibbo, Phys. Rev. Lett. **10**, 531 (1963).
- [36] M. Kobayashi and T. Maskawa, Prog. Theo. Phys. **49**, 652 (1973).
- [37] J. Ellis and D.V. Nanopoulos, Phys. Lett. B **110**, 82 (1944);
M.J. Duncan, Nucl. Phys. **B221**, 285 (1983);
J.F. Donoghue, H.P. Nilles, and D. Wyler, Phys. Lett. B **128**, 55 (1983);
M. Dugan, B. Grinstein, and L. Hall, Nucl. Phys. **B255**, 413 (1985);
S. Bertolini, F. Borzumati, A. Masiero, and G. Ridolfi, Nucl. Phys. **B353**, 591 (1991) .
- [38] L.J. Hall, V.A. Kostelecky, and S. Raby, Nucl. Phys. **B267**, 415 (1986);
F. Borzumati and A. Masiero, Phys. Rev. Lett. **57**, 961 (1986);
T. Kosmas, G. Leontaris, and J. Vergados, Phys. Lett. B **219**, 457 (1989);
A. Gabbiani and A. Masiero, Nucl. Phys. **B322**, 235 (1989);
R. Barbieri, L. Hall, A. Strumia, Nucl. Phys. **B445**, 219 (1995) .
- [39] A. Bartl, W. Majerotto, and W. Porod, Z. Phys. C–Particles and Fields **64**, 499 (1994); erratum ibid. Z. Phys. C–Particles and Fields **68**, 518 (1995).
- [40] J.-F. Grivaz, Rapporteur Talk, International Europhysics Conference on High Energy Physics, Brussels, 1995.

- [41] L. Rolandi (ALEPH), H. Dijkstra (DELPHI), D. Strickland (L3), G. Wilson (OPAL), Joint Seminar on First Results, CERN, December 12, 1995;
ALEPH Coll., CERN-PPE/96-10, Jan. 96;
L3 Coll., H. Nowak, and A. Sopczak, L3 Note 1997, Jan. 1996;
OPAL Coll., S. Asai and S. Komamiya, OPAL Physics Note PN-205, Feb. 1996.
- [42] DELPHI Coll. , Phys. Lett. B **382**, 323 (1996); Phys. Lett. B **387**, 651 (1996).
- [43] OPAL Coll., Phys. Lett. B **377**, 273 (1996), Phys. Lett. B **389**, 197 (1996), Phys. Lett. B **389**, 616 (1996), Phys. Lett. B **396**, 301 (1997), Z. Phys. C—Particles and Fields **73**, 201 (1997) .
- [44] ALEPH Coll., Phys. Lett. B **373**, 246 (1996), Phys. Lett. B **384**, 461 (1996), Z. Phys. C—Particles and Fields **72**, 549 (1996) .
- [45] L3 Coll., Phys. Lett. B **377**, 289 (1996) .
- [46] OPAL Coll., CERN-PPE/97-046, CERN-PPE/97-083;
ALEPH Coll., CERN-PPE/97-056; CERN-PPE/97-071; CERN-PPE/97-084;
DELPHI-PPE/97-085; DELPHI-PPE/97-107 .
- [47] J.-F. Grivaz, **hep-ph/9709504**, LAL 97-060; **hep-ph/9709505**, LAL 97-061.
- [48] S. Abachi et al., Phys. Rev. Lett. **76**, 2222 (1996).
- [49] CDF Coll., F. Abe et al., Phys. Rev. Lett. **76**, 2006 (1996).
- [50] X. Tata, **hep-ph/9510287**, UH-511-833-95.
SUPERSYMMETRY: WHERE IT IS AND HOW TO FIND IT.
Jun 1995. 55pp. Talk given at Theoretical Advanced Study Institute in Elementary Particle Physics (TASI 95): QCD and Beyond, Boulder, CO, 4-30 Jun 1995. In "Boulder 1995, QCD and beyond" 163-219.
- [51] K.I. Hikasa and M. Kobayashi, Phys. Rev. D **36**, 724 (1987).
- [52] M. Drees and K.I. Hikasa, Phys. Lett. B **252**, 127 (1990).
- [53] H. Eberl, A. Bartl, and W. Majerotto, Nucl. Phys. **B472**, 481 (1996).
- [54] A. Bartl, H. Eberl, S. Kraml, W. Majerotto, and W. Porod, Z. Phys. C—Particles and Fields **73**, 469 (1997).
- [55] W. Beenaker, R. Höpker, and P.M. Zerwas, Phys. Lett. B **349**, 463 (1995).
- [56] Proc. of the Workshop on Physics at LEP2, CERN 96-01, Vol. I, p. 463, eds. G. Altarelli, T. Sjöstrand, and F. Zwirner.

- [57] J.F. Gunion, H.E. Haber, and M. Sher, Nucl. Phys. **B306**, 1 (1988);
J.A. Casas, A. Lleyda, and C. Muñoz, Nucl. Phys. **B471**, 3 (1996);
A. Kusenko, P. Langacker, and G. Segre, Phys. Rev. D **54**, 5824 (1996);
A. Strumia, Nucl. Phys. **B482**, 24 (1996);
J. A. Casas, **hep-ph/9707475**, IEM-FT-161/97.
- [58] F.M. Borzumati, **hep-ph/9702307**, WIS-96/50/DEC.-PH;
S. Dimopoulos, S. Thomas, and J.D. Wells, Nucl. Phys. **B488**, 39 (1997) .
- [59] D. Schulte and R. Settles, Proceedings of the Workshop “Physics with e^+e^- Linear Colliders”, Annecy – Gran Sasso – Hamburg, Feb. 4 - Sept. 1, 1995, ed. P.M. Zerwas, p. 527, DESY 96-123D.
- [60] M.M. Nojiri, Phys. Rev. D **51**, 6281 (1995);
M.M. Nojiri, K. Fujii, and T. Tsukamoto Phys. Rev. D **54**, 6756 (1996).
- [61] C. Kolda and S.P. Martin, Phys. Rev. D **53**, 3871 (1996) and references therein.
- [62] A. Sopczak, Proceedings of the Workshop “ e^+e^- collisions at 500 GeV: The Physics Potential”, Munich – Annecy – Hamburg, Nov. 92 - April 93, ed. P.M. Zerwas, p. 121, DESY 93-123C.
- [63] A. Bartl, W. Majerotto, and B. Mösslacher, Proceedings of the workshop on „ e^+e^- collisions at 500 GeV”: the physical potential, ed. P.M. Zerwas, p. 641, 1992, DESY 92-123B.
- [64] ALEPH Coll. CERN-PPE/97-71, June 97;
DELPHI Coll., CERN-PPE/97-85, July 97.
- [65] H. Eberl, private communication.
- [66] G. Passarino and M. Veltman, Nucl. Phys. **B160**, 151 (1979).
- [67] A. Denner, Fortschr. Phys. **41**, 307 (1993).
- [68] M.E. Peskin, Seventeenth SLAC Summer Institute, Physics at the 100 GeV mass scale, SLAC-PUB-5210 (1990).
- [69] É.A. Kuraev and V.S. Fadin, Sov. J. Nucl. Phys. **41**, 466 (1985).

Zusammenfassung

Die Vorhersagen des Standardmodells der Elementarteilchenphysik stimmen mit einer erstaunlichen Genauigkeit mit den experimentellen Daten überein. Trotz dieses großartigen Erfolges muß dieses Modell als Grenzfall einer übergeordneten Theorie angesehen werden. Supersymmetrie gilt als einer der aussichtsreichsten Erweiterungen des Standardmodells. Im Rahmen dieser neuen Theorie wird die Poincaré-Algebra um fermionische, antikommutierende Generatoren erweitert, die zu einer Symmetrie führen, die fermionische und bosonische Freiheitsgrade ineinander überführt. Im Rahmen des Minimalen Supersymmetrischen Modells wird dieses Konzept auf eine phänomenologische Grundlage gestellt.

Diese grundlegende Veränderung der Symmetrie hat eine wesentliche Erweiterung des Teilchengehaltes zur Folge: Zu den Leptonen und Quarks kommen die sogenannten Sleptonen und Squarks als Partner hinzu. Der Higgssektor muß um ein Duplett erweitert werden. Dies impliziert die Existenz von fünf physikalischen Higgs-Bosonen. Die supersymmetrischen Partner der Eich- und Higgs-Bosonen treten als Mischzustände auf, die Charginos und Neutralinos genannt werden. Da man bis heute keine supersymmetrischen Teilchen gefunden hat, muß Supersymmetrie gebrochen sein. Dieser Brechung wird durch die Einführung sogenannter „soft SUSY breaking“ Terme Rechnung getragen. Diese werden unterteilt in die Massenterme für die Gauginos und die Sfermionen, trilineare Kopplungen zwischen Higgs-Bosonen und Sfermionen und einem bilinearen Term im Higgs-Sektor.

Es hat sich experimentell gezeigt, daß das Tau-Lepton, das Bottom-Quark und im besonderen das Top-Quark eine wesentlich größere Masse haben als die entsprechenden Fermionen der ersten beiden Generationen. Diesem Umstand wird in den Modellen durch entsprechend große Yukawakopplungen Rechnung getragen. Diese Yukawakopplungen beeinflussen auch wesentlich die Phänomenologie der entsprechenden supersymmetrischen Partner. In der vorliegenden Arbeit werden systematisch die Zerfallsbreiten sämtlicher Zweikörperzerfälle auf Tree-Level berechnet. Im Falle des leichten Stops, einem der beiden Partner des Top-Quarks, ist es darüber hinaus notwendig, die Zerfallsbreiten der wichtigsten Dreikörperzerfälle zu berechnen. Damit ist die Grundlage zur Erarbeitung der Phänomenologie dieser Teilchen an laufenden und zukünftigen Beschleunigern gegeben. Je nach Massenbereich sind dies der LEP-Beschleuniger (CERN), Tevatron (Fermilab), LHC (CERN) und ein

zukünftiger Leptonbeschleuniger mit einem Energiebereich von 300 GeV bis 2 TeV.

Im Folgenden bezeichnen wir die supersymmetrischen Partner des Top-Quarks, des Bottom-Quarks, des Tau-Leptons und des Tau-Neutrinos als Stops, Sbottoms, Staus und Tau-Sneutrino. Die Yukawakopplungen in den Massenmatrizen dieser Teilchen haben zur Folge, daß die elektroschwachen Eigenzustände mischen. Die physikalischen Teilchen werden durch die Massen und den Mischungswinkel charakterisiert. Die Produktion dieser Teilchen bei e^+e^- -Beschleunigern hängt in einer charakteristischen Weise vom Mischungswinkel ab. Diese Abhängigkeit ist wesentlich ausgeprägter, falls polarisierte Elektronen zur Verfügung stehen.

Die großen Yukawakopplungen und die Mischung der elektroschwachen Eigenzustände haben zur Folge, daß sich die Zerfälle dieser Teilchen wesentlich von den Zerfällen der entsprechenden Teilchen der ersten beiden Generationen unterscheiden. Im Falle der Zerfälle in Charginos und Neutralinos treten Interferenzen zwischen den Gaugino- und Higgsinokomponenten dieser Teilchen auf, die abhängig von den Parametern positiv oder negativ sein können. Im Besonderen gibt es Szenarien, in denen aufgrund dieser Interferenzen der Zerfall in das schwerste Chargino bzw. in das schwerste Neutralino am wichtigsten ist.

Ein wesentlicher Aspekt ist die Tatsache, daß aufgrund der Mischung und der Massenaufspaltung Zerfälle in Eich- und Higgsbosonen möglich sind. Es zeigt sich, daß diese Zerfälle dominieren können, besonders im Fall der Stops und Sbottoms. Folgende Punkte haben sich als wichtig erwiesen: Kinematische Effekte sind im Falle der Zerfälle in Eichbosonen besonders ausgeprägt. Die Zerfallsbreite in ein Z -Boson ist umso größer je größer die Mischung ist. Der Zerfall in ein W -Boson wird umso wichtiger je größer die Links-Komponente der Sfermionen ist. Beide Tatsachen lassen sich dadurch verstehen, daß die analogen Kopplungen der Eichbosonen an die entsprechenden Fermionen deren Chiralität erhalten. Im Gegensatz dazu ändern die Kopplungen der Higgsbosonen an die Fermionen deren Chiralität. Entsprechend dazu stellt sich heraus, daß die Zerfälle in Higgsbosonen besonders wichtig sind falls das eine Sfermion überwiegend ein Linkszustand und das andere Sfermion überwiegend ein Rechtszustand ist. Die einzige Ausnahme ist hier das pseudoskalare Higgs, da dessen Kopplungen unabhängig von der Mischung im Sfermionsektor ist.

Im Falle des leichten Stops kann nun der Fall auftreten, daß sämtliche Zweikörperzerfälle auf Tree-Level kinematisch verboten sind. In solch einem Szenario sind die Dreikörperzerfälle dominant gefolgt von dem „Flavour Changing“ Zerfall in ein Charm-Quark und das leichteste Neutralino. Auch im Falle des leichten Sbottoms haben wir Szenarien gefunden, in denen der „Flavour Changing“ Zerfall in ein Charm-Quark und das leichteste Chargino wichtig sein kann. In beiden Fällen sind die totalen Zerfallsbreiten so klein, daß höchstwahrscheinlich Hadronisation dieser Teilchen wichtig sein wird.

Es hat sich herausgestellt, daß die Phänomenologie der Stops, Sbottoms, Staus

und des Tau-Sneutrinos sehr reichhaltig ist. Eine genaue Bestimmung ihrer Eigenschaften wird uns Aufschluß über die „SUSY breaking“ Parameter geben und darüber hinaus hoffentlich auch Einsicht in den Mechanismus der Supersymmetriebrechung.

Lebenslauf

Personalien: Name: Werner Porod
 Geburtsdatum: 10. August 1967
 Geburtsort: Waidhofen an der Ybbs
 Eltern: Stefanie Porod, Hausfrau
 Klaus Porod, Justizwachbeamter

Bildungsgang: 4 Jahre Volksschule in Feldkirch-Tisis
 2 Jahre Hauptschule in Feldkirch-Gisingen
 6 Jahre Gymnasium in Feldkirch-Levis
 7 Semester Physik-Diplomstudium an der TU-Graz
 10 Semester Physik-Diplomstudium an der Universität Wien
 Abschluß des Diplomstudiums mit Auszeichnung am 4.8.1993
 9 Semester Physik-Doktoratstudium an der Universität Wien

Zivildienst: abgeleistet vom 1.10.1996 bis 31.8.1997 in der Pfarre St. Cyril
 und Method

Mitwirkung an folgenden Lehrveranstaltungen:
 Tutorium zum Proseminar zur theoretischen Physik
 für Lehramtskanidaten 1 im WS 1992/93 und 1993/94
 Tutorium zum Proseminar zur theoretischen Physik
 für Lehramtskanidaten 2 im SS 1993 und 1994

Auslandsaufenthalte:
 Summerschool on high energy physics and cosmology,
 International Center for Theoretical Physics in Triest,
 13.6.94-29.7.94

 27. Herbstschule für Hochenergiephysik,
 Maria Laach, 5.9.1995-15.9.1995